Enhancing the Kinetics of Pyrite Catalyzed Leaching of Chalcopyrite

by

Ghazaleh Taghi Nazari

BASc, The University of British Columbia, 2009

A THESIS SUBMITTED IN PARTIAL FULFILMENT OF
THE REQUIREMENT FOR THE DEGREE OF

DOCTOR OF PHILOSOPHY

in

THE FACULTY OF GRADUATE STUDIES

(Materials Engineering)

THE UNIVERSITY OF BRITISH COLUMBIA
(Vancouver)

March 2012

Abstract

An investigation has been conducted into the kinetics of chalcopyrite leaching in acidic ferric/ferrous sulfate media at atmospheric pressure and low temperature in the presence of pyrite. It has been found that pyrite samples from different sources affect the rate of chalcopyrite leaching differently. Some pyrite samples accelerate the rate significantly while others have little or no influence. The effectiveness of pyrite has a strong correlation with the level of silver occurring in the pyrite.

In this study, the use of silver-enhanced pyrite in the Galvanox™ process to improve the extraction of copper from chalcopyrite was investigated. The catalytic properties of pyrite have been improved such that all pyrite samples accelerate the rate of copper extraction regardless of their sources. Under appropriate conditions, complete copper extraction can be obtained in the presence of silver-enhanced pyrite in 10 to 15 hours. Silver-enhanced pyrite can also be effectively recycled with minimal loss of effectiveness.

A comprehensive understanding of the mechanisms involved in the process of chalcopyrite leaching in the presence of silver-enhanced pyrite was developed. It has been found that the acceleration of the rate of chalcopyrite leaching is due to the galvanic interaction between pyrite and chalcopyrite particles. An important factor in any galvanic process is maintaining electrical contact between two minerals to ensure the transport of electrons from the anode to the cathode. As chalcopyrite leaching proceeds, layers of extremely high electrical resistivity form around chalcopyrite particles, which limit the transport of electrons from chalcopyrite to pyrite and inhibit the galvanic interaction between these two minerals. However, in this study, it has been shown that, in the presence of silver-enhanced pyrite, around 10% of the added silver gradually leaves pyrite during leaching and reacts with the elemental sulfur layer on chalcopyrite to form silver sulfide. Although the amount of silver sulfide is very low and the sulfur layer

does not become very conductive, it does become conductive enough to allow the transport of electrons at a rate sufficient to support the leaching reactions at rates observed in the process. With a conductive path between pyrite and chalcopyrite, the galvanic interaction between these two minerals can now occur.

Preface

This thesis presents research conducted by Ghazaleh Nazari in collaboration with Dr. David Dixon and Dr. David Dreisinger. Ghazaleh Nazari conducted all the testing and wrote the manuscripts. The details of publications are as follows:

A version of Chapter 4 has been published as “G. Nazari., D.G. Dixon., D.B. Dreisinger. 2011. Enhancing the kinetics of chalcopyrite leaching in the Galvanox™ process. *Hydrometallurgy* 105, 251–258”.

A version of Chapter 5 has been published as “G. Nazari., D.G. Dixon., D.B. Dreisinger. 2012. The role of galena associated with silver-enhanced pyrite in the kinetics of chalcopyrite leaching during the Galvanox™ process. *Hydrometallurgy*, 111–112, 35–45”.

A part of Chapter 8 has been published as “G. Nazari., D. G. Dixon., D.B. Dreisinger. 2012. The role of silver-enhanced pyrite in enhancing the electrical conductivity of sulfur product layer during chalcopyrite leaching in the Galvanox™ process. *Hydrometallurgy* 113–114, 177–184”.

A part of Chapter 8 has been published as “G. Nazari., D.G. Dixon., D.B. Dreisinger. 2012. The mechanism of chalcopyrite leaching in the presence of silver-enhanced pyrite in the Galvanox™ process. *Hydrometallurgy*, 113–114, 122–130”.

Table of Contents

List of Tables

List of Figures

List of Symbols

E^O	Standard reduction potential
E	Reduction potential
ΔG^O	Standard Gibbs free energy
T	Temperature
K_{sp}	Solubility product constant
P_{80}	80%-mass-passing particle size
Cp	Chalcopyrite
Py	Pyrite
I	Current
i	Current density
i_d	Dissolution current
$I_{c,cp}$	Cathodic currents on chalcopyrite
$I_{c,py}$	Cathodic currents on pyrite
$I_{a,cp}$	Anodic currents on chalcopyrite
L	Length
A	Total surface area
A_c	Cathodic surface area
A_a	Anodic surface area
A_{cp}	Surface areas of chalcopyrite
A_{py}	Surface areas of pyrite
Θ_A	Ratio of cathodic to anodic area
λ	Fraction of the cathodic to anodic to area on chalcopyrite
m	Mass
M	Molar mass
F	Faraday's constant (96485 C/mol)
t	Time
R	Electrical resistance
ρ	Electrical resistivity

η_a	Anodic overpotential
α	Charge transfer coefficient
ΔE	Potential difference

Acknowledgements

First and foremost, I would like to thank my supervisors, Dr. David Dixon and Dr. David Dreisinger, for their guidance and support. It has been an honor to be their student. I appreciate all their contributions of time and ideas to make my Ph.D. study interesting and productive. While they provided me with valuable input, they have been supportive and given me the freedom to pursue various paths in my study.

I gratefully acknowledge the financial support of the Natural Science and Engineering Research Council of Canada, particularly in the award of a Postgraduate Doctoral Scholarship.

It has been a great privilege to spend all these years of undergraduate and graduate studies in the Department of Materials Engineering at the University of British Columbia. All its members and memories always remain in my mind.

I would also like to thank my parents for all the love, encouragement, motivation, and support they have given me.

Chapter 1 Introduction

1.1 Background

Chalcopyrite mineral is the most important source of copper in the world (Dutrizac, 1978), and accounts for 70% of the world's known copper reserves (Wang, 2005). Extensive research in the field of hydrometallurgy was done in order to develop an efficient process to extract copper from chalcopyrite, and many hydrometallurgical processes for copper recovery have been proposed. These processes can be categorized according to the type of lixiviant used, such as sulfate, chloride, ammonia, and nitrate. Among these processes, it has been found that ferric sulfate leaching has several advantages such as simplicity of the leaching reaction, low operational cost and low capital cost, and the ease with which copper is recovered by solvent extraction and electrowinning.

In spite of these advantages, copper recovery in ferric sulfate leaching of chalcopyrite is generally low. The reasons for chalcopyrite's resistance to leaching in ferric sulfate media have not been clearly established. Initial reaction rates have been noted to decline rapidly with time, leading many investigators to conclude that a passivating layer forms on the mineral surface (Hackl, 1995). Formation of the passive layer on the surface of the mineral hinders further copper dissolution. In spite of extensive research, the nature of this passive layer is not yet clear. However, there are three different hypotheses to explain the structure of this impermeable layer. One theory suggests the formation of the sulfur layer which limits the oxidation reaction (Dutrizac, 1989; McMillan *et al*., 1982; Muñoz *et al*., 1979). Muñoz *et al*. (1979) suggested that the transport of electrons through the sulfur layer is the rate limiting step, while Durtrizac (1989) believes that the sulfur layer limits the diffusion of reactants and products to and from the chalcopyrite core. Another hypothesis suggests the formation of a copper-rich polysulfide layer which develops on the surface as a result of solid-state changes to the mineral during leaching (Hackl, 1995). A third theory

suggests that the passivating layer consists of iron salts (Pinches *et al*., 1976). These three hypotheses are explained in detail in Chapter 3.

It has been found that one of the most effective methods to increase the reaction rate of chalcopyrite leaching is the addition of pyrite to facilitate the galvanic interaction between pyrite and chalcopyrite (Dixon *et al*., 2008). This process, known as Galvanox™, has several advantages over other hydrometallurgical processes. Galvanox™ runs under atmospheric conditions, so it requires only low-cost leaching tanks. Moreover, the sulfur yield at this temperature is high (>95%) which leads to low oxygen consumption and low sulfuric acid generation. The operating temperature is below the melting point of sulfur which eliminates the use of surfactants. This process also does not require fine grinding.

Galvanox™ has been described as galvanically-assisted atmospheric leaching of copper from chalcopyrite concentrates. In this process, pyrite provides an alternative surface for ferric reduction. Providing a larger surface area for the cathodic reaction on pyrite than for the anodic reaction on chalcopyrite also increases the anodic dissolution rate (Tshilombo, 2004).

As discussed earlier, leaching of chalcopyrite occurs slowly due to the formation of the passivating layer at a potential higher than the passive potential. Therefore, it is important to control the potential of the system such that it remains in the active region of the chalcopyrite. When chalcopyrite leaches, ferrous ions are produced. In the presence of oxygen, the oxidation of ferrous to ferric occurs rapidly and readily at elevated temperature such that the oxidation-reduction potential (ORP) of the leach solution also increases readily. Therefore, the potential of the system shifts to the passive region of the mineral (Elsherif, 2002). The average reported passive potential of chalcopyrite at high temperature (80°C) in sulfuric acid (pH 0.5) and ferric/ferrous sulfate (5 g/L total iron) media is 757 mV *vs* SHE (Viramontes-Gamboa *et al*., 2007). When pyrite is present in the leach slurry, ferric reduction increases and this allows the system

to maintain the solution potential within the active region of the mineral. Figure 1.1 and Figure 1.2 may help to explain this concept.

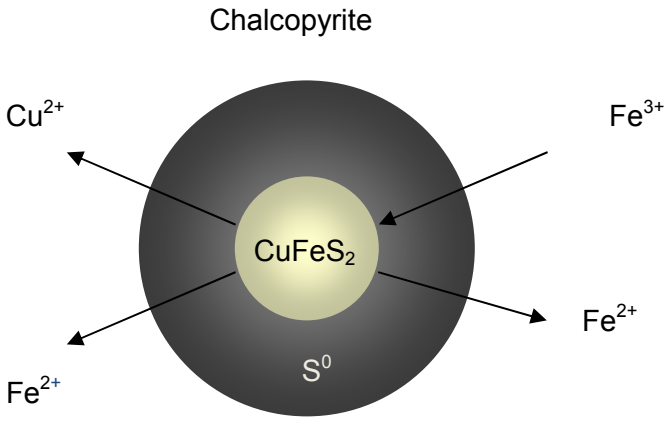

Figure 1.1 Schematic diagram of typical electrochemical leaching mechanism

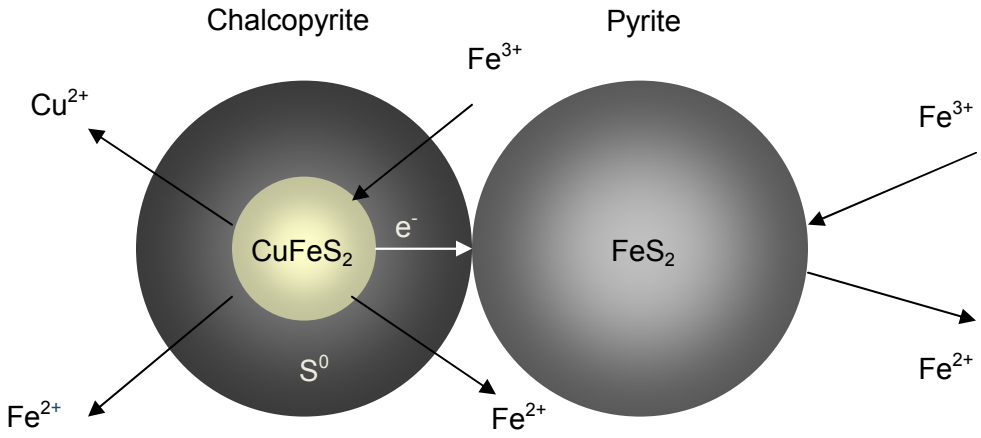

Figure 1.2 Schematic diagram of galvanically assisted electrochemical leaching mechanism

It is worth noting that pyrite has the highest rest potential of the major sulfides (Majima, 1969). The reported rest potential of pyrite at 25°C and pH 4 is 0.66 V (*vs* SHE) (Abraitis *et al*., 2004; Majima, 1969). In another study (Doyle and Mirza,

1996), a rest potential range of 0.558 to 0.699 V (*vs* SHE) at 25°C and pH 1 for pyrite has been was reported. The higher the rest potential, the more noble the mineral. Therefore, in the Galvanox™ process, the selective leaching of chalcopyrite over pyrite occurs (Dixon *et al*., 2008). Furthermore, due to high rest potential of pyrite, it remains more or less inert and can be recycled efficiently (Dixon *et al*., 2008).

1.2 Problem Definition

The most recent studies of the Galvanox™ process indicate that pyrite samples from various sources influence the rate of chalcopyrite leaching differently. Some of the pyrite samples accelerate leaching significantly, while others have only a minor effect on the leach rate. The variation in the catalytic properties of pyrite causes a process uncertainty. It has been found that the effectiveness of pyrite has a strong correlation with the amount of silver associated with the pyrite.

1.3 Objectives

Considering the results of the Galvanox™ tests indicating the importance of silver on pyrite, it was decided to examine the effects of silver-enhanced pyrite (pyrite pretreated with silver ions) on the kinetics of the Galvanox™ process. Reviewing the literature reveals several studies on the interaction of pyrite with silver ions. It has been shown that by introducing the pyrite to a solution containing silver ions, the silver ions are taken up by the pyrite (Bancroft and Hyland, 1990; Buckley *et al*., 1989; Hiskey *et al*., 1987; Hiskey and Pritzker, 1988; Maddox *et al*., 1996; Scaini *et al*.1995 and 1997). Also, it has been proved that pyrite facilitates the leaching of chalcopyrite (Berry *et al*., 1978; Dixon *et al*., 2008; Mehta and Murr, 1983; Muñoz *et al*., 2008; Nowak *et al*., 1984, Tshilombo, 2004). However, there are no studies on the effects of silver-enhanced pyrite on the rate of chalcopyrite leaching.

Hence, in this project, techniques to enhance the catalytic properties of pyrite were studied. Specifically, the effects of silver-enhanced pyrite (pyrite pretreated with silver) on the kinetics of the chalcopyrite leaching were investigated. Various experiments and analyses were conducted to understand the effects of silver on the kinetics of the Galvanox™ process. The aim of this work was to improve the Galvanox™ process by enhancing the catalytic properties of pyrite. Another goal of this project was to discover the optimized conditions for this process in order to render it commercially feasible. Understanding the mechanism of this process was also an important aim of this project.

In summary, the primary objectives of this project were:

- To enhance the catalytic properties of pyrite such that all pyrite samples accelerate the rate of chalcopyrite leaching in the Galvanox™ process regardless of the source of pyrite and hence, eliminate the source of pyrite as a process uncertainty.

- To investigate the use of silver-enhanced pyrite in the Galvanox™ process to improve the extraction of copper from chalcopyrite. Effects of various parameters, such as the amount of silver, the silver-to-pyrite ratio, and solution potential were fully examined in order to maximize copper extraction while minimizing the cost of reagents.

- To develop a comprehensive understanding of the mechanisms involved in the process of chalcopyrite leaching in the presence of silver-enhanced pyrite. A large number of experiments were designed to reveal the mechanism of this process. In addition, various methods and instruments were used to analyze the surfaces of reacted and un-reacted pyrite and chalcopyrite particles in order to understand the nature of the interaction among the various species involved.

Achieving these objectives may lead to a more efficient extraction of copper than is currently possible with either pyrite-catalyzed leaching without added silver (the Galvanox™ process) or silver-catalyzed leaching (e.g., the BRISA process).

In order to achieve these objectives, a number of experiments were designed and conducted to investigate the use of silver-enhanced pyrite with the aim of improving the Galvanox™ process. The effects of various parameters to maximize copper extraction while minimizing the amount of added silver were fully examined. Furthermore, the effects of impurities associated with natural pyrite were studied. The results of these experiments are shown in Chapter 4.

After observing the significant role of silver-enhanced pyrite in accelerating the rate of chalcopyrite leaching, it was important to understand the mechanism involved in this process. The morphology and elemental compositions of pyrite samples were analyzed after the pretreatment with silver ions. It was noted that silver could only be detected in association with galena. In addition, it has been reported that the dissolution of chalcopyrite is favored in the presence of galena (Nova and Gonzalez, 2006). In their study, the electrochemical behavior of pure chalcopyrite and chalcopyrite concentrate containing galena were compared and it was observed that the dissolution current was significantly higher in the concentrate containing galena. Therefore, it was a subject of interest to examine the effect of galena on accelerating the rate of chalcopyrite leaching in both the absence and presence of pyrite and silver in the leaching slurry. Based on the detection of silver in galena, it was also important to determine whether chalcopyrite oxidation could be accelerated by pretreating galena with silver ions. The results are presented in Chapter 5.

In addition, considering the known catalytic properties of silver to accelerate the leaching of copper from chalcopyrite (Banerjee *et al.*, 1990; Miller *et al*., 1981; Price and Warren, 1986) and a stronger affinity of silver to interact with chalcopyrite than with pyrite (Muñoz *et al*., 2008) , it was critical to understand if

there is any beneficial effect of pretreating pyrite with silver and introducing the silver-enhanced pyrite to the leach slurry over adding silver directly to the chalcopyrite leach slurry. A series of experiments was conducted to compare these processes. The results are shown in Chapter 6.

Furthermore, the interaction of silver and pyrite was studied under the conditions of silver-enhanced pyrite preparation in the Galvanox™ process. It was also important to understand the behaviour of silver and pyrite after introducing silver-enhanced pyrite to the leach slurry. The results of this study are presented in Chapter 7.

Considering the results obtained in Chapter 5, 6, and 7, a model was proposed to explain the mechanism of silver-enhanced pyrite catalyzed leaching of chalcopyrite in ferric sulfate media. Several experiments were designed and examined to prove the proposed mechanism. The results are shown in Chapter 8.

Chapter 2 Hydrometallurgical Processes for Chalcopyrite Leaching

2.1 Introduction

Extensive research in the field of hydrometallurgy has been conducted in order to develop an efficient process to extract copper from chalcopyrite. As a result, there are many different hydrometallurgical processes for copper recovery from chalcopyrite. These processes can be grouped according to leaching media as sulfate, chloride, sulfate/chloride, ammonia, and nitrogen processes. In this chapter, a description of all these processes is given. Table 2.1 lists the major processes in each category.

Table 2.1 Sulfate chloride, sulfate/chloride, ammonia, and nitrogen processes

Lixiviant	Process	Temperature (°C)	Pressure (atm)	P_{80} (µm)	Sulfur Product	Recovery (%)	Retention Time	Scale of Development	References
Sulfate	Activox	90-110	10 to 12	5-10	S^0 and SO_4^{2-}	99	1-2 h	8	Corrans and Angove, 1993
	Albion	85-90	1	10-15	S^0	98	22 h	6-7	Hourn and Halbe, 1999
	AAC-UBC	150	10 to 12	10-15	S^0	95	1 h	6	Dreisinger *et al*., 2003
	Dynatec	150	10 to 12	37	S^0	98	2 h	5-6	Collins and Kofluk, 1998
	Galvanox™	80	1	75	S^0	99	< 12 h	5-6	Dixon *et al*., 2008
	TPOX	200-230	30 to 40	37	SO_4^{2-}	98	1 h	9	King and Dreisinger, 1995
	BRISA	70	1	-	S^0	96	8-10 h	5	Romero *et al*., 2003
	BacTech/Mintek	40-50	1	5-10	S^0 and SO_4^{2-}	94	30 days	6	Van Staden, 1998
	BioCOP™	65-80	1	37	SO_4^{2-}	94	10 days	8	Tunley, 1999
	GeoCoat	50	1	-	SO_4^{2-}	99	210 days	6	Johansson *et al*., 1999
Chloride	CLEAR	145	1	-	SO_4^{2-}	98	1-7 h	9	Schweiter and Livingstone, 1982
	Cuprex	95-100	1	-	S^0 and SO_4^{2-}	96	9-10 h	6	Dalton *et al*., 1991
	CYMET	98	1	-	S^0 and SO_4^{2-}	99	6 h	6	Peacey *et al*., 2003
	HydroCopper	85-95	1	-	S^0	98	10-20 h	8	Lundstrom *et al*., 2005
	Intec	85	1	-	S^0	99	16 h	8	Moyes and Houllis, 2002
	Sumitomo	95	1	6-10	S^0	99	3-6 h	6	Asano *et al*., 2007
Sulfate/ Chloride	CESL	140-150	10 to 12	37	S^0	95-98	1-2 h	8	Jones and Hestrin, 1998
	Noranda	140	18	-	S^0	95	1 to 2 h	5	Stanley and Subramanian., 1977
	PLATSOL™	220-230	30 to 40	15	SO_4^{2-}	99	70 min	7	Ferron *et al*., 2001
Ammonia	Arbiter	75-80	1	53	SO_4^{2-}	96	1 h	8	Arbiter and McNulty, 1999
	Escondida	35	1	53	S^0	40	3 h	6	Duyvesteyn *et al*., 1993
Nitrogen	NSC	180	9.75	10	S^0 and SO_4^{2-}	99	30 min	6	Anderson, 2003

1 Basic principles observed and reported
2 Technology concept and/or application formulated
3 Analytical and experimental critical function and/or characteristic proof-of concept
4 Component validation at laboratory scale
5 Integrated component validation at bench/lab scale
6 Pilot plant scale validation
7 Industrial scale validation
8 Demo plant
9 Applied industrially

2.2 Sulfate Processes

The processes based on the sulfate medium are the most established technology for chalcopyrite leaching. Some sulfate processes are briefly discussed below. Among all the processes, it has been found that ferric sulfate leaching has several advantages such as simplicity of the leaching reaction, low operational cost and low capital cost, and the ease with which copper is recovered by solvent extraction and electrowinning.

In general, ferric sulfate leaching of chalcopyrite can be represented by the following reactions (Dutrizac and McDonald, 1974):

$$CuFeS_2 + 2\ Fe_2(SO_4)_3 = CuSO_4 + 5\ FeSO_4 + 2\ S^0 \qquad (2.2.1)$$

$$CuFeS_2 + 8\ Fe_2(SO_4)_3 + 8\ H_2O = CuSO_4 + 17\ FeSO_4 + 8\ H_2SO_4 \qquad (2.2.2)$$

Ferric ions are regenerated via oxidation of ferrous to ferric according to the following reaction:

$$4\ FeSO_4 + O_2 + 2\ H_2SO_4 = 2\ Fe_2(SO_4)_3 + 2\ H_2O \qquad (2.2.3)$$

Oxygen consumption is substantially higher when sulfate is a reaction product rather than elemental sulfur. Each mole of sulfur consumes 1.5 moles of oxygen when oxidized to sulfate according to the following reaction:

$$S + 1.5\ O_2 + H_2O = H_2SO_4 \qquad (2.2.4)$$

Three additional moles of oxygen are required for each mole of chalcopyrite when sulfate is a reaction product. Therefore, high yields of elemental sulfur are desirable to reduce the oxygen consumption.

There are various strategies to recover PGMs (ruthenium, rhodium, palladium, osmium, iridium, and platinum) in sulfate oxidation processes. One is to dissolve the base metals and PGMs and then separate each metal. Another method is to oxidize the base metal and leave the PGMs in a highly concentrated residue suitable for refining. Another strategy is to dissolve the base metals and leave the PGMs in an intermediate residue for further concentration and then refining (Milbourne *et al*., 2003). Gold in residues can be recovered by cyanidation of copper leach residues. However, the presence of elemental sulfur increases the cost of recovery significantly due to the formation of SCN^- via following reaction:

$$S^0 + NaCN = NaSCN \qquad (2.2.5)$$

Chloride and bromide are other alternative reagents for PGMs recovery.

A summary of important sulfate processes is given below.

2.2.1 The Activox Process

The Activox process (Corrans and Angove, 1993) was developed for the treatment of a wide variety of sulfide mineral concentrates. This process consists of activation of the mineral surfaces by fine grinding (P_{80} = 5 to 10 µm). the total surface area increases by decreasing the initial mineral particle size which leads to increasing copper extraction. This process operates at 90 to 110°C and oxygen pressure of 10 to 12 atm (Dreisinger, 2006). Leaching temperature in this process is lower than the melting point of sulfur (119°C); hence, addition of a surfactant is not required. The oxidation reactions in the Activox process occur through the following reactions:

$$CuFeS_2 + O_2 + 2\ H_2SO_4 = CuSO_4 + FeSO_4 + 2\ H_2O + 2\ S^0 \qquad (2.2.6)$$

$$CuS + 0.5\ O_2 + H_2SO_4 = CuSO_4 + S^0 + H_2O \qquad (2.2.7)$$

$$Cu_2S + O_2 + 2\ H_2SO_4 = 2\ CuSO_4 + S^0 + 2\ H_2O \quad (2.2.8)$$

Elemental sulfur formed in this process remains in the leaching residue, which decreases the oxygen consumption but also leads to difficulty in the recovery of precious metals from leaching residues. Gold and silver are recovered from a non-sulfidic leach residue by cyanidation. As mentioned above, the presence of elemental sulfur leads to the formation of SCN^-, which would increase the cost of recovery.

If sufficient acid is not present during the leaching process, copper may precipitate as a basic copper sulfate in the leach residue. This copper is recovered by acid washing the leach residue. Most of the iron precipitates as goethite or jarosite. The Activox process for copper was demonstrated at the Tati Hydrometallurgical Demonstration Plant (THDP) in 2004 (Ramachandran *et al*., 2007).

2.2.2 The Albion Process (NENATECH)

The Albion process (Hourn and Halbe, 1999) is another sulfate-based process employing fine grinding (P_{80} = 10 to 15 µm) at 85 to 90°C and atmospheric pressure. Elemental sulfur formed in the process remains in the leaching residue leading to difficulty in recovering precious metals. The Albion leach process is a ferric leach, with the following overall reactions:

$$CuFeS_2 + 2\ Fe_2(SO_4)_3 = CuSO_4 + 5\ FeSO_4 + 2\ S^0 \quad (2.2.9)$$

$$Cu_2S + Fe_2(SO_4)_3 = CuSO_4 + 2\ FeSO_4 + CuS \quad (2.2.10)$$

$$CuS + Fe_2(SO_4)_3 = CuSO_4 + 2\ FeSO_4 + S^0 \quad (2.2.11)$$

Gold is recovered from leach residues by cyanidation. Relatively low process risk and lower operating cost are some of the advantages of the Albion process. This process has been successfully used by Xstrata at their Mt Isa plant to leach arsenic-containing smelter dusts and has full scale application in gold and zinc processing. The Albion process has been demonstrated at the continuous pilot plant scale for copper recovery but has not yet been applied commercially.

2.2.3 The Anglo American-University of British Columbia Process

Anglo American Corporation and the University of British Columbia have developed a process for chalcopyrite leaching under moderate oxygen pressure (10 to 12 atm) at 150°C. As the operating temperature is higher than the melting point of sulfur, surfactants are required to prevent coating of unreacted chalcopyrite by liquid sulfur (Dreisinger *et al*., 2003). In this process, surfactants such as calcium lignosulfonate and ortho-phenylenediamine (OPD) are used to disperse the molten sulfur. Viscosity of sulfur decreases from 115 to 159°C but increases dramatically at temperatures higher than 159°C. Hence, the operating temperature must be lower than 159°C. In the AAC/UBC process, chalcopyrite is oxidized according to the following reactions:

$$CuFeS_2 + {}^{5}/_{4}\ O_2 + {}^{5}/_{3}\ H_2SO_4 = CuSO_4 + {}^{1}/_{3}\ (H_3O)Fe_3(SO_4)_2(OH)_6 + {}^{1}/_{6}\ H_2O + 2\ S^0 \quad (2.2.12)$$

$$CuFeS_2 + {}^{5}/_{4}\ O_2 + H_2SO_4 = CuSO_4 + {}^{1}/_{2}\ Fe_2O_3 + H_2O + 2\ S^0 \quad (2.2.13)$$

$$CuFeS_2 + {}^{17}/_{4}\ O_2 + {}^{11}/_{6}\ H_2O = CuSO_4 + {}^{1}/_{3}(H_3O)Fe_3(SO_4)_2(OH)_6 + {}^{1}/_{3}\ H_2SO_4 \quad (2.2.14)$$

$$CuFeS_2 + {}^{17}/_{4}\ O_2 + H_2O = CuSO_4 + {}^{1}/_{2}\ Fe_2O_3 + H_2SO_4 \quad (2.2.15)$$

Copper is recovered by SX/EW to produce premium copper cathode, iron is precipitated as hematite and jarosite, and sulfide mainly exists as elemental sulfur, although sulfur oxidizes to sulfate to some extent (25 to 35%) (Dreisinger *et al*., 2003). Thus, oxygen consumption in this process is lower than high pressure/temperature processes but higher than low temperature/pressure processes. This process is a mid-range autoclave process. Gold and silver are recovered from the non-sulfidic leach residue by cyanidation. Gold extractions exceed 80% while silver recovery is low due to formation of argentojarosite. The AAC/UBC process has been evaluated in a continuous, fully integrated pilot plant.

2.2.4 The Dynatec Process

The Dynatec process was first developed for the treatment of zinc concentrates and refractory gold ores (Collins and Kofluk, 1998). The feed is ground to 30 to 40 μm. This process operates at 150°C. Recently, the Dynatec process was used to dissolve copper from chalcopyrite under 10 to 12 atm pressure (Peacey *et al*., 2003). Similar to the AAC/UBC process, the addition of surfactant is required to avoid coating of unleached mineral by molten sulfur. The Dynatec process uses coal as an additive to disperse molten sulfur. Sulfur largely exists as elemental sulfur in the leach residue. Iron is precipitated as hematite and jarosite (Peacey *et al*., 2003). The process chemistry is as follows.

Leaching:

$$CuFeS_2 + O_2 + 2\ H_2SO_4 = CuSO_4 + FeSO_4 + 2\ H_2O + 2\ S^0 \qquad (2.2.16)$$

$$CuFeS_2 + 2\ Fe_2(SO_4)_3 = CuSO_4 + 5\ FeSO_4 + 2\ S^0 \qquad (2.2.17)$$

$$CuS + {}^1/_2\ O_2 + H_2SO_4 = CuSO_4 + S^0 + H_2O \qquad (2.2.18)$$

$$Cu_2S + O_2 + 2\ H_2SO_4 = 2\ CuSO_4 + S^0 + 2\ H_2O \quad (2.2.19)$$

Iron Precipitation:

$$FeSO_4 + {}^1/_4\ O_2 + H_2O = {}^1/_2\ Fe_2O_3 + {}^1/_4\ H_2SO_4 \quad (2.2.20)$$

$$3\ FeSO_4 + {}^3/_4\ O_2 + {}^{11}/_2\ H_2O = (H_3O)Fe_3(SO_4)_2(OH)_6 + H_2SO_4 \quad (2.2.21)$$

Similar to the AAC/UBC process, this process is a mid-range autoclave process, hence PGMs are not dissolved. In addition to the operating conditions of the process that leads to the formation of sulfur and complicates PGMs recovery, the presence of coal decreases the PGMs recovery. Both sulfur and coal would tend to pick up PGM values. Gold and silver are recovered from the non-sulfidic leach residue by cyanidation. This process has been run in three mini-pilot plant campaigns. The Dynatec process is still under development and has not yet been commercialized.

2.2.5 The Galvanox™ Process

The Galvanox™ process is the atmospheric leaching of primary copper concentrates (Dixon and Tshilombo, 2005). It has been shown that in the presence of pyrite, the kinetics of leaching is accelerated significantly. It is strictly chemical and therefore requires no microbes. Fine grinding is not required in this process. Also, since the operating temperature is low, and the chemical conditions are mild, the near-quantitative yield of elemental sulfur is observed. This decreases both oxygen consumption and the necessity to neutralize large quantities of sulfuric acid. The operating temperature (80°C) is below the melting point of sulfur which eliminates the need for surfactants. The Galvanox™ chemistry is shown below.

Ferric leaching of chalcopyrite:

$$CuFeS_2 + 2\ Fe_2(SO_4)_3 = CuSO_4 + 5\ FeSO_4 + 2\ S^0 \quad (2.2.22)$$

Oxidation of ferrous with dissolved oxygen gas:

$$4\ FeSO_4 + O_2 + 2\ H_2SO_4 = 2\ Fe_2(SO_4)_3 + 2\ H_2O \quad (2.2.23)$$

Overall leaching reaction:

$$CuFeS_2 + O_2 + 2\ H_2SO_4 = CuSO_4 + FeSO_4 + 2\ S^0 + 2\ H_2O \quad (2.2.24)$$

Iron Oxyhydrolysis:

$$4\ FeSO_4 + O_2 + 4\ H_2O = 2\ Fe_2O_3 + H_2SO_4 \quad (2.2.25)$$

Copper electrowinning:

$$CuSO_4 + H_2O = Cu^0 + {}^1/_2\ O_2 + H_2SO_4 \quad (2.2.26)$$

Overall process chemistry:

$$CuFeS_2 + {}^5/_4\ O_2 = Cu^0 + 2\ S^0 + {}^1/_2\ O_2 + {}^1/_2\ Fe_2O_3 \quad (2.2.27)$$

Complete copper recovery in the Galvanox™ process can be achieved at a considerably higher rate than other ferric sulfate leaching processes (Dixon *et al*., 2008). Recycling pyrite and recovery of copper from tailings have been evaluated in a continuous mode in the Galvanox™ process on pilot plant scale (Dixon *et al*., 2007).

As mentioned above, this process runs under atmospheric pressure and low temperature which leads to oxidation of sulfide to elemental sulfur. Under these conditions most of PGMs remain in the solid residue. Recovery of PGMs is feasible through cyanide or thiosulfate leaching of copper residues.

2.2.6 The Total Pressure Oxidation Process

The Total Pressure Oxidation process operates under high temperature (220°C) and high pressure (30 to 40 atm) conditions to achieve high copper extractions (King and Dreisinger, 1995). This process was initially developed for the treatment of gold ores. The advantages of this process are rapid and complete chalcopyrite leaching, and a high degree of iron hydrolysis, mainly as hematite (Glen *et al*., 2003). However, the oxygen consumption is high due to the total conversion of sulfur to sulfate. In this process, oxidation of chalcopyrite and covellite occurs through the following reactions:

$$CuFeS_2 + {}^{17}/_4\ O_2 + {}^{1}/_2\ H_2SO_4 = CuSO_4 + {}^{1}/_2\ Fe_2(SO_4)_3 + {}^{1}/_2\ H_2O \qquad (2.2.28)$$

$$CuS + 2\ O_2 = CuSO_4 \qquad (2.2.29)$$

Iron Hydrolysis occurs as follows:

$$Fe_2(SO_4)_3 + 3\ H_2O = Fe_2O_3 + 3\ H_2SO_4 \qquad (2.2.30)$$

Lime consumption to neutralize acidic bleed solution is also high unless the acidic solution can be used for heap leaching, as used by Phelps Dodge (Marsden *et al*., 2003). This process has typically been employed industrially where the acid generated can be used elsewhere.

Under total oxidation conditions, the sulfide content of the ore is completely oxidized to sulfate. PGMs follow iron and report to the hematite residue as an

oxide or in elemental form. Then a secondary leach is required to recover PGMs. In this step, a chelating agent may be used to hold the metals in solution. This step will be followed by ion exchange to recover PGMs from solution.

The TPOX process has been successfully commercialized at both Freeport McMoran's Baghdad Operation in Arizona and First Quantum's Kansanshi Copper Operation in Zambia.

2.2.7 The BRISA Process

Carranza *et al*. (1997) have developed a process for copper recovery from chalcopyrite which is known as BRISA. This process is comprised of two steps; chalcopyrite leaching in ferric sulfate solution, and biooxidation of ferrous to ferric using mesophilic bacteria. The reactions in these two steps are shown below.

Chalcopyrite leaching in ferric sulfate solution:

$$CuFeS_2 + {}^{17}/_4\ O_2 + {}^{1}/_2\ H_2SO_4 = CuSO_4 + {}^{1}/_2\ Fe_2(SO_4)_3 + {}^{1}/_2\ H_2O \qquad (2.2.31)$$

Depending upon the pH, the ferric sulfate may undergo hydrolysis in the leaching medium according to the following reaction:

$$3\ Fe_2(SO_4)_3 + 14\ H_2O = 2\ (H_3O)Fe_3(SO_4)_2(OH)_6 + 5\ H_2SO_4 \qquad (2.2.32)$$

Biooxidation of ferrous to ferric using bacteria:

$$4\ FeSO_4 + 2\ H_2SO_4 + O_2 = 2\ Fe_2(SO_4)_3 + 2\ H_2O \qquad (2.2.33)$$

Leaching is performed at 70°C and pH 1.25 and 2 mg Ag/g concentrate. Copper recovery of > 95% is obtained in 10 hours. Palencia *et al*. (1998) have shown that all silver added as a catalyst remains in the leached residue as Ag_2S and Ag^0.

Silver may be recovered from the leach residue by leaching them with an acid-brine medium with 200 g/L of NaCl and 0.5 M sulfuric acid (Romero *et al*., 1998). The BRISA process has been evaluated at laboratory scale.

2.2.8 The BacTech/Mintek Process

BacTech and Mintek have developed a bioleaching process for the treatment of various copper concentrates. Bioleaching is the extraction of a metal from sulfide ores or concentrates using microorganisms. Bioleaching involves the use of microorganisms to catalyze the oxidation of iron sulfides to produce ferric sulfate and sulfuric acid. Ferric sulfate oxidizes the copper sulfide minerals (Ramachandran *et al*., 2007). The bacteria involved in the copper sulfide minerals leaching and the treatment of other sulfide minerals depend on the operating temperature.

In the BacTech/Mintek process, moderate and extreme thermophilic cultures at 40 to 50°C and 70°C, respectively, are used for chalcopyrite concentrate leaching. In this process, leaching and ferrous biooxidation are carried out in separate tanks.

Chalcopyrite oxidation:

$$CuFeS_2 + 2\ Fe_2(SO_4)_3 = CuSO_4 + 5\ FeSO_4 + 2\ S^0 \qquad (2.2.34)$$

Sulfur biooxidation:

$$2S^0 + 3O_2 + 2H_2O = 2H_2SO_4 \qquad (2.2.35)$$

Ferrous biooxidation:

$$4FeSO_4 + 2\ H_2SO_4 + O_2 = 2\ Fe_2(SO_4)_3 + 2\ H_2O \qquad (2.2.36)$$

Feed is ground to P_{80} = 10 μm. The sulfide is converted to elemental sulfur and sulfate. Sulfate is precipitated as gypsum, and soluble iron is precipitated as hydronium jarosite (Van Staden, 1998). A large pilot plant of the BacTech/Mintek process was successfully operated at the research facilities of Peñoles in Monterrey, Mexico.

2.2.9 The BioCOP™ Process

The BioCOP™ process has been developed by BHP Billiton to dissolve copper from chalcopyrite (Tunley, 1999). In this process, thermophiles leach chalcopyrite at 70 to 80°C. Pre-leaching ahead of oxidation leaching is helpful for copper recovery when treating secondary copper sulfides but it has minor effect on chalcopyrite leaching (Peacey *et al*., 2003). Oxygen consumption is high due to the complete oxidation of sulfur to sulfate (Ramachandran *et al*., 2007) similar to the high temperature total pressure oxidation process described earlier.

$$2\ S^0 + 3\ O_2 + 2\ H_2O = 2\ H_2SO_4 \qquad (2.2.37)$$

Comparing the BioCOP™ and the total pressure oxidation processes, it has been shown (Dreisinger, 2006) that the BioCOP™ process has higher operating cost. In 2000, Billiton and CODELCO formed a joint venture called Alliance Copper to commercialize the BioCOP™ technology. This process has been commercialized at Chuquicamata in Chile in a 20,000 tpa Copper demonstration plant.

2.2.10 The GeoCoat™ Process

The GeoCoat™ process involves the coating of concentrate onto sized support barren rocks or low grade ores, then heap bioleaching the coated material. The heap is inoculated with suitable cultures and irrigated with acidic solutions containing iron and nutrients. The operating temperature is 60 to 70°C. This process has overcome two major problems in heap leaching: obstruction of liquid

and air flow by fine particles of ore, and limited exposure of sulfide particles to air, leach solution, and microbes (Johansson *et al*., 1999). This process has been examined at laboratory and pilot plant level.

2.3 Chloride Processes

Ferric chloride and cupric chloride solutions have been the favored oxidants for chalcopyrite concentrates, because of their high leaching efficiency and the fact that sulfur is liberated in the elemental form (McLean, 1982). The principal chemical reactions in the ferric chloride and cupric chloride leaching are shown below:

$$CuFeS_2 + 3\ CuCl_2 = 4\ CuCl + FeCl_2 + 2\ S^0 \quad (2.3.1)$$

$$CuFeS_2 + 4\ FeCl_3 = CuCl_2 + 5\ FeCl_2 + 2\ S^0 \quad (2.3.2)$$

$$CuFeS_2 + 3\ FeCl_3 = CuCl + 4\ FeCl_2 + 2\ S^0 \quad (2.3.3)$$

$$S^0 + 4\ H_2O + 6\ CuCl_2 = 6\ CuCl + 6\ HCl + H_2SO_4 \quad (2.3.4)$$

Oxidative leaching in the presence of high chloride levels dissolves some silver and gold. Silver can be recovered by cementation with copper. Copper is recovered by SX/EW. Gold can be recovered through cyanidation leaching. However, due to the presence of elemental sulfur the direct recovery of gold from the leach residue is difficult and expensive.

Chloride processes have several advantages over sulfate processes. Faster kinetics, low operating temperature, oxidation of sulfide to sulfur (low oxygen consumption), high solubility of metals (lower solution volume and smaller tanks) are some of these advantages. However, these processes have some drawbacks which limit their application such as high corrosive nature of the

chloride solution, difficulty in producing a high purity copper cathode (Agrawal and Sahu, 2010).

Initially, chloride-based processes found little application because of the highly corrosive nature of the solutions, but these problems have been largely overcome with the advent of modern materials of construction such as fiber-reinforced plastic, polypropylene, butyl rubber and titanium (Wang, 2005).

Previous studies have shown that very few of the chloride leaching processes permit the direct production of high purity copper, even when applied mainly to clean chalcopyrite concentrates (Szymanowski, 1993). In most cases further expensive fire refining and electrowinning are necessary to produce wire bar or cathode grade material. For example, the CLEAR process only produced blister-grade copper containing all the silver present in the original leach solution, necessitating further electrorefining (Fletcher, 1986).

It should be also noted that very high efficiency of chloride leaching brings its own problems, many other base metals and minor metals which are present as sulfide such as Zn, Pb, Ag, As, Sb, Bi, Cd, and Hg are leached very effectively in chloride media (Dalton *et al*., 1991). Reactions (2.3.5) and (2.3.6) show the leaching reactions of silver and zinc sulfide in ferric chloride solution:

$$Ag_2S + 2\ FeCl_3 = 2\ AgCl + 2\ FeCl_2 + S^0 \qquad (2.3.5)$$

$$ZnS + 2\ FeCl_3 = ZnCl_2 + 2\ FeCl_2 + S^0 \qquad (2.3.6)$$

Hence, without a purification stage, the presence of these metals has a very serious effect on the quality of the copper produced (Andersen *et al*., 1980). Some of the important chloride leaching processes are discussed below.

2.3.1 The CLEAR Process

The CLEAR process was developed primarily for the treatment of chalcopyrite concentrates. The principal oxidant is cupric chloride. This process produces cuprous chloride solution from which copper is electrowon. Copper is deposited as a powder in electrowinning. The CLEAR process did not focus on PGM recovery. This process progressed beyond the laboratory development stage in 1976. The CLEAR process reached commercial operation for a period of six years but it was not economically successful and closed in 1982 (Schweiter and Livingstone, 1982). In addition to economic reasons, the plant was unsuccessful because the copper product could not meet LME specifications.

2.3.2 The Cuprex Process

In the Cuprex process, copper sulfide concentrates are leached with ferric chloride solutions. Copper is extracted by solvent extraction and recovered by electrowinning as copper powder. Chlorine generated at the anode was recovered to oxidize the cuprous chloride formed during electrowinning (Dalton *et al*., 1991). The Cuprex process did not focus on PGM recovery. This process had been developed at pilot plant scale.

2.3.3 The CYMET Process

In the CYMET process, the copper sulfide concentrates are leached in a ferric chloride/cupric chloride/ sodium chloride brine solution. Iron precipitates as jarosite. Copper is recovered by hydrogen reduction. The product is melted to copper wirebars (Peacey *et al*., 2003). The CYMET process has been evaluated at pilot plant scale.

2.3.4 The HydroCopper Process (Outokumpu)

In this process, developed by Outotec, chalcopyrite concentrates are leached at atmospheric pressure with a cupric chloride/brine solution. The leach temperature is 85 to 95°C and air or oxygen is used as the oxidant. Sulfide is removed as elemental sulfur and gold dissolves as a chloro-complexes. Hence, gold is leached and recovered by absorption onto resin (Baxter *et al*., 2010). Copper is extracted by precipitating the cuprous oxide using caustic soda. All impurity metals are removed before Cu_2O precipitation, because otherwise they would report to the copper product.

$$CuFeS_2 + CuCl_2 + {}^3/_4\ O_2 = 2\ CuCl + {}^1/_2\ Fe_2O_3 + 2\ S^0 \qquad (2.3.7)$$

$$CuCl + {}^1/_2\ Cl_2 = CuCl_2 \qquad (2.3.8)$$

$$CuCl + NaOH = {}^1/_2\ Cu_2O + NaCl + {}^1/_2\ H_2O \qquad (2.3.9)$$

In this process, a multistage scheme has been developed consisting of chemical precipitation of impurity metals by pH increases and cementation of silver (Hamalainen *et al*., 2003). Cuprous oxide is reduced by hydrogen to copper:

$$ {}^1/_2\ Cu_2O + {}^1/_2\ H_2 = Cu + {}^1/_2\ H_2O \qquad (2.3.10)$$

Then copper is melted and cast into a copper product (Leimala *et al*., 2003). This process has been engineered and recently demonstrated on the Zangezur concentrate in Outotec's demonstration plant in Pori, Finland.

2.3.5 The Intec Process

The Intec process is a chloride based leaching system which uses $BrCl_2^-$ to oxidize copper sulfides. This process operates at high potential of 1000 mV (*vs*

SHE). In this process, PGMs can be dissolved in high extent, due to the presence of the chelating agent. The bromo-chloride is a strong oxidant and allows the extraction of gold and PGMs even in the presence of elemental sulfur. Recovery of precious metals without the need for retreatment of the environmentally stable solid residue is one of the advantages of the Intec process (Moyes *el al*.). In this process, sulfur is recovered in the solid residues in the elemental form.

$$CuFeS_2 + {}^3/_4\ O_2 = Cu + {}^1/_2\ Fe_2O_3 + 2\ S^0 \qquad (2.3.11)$$

This process consists of three stages: leaching, purification, and electrowinning. The primary copper product is in the form of dendrites that is washed and dried under an inert atmosphere, melted and cast into shapes (Moyes and Houllis, 2002). The Intec process for copper has been run at the demonstration plant scale (Milbourne *et al*., 2003).

2.3.6 The Sumitomo Process

In this process, copper sulfide is leached by chlorine gas under atmospheric pressure. In this process, copper in chalcopyrite can be leached by controlling oxidation reduction potential and chloride ion concentration. Leaching in this process occurs through following reactions:

$$CuFeS_2 + 3\ Cu^{2+} = 4\ Cu^{+} + Fe^{2+} + 2S^0 \qquad (2.3.12)$$

$$2\ Cu^{+} + Cl_2 = 2\ Cu^{2+} + 2\ Cl^{-} \qquad (2.3.13)$$

Cuprous in leached liquor is separated from ferrous by solvent extraction. Pure copper powder is produced by electrowinning (Asano *et al*., 2007). In this process, iron is recovered as metal by electrowinning instead of goethite or hematite waste via these reactions:

Cathode: $Fe^{2+} + 2\ e^{-} = Fe$ (2.3.14)

Anode: $Fe^{2+} = Fe^{3+} + e^{-}$ (2.3.15)

The Sumitomo process has been applied at the laboratory and pilot plant scale. This process is under optimization through the pilot plant tests.

In summary, despite the effectiveness of chloride leaching, progression toward commercialization has been slow and only one process, CLEAR, has been operated commercially. The CLEAR process operated for six years until it was closed due to various technical and economic reasons (Liddicoat and Dreisinger, 2007). The product still required further refining to achieve wirebar or cathode grade material.

Product impurity, undesirable copper cathode morphology, and handling corrosive process liquors are some of the major drawbacks in chloride leaching processes (Hoffman, 1991).

2.4 Sulfate-Chloride Processes

Chloride addition to sulfate leaching improves the leaching kinetics and allows lower temperature leaching. In these processes, sulfide is oxidized to elemental sulfur and copper is recovered by SX/EW. The main sulfate-chloride leaching processes are discussed below.

2.4.1 The CESL Process

The CESL process uses mixed sulfate-chloride solution and operates at about 150°C and 10 to 12 atm total pressure (Dreisinger, 2006) with a chloride concentration of 10 to 15 g/L. The feed is ground to 40μm. In this process,

chalcopyrite dissolves to form a basic copper sulfate salt, hematite and elemental sulfur:

$$3\ CuFeS_2 + {}^{15}/_4\ O_2 + H_2O + H_2SO_4 = CuSO_4{\cdot}2Cu(OH)_2 + {}^{3}/_2\ Fe_2O_3 + 6\ S^0 \quad (2.4.1)$$

Then, the basic copper sulfate is dissolved under more acidic conditions:

$$CuSO_4.\ 2\ Cu(OH)_2 + 2\ H_2SO_4 = 3\ CuSO_4 + 4\ H_2O \quad (2.4.2)$$

It is important to note that chloride catalyzes the oxidation of chalcopyrite.

A small amount of surfactant is added to the autoclave slurry to act as a sulfur dispersant. The surfactant keeps the molten sulfur as small droplets in the autoclave and avoids coating of copper concentrate particles by liquid sulfur. After solid/liquid separation, basic copper precipitates are dissolved in an atmospheric leach step using the acidic raffinate recycled from solvent extraction/ electrowinning (Jones and Hestrin, 1998). The solvent extraction step excludes chloride as an impurity to produce a suitable electrolyte for electrowinning.

In terms of PGMs recovery in the CESL process, previously, the following steps had been taken. The first step was removal of elemental sulfur using a hot perchloroethylene leach. The second step was total oxidation of the remaining sulfides to release refractory gold. The third step was neutralization, followed by cyanide leaching of the solids for gold recovery (Jones, 2002). However, the high cost of solvent, difficult solvent recovery, and high capital and operating costs were some of the disadvantages of this process (Barr *et al*., 2007). Recently, a new gold process has been developed (Jones, 2011). As discussed earlier, gold and silver recovery by cyanidation is unsatisfactory due to high consumption of cyanide as a result of thiocyanate and copper cyanide formation. However, it has been shown that cyanide consumption can be reduced by a combination of process steps which include pressure cyanidation of residue with high pressure

oxygen to leach gold and silver into solution for short retention times to minimize thiocyanate, partial suppression of copper cyanide formation, and finally by recovering cyanide as efficiently as possible from the (reduced) copper cyanide complexes.

The CESL technology has been applied on a 10,000 t/a copper demonstration plant and is currently being operated by Vale at the Sossego Mine in Brazil (Defreyne and Cabral, 2009).

2.4.2 The Noranda Antlerite Process

This process was developed by Noranda in late 1970's for the treatment of chalcopyrite (Stanley and Subramanian, 1977). The oxidant is a mixture of HCl-$CuCl_2$-$CuSO_4$. This process consists of two steps: 1) conversion of chalcopyrite and other copper sulfide minerals to antlerite (basic copper sulfate), $CuSO_4 \cdot 2Cu(OH)_2$, hematite and elemental sulfur in cupric sulfate and cupric chloride solution at 135 to 145°C and 200 psi oxygen, and 2) leaching of the antlerite residue with sulfuric acid at pH 2.5 to produce a pregnant electrolyte for copper electrowinning. This process was tested at laboratory scale.

2.4.3 The PLATSOL™ Process

The PLATSOL™ process was primarily developed to treat a copper/nickel/PGM concentrate. This process consists of total pressure oxidation in the presence of chloride ions (5 to 10 g/L NaCl) to dissolve copper, nickel and PGMs. The feed is ground to 15 to 20 µm. Similar to the Total Pressure Oxidation process, temperature and pressure are at 220°C and 30 to 40 atm, respectively (Ferron *et al.*, 2002). Chalcopyrite and PGMs oxidize according to the following reactions:

$$CuFeS_2 + {}^{17}/_4\ O_2 + H_2SO_4 = CuSO_4 + {}^{1}/_2\ Fe_2(SO_4)_3 + H_2SO_4 \qquad (2.4.3)$$

$$Au + {}^{3}/_{4}\ O_2 + 4\ HCl = HAuCl_4 + {}^{3}/_{2}\ H_2O \quad (2.4.4)$$

$$Pt + O_2 + 6\ HCl = H_2PtCl_6 + 2\ H_2O \quad (2.4.5)$$

$$Pd + {}^{1}/_{2}\ O_2 + 4\ HCl = H_2PdCl_4 + H_2O \quad (2.4.6)$$

In this process, PGMs are readily dissolved due to the presence of suitable complexing agents. PGM recovery from solution is achieved by cementation using CuS or NaHS (Ferron *et al*., 2001). The precipitation of PGMs occurs by the following reactions:

$$HAuCl_4 + {}^{3}/_{2}\ CuS + {}^{3}/_{2}\ H_2SO_4 = Au + {}^{3}/_{2}\ CuSO_4 + 4\ HCl + {}^{3}/_{2}\ S^0 \quad (2.4.7)$$

$$H_2PtCl_6 + 2\ CuS + 2\ H_2SO_4 = Pt + 2\ CuSO_4 + 6\ HCl + 2\ S^0 \quad (2.4.8)$$

$$H_2PdCl_4 + CuS + H_2SO_4 = Pd + CuSO_4 + 4\ HCl + S^0 \quad (2.4.9)$$

PolyMet Mining has planned to use the PLATSOL™ process for their NorthMet project in Minnesota, USA.

2.5 Ammonia Processes

Summaries of two ammonia leaching processes are given below.

2.5.1 The Arbiter Process

The Arbiter process was developed to treat chalcopyrite, chalcocite, and covellite in ammonia media by Anaconda (Arbiter and Fletcher, 1994). In this process, copper concentrate was leached with ammonia and oxygen, at low partial pressure and around 75 to 80°C. Then, an intermediate insoluble copper (I) ammonium sulfite ($Cu_2SO_3 \cdot (NH_4)_2SO_3 \cdot 2H_2O$) was generated by adding SO_2 to

copper (II) ammine leach solution (Muir, 2008). Copper powder and ammonium sulfate were generated after autoclaving the precipitate at 150°C. The plant was shut down after running a one hundred tonne per day demonstration plant for four years. The major problem in this process that led to the plant shutdown was sulfate disposal. There was a poor regional demand for ammonium sulfate and the cost of neutralization was high (Arbiter and McNulty, 1999).

2.5.2 The Escondida Process

This process was developed to treat Escondida copper concentrates in ammonia media. In this process, air and ammonium were used to oxidize copper sulfides. The plant was designed to leach only 40% of the copper from copper sulfide to avoid ammonium sulfate production. The aim of this process was to recover the copper that was readily soluble in a mildly oxidizing environment (Duyvesteyn *et al*., 1993). By controlling the oxidation potential, the formation of sulfate ions and, consequently, of ammonium sulfate is reduced. Furthermore, the mild leaching conditions also prevent the dissolution of unwanted impurities which leads to the production of ultra high purity electrowon copper (Duyvesteyn *et al*., 1993). This process was successfully applied for several years to elevate the plant capacity at Escondida. The plant was closed after smelter expansion (Chmielewski *et al*., 2009).

2.6 Nitrogen Species Catalyzed Leaching Process

The application of nitrogen species catalyzed pressure oxidation of chalcopyrite concentrate has been studied (Anderson, 1999). The commonly reported leach reaction of a sulfide mineral with nitric acid in conjunction with sulfuric acid is shown below:

$$3\ MeS + 2\ HNO_3 + 3\ H_2SO_4 = 3\ MeSO_4 + 3\ S^0 + 2\ NO + 4\ H_2O \qquad (2.6.1)$$

Anderson *et al*. (1996) showed that the actual reaction species is NO^+ not NO_3^-. Based on their study, addition or presence of NO_2^- instead of NO_3^- accelerates the formation of NO^+. A convenient source of nitrous acid is sodium nitrite. By adding this species in acidic media, reactions (2.6.2) and (2.6.3) occur.

$$NaNO_2 + H^+ = HNO_2 + Na^+ \quad (2.6.2)$$

$$HNO_2 + H^+ = NO^+ + H_2O \quad (2.6.3)$$

Then NO^+ oxidizes the sulfide mineral:

$$2\ MeS + 4\ NO^+ = 2\ Me^{2+} + 2\ S^0 + 4\ NO \quad (2.6.4)$$

Nitrogen oxide transfers out of solution. In the pressure leach system, nitrogen oxide accumulates in the headspace of the reactor and reacts with oxygen to form nitrogen dioxide gas (reaction 2.6.5). The NO is then regenerated to NO^+ as shown in reaction (2.6.7).

$$2\ NO(g) + O_2(g) = 2\ NO_2(g) \quad (2.6.5)$$

$$2\ NO_2(g) = 2\ NO_2(aq) \quad (2.6.6)$$

$$2\ NO_2(aq) + 2\ NO(g) + 4\ H^+ = 4NO^+(aq) + 2\ H_2O \quad (2.6.7)$$

Since nitrogen species is continuously regenerated, its role in the overall reaction is not obvious. The net reaction is the oxidation of the sulfide mineral in acidic solution with oxygen.

$$2\ MeS + 4\ H^+ + O_2 = 2\ Me^{2+} + 2S^0 + 2\ H_2O \quad (2.6.8)$$

The Nitrogen Species Catalyzed (NSC) sulfuric acid pressure leach has been tested on a chalcopyrite concentrate at the laboratory and pilot plant scale and is suitable for leaching of copper concentrates containing precious metals. In the NSC process, silver is recovered from leach solution by precipitating as AgCl followed by reduction to silver metal. Gold reacts with the sulfur residues in alkaline leach solution. Gold leached by the alkaline sulfide system is recovered by SX/EW (Anderson, 2003). This process may provide a non-cyanide approach for gold recovery.

2.7 Conclusions

Hydrometallurgical processes to extract copper from chalcopyrite can be categorized according to the type of lixiviant used. These processes can be grouped as sulfate, chloride, sulfate-chloride, ammonia, and nitrogen processes. The most important and common ones are sulfate and chloride processes. In this Chapter, it has been described that sulfate processes are the most established technology due to the simplicity of their leaching reactions, low capital and operating cost and the conventional solvent extraction and electrowinning. In this media, the kinetics of chalcopyrite leaching is slow compared to chloride and nitrogen catalyzed processes. Chloride processes have several advantages over sulfate processes. The kinetics of chalcopyrite leaching are significantly faster in chloride media. Low operating temperature, high solubility of metals, and low sulfuric acid generation are some of other advantages of chloride processes. In spite of these, the application of chloride processes is limited due to the highly corrosive nature of chloride solutions and difficulty in producing a high purity copper cathode. Ferric/cupric chloride is a strong oxidant which oxidizes many other base metals and minor metals. The presence of these elements negatively affects the quality of the copper produced. Hence, product impurity, undesirable copper cathode morphology, and handling corrosive process liquors are some of the major drawbacks in chloride leaching process.

Chapter 3 Ferric Sulfate Leaching of Chalcopyrite

3.1 Introduction

Among the processes described in Chapter 2, atmospheric leaching in sulfate media is one of the most attractive hydrometallurgical processes to extract copper from chalcopyrite. There are several advantages to this process, including the simplicity of the leaching reactions, low capital requirements, low operating cost, and operational simplicity (Hiroyoshi *et al*., 2001). Despite these advantages, slow leaching kinetics and low levels of extraction have plagued the process. These have been attributed to the formation of a passive layer that prevents the transport of reactants and products to and from chalcopyrite. Extremely slow rates of chalcopyrite leaching have been shown in many studies. For example, Muñoz *et al*. (1979) leached fine chalcopyrite at 90°C and obtained only 58% copper extraction in 100 hours. In another study by Dutrizac (1982), about 50% copper extraction was obtained from chalcopyrite oxidation in 50 hours. 80% copper extraction from very fine chalcopyrite (< 5 μm) at 90°C and 10 hours was reported by Le Houillier and Ghali (1982).

Two major considerations were taken into account to overcome the slow and incomplete leaching of chalcopyrite in sulfate media: the extent and the rate of the reactions. The former depends on the thermodynamic tendency of the chemical system which determines the overall reaction driving force. The latter, the reaction kinetics, depends on a combination of physical, chemical, and mass transfer factors. The kinetics and thermodynamics of chalcopyrite leaching in ferric sulfate media are explained in this Chapter.

3.2 Thermodynamics of Chalcopyrite Dissolution

To predict the thermodynamic behaviour of chalcopyrite dissolution, the Pourbaix diagram for the Cu-Fe-S-H_2O system (Figure 3.1) was considered. According to

this figure, the dissolution of chalcopyrite in acidic solution takes place through solid transformations via different intermediate sulfides (Cordoba *et al*., 2008(I)).

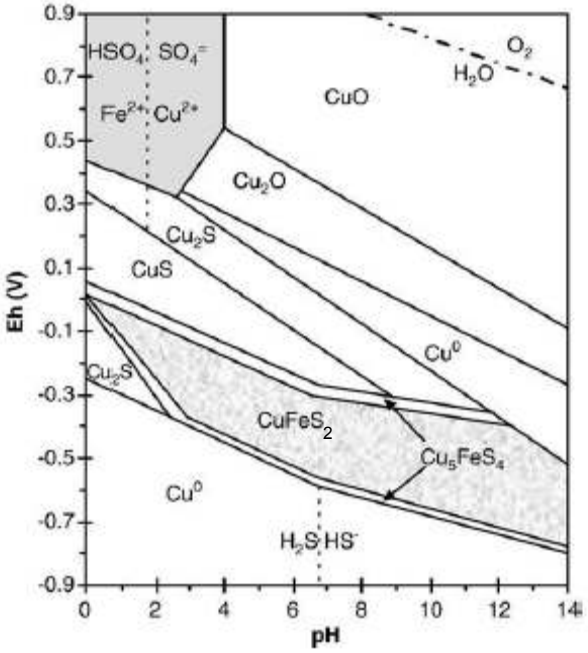

Figure 3.1 Pourbaix diagram for the Cu-Fe-S-H_2O system at 25°C at standard conditions (Cordoba *et al*., 2008(I) after Garrels and Christ, 1965)

The diagram has been simplified and includes only the sulfide minerals commonly found with chalcopyrite such as bornite (Cu_5FeS_4), covellite (CuS), chalcocite (Cu_2S), and copper oxides (Cu_2O and CuO). This diagram indicates that a pH lower than 4 and an oxidizing redox potential higher than 0.4 V is required to dissolve copper from chalcopyrite (Cordoba *et al*., 2008(I)). These conditions are achieved using oxidizing agents such as ferric sulfate. Ferric sulfate leaching of chalcopyrite can be represented by the following reactions (Dutrizac and McDonald, 1974):

$$CuFeS_2 + 2\ Fe_2(SO_4)_3 = CuSO_4 + 5\ FeSO_4 + 2\ S^0 \qquad (3.2.1)$$

$$CuFeS_2 + 8\ Fe_2(SO_4)_3 + 8\ H_2O = CuSO_4 + 17\ FeSO_4 + 8\ H_2SO_4 \qquad (3.2.2)$$

However, it should be noted that the kinetics of reaction are not considered in the Pourbaix diagram. In order to evaluate the feasibility of these reactions, one might consider the kinetics of these reactions in practical leaching times (in hours or days). For instance, according to this diagram, covellite oxidizes to chalcocite and sulfate ions through the following reaction:

$$2\ CuS + 4\ H_2O = Cu_2S + SO_4^{2-} + 8\ H^+ + 6\ e^- \qquad (3.2.3)$$

However, this reaction occurs only over geological time (Peters, 1992).

In addition, the sulfur Pourbaix diagram shows that the elemental sulfur is thermodynamically stable over a narrow potential range at pH values lower than about 9. However, it has been shown that sulfur is far more stable with respect to oxidation in hydrometallurgical time frames of hours to days. Figure 3.2 shows the extended sulfur stability region.

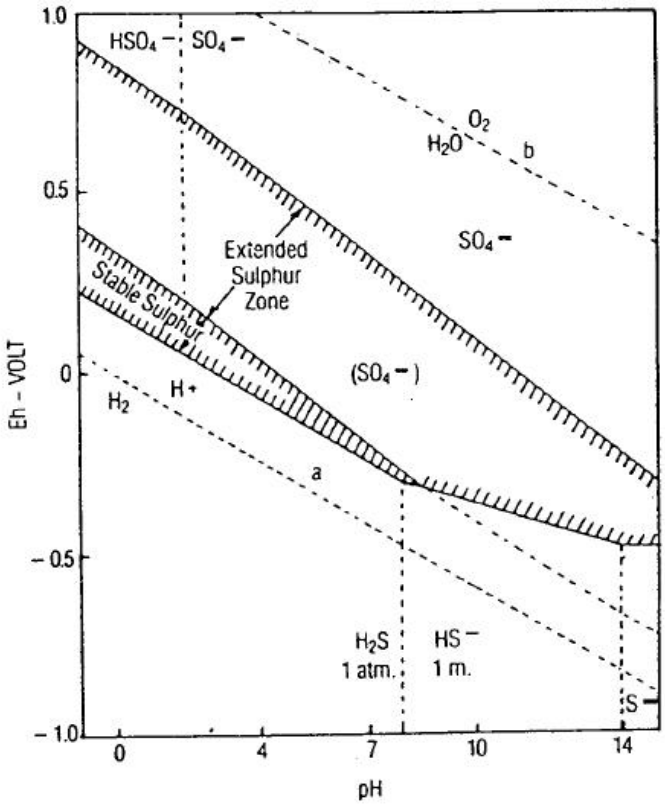

Figure 3.2 The Potential-pH diagram for the S-H_2O system, showing the region of sulfur stability and the extended stability by a 300 kJ/mole barrier to the formation of sulfate (Peters, 1986)

This diagram more accurately reflects the sulfur behaviour in hydrometallurgical processes. For instance, it is well known that sulfur is not oxidized by ferric ions at a significant rate. Previously, the oxidation of sulfur in the temperature range of 60 to 170°C and oxygen partial pressure of 0.10 to 0.69 MPa has been studied.

$$S + \tfrac{1}{2} O_2 + H_2O = H_2SO_4 \qquad (3.2.4)$$

It has been observed that this reaction depends greatly on temperature and oxygen pressure (Habashi and Bauer, 1966). According to this study, the rate of sulfur oxidation increases above the sulfur melting point and with increasing the temperature. However, it should be noted that increasing the temperature

moderately in the range of 120 to 160°C is not useful, since molten sulfur wets and agglomerates the sulfide particles (Vizsolyi *et al*., 1967), unless surfactants are used to avoid agglomeration. However, rapid and complete copper recovery can be obtained at higher temperatures. According to previous studies, 98% copper extraction was achieved in ferric sulfate media at 200°C and 0.79 MPa oxygen in only 30 minutes (Stanczyk, 1963). King *et al*. (1993) leached four different copper concentrates and obtained 98% copper extraction within 3 hours at 200°C and 0.69 MPa oxygen pressure. The rapid copper extraction at very high temperature is attributed to complete oxidation of elemental sulfur to sulfate.

In another study by Corriou and Kikindai (1981), the oxidation of elemental sulfur to sulfate in the temperature range of 125 to 230°C and oxygen partial pressure range of 0.1 to 5 MPa was investigated. It has been found that below the sulfur melting point, sulfur oxidation is negligible. Activation energies have been compared in the temperature range of 125 to 160°C and 175 to 230°C. It has been found that the activation energy is considerably lower in the higher temperature range of 175 to 230°C (Corriou and Kikindai, 1981). This observation has been attributed to the change of allotropic composition of molten sulfur above 160°C. Below 160°C sulfur primarily exists as a ring of eight sulfur atoms, known as cyclooctasulfur, S_8. Above 160°C, S_8 rings start to break apart to form linear sulfenyl diradicals. These radicals react with other S_8 rings in a chain reaction which leads to formation of long-chain polymers (Hackl, 1995).

Many researchers have investigated the dissolution of chalcopyrite concentrates in ferric sulfate. Based on their studies, at 95°C around 75% of chalcopyrite dissolves according to reaction (3.2.1) and the remaining 25% by reaction (3.2.2) (Sullivan, 1933). The lower rate of sulfate production is attributed to the limited solubility of dissolved oxygen at 95°C, and not to the action of ferric ions (Cordoba *et al*., 2008(I)). Some other researchers concluded that the stoichiometry of chalcopyrite dissolution at atmospheric pressure should be described by reaction (3.2.1) (Dutrizac *et al*., 1969). Later, another study by

Dutrizac (1989) confirmed the high elemental sulfur yield (94%) at temperatures of about 95°C.

3.3 Kinetics of Chalcopyrite Dissolution

As discussed earlier, chalcopyrite dissolution in acidic ferric media at atmospheric pressure can be represented by reaction (3.2.1). This reaction can also be expressed by anodic and cathodic half-cell reactions as follows (Tshilombo, 2004):

Anodic: $CuFeS_2 = Cu^{2+} + Fe^{2+} + 2\ S^0 + 4\ e^-$ $E^O = 0.47$ V (SHE) (3.2.5)

Cathodic: $4\ Fe^{3+} + 4\ e^- = 4\ Fe^{2+}$ $E^O = 0.77$ V (SHE) (3.2.6)

Reactions (3.2.5) and (3.2.6) occur simultaneously on the surface of the chalcopyrite at a rate such that the difference between electron production and consumption is zero. Consequently, the dissolution potential and rate can be obtained by combining the cathodic branch and the anodic branch of these two half-cell reactions in an Evans diagram. The point at which the cathodic and anodic rates are equal is called the “dissolution rate” and the corresponding potential is the “mixed potential.” Therefore, in order to understand the overall rate of reaction, it is important to study the electrochemical behaviour of these reactions. In previous studies, the importance of the redox potential on kinetics of chalcopyrite leaching has been noted (Hiroyoshi *et al*., 2002, 2004, 2007, 2008). According to previous studies (Hiroyoshi *et al*., 2000, 2001, 2007; Kametani and Aoki, 1985; Okamoto *et al*., 2003, 2004, 2005; Petersen and Dixon, 2006), in the case of chalcopyrite leaching, the leaching rate increases with increasing redox potential and reaches a maximum at an optimum redox potential and then decreases at higher potential (the “passive potential”). At very high potentials the rate increases again (the “transpassive potential”). Hence, controlling the solution potential is necessary to obtain rapid kinetics (Ahonen and Tuovinen, 1993;

Bruynesteyn *et al*., 1986; Dixon and Tshilombo, 2005; Gericke and Pinches, 1999; Lawrence *et al*., 1985; Third *et al*., 2000, 2002; Van der Merwe *et al*., 1998; Pinches, 1997). In addition, there is a report from a leaching operation at the Kosaka mine in Japan that shows the copper recovery from chalcopyrite has been maximized by controlling the concentration ratio of ferric to total soluble iron at 0.2. This ratio corresponds to the redox potential of 0.63 V *vs* SHE (Hiroyoshi *et al*., 2008).

According to the previous studies, chalcopyrite leaches extremely slowly in ferric sulfate media. Muñoz *et al*. (1979) reported 58% copper extraction of very fine chalcopyrite (12 μm) after 100 hours. Some of the previous studies have indicated that the extremely low rate of leaching in ferric sulfate media is due to slow diffusion of reactants or products through a passivating layer. These researchers reported a parabolic rate law (Dutrizac, 1989; Dutrizac *et al*., 1969; Parker *et al*., 1981). Most of the researchers found a strong dependence of reaction rate on particle size. They found that the leaching rate was inversely related to the square of the initial particle size (Muñoz *et al*., 1979). This idea supports a diffusion-controlled mechanism of chalcopyrite dissolution. In contrast, some researchers found that the leaching curve is linear over an extended leaching period (Jones and Peters, 1976). In another study (Hirato *et al*., 1987), initially parabolic kinetics was reported followed by linear kinetics. In this study, observation of parabolic kinetics was attributed to the formation of elemental sulfur. Then, it was suggested that this layer was peeled off, and no sulfur layer was observed where linear kinetics were noted which suggests a reaction-controlled mechanism. On the other hand, Parker *et al*. (1981) studied the electrochemical behaviour of chalcopyrite leaching and showed that the oxidative dissolution of chalcopyrite was controlled by the formation of an un-stable, metal-deficient polysulfide film on the surface of chalcopyrite. In this study, diffusion of reactants through the sulfur layer was not considered as a rate-limiting step.

In spite of the broad research, the structure of the passivating layer that slows down the transport of reactants to the chalcopyrite core is not yet known. However, there are three different hypotheses to explain the nature of this layer; formation of a sulfur layer, formation of copper polysulfide, and precipitation of iron compounds.

- Formation of a Sulfur Layer

Some researchers claim that the formation of elemental sulfur on chalcopyrite surface limits the oxidative dissolution of chalcopyrite (Dutrizac, 1989). Muñoz *et al*. (1979) also suggested that transport of electrons through the elemental sulfur, which is the reaction product, is rate limiting. It has been reported that, if leaching is interrupted and the sulfur is removed, the initial reaction rate is restored (Wan *et al*., 1984). In another study, chalcopyrite was leached in the presence of carbon tetrachloride, which is a sulfur solvent. In this study, it was observed that the rate of chalcopyrite oxidation was significantly higher (Havlik and Kammel, 1995). Similarly, when chalcopyrite is oxidized by ozone in 0.5 M H_2SO_4 and the product of sulfide oxidation is sulfate, 90% of copper is recovered in 48 hours at 22°C (Klauber *et al*., 2001). Conversely, some researchers concluded that chalcopyrite leaches slowly even if S^0 is removed during the leach with an organic solvent (Buttinelli *et al*., 1992).

- Formation of Copper Polysulfide

Another hypothesis suggests the formation of the copper polysulfide as a result of solid-state changes which inhibits further copper dissolution. Hackl (1995) proposed the following sequence of reactions to describe the oxidative leaching and passivation of chalcopyrite in sulfate media:

Fastest (y >> x):

$$CuFeS_2 = Cu_{1-x}Fe_{1-y}S_2 + x\ Cu^{2+} + y\ Fe^{2+} + 2(x+y)\ e^- \qquad (3.2.7)$$

Slower:

$$Cu_{1-x}Fe_{1-y}S_2 = Cu_{1-x-z}S_2 + z\ Cu^{2+} + (1-y)\ Fe^{2+} + 2(1+z-y)\ e^- \quad (3.2.8)$$

Slowest:

$$Cu_{1-x-z}S_2 = (1-x-z)\ Cu^{2+} + 2\ S^0 + 2\ (1-x-z)\ e^- \quad (3.2.9)$$

In the initial reaction (3.2.7), iron leaches preferentially to copper to form an intermediate iron-deficient sulfide phase. In a second step, reaction (3.2.8), the remaining iron and additional copper leaches out of the iron-deficient copper-iron polysulfide to form a copper polysulfide. In a study by Holliday and Richmond (1990), it has been shown that the ratio of ferrous to cupric dissolved initially is 5 to 1. According to this study, the following reaction has been proposed to describe the formation of passive copper polysulfide from chalcopyrite:

$$CuFeS_2 = {}^1/_5\ Cu^{2+} + Fe^{2+} + Cu_{0.8}S_2 + {}^{12}/_5\ e^- \quad (3.2.10)$$

Hackl believes that the slowest step is the decomposition of the copper polysulfide to cupric ions (reaction 3.2.9) and elemental sulfur, with polysulfide chains restructuring to form S_8 rings (Hackl, 1995). The same sequence of reactions to describe the composition of the passivating layer has been reported by several authors (Baur *et al*., 1974; Jones, 1974; Linge, 1976). Parker *et al*. (1981) suggested a metal-deficient, copper-rich polysulfide as a barrier for copper dissolution.

- Precipitation of Iron Compounds

Still another passivation theory suggests that the impermeable layer is comprised of precipitated iron compounds. The corresponding reactions are as follows:

$$2\ Fe(OH)_2 + H_2O + {}^1/_2\ O_2 = 2\ Fe(OH)_3 \quad (3.2.11)$$

$$3\ Fe_2(SO_4)_3 + Na_2SO_4 + H_2O = 2\ NaFe_3(SO_4)_2(OH)_6 + 6\ H_2SO_4 \quad (3.2.12)$$

According to this hypothesis, precipitation of iron-hydroxy compounds leads to the slow kinetics and low copper recovery (Cordoba *et al*., 2008(I); Gomez *et al*., 1996; Parker *et al*., 2003; Sandstrom *et al*., 2005; Stott *et al*., 2001). This hypothesis has received less support (Pinches *et al*., 1976). Under some leaching conditions iron compounds are associated with the sulfur layer. However, it is doubtful that this layer could be responsible for the extremely slow leaching rate (Braithwaite and Wadsworth, 1976; Hackl *et al*., 1995). In addition, it has been noted that at high temperature and high pressure processes, iron readily and rapidly precipitate as hematite or basic iron sulfate. However, formation of these species does not seem to impede chalcopyrite oxidation (Hackl *et al*., 1995). It was reported that the precipitation of iron compounds reduces the concentration of ferric ions in solution, which will directly affect the ferric ion oxidative leaching (Klauber *et al*., 2001).

3.4 Conclusions

In summary, in spite of advantages of ferric sulfate media over chloride, ammonia, and nitrogen media due to simplicity of the leaching reactions, lower capital and operating costs, and the simplicity of the electrowinning process following solvent extraction, the rate and level of copper extraction are extremely low. The slow reaction rate is attributed to the formation of a passivating layer, either elemental sulfur, or iron-deficient copper polysulfide, or iron precipitates. This passivating layer prevents the transport of reactants/product to and from the chalcopyrite surface. This layer may also inhibit the transport of electrons to and from the chalcopyrite surface. Unless particles are ultrafine, a rapid and complete copper extraction in ferric sulfate media is only observed at high temperature and high pressure when sulfur is completely oxidized to sulfate.

Chapter 4 Enhancing the Kinetics of Chalcopyrite Leaching in the Galvanox™ Process

4.1 Objectives

As mentioned in previous chapters, pyrite is an effective catalyst during atmospheric leaching of chalcopyrite in iron sulfate media via the Galvanox™ process. However, not all pyrite samples have the same catalytic effect on the process. Recent studies on the Galvanox™ process have indicated that pyrite samples from different sources can influence the rate of chalcopyrite leaching differently. Some pyrite samples accelerate the leaching rate significantly, while others have less effect on the process. Furthermore, a strong correlation has been noted between the level of silver occurring in the pyrite samples and their effectiveness as catalysts for chalcopyrite leaching.

In this chapter, the use of silver-enhanced pyrite with the aim of improving the Galvanox™ process was investigated. The effects of various parameters to maximize copper extraction while minimizing the amount of added silver were fully examined. Furthermore, the effects of impurities associated with natural pyrite were studied in this section. Hydrometallurgical process waters may contain dissolved chloride. Due to very low silver chloride solubility, it was important to understand if the presence of dissolved chloride in leaching solutions would have any detrimental effect on the kinetics of this process.

4.2 Experimental

The procedure to pretreat pyrite with silver ions and to prepare silver-enhanced pyrite will be described in the next section followed by the batch leaching set-up.

4.2.1 Pyrite Pretreatment with Silver Ions

Pyrite was pretreated with silver according to the following procedure: 500 mL of solution containing the desired amount of silver, added as silver nitrate solution, was prepared. The solution was well mixed using a magnetic stirrer. 50 g of ground pyrite were added and allowed to react with the silver until no silver was detected in the solution. The behavior of silver was studied by following the silver concentration in the aqueous phase before and after addition of pyrite at various time intervals. The silver content was determined by atomic absorption spectroscopy. Pulp density was held at 100 g/L to ensure a high degree of mixing by the magnetic stirrer in the glass beaker. After treating the pyrite with silver ions, the solid residue was filtered and rinsed several times with water to wash any unreacted silver off of the pyrite surfaces.

4.2.2 Leaching Experiments

Batch leaching experiments were conducted in a sealed 2-L jacketed glass reactor. The temperature was maintained at 80°C with a circulating water bath. The reactor was equipped with three baffles made of 316 stainless steel and a six-bladed Rushton turbine impeller with a motor and speed controller manufactured by Applikon Dependable Instruments (ADI). Impeller speed was maintained at 1200 rpm.

Each reactor was connected to a multi-channel digital controller (ADI 1030 Bio-controller). A pH probe, a redox potential probe and a thermocouple were connected to the controller and inserted into the reactor. The outputs of these probes were recorded to the computer from the controller. In each experiment, the solution potential was set at specific point. The controller was also equipped with two analogue outputs. When the solution potential fell below the set point, an analogue signal was sent to a digital gas mass flow meter (Aalborg GFCS), upon which oxygen from a cylinder passed into the reactor through a sparger

until the potential set point was reached. The rate of oxygen flow decreased as the potential became closer to the set point. Each reactor was also equipped with a condenser, which allowed excess oxygen to exit while condensing the associated water vapor and returning it to the reactor.

The leach reactor was filled with 1.5 L of solution with the required concentration of sulfuric acid, corresponding to 150% of the stoichiometric requirement based on the following overall leach reaction (4.2.1):

$$CuFeS_2 + O_2 + 2\ H_2SO_4 = CuSO_4 + FeSO_4 + 2\ H_2O + 2\ S^0 \qquad (4.2.1)$$

The reactor was then sealed and the condenser, stirring motor and oxygen tube were installed. Before adding the concentrate, the solution was heated to the desired temperature using a recirculating water bath. Ferrous and ferric salts were added after reaching the desired temperature, and the agitation speed was set to 1200 rpm. Before starting the leach test, the pH probe was calibrated using buffer solutions at pH 1 and pH 4. The redox potential probe was also placed in a standard solution (470 mV *vs* Ag/AgCl at 25°C) to ensure that it was working properly. Then, the concentrate and pyrite were added to the reactor. Slurry samples of approximately 2 mL were taken periodically for analysis. Samples were filtered and assayed for copper content by atomic absorption spectroscopy. At the end of each test, all contents of the reactor were emptied to a flask and filtered. The solid residue was collected for analysis by multiacid digestion and induction coupled plasma (ICP) spectroscopy. The dried residue was weighed, then coned and quartered to obtain a representative sample for analysis. Solid assays were conducted by a local commercial laboratory (International Plasma Laboratory (IPL), Richmond, BC).

4.2.3 Materials

A copper concentrate containing 27% copper and three pyrite samples containing 97.6%, 70.8%, and 98.7% pyrite from three different sources were used. To obtain the elemental compositions of the minerals, representative samples were sent to a local commercial laboratory (International Plasma Laboratory (IPL), Richmond, BC) for Induction Coupled Plasma (ICP) analysis. The mineralogical compositions of minerals were obtained by quantitative Rietveld XRD analysis. The sample was reduced into fine powder to the optimum grain-size range for X-ray analysis (<10μm) by grinding under ethanol in a vibratory McCrone Micronizing Mill for 7 minutes. Step-scan X-ray powder-diffraction data were collected over a range 3-80°2θ with Co (Kα) radiation on a Bruker D8 Focus Bragg-Brentano diffractometer equipped with an Fe monochromator foil, 0.6 mm (0.3°) divergence slit, incident- and diffracted-beam Soller slits and a LynxEye detector. The long fine-focus Co X-ray tube was operated at 35 kV and 40 mA, using a take-off angle of 6°.

Mineralogical and elemental compositions of the concentrate and pyrite samples are summarized in Table 4.1 and Table 4.2, respectively. A Malvern Mastersizer was used in order to obtain particle size distributions of the samples. The P_{80} of Pyrite #1, Pyrite #2, and Pyrite #3 are 274 μm, 245 μm, and 226 μm. The P_{80} of copper concentrate is 46 μm.

Table 4.1 Rietveld XRD analysis of copper concentrate and pyrite samples

Mineral	Ideal Formula	Copper Conc (%)	Pyrite #1 (%)	Pyrite #2 (%)	Pyrite #3 (%)
Pyrite	FeS_2	15.9	97.6	70.8	98.7
Chalcopyrite	$CuFeS_2$	78	—	4.0	—
Quartz	SiO_2	1	0.6	1.9	0.3
Biotite	$K(Mg,Fe^{2+})_3AlSi_3O_{10}(OH)_2$	1.8	—	—	0.4
Dolomite	$CaMg(CO_3)_2$	1.1	—	12.2	—
Plagioclase	$NaAlSi_3O_8 – CaAl_2Si_2O_8$	2.2	—	—	—
Anhydrite	$CaSO_4$	—	1.8	—	—
Gypsum	$CaSO_4.2H_2O$	—	—	3.4	0.5
Calcite	$CaCO_3$	—	—	—	0.1
Pyrrhotite	$Fe_{1-x}S$	—	—	2.1	—
Clinochlore	$(Mg,Fe^{2+})_5Al(Si_3Al)O_{10}(OH)_8$	—	—	2.2	—
Muscovite	$KAl_2AlSi_3O_{10}(OH)_2$	—	—	3.4	—

Table 4.2 Elemental analysis of copper concentrate and pyrite samples

Element	Copper Conc	Pyrite #1	Pyrite #2	Pyrite #3
Cu	27.00 %	0.13 %	1.8 %	11 ppm
Fe	31.14 %	45.43 %	38.02 %	45.94 %
S	36.70 %	52.62 %	45.3 %	52.75 %
Mg	0.27 %	0.04 %	1.88 %	< 0.01 %
Co	0.16 %	—	68 ppm	—
Pb	—	0.14 %	48 ppm	< 2 ppm
As	130 ppm	—	49 ppm	8 ppm
Ag	15.5 ppm	21 ppm	2 ppm	0.4 ppm
Ca	0.47 %	0.56 %	4.05 %	0.16 %
Al	0.51 %	0.02 %	0.41 %	0.08 %
Zn	0.01 %	—	441 ppm	6 ppm
Si	1.14 %	0.28 %	1.18 %	0.14 %

4.3 Results and Discussion

The first test was conducted to observe the rate of copper extraction in ferric sulfate solution at 470 mV (*vs* Ag/AgCl) in the absence of added pyrite. Figure 4.1 indicates very slow kinetics and incomplete copper extraction under these conditions. Under these conditions, only 42% copper extraction was achieved after 90 hours and it was proceeding very slowly.

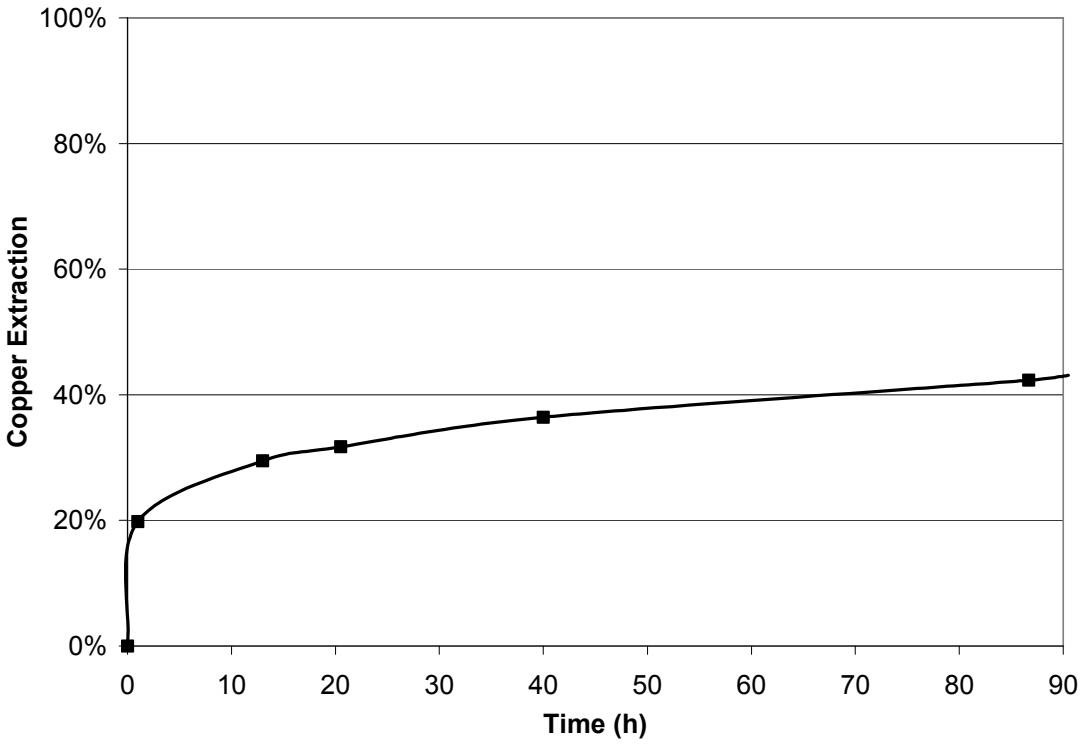

Figure 4.1 Chalcopyrite leaching in ferric sulfate media at a potential set point of 470 mV and 80°C

Initially, pyrite samples from various sources were examined in order to obtain a broader understanding of their catalytic properties. The first series of tests was conducted to investigate the effect of adding pyrite from three different sources. The results are shown in Figure 4.2.

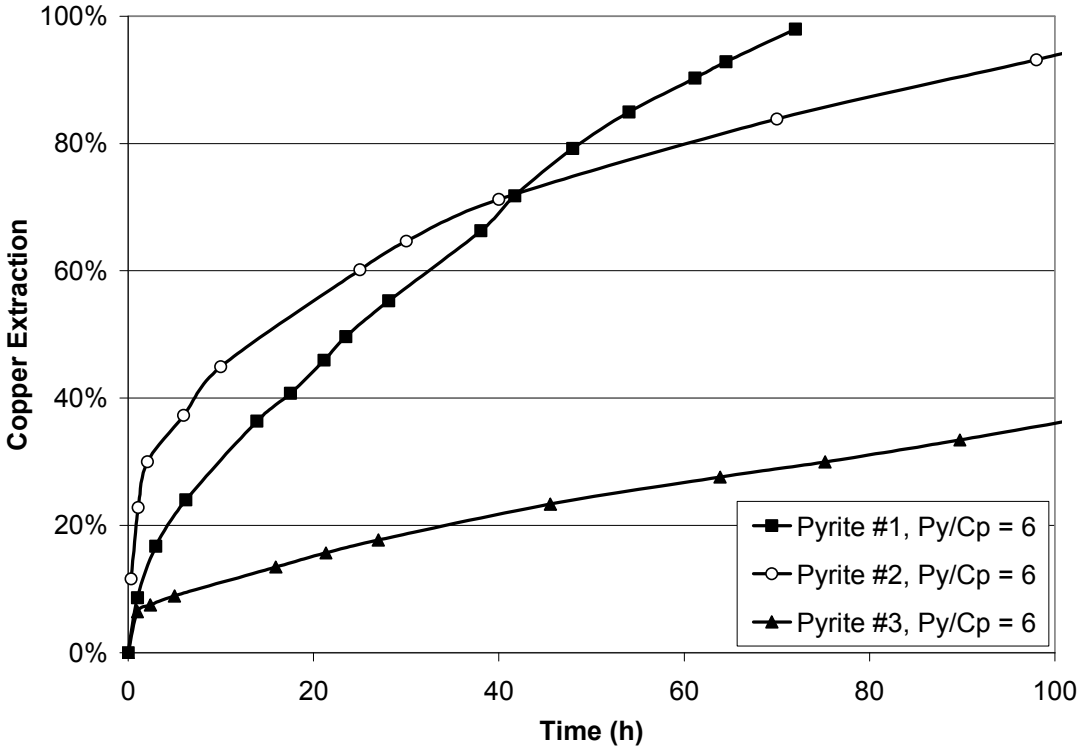

Figure 4.2 Effect of pyrite addition on copper extraction using plain pyrite at a potential set point of 470 mV, 10 g/L Cu concentrate, and 80°C

The results shown in Figure 4.2 indicate that although the kinetics of chalcopyrite leaching increases in the presence of natural pyrite, a long time is still required for complete copper extraction.

These tests were then repeated, but with the addition of silver at a silver-to-pyrite ratio of 100 ppm. The results are shown in Figure 4.3 and show a dramatic increase in copper leaching kinetics.

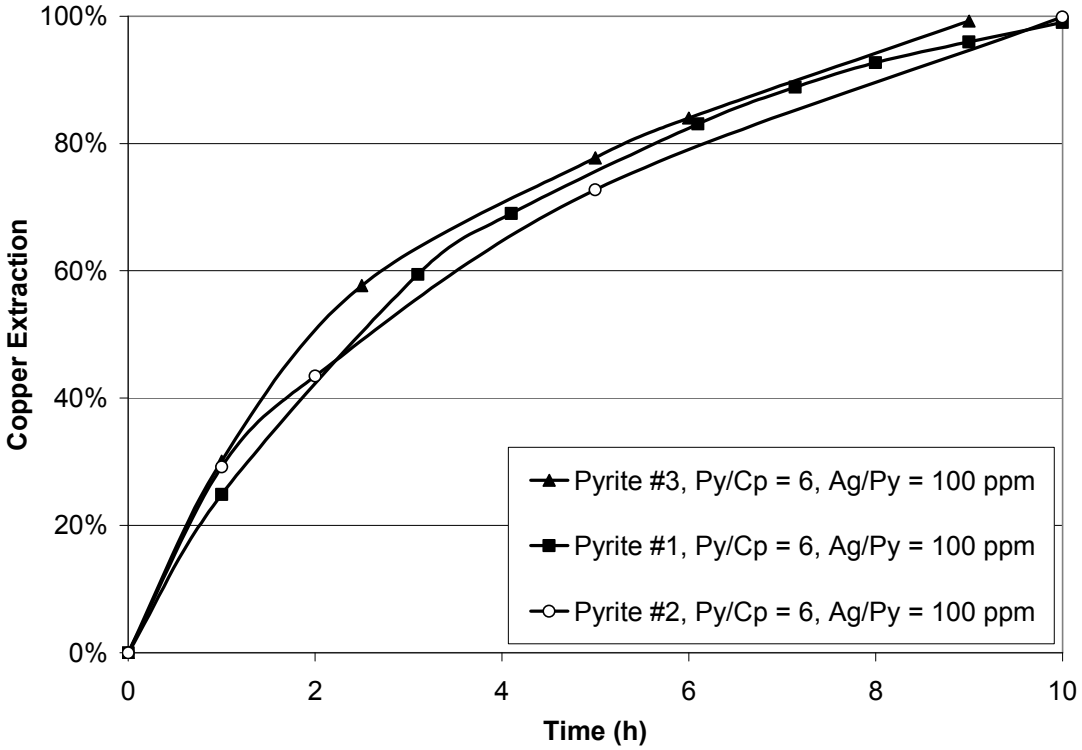

Figure 4.3 Effect of silver-enhanced pyrite at a silver-to-pyrite ratio of 100 ppm, a potential set point of 470 mV, 10 g/L Cu concentrate, and 80°C

The results shown in Figure 4.3 also indicate that, in spite of major differences in the catalytic properties of natural pyrite from different sources, shown in Figure 4.2, all three silver-enhanced pyrite samples have an identical catalytic effect on chalcopyrite leaching.

For comparison purposes, the results of copper extraction using various natural pyrite samples and silver-enhanced pyrite samples are all shown in Figure 4.4 to reveal the significant improvement on the kinetics of copper extraction in the presence of silver-enhanced pyrite.

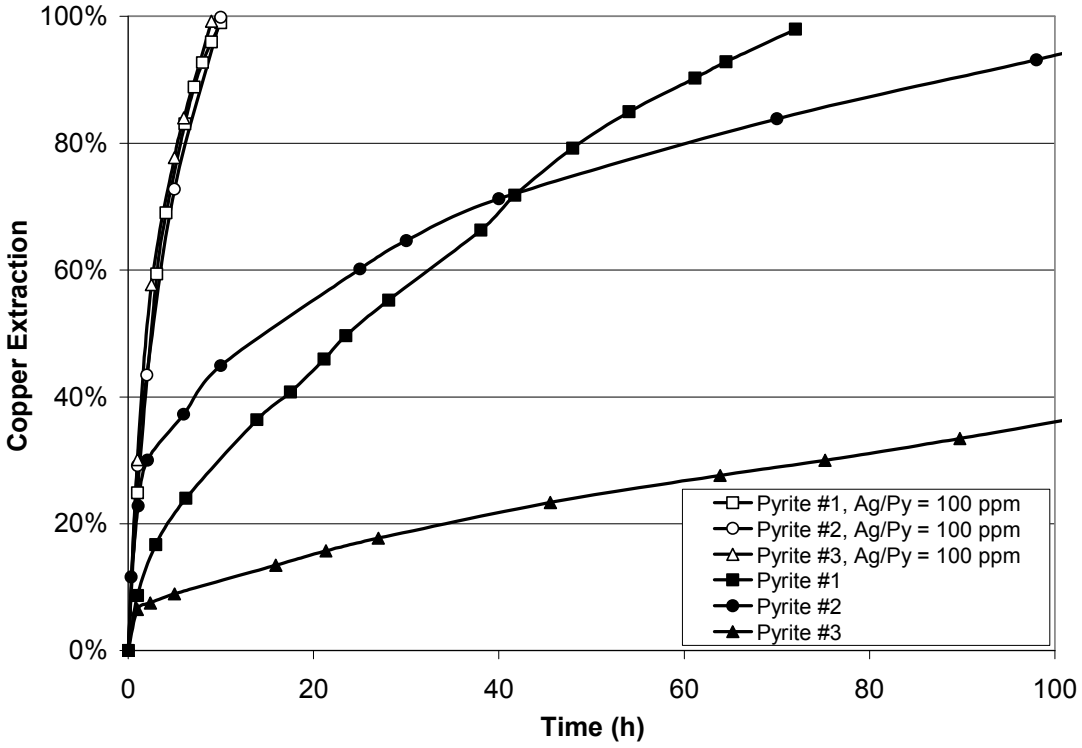

Figure 4.4 Comparison of natural pyrite and silver-enhanced pyrite at a potential set point of 470 mV, 10 g/L Cu concentrate, and 80°C

It was important to evaluate the reproducibility of the results. Similar experiments were conducted at a silver to pyrite ratio of 200 ppm and a pyrite to chalcopyrite ratio of 2. The results are shown in Figure 4.5.

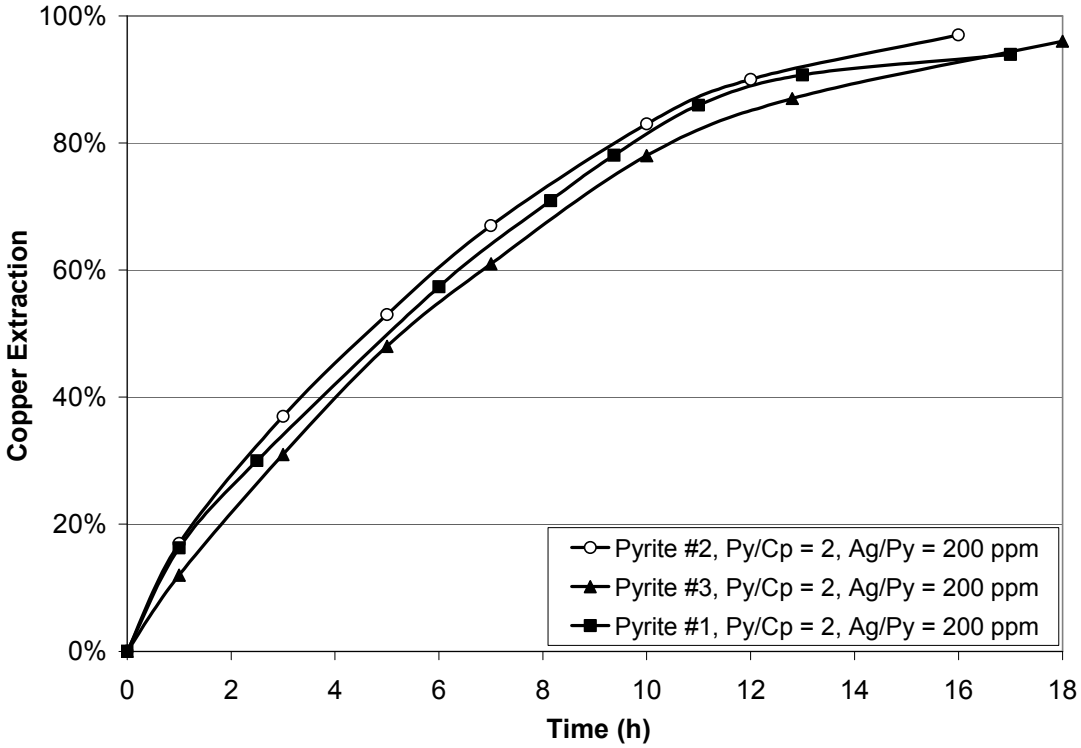

Figure 4.5 Effect of silver-enhanced pyrite at a silver-to-pyrite ratio of 200 ppm, a potential set point of 470 mV, 10 g/L Cu concentrate, and 80°C

Figure 4.5 confirms the reproducibility of the results and shows that these three pyrite samples behave similarly in this process. Given this similarity, all further results presented in this chapter are based only on Pyrite #1, unless otherwise is noted.

Figure 4.6 and Figure 4.7 present the particle size distributions of copper concentrate and pyrite, respectively. Figure 4.6 shows that the concentrate as received was not ground ultrafine (P_{80} = 46 µm). The pyrite particles were considerably larger, as shown in Figure 4.7 (P_{80} = 274 µm).

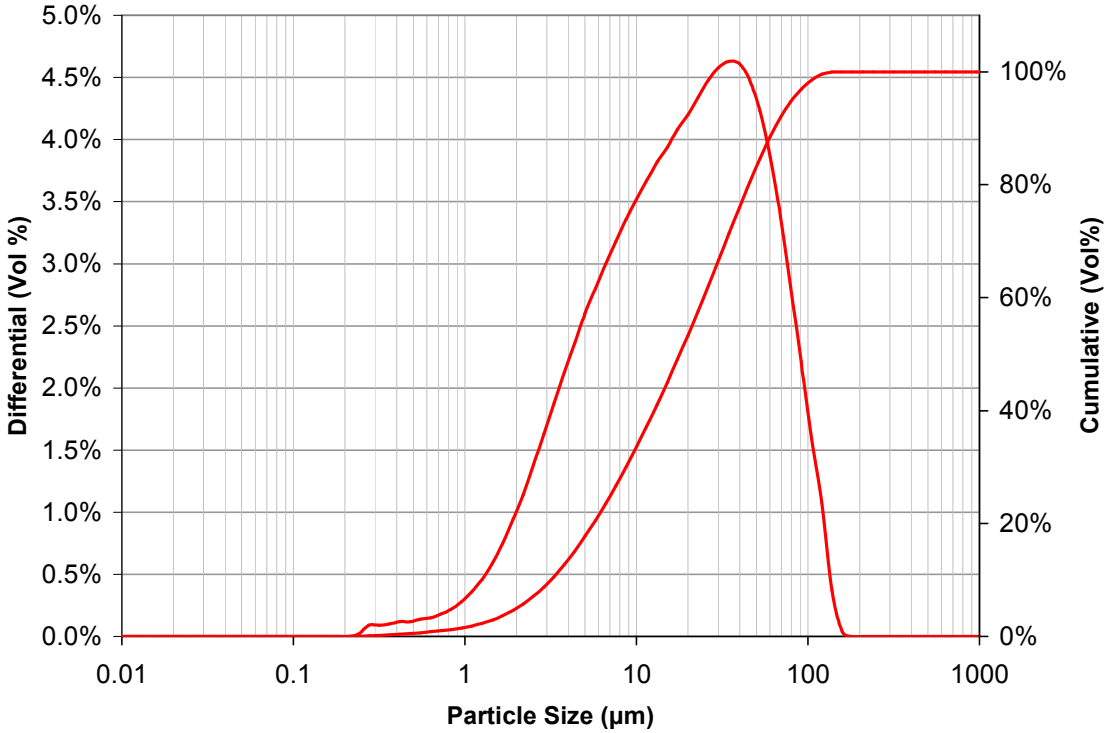

Figure 4.6 Particle size distribution of copper concentrate

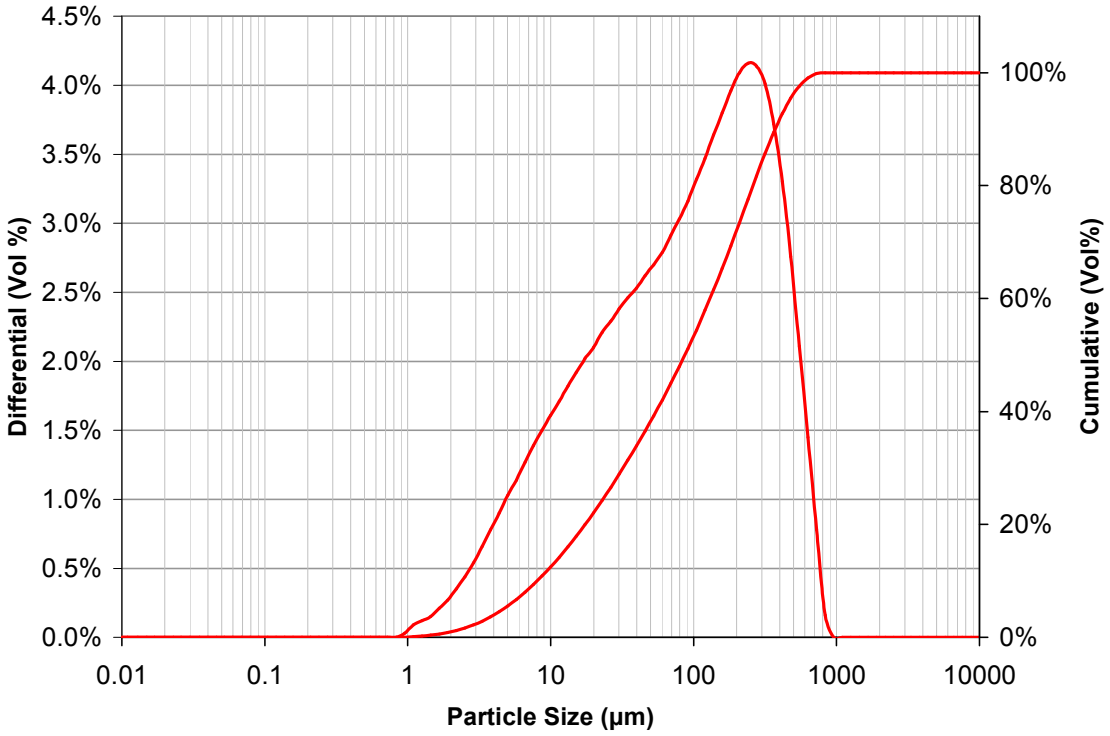

Figure 4.7 Particle size distribution of pyrite

A large number of leaching experiments have been conducted in order to develop an understanding of the effects of several variables on the kinetics of copper extraction from chalcopyrite using silver-enhanced pyrite. Selected results are shown below. All redox potentials are reported *vs* the KCl-saturated Ag/AgCl reference electrode.

Five variables were systematically investigated in this study to determine their effect on the rate of chalcopyrite leaching and discover the optimized conditions:

1. Mass ratio of silver-enhanced pyrite to chalcopyrite
2. Silver concentration of pyrite
3. Redox potential
4. Pyrite recycle
5. Pulp density

Then, under optimized conditions, the effects of impurities associated with pyrite and the influence of chloride concentration in leaching solutions were investigated

Two tests were conducted to observe the effect of adding Pyrite #1 to chalcopyrite at two different ratios. For both tests the solution potentials were set at 470 mV. The pyrite residues were collected and recycled to subsequent tests. The results are shown in Figure 4.8. While this pyrite did facilitate the complete recovery of copper from the chalcopyrite, the necessary leach times were very long (75 hours or more), and the required pyrite-to-chalcopyrite ratios were high. Samples of this same pyrite material were used in all subsequent tests reported below.

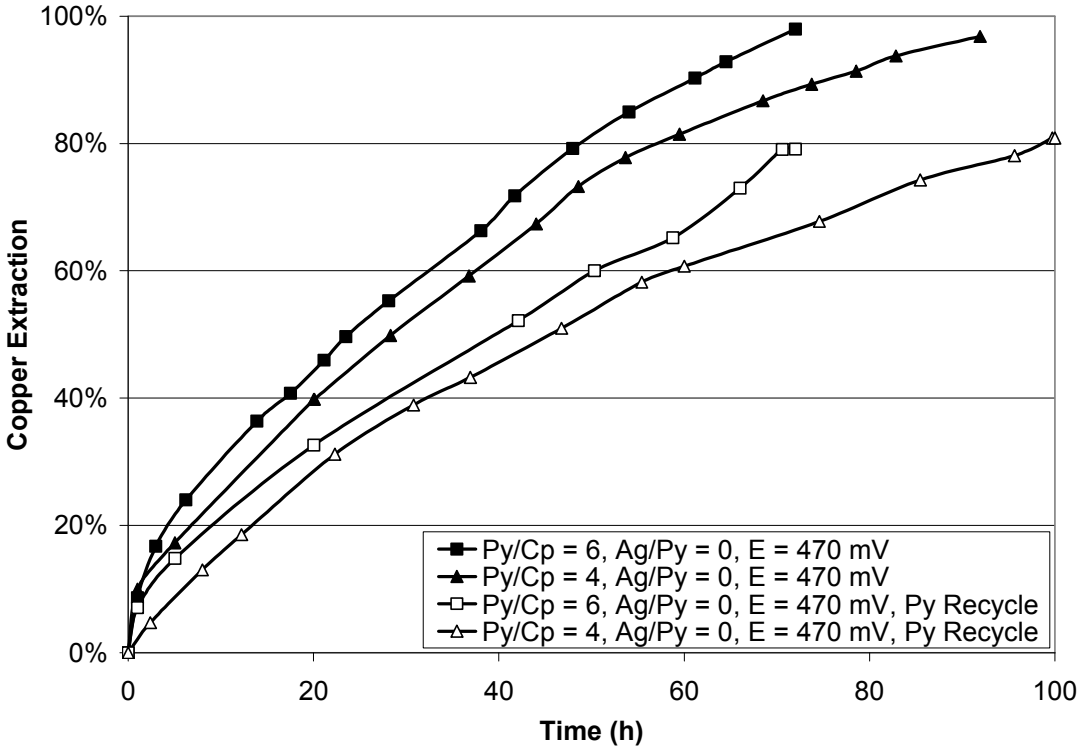

Figure 4.8 Effect of pyrite addition on copper extraction using plain pyrite and the recycled plain pyrite at a potential set point of 470 mV, 10 g/L Cu concentrate, and 80°C

4.3.1 Effect of the Mass Ratio of Silver-enhanced Pyrite to Chalcopyrite

In order to determine the effect of silver-enhanced pyrite addition, leaching experiments were performed at pyrite-to-chalcopyrite mass ratios of 2, 4, and 6. Each of these three ratios was tested at 50 ppm, 100 ppm, and 200 ppm silver-to-pyrite ratios. Figure 4.9, Figure 4.10, and Figure 4.11 show the effects of addition of silver-enhanced pyrite on the kinetics of chalcopyrite leaching at a constant silver-to-pyrite ratio of 50 ppm, 100 ppm, and 200 ppm, respectively.

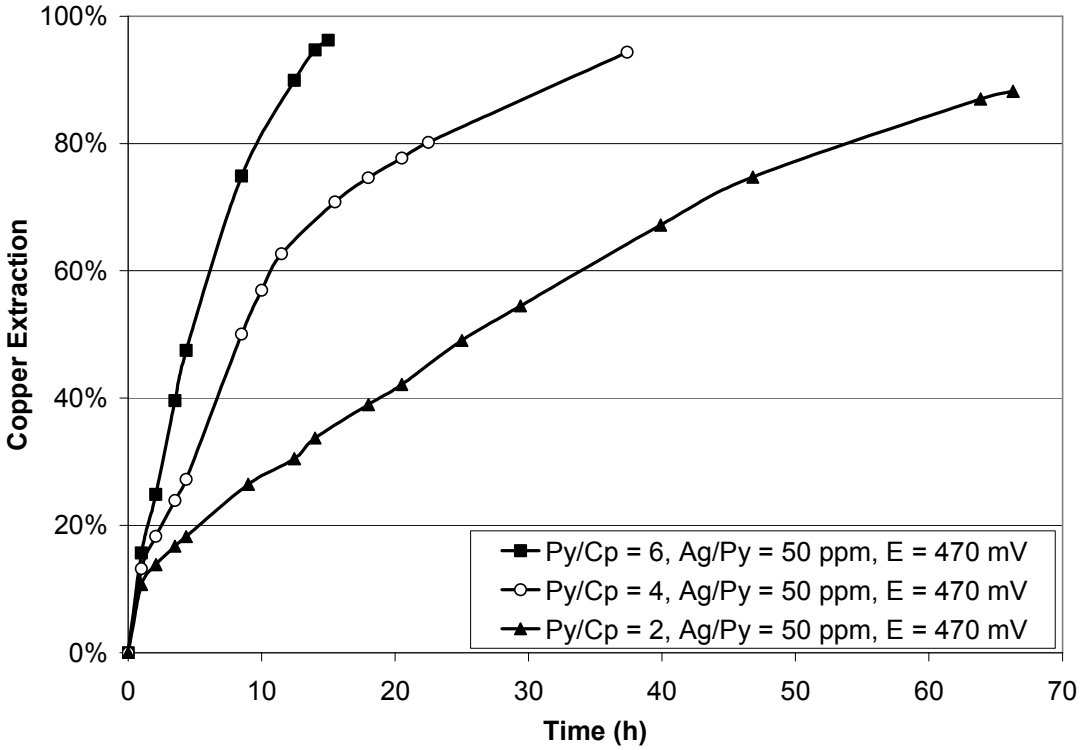

Figure 4.9 Effect of silver-enhanced pyrite at various pyrite-to-chalcopyrite ratios, a silver-to-pyrite ratio of 500 ppm, a potential set point of 470 mV, 10 g/L Cu concentrate, and 80°C

Figure 4.9 shows the effect of addition of silver-enhanced pyrite at a silver-to-pyrite ratio of 50 ppm and three different pyrite-to-chalcopyrite ratios. In these tests, known amounts of pyrite were soaked in solution containing specific quantities of dissolved silver to make up 50 ppm of silver on pyrite, or 50 g Ag per tonne of pyrite. This figure clearly shows that the rate of chalcopyrite leaching increased by increasing the ratio of pyrite to chalcopyrite. At the silver-to-pyrite ratio of 50 ppm and the pyrite-to-chalcopyrite ratio of 6, 97% copper extraction was obtained in 15 hours. However, at the same silver-to-pyrite ratio but at a lower pyrite-to-chalcopyrite ratio of 2, almost 90% copper recovery was obtained in 70 hours.

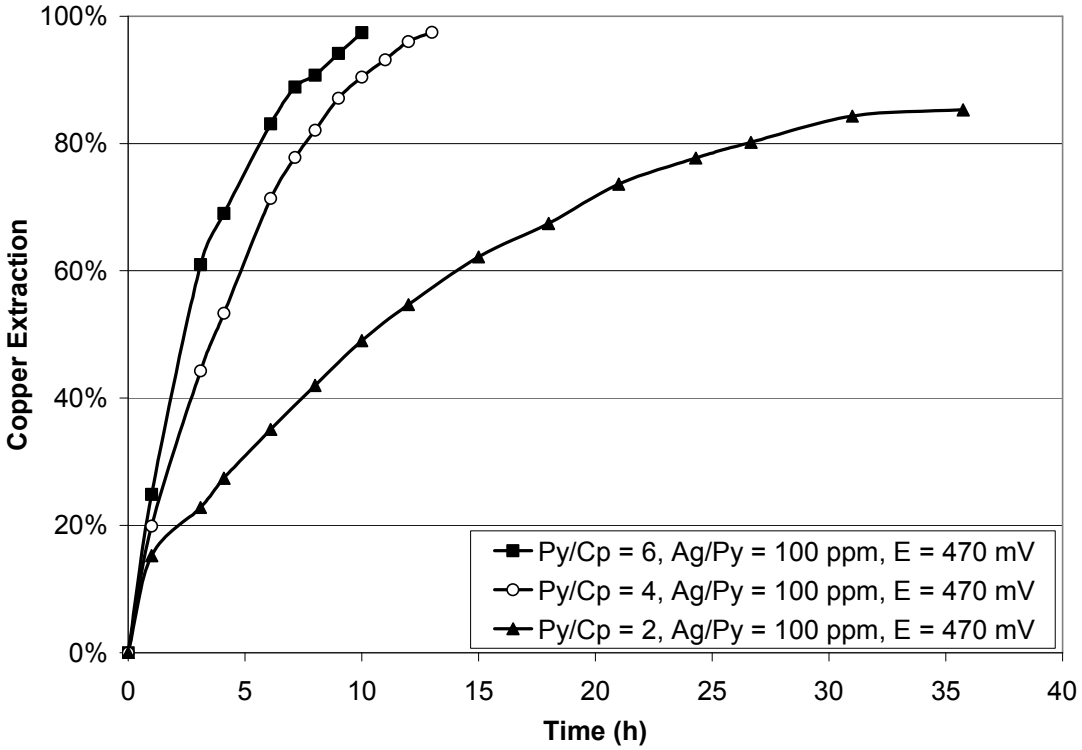

Figure 4.10 Effect of silver-enhanced pyrite at various pyrite-to-chalcopyrite ratios, a silver-to-pyrite ratio of 100 ppm, a potential set point of 470 mV, 10 g/L Cu concentrate, and 80°C

Figure 4.10 shows the results of addition of silver-enhanced pyrite at a silver-to-pyrite ratio of 100 ppm. Similarly, known amounts of pyrite were soaked in solution containing specific quantities of dissolved silver to make up 100 g Ag per tonne of pyrite, respectively. Although the rate of leaching is faster at the pyrite-to-chalcopyrite ratio of 6 than that at a ratio of 4, the difference is insignificant. Conversely, Figure 4.10 shows the significant difference in the rate of chalcopyrite leaching at the pyrite-to-chalcopyrite ratio of 4 and 2. The copper extraction was complete at the pyrite-to-chalcopyrite ratio of 6 and 4, after 10 and 13 hours, respectively. However, at the pyrite-to-chalcopyrite ratio of 2, only 85% copper extraction was achieved after 36 hours.

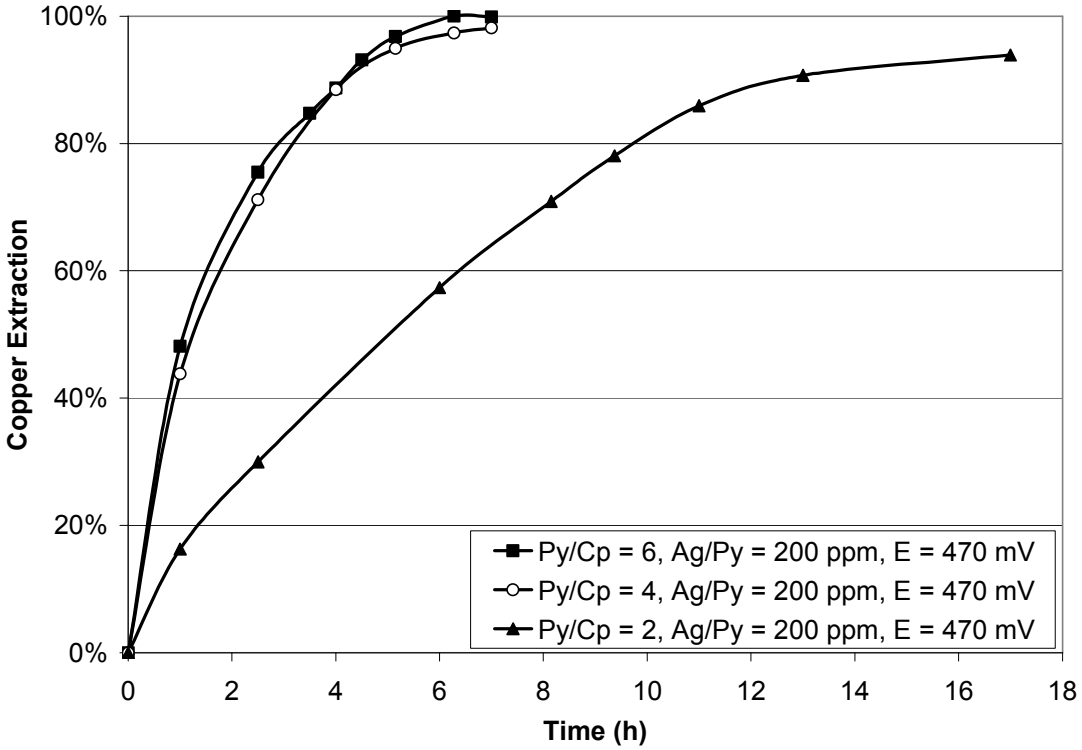

Figure 4.11 Effect of silver-enhanced pyrite at various pyrite-to-chalcopyrite ratios, a silver-to-pyrite ratio of 200 ppm, a potential set point of 470 mV, and 80°C

Figure 4.11 also clearly shows the significant effect of silver-enhanced pyrite on the kinetics of chalcopyrite leaching. The results are in agreement with previous results shown in Figure 4.9 and Figure 4.10. Figure 4.11 shows that the rate of copper extraction is almost identical at the pyrite-to-chalcopyrite ratio of 6 and 4 and both were complete in 6.3 hours and 7 hours, respectively. As discussed earlier, Figure 4.9 and Figure 4.10 show that the rate of chalcopyrite leaching increases by increasing the ratio of pyrite to chalcopyrite. However, Figure 4.11 shows that at higher ratio of silver to pyrite (200 ppm), this improvement is not noticeable at high ratio of pyrite to chalcopyrite (i.e. ratio of 6 and 4). This observation may be attributed to the change of a rate limiting step in this process. The reaction might be chemical reaction control instead of diffusion control, at high pyrite-to-chalcopyrite ratios and high silver-to-pyrite ratios.

Overall, at the highest pyrite-to-chalcopyrite ratio of 6:1, and the silver-to-pyrite ratio of 200 ppm, leaching was complete within roughly 6.3 hours. Conversely, at the lowest pyrite-to-chalcopyrite ratio of 2, and the lowest silver-to-pyrite ratio of 50 ppm, almost 90% copper extraction was obtained in 70 hours.

It is important to note that, for instance, at a silver-to-pyrite ratio of 100 ppm, by increasing the mass ratio of pyrite to chalcopyrite, the amount of silver used for that test in proportion to the amount of copper present also increases. Hence, increasing the ratio of pyrite to chalcopyrite may not be the only reason for the improved leaching rates in these tests. Figure 4.12 presents the results for a total amount of 5 mg silver. In one of the tests, the ratio of pyrite to chalcopyrite is twice the other, whereas the ratio of silver to pyrite is half.

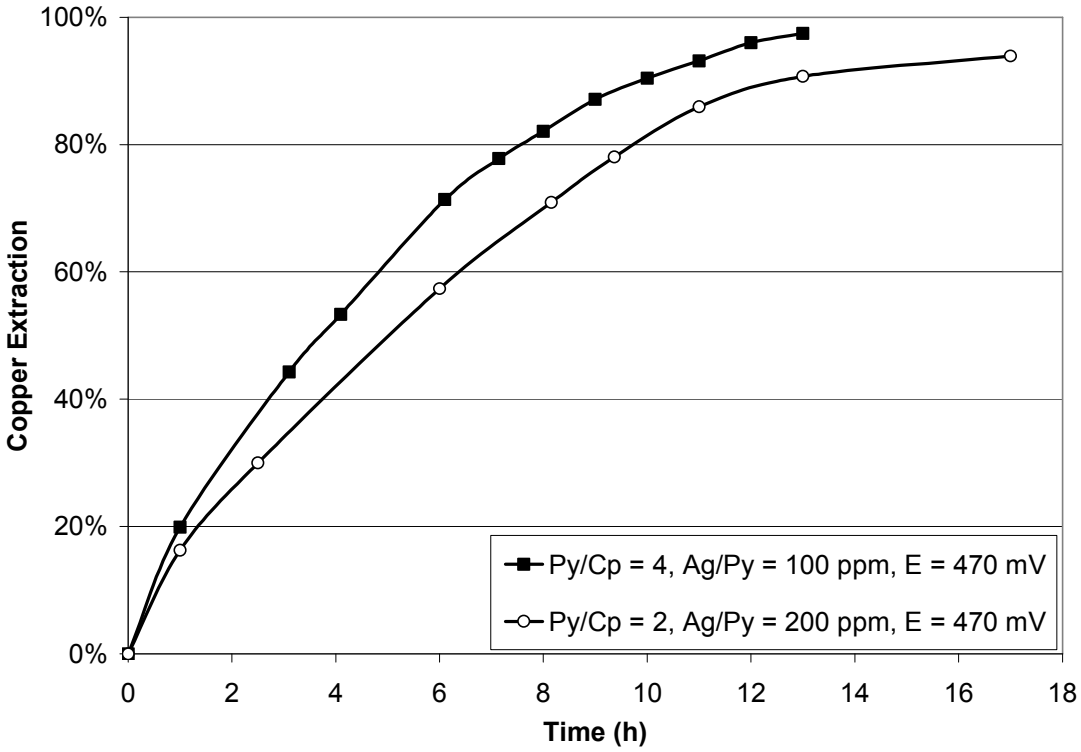

Figure 4.12 Effect of pyrite and silver concentrations at 5 mg Ag total, a potential set point of 470 mV, and 80°C

Figure 4.12 shows that although the total amounts of silver in both cases are equal, the leaching rate is measurably faster at a higher pyrite-to-chalcopyrite ratio. This confirms the beneficial role of pyrite in the process.

4.3.2 Effect of Silver Concentration on Pyrite

In order to delineate the effect of silver-to-pyrite ratio, this parameter was varied at fixed ratios of pyrite to chalcopyrite. Silver-to-pyrite ratios of 50, 100, and 200 ppm were tested at a pyrite-to-chalcopyrite ratio of 2, 4, and 6. Results are shown in Figure 4.13, Figure 4.14, and Figure 4.15.

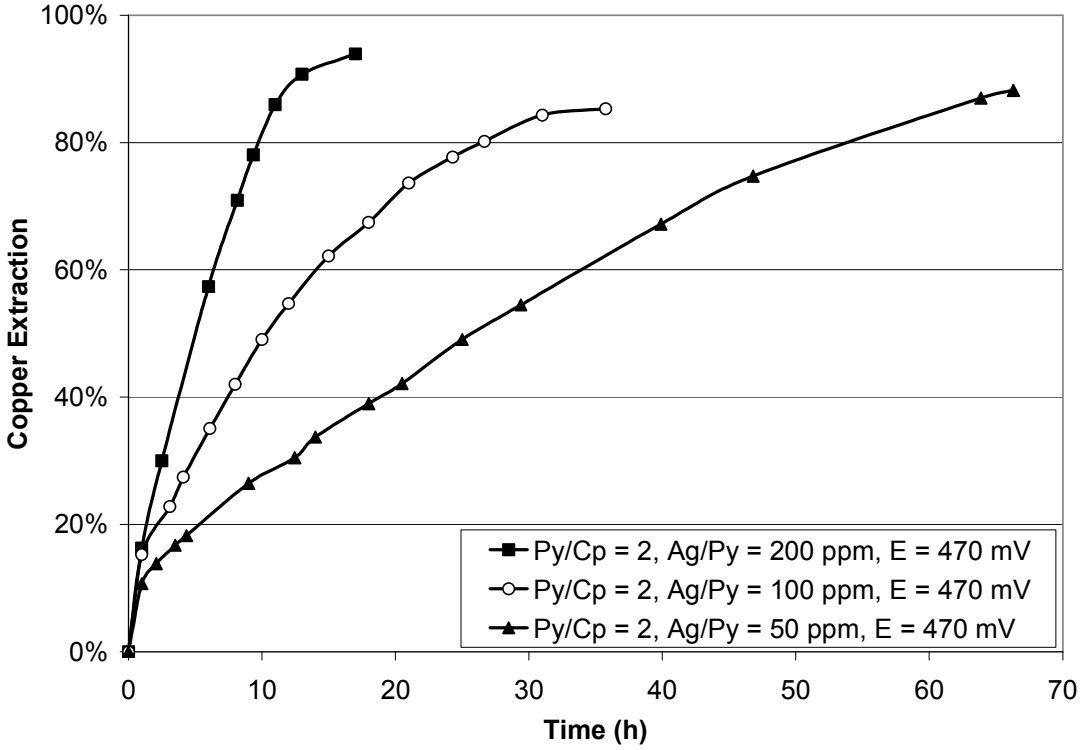

Figure 4.13 Effect of silver-to-pyrite ratio at a constant pyrite-to-chalcopyrite ratio of 2, a potential set point of 470 mV, 10 g/L Cu concentrate, and 80°C

Figure 4.13 shows that increasing the concentration of silver on pyrite increases the rate of copper extraction, significantly. At a fixed pyrite-to-chalcopyrite ratio of

2, 93% copper extraction was obtained after 17 hours in the presence of silver-enhanced pyrite at a silver-to-pyrite ratio of 200 ppm, while 88% copper extraction was achieved after 66 hours when the silver-to-pyrite ratio was 50 ppm.

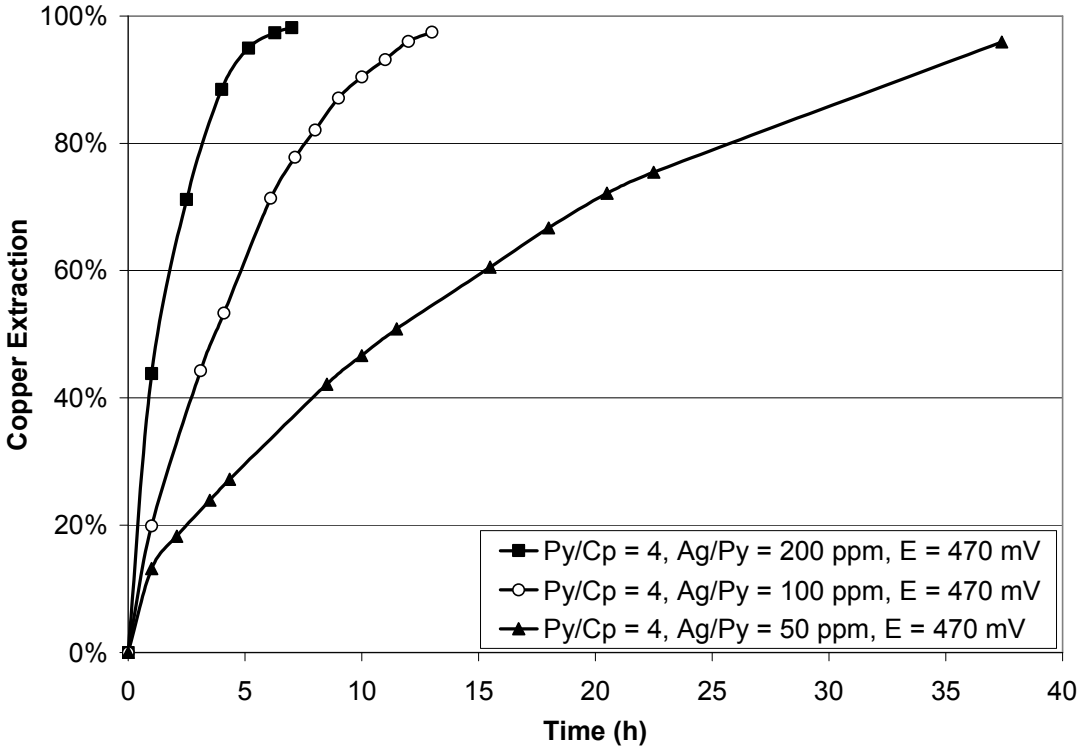

Figure 4.14 Effect of silver-to-pyrite ratio at a constant pyrite-to-chalcopyrite ratio of 4, a potential set point of 470 mV, 10 g/L Cu concentrate, and 80°C

Figure 4.14 shows the effect of addition of silver-enhanced pyrite at various silver concentrations and a fixed pyrite-to-chalcopyrite ratio of 4. Similarly, faster kinetics is observed at higher silver concentrations. 99% copper extraction was obtained at a fixed pyrite-to-chalcopyrite ratio of 4 and silver-to-pyrite ratios of 200 ppm and 100 ppm after 7 and 13 hours, respectively. The leaching rate is significantly slower at a silver-to-pyrite ratio of 50 ppm. The results show that 94% copper recovery was obtained after 37 hours.

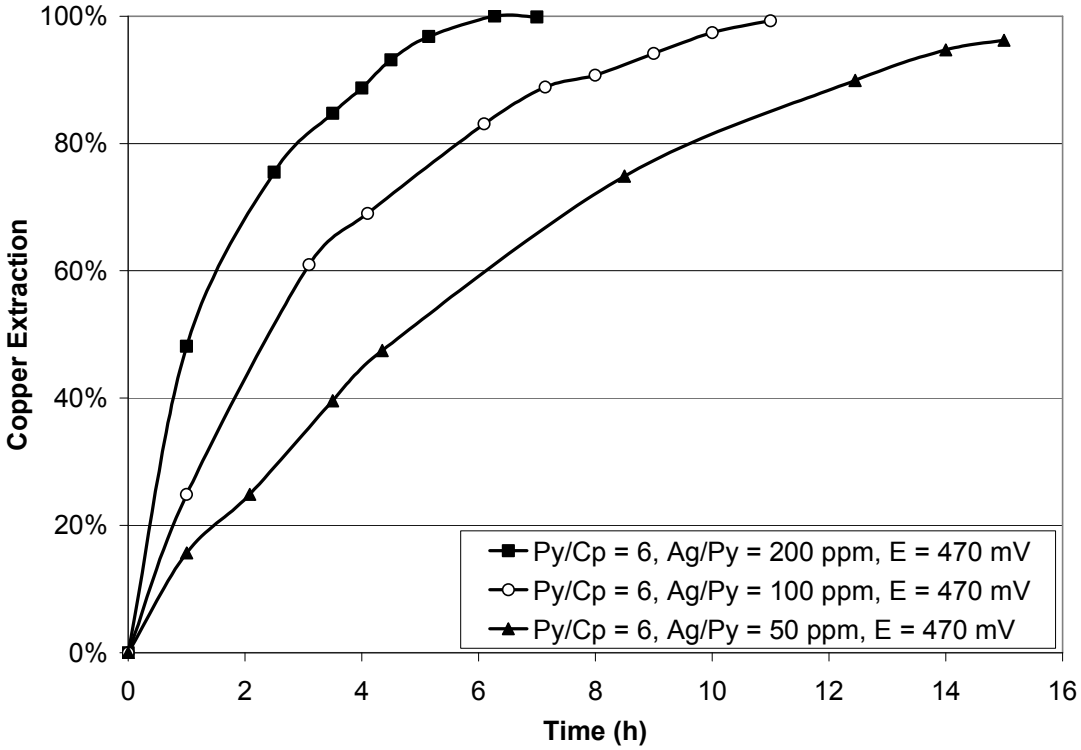

Figure 4.15 Effect of silver-to-pyrite ratio at a constant pyrite-to-chalcopyrite ratio of 6, a potential set point of 470 mV, 10 g/L Cu concentrate, and 80°C

Figure 4.15 shows the results of silver-enhanced pyrite addition at a fixed pyrite-to-chalcopyrite ratio of 6 and various silver-to-pyrite ratios of 50 ppm, 100 ppm, and 200 ppm. At a silver-to-pyrite ratio of 200 ppm, leaching is complete in about 6.3 hours. The leaching rate decreases at a lower silver-to-pyrite ratio of 4 and 2 such that 100% and 96% copper recoveries were obtained after 11 and 15 hours, respectively.

4.3.3 Effect of Solution Potential

Previously, Dixon *et al*. (2008) have shown that increasing the solution potential set point from 425 to 470 mV accelerates chalcopyrite leaching rates in the presence of pyrite. Hence, the first series of experiments was conducted at a

potential set point of 470 mV. In order to inhibit the oxidation of pyrite and the attendant loss of reacted silver, it was subsequently decided to decrease the solution potential set point.

Figure 4.16 shows the effect of varying the solution potential set point. This figure clearly indicates that copper extraction was faster at 440 and 450 mV than at 470 mV. However, dropping the solution potential to 420 mV gave a much slower rate. The rest potential of this pyrite at a silver-to-pyrite ratio of 100 ppm in a solution containing 65 g/L sulfuric acid and 80°C was measured and it was 452-455 mV *vs* Ag/AgCl. According to Figure 4.16, the fastest rate was achieved at 450 mV. This faster rate at lower potential can be attributed to a decrease in both pyrite and silver oxidation and, therefore, in the loss of reacted silver to solution. At higher potentials, more pyrite and silver are oxidized and more silver is lost. The solid assay results of pyrite samples after the leaching tests were obtained. The results showed that the silver concentrations of the enhanced pyrite were 42, 74, 78, 75 ppm in experiments conducted at the potential set point of 470, 450, 440, and 420 mV, respectively. The results indicate that the silver content of the pyrite were decreased with increasing the solution potential above 450 mV. At potential lower than 450 mV, the silver concentrations of pyrite were almost identical. In addition, about 4.5 to 5% of pyrite was oxidized at 470 mV, while no pyrite oxidation was occurred at lower potentials. However, the anodic decomposition of chalcopyrite is also retarded at lower potentials, as also observed in conventional Galvanox™ leaching (Dixon *et al*., 2008). Therefore, the solution potential has to be controlled high enough to accelerate the oxidation of chalcopyrite and low enough to inhibit the oxidation of silver and pyrite.

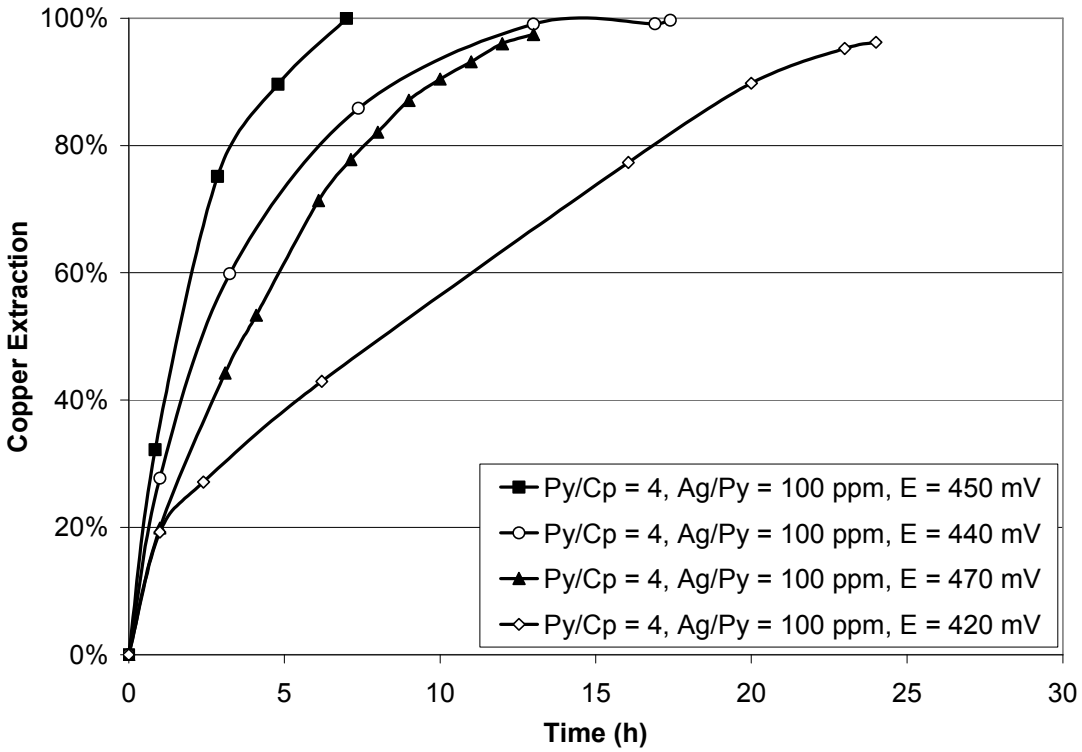

Figure 4.16 Effect of potential at a constant pyrite-to-chalcopyrite ratio of 4, a constant silver-to-pyrite ratio of 100 ppm (1.23 g Ag per kg of contained Cu), 10 g/L Cu concentrate, and 80°C

In Figure 4.17, the rates of leaching at two different solution potential set points are compared. In each of these tests, the ratio of pyrite to chalcopyrite was 2. This figure shows the significant improvement in chalcopyrite leaching at lower solution potential. At 450 mV and a silver-to-pyrite ratio of 50 ppm, leaching was complete after 23 hours whereas at 470 mV, only 88% copper extraction was achieved after 66 hours.

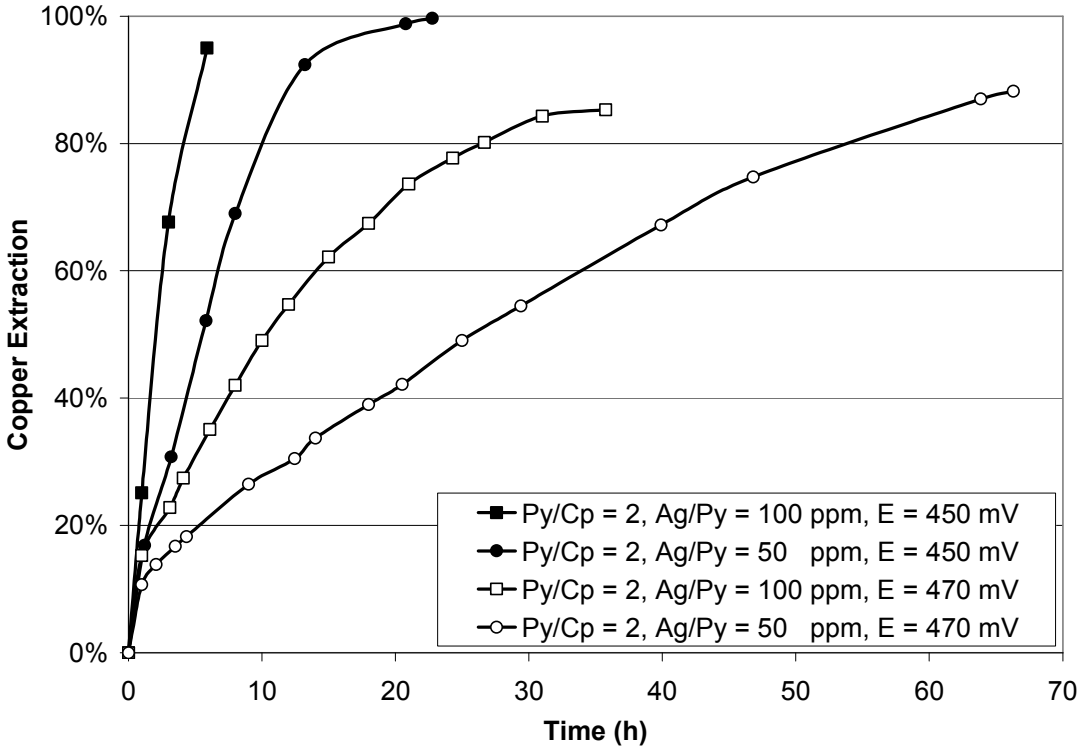

Figure 4.17 Comparison of two different solution potential set points (450 and 470 mV) and silver-to-pyrite ratios (50 and 100 ppm) at a constant pyrite-to-chalcopyrite ratio of 2, 10 g/L Cu concentrate , and 80°C

It is also interesting to note that at a solution potential set point of 470 mV and a silver-to-pyrite ratio of 100 ppm, only 85% extraction was achieved after 36 hours. Hence, although the amount of silver was reduced to half of the other test, due to the lower potential the leaching occurred at a much faster rate.

4.3.4 Effect of Pyrite Recycle

The feasibility of recycling pyrite for treating subsequent charges of concentrate was also examined. In each of the tests, upon completion of the first test, the supernatant solution was decanted from the reactor while retaining the residue. Then, new solution containing the desired amounts of sulfuric acid was added.

This new solution was heated to 80°C and then the required amounts of ferric and ferrous sulfate and a new charge of fresh concentrate were added.

Figure 4.18 shows the results of recycling pyrite from the tests that were presented in Figure 4.16. The recycle tests followed the same trend as the initial tests. Similarly, the fastest and slowest copper extraction was observed at 450 and 420 mV, respectively. This indicates that the silver-enhanced pyrite retained its catalytic properties. However, it should be noted that the leach times were all longer in the recycle tests, by roughly a factor of two. Solid assay results confirm that the recycled pyrite contained less reacted silver than the freshly enhanced pyrite.

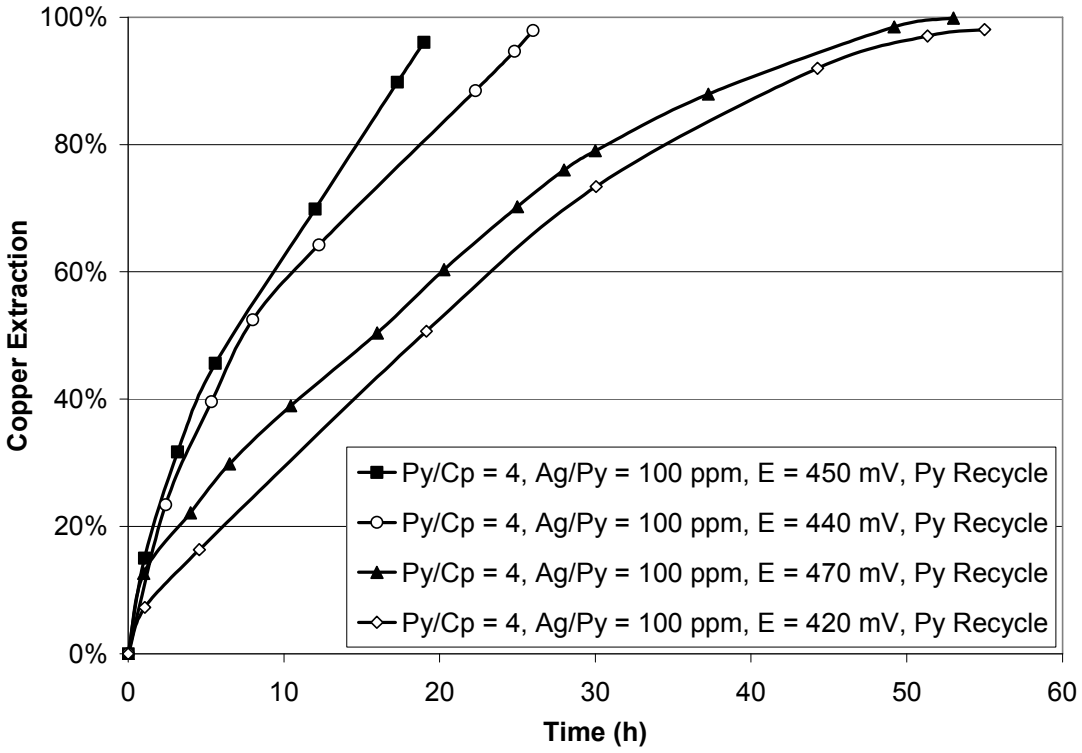

Figure 4.18 Effect of potential with recycled pyrite at a constant pyrite-to-chalcopyrite ratio of 4, a constant silver-to-pyrite ratio of 100 ppm (1.23 g Ag per kg of contained Cu), 10 g/L Cu concentrate, and 80°C

4.3.5 Effect of Pulp Density

While it has been demonstrated that recycled pyrite is an effective catalyst, it has also been noted that some of the reacted silver, and with it some of the catalytic effectiveness, is lost upon recycle. However, it was also determined that the concentration of silver dissolved in the leach solution at the end of each test was always about the same (0.2 to 0.5 ppm), and probably represented a solubility limit for silver under the prevailing conditions. It was hypothesized that increasing the concentration of pyrite in the reactor would decrease the relative loss of reacted silver to solution.

Figure 4.19 shows the effect of increasing the pulp density on the rate of chalcopyrite leaching. Previous tests were run with 10 g of copper concentrate per L of solution whereas Figure 4.19 shows the results of three tests run with 70 g of copper concentrate per L of solution, or 105 g total. In the first test, 175 g of fresh silver-enhanced pyrite with a silver-to-pyrite ratio of 100 ppm were added to give a pyrite-to-chalcopyrite ratio of 2:1. In the second and third tests, solid residues from the previous tests were recycled with fresh charges of copper concentrate, plus an additional 10% of the original charge, or 17.5 g, of fresh silver-enhanced pyrite. As shown in Figure 4.19, leaching with recycled residue occurs just as rapidly as leaching with freshly enhanced pyrite, and there is no loss of catalytic ability even after recycling the pyrite a second time. In fact, the second recycle test gave slightly faster leaching than the others, suggesting that the 10% makeup of silver-enhanced pyrite was more than adequate to ensure optimum catalytic effectiveness. In any case, the addition of 10% silver-enhanced pyrite to each recycle test corresponds to the addition of just 60 mg of silver per kg of contained copper.

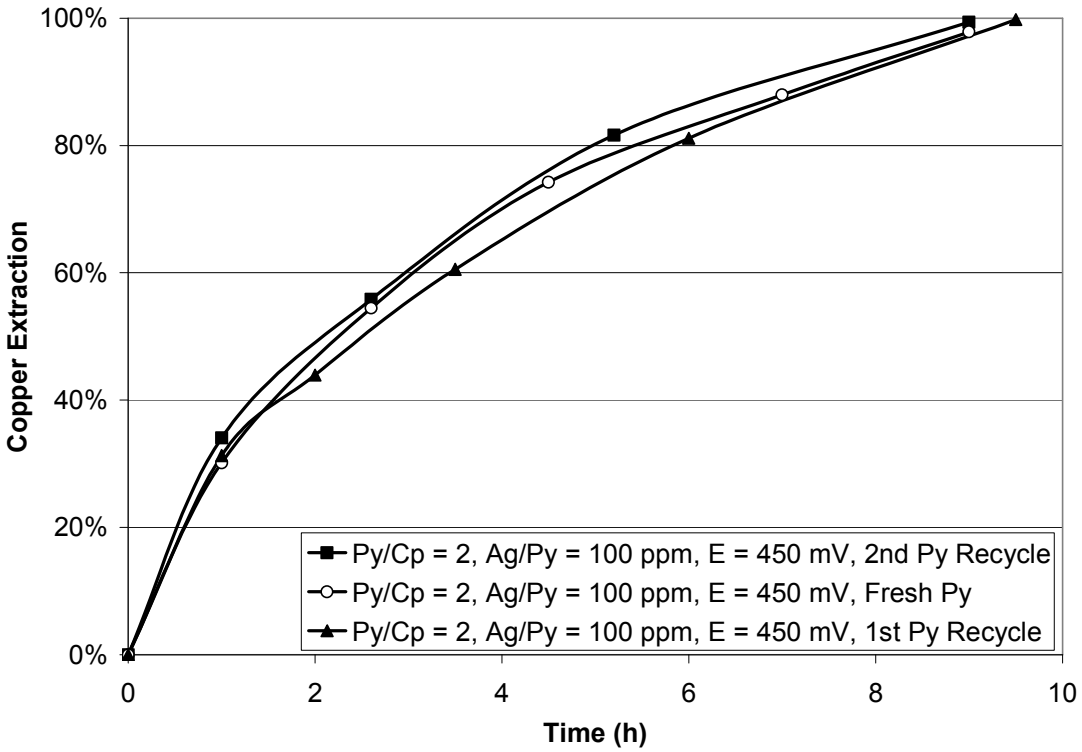

Figure 4.19 Effect of higher pulp density at a constant pyrite-to-chalcopyrite ratio of 2, an initial silver-to-pyrite ratio of 100 ppm, a potential set point of 450 mV, at 70 g/L Cu concentrate, and 80°C

The mass of copper concentrate per liter of solution was 70 g/L and the net increase in copper concentration in each test was roughly 19 g/L (ΔCu = 19 g/L). In commercial practice, following leaching and solid liquid separation, the pregnant leach solution (PLS) would be introduced to conventional solvent extraction, where each mole of copper removed from the aqueous solution would be replaced with one mole of sulfuric acid. In high copper tenor solutions, a significant amount of acid is produced which can affect the loading behaviour of the organic extractant by shifting the equilibrium toward stripping. Hence, in this process, the main factor limiting pulp density in the leach circuit is the capacity of the subsequent solvent extraction circuit.

4.3.6 Effect of Impurities Associated with Pyrite

In this section, Pyrite #2 containing only 70.8% pyrite was used to investigate the effect of impurities associated with pyrite on their effectiveness in this process.

The first test was conducted to observe the effect of adding Pyrite #2 as received on the rate of chalcopyrite leaching. This experiment was carried out at a pyrite-to-chalcopyrite ratio of 2, a silver-to-pyrite ratio of 100 ppm, and a solution potential set point of 450 mV. Upon completion of the first test, the supernatant solution was decanted from the reactor while retaining the residue. Then, new solution containing the desired amounts of sulfuric acid was added. This new solution was heated to 80°C and then the required amounts of ferric and ferrous sulfate and a new charge of fresh concentrate plus an additional 5% of the silver-enhanced pyrite were added. The results are shown in Figure 4.20.

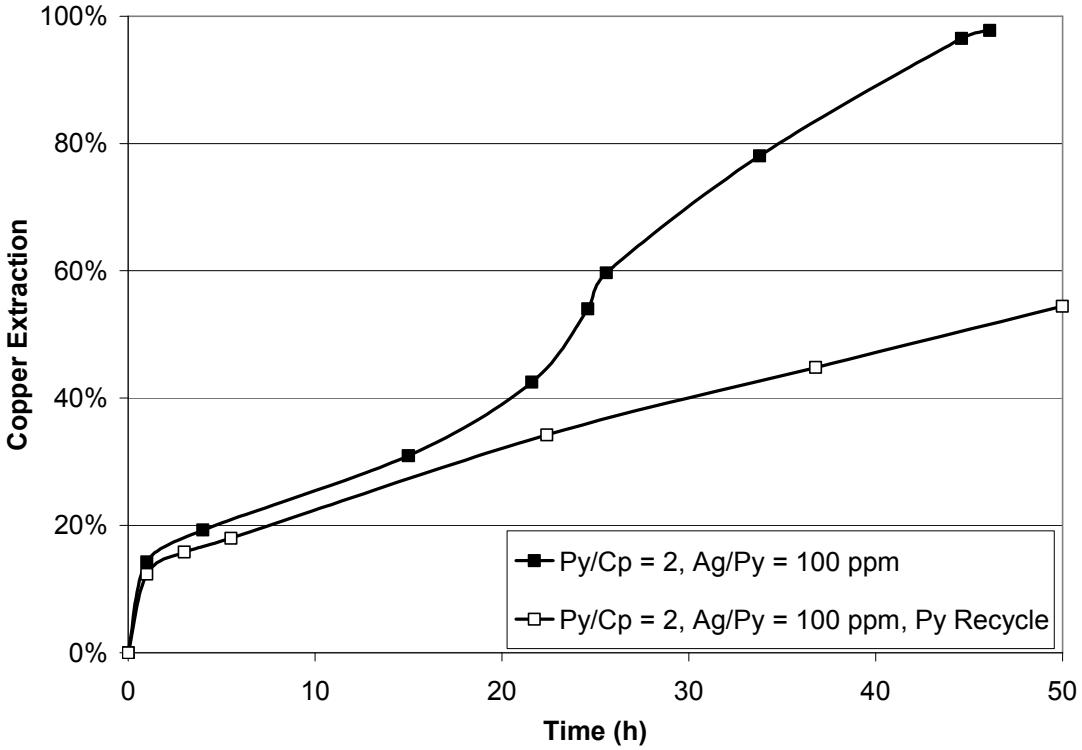

Figure 4.20 Effect of addition of Pyrite #2 at a pyrite-to-chalcopyrite ratio of 2, an initial silver-to-pyrite ratio of 100 ppm, a potential set point of 450 mV, 70 g/L Cu concentrate, and 80°C

Figure 4.20 indicates that the complete copper extraction using freshly silver-enhanced pyrite was obtained in about 50 hours. Although the initial rates of copper extraction in both tests were similar, the rate increased rapidly after 25 hours in the presence of the freshly silver-enhanced pyrite. This increase was not observed in the presence of recycled pyrite. Figure 4.20 shows that only 54% copper extraction was obtained after 50 hours.

As mentioned, Pyrite #2 contains only about 70.8% pyrite. When Pyrite #2 is pretreated with silver ions, some of the silver ions can be adsorbed/ reacted into/ with the impurities instead of pyrite. Hence, the ratio of silver to pyrite can be lower than 100 ppm. Adsorption of silver to these impurities, by itself, does not have any beneficial effect on accelerating the rate of copper extraction. The

slower initial rate of chalcopyrite leaching, compared to the results shown earlier in this chapter, might be explained by the lower ratio of silver to pyrite. The rapid increase in the kinetics of chalcopyrite leaching after 25 hours, shown in Figure 4.20, can be attributed to the release of silver ions from these impurities due to their dissolution in acidic ferric media. Upon release of silver ions to the solution, they may react with chalcopyrite and the rate of copper extraction increases due to the catalytic properties of silver ions. For this reason, in the first experiment, in the presence of freshly silver-enhanced pyrite, complete copper extraction was achieved. The silver ions that reacted with chalcopyrite formed silver sulfide and stayed with the chalcopyrite residue. Silver recovery from silver sulfide is not feasible under mild oxidizing conditions of the Galvanox™ process. Hence, silver ions lose their catalytic properties. This explanation is in agreement with the results of the recycle test, shown in Figure 4.20, which indicates the slow rate of leaching through the process. Due to the presence of impurities and reaction of silver ions with these impurities, silver ions did not retain their catalytic properties in the recycle test. Upon dissolution of impurities, silver ions reacted with chalcopyrite and stayed with sulfur (chalcopyrite residue) which could not be recovered directly in this process. As a result, the ratio of silver-to-Pyrite #2 in the recycle test was considerably lower than the initial ratio. The kinetics of the recycle test are almost identical to the initial rate of the first test. This rate presents the kinetics of chalcopyrite leaching in the presence of silver-enhanced pyrite at a silver-to-pyrite ratio considerably lower than 100 ppm. As discussed above, due to the presence of impurities, the ratio of silver-to- pyrite is lower than 100 ppm. Previously, it has been shown that in this process, silver-enhanced pyrite only loses about 5-10% of its catalytic properties in each leach test. Hence, by addition of 10% freshly enhanced pyrite the catalytic properties of pyrite are retained. Consequently, the rate of the recycle test, shown in Figure 4.20, is the rate of chalcopyrite leaching in the presence of silver-enhanced pyrite at a very low silver-to-pyrite ratio.

Two experiments were conducted at two ratios of pyrite to chalcopyrite. These experiments were carried out at pyrite-to-chalcopyrite ratios of 4, and 2, and a silver-to-pyrite ratio of 100 ppm. Pyrite #2 was acid washed in a concentrated sulfuric acid solution to dissolve dolomite (12.2%) associated with this pyrite sample. The results shown in Figure 4.21 indicate that the rate of chalcopyrite leaching is faster at a higher ratio of pyrite to chalcopyrite. In addition, Figure 4.21 shows that at the pyrite-to-chalcopyrite ratio of 2, although the rate of leaching was faster at the beginning, this reaction was complete after about 50 hours. In this experiment, due to removal of dolomite prior to pyrite pretreatment with silver, a large proportion of silver ions reacted with pyrite. Therefore, a rapid increase on the rate of chalcopyrite leaching was not observed in the middle of the process, unlike the results shown in Figure 4.20.

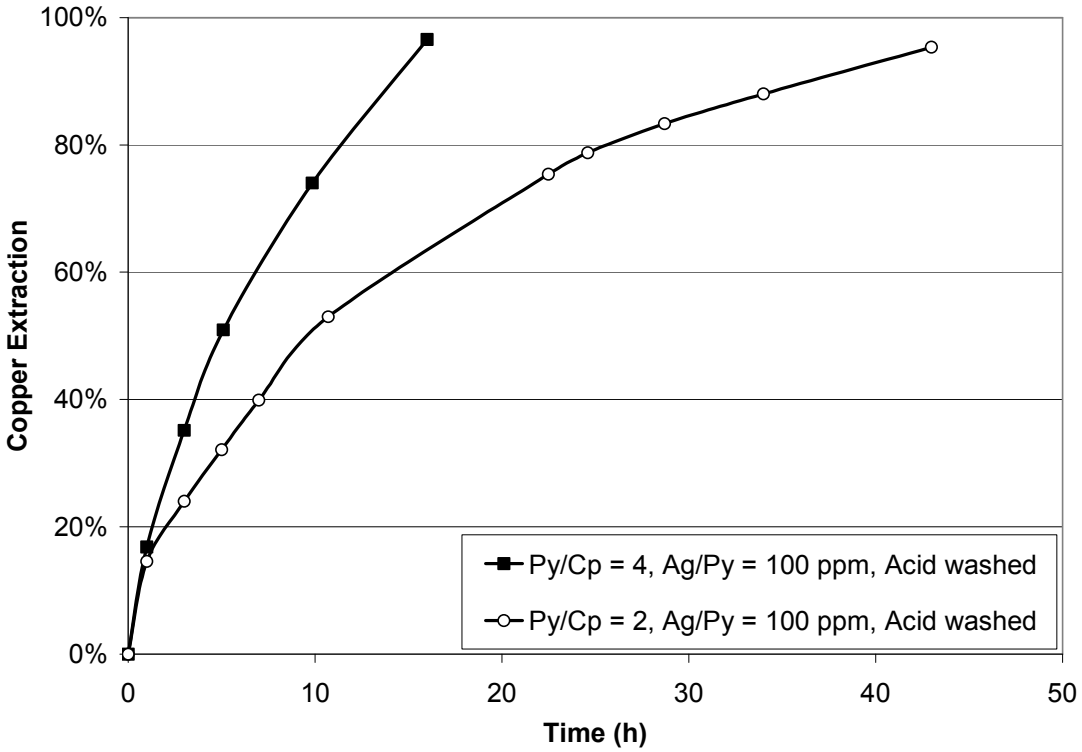

Figure 4.21 Effect of various pyrite pretreatments at a constant silver-to-pyrite ratio of 100 ppm, a potential set point of 450 mV, 70 g/L Cu concentrate , and 80°C

pH variations with time in these experiments (Figure 4.21) are shown in Figure 4.22. The results show that pH decreases during the first hour of both experiments. Based on the variation of pH at the beginning of these tests, the hypothesis was that some of the pyrite/pyrrhotite leaches quickly at the beginning of the experiment and loses its silver to the solution or chalcopyrite. Therefore, silver-enhanced pyrite does not retain its catalytic properties and silver is lost before it has been used efficiently. In previous studies, it has been shown that the rest potential of pyrrhotite is considerably lower than that of pyrite (Almeida and Giannetti, 2003; Jibiki, 1971). Hence, pyrrhotite is oxidized at 450 mV (Ag/Ag/Cl) and loses any silver associated with it.

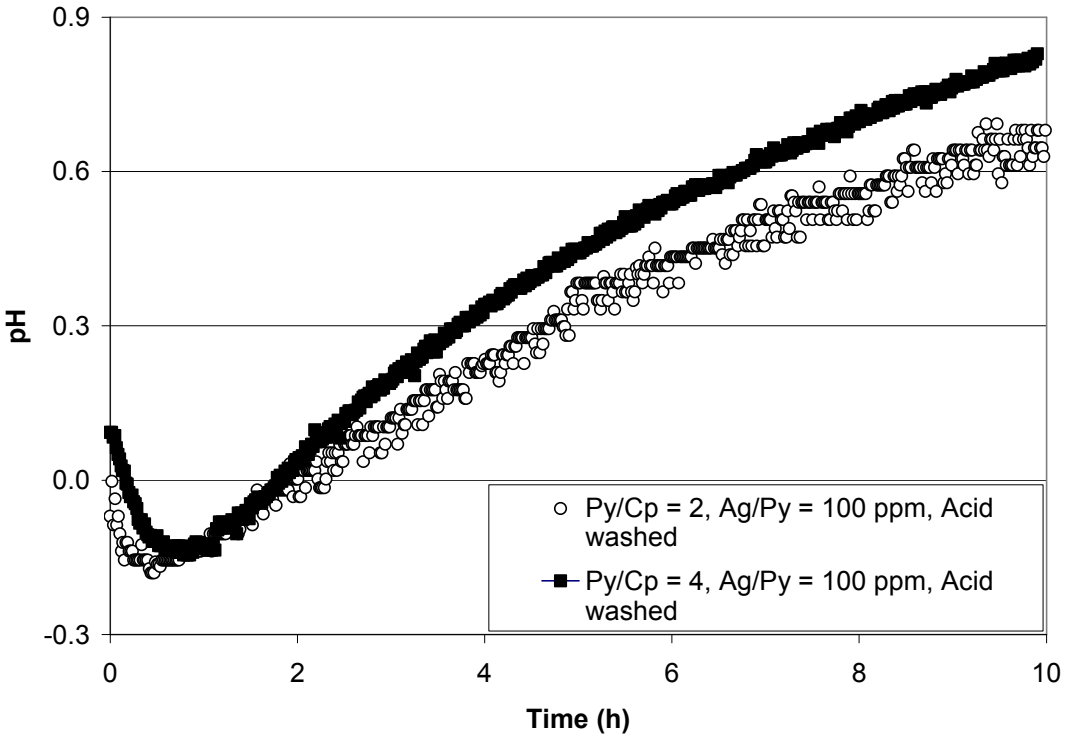

Figure 4.22 Variation of pH during the first 10 hours of chalcopyrite leaching at a constant silver-to-pyrite ratio of 100 ppm, a potential set point of 450 mV, 70 g/L Cu concentrate, and 80°C

In order to examine this hypothesis, two experiments were conducted using the same acid-washed pyrite. In these experiments, the acid treated pyrite was

introduced to the solution containing sulfuric acid, ferric and ferrous sulfate at potential 450 mV (*vs* Ag/AgCl). The decrease of pH was noted. Then after about 40 min, when the pH was almost constant, silver was added to the solution. After about 20 min, the copper concentrate was added to the reactor. Figure 4.23 clearly shows the significant improvement on the rate of copper recovery when the concentrate was added after an hour.

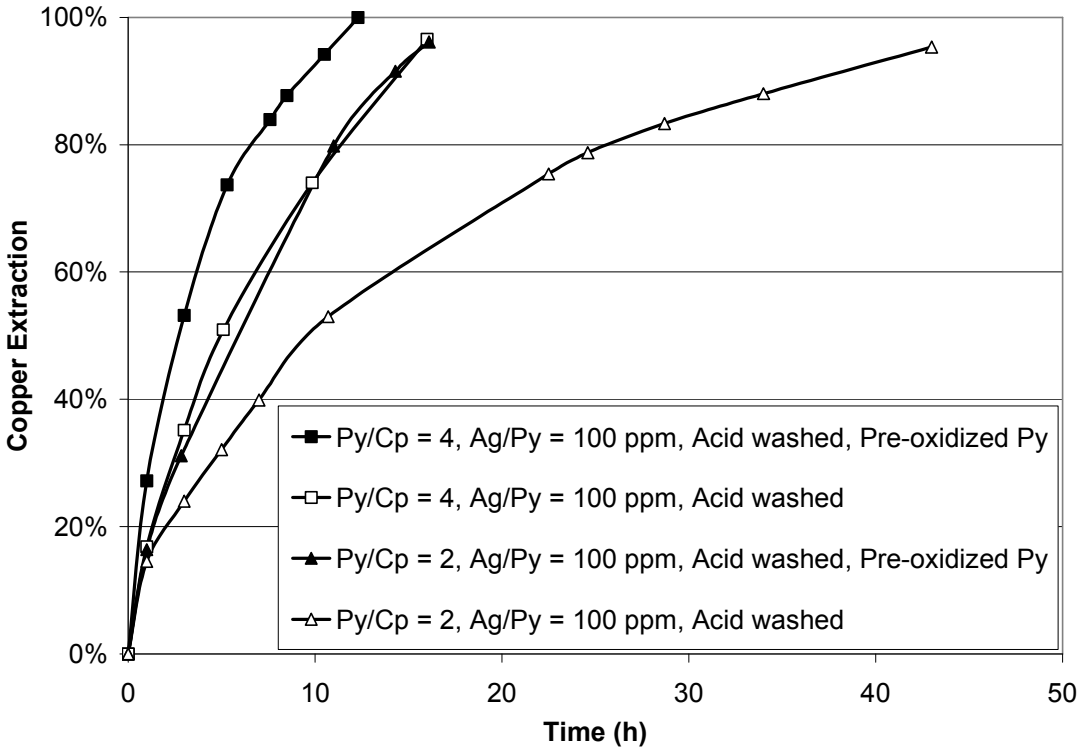

Figure 4.23 Effect of introducing a charge of copper concentrate after an hour at a constant silver-to-pyrite ratio of 100 ppm, a potential set point of 450 mV, 70 g/L Cu concentrate, and 80°C

For comparison purposes, the results of various pyrite pretreatments to eliminate impurities and enhance the catalytic properties of pyrite are all shown in Figure 4.24. These experiments were all carried out at a pyrite-to-chalcopyrite ratio of 2 and a silver-to-pyrite ratio of 100 ppm. Figure 4.24 shows the dramatic improvement on the kinetics of chalcopyrite leaching as a result of eliminating

impurities and oxidizing the easily leached pyrite and pyrrhotite prior to the treatment with silver ions.

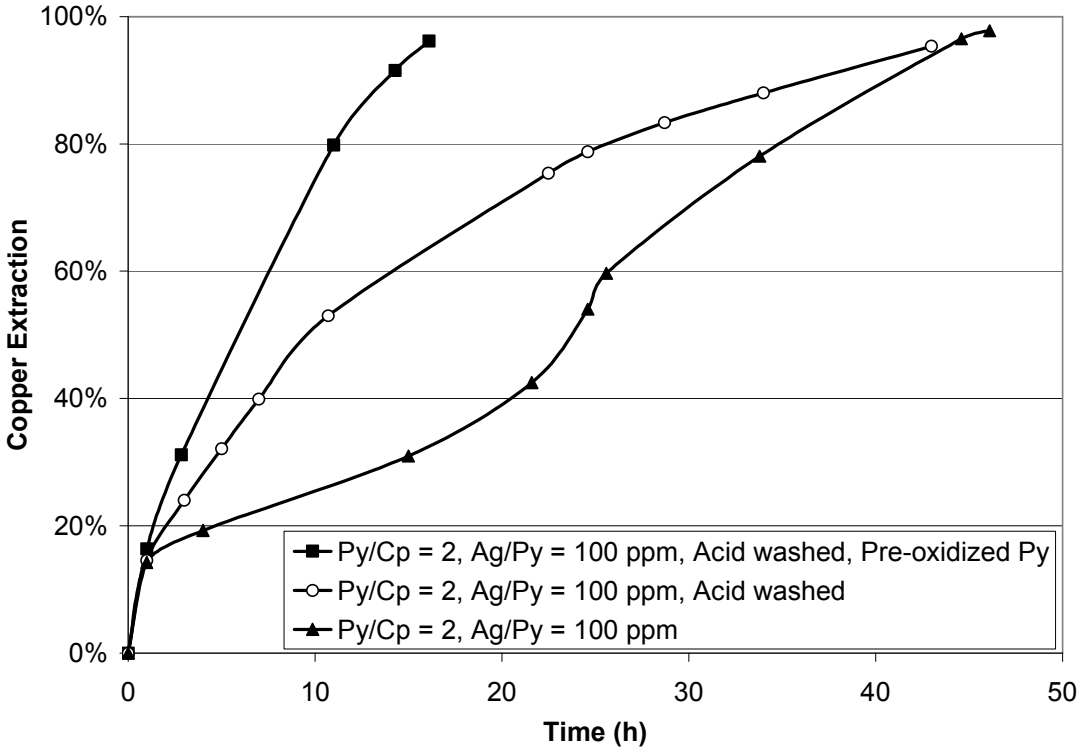

Figure 4.24 Effect of various pyrite pretreatments on the rate of copper recovery at a constant silver-to-pyrite ratio of 100 ppm, a potential set point of 450 mV, 70 g/L Cu concentrate, and 80°C

Figure 4.25 shows the results of copper extraction at three different ratios of pyrite to chalcopyrite: 2, 4, and 6. In all of these experiments, copper concentrate was added after one hour. Figure 4.25 shows rapid copper extraction at all three ratios, especially at pyrite-to-chalcopyrite ratios of 4 and 6.

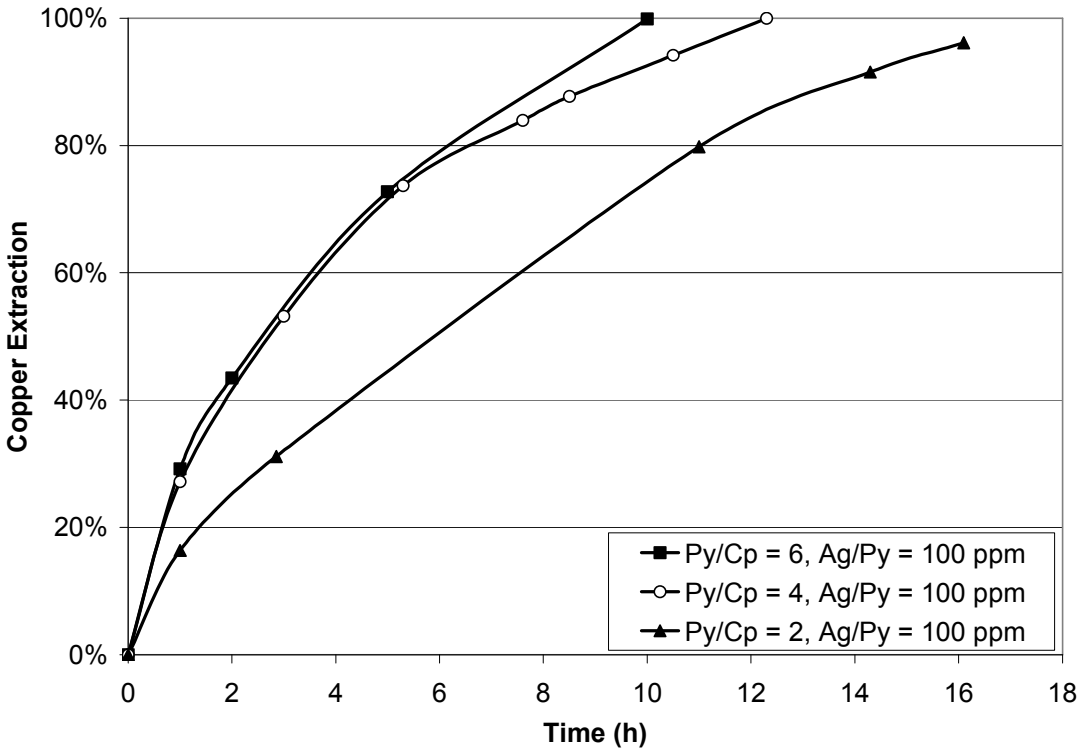

Figure 4.25 Effect of pyrite-to-chalcopyrite ratio where copper concentrate was added after one hour. At a constant silver-to-pyrite ratio of 100 ppm, a potential set point of 450 mV, 70 g/L Cu concentrate, and 80°C

Figure 4.20 shows that Pyrite #2 has not been successfully recycled. It was important to evaluate the feasibility of this pyrite after the pretreatments described above. Therefore, upon completion of the first test at the pyrite-to-chalcopyrite ratio of 6, and silver-to-pyrite ratio of 100 ppm, the solid residue was recycled to the subsequent test to treat a new charge of copper concentrate. The results are shown in Figure 4.26.

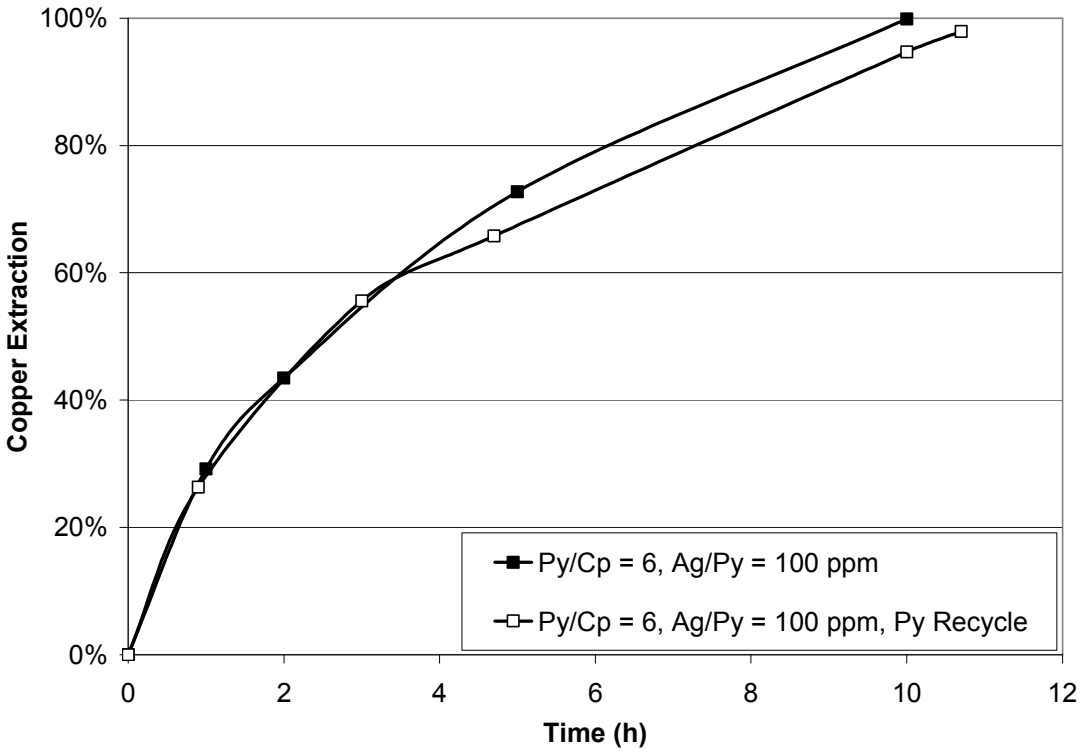

Figure 4.26 Effects of recycling Pyrite #2 after required pretreatment at a pyrite-to-chalcopyrite ratio of 6, a silver-to-pyrite ratio of 100 ppm, a potential set point of 450 mV, 70 g/L Cu concentrate, and 80°C with additional 5% silver-enhanced pyrite in the recycle test

Figure 4.26 indicates that the recycled pyrite with the addition of 5% freshly silver-enhanced pyrite is as effective as freshly enhanced pyrite. Hence, there is only a minor loss of catalytic ability after recycling the pyrite. The addition of 5% silver-enhanced pyrite to each recycle test corresponds to the addition of 91 mg of silver per kg of contained copper at a pyrite-to-chalcopyrite ratio of 6:1.

These results confirm the importance of controlling the conditions of the system, such that loss of silver from pyrite is minimized. This observation is in agreement with the previous discussion regarding the solution potential control at the level lower than the rest potential of pyrite to avoid its oxidation and the loss of silver from pyrite.

4.3.7 Effects of Chloride Concentration

The solubility of silver chloride is very low (K_{sp} = 1.8×10^{-10}). It is known that dissolved chloride up to about 200 ppm is often found in hydrometallurgical process waters, and that chloride can precipitate silver as silver chloride, due to its low solubility limit. Thus, it was of interest to evaluate the effects of chloride concentration on the silver-enhanced catalyzed leaching process.

Leaching tests were carried out using a pyrite-to-chalcopyrite ratio of 2, a silver-to-pyrite ratio of 100 ppm, and dissolved chloride concentrations of 0, 50, 200, and 1000 ppm. The redox potential was controlled at 450 mV. To examine the feasibility of recycling the pyrite, upon completion of the first tests, the supernatant solution was decanted from the reactor while retaining the residue. The new leaching solution was added to the reactor and it was heated to 80°C. Then, the 10% make up of silver-enhanced pyrite and a new charge of fresh concentrate were introduced the leach slurry. The results of leaching experiments in the presence of freshly silver-enhanced pyrite and recycled pyrite at various chloride concentrations are shown in Figure 4.27 and Figure 4.28.

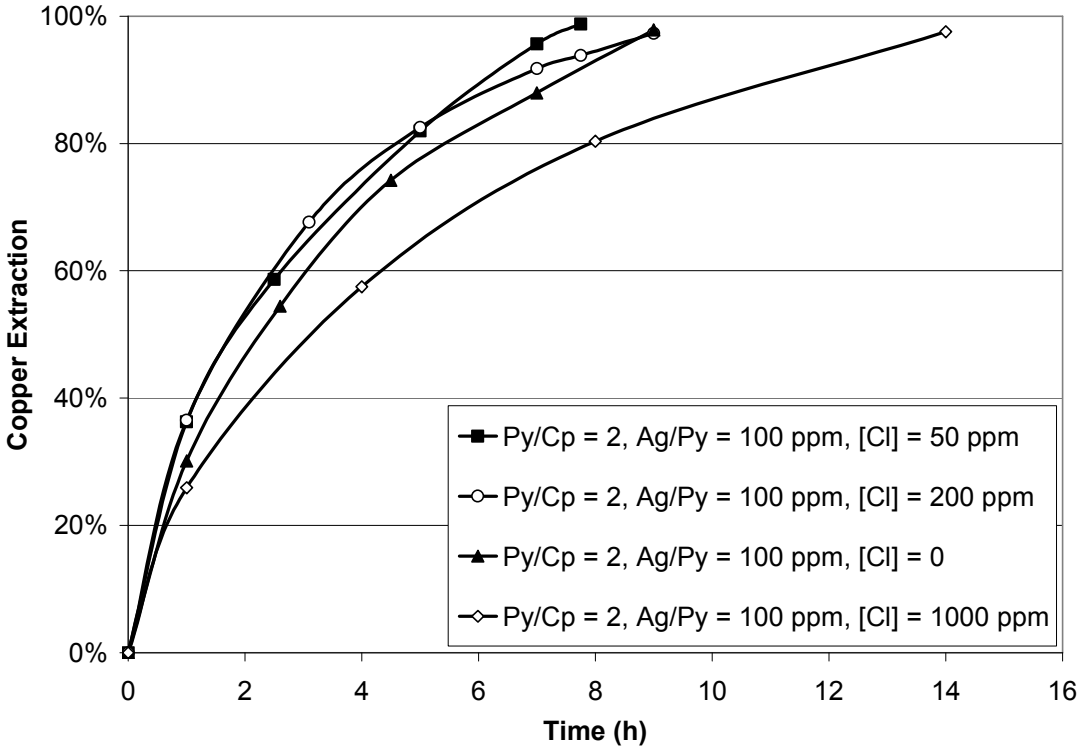

Figure 4.27 Effects of chloride concentration at a pyrite-to-chalcopyrite ratio of 2, a silver-to-pyrite ratio of 100 ppm, a potential set point of 450 mV, 70 g/L Cu concentrate, and 80°C

The results, shown in Figure 4.27, indicate that chloride concentration up to 200 ppm has no or little detrimental effect on the kinetics of chalcopyrite leaching, and chloride concentration up to 1000 ppm can be tolerated.

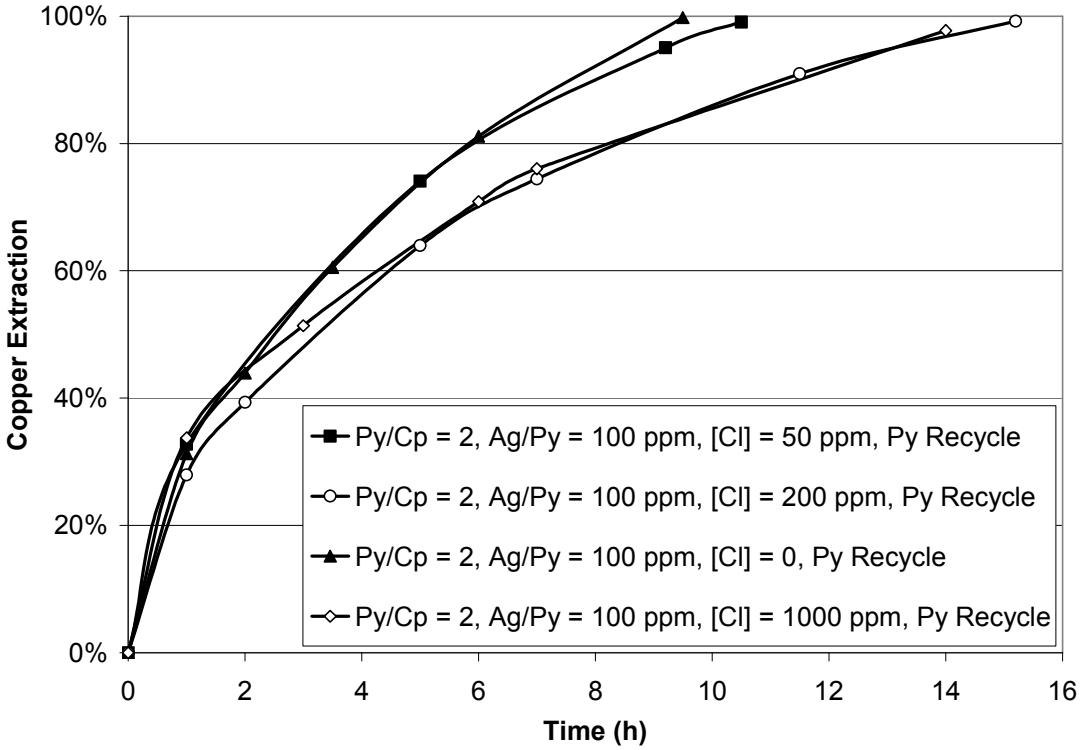

Figure 4.28 Effects of chloride concentration with recycled pyrite at a pyrite-to-chalcopyrite ratio of 2, a silver-to-pyrite ratio of 100 ppm, a potential set point of 450 mV, 70 g/L Cu concentrate, 80°C, and additional 10% silver-enhanced pyrite

Figure 4.28 shows that pyrite can be effectively and efficiently recycled to the subsequent leach tests with the addition of only 10% freshly silver-enhanced pyrite, and silver-enhanced pyrite retains its effectiveness as a catalyst upon recycle.

4.4 Conclusions

With the new process described in this chapter, the catalytic properties of pyrite are improved such that all pyrite samples accelerate the rate of copper extraction from chalcopyrite significantly. To enhance the catalytic properties of pyrite, ground samples of natural pyrite were pretreated with small amounts of silver ion

by soaking the ground pyrite in a dilute solution of soluble silver salt such as silver nitrate before introducing the pyrite into the leaching reactor. Even at room temperature, the finely divided pyrite typically adsorbs all of the silver from solution in just a few minutes. As little as 50 ppm Ag on pyrite, or 50 g Ag (about 1.5 troy ounces) per tonne of pyrite, is sufficient to ensure rapid chalcopyrite leaching kinetics in the Galvanox™ process.

In this new process, which is an improvement on the Galvanox™ process, the catalytic properties of pyrite are improved such that all pyrite samples accelerate the rate of copper extraction from chalcopyrite significantly. The effects of several variables such as mass ratio of pyrite to chalcopyrite, ratio of silver to pyrite, solution potential, and pulp density were evaluated in order to discover the optimized conditions for this process. It was observed that the rate of chalcopyrite leaching increases by increasing ratios of pyrite to chalcopyrite and silver to pyrite. Effects of solution potential on leaching kinetics were also examined. The results showed that the fastest kinetics was observed at a solution potential of 450 mV. The slower rate at higher potential was attributed to an increase in pyrite oxidation and the loss of added silver to solution. The slower rate at lower potential was attributed to a decrease in a driving force required for chalcopyrite oxidation.

The results showed that a proportion of added silver left pyrite during chalcopyrite leaching. Hence, although recycled pyrite was still an effective catalyst, the rate of reaction was slower after each recycle. It was noted that the absolute loss of silver from pyrite was almost constant regardless of the concentration of pyrite in the leach slurry or the ratio of silver to pyrite. Thus, effects of pulp density on the kinetics of chalcopyrite leaching was also examined for the purpose of reducing the relative loss of silver and maintaining the catalytic properties of silver-enhanced pyrite in subsequent leach tests. Faster kinetics and more efficient pyrite recycling were observed at higher pulp densities. These

observations were attributed to the lower relative loss of reacted silver to solution at higher pulp densities.

Under optimized conditions, it was found that the addition of as little as 60 mg of silver per kg of copper is sufficient to ensure the complete copper extraction within 15 hours of leaching and the recycled pyrite is equally as effective as freshly enhanced pyrite as a catalyst.

Effects of impurities associated with pyrite samples in the process of silver-enhanced pyrite catalyzed leaching were also investigated. It was demonstrated that even a pyrite sample with a high level of impurities could be enhanced with silver ions. However, due to the presence of impurities and possible reactions of silver ions with this species, some pretreatment steps were required to obtain the optimum catalytic properties. It was shown that the detrimental effects of impurities were eliminated when pyrite was pretreated in leach solutions containing sulfuric acid, ferric and ferrous sulfate. Hence, pretreating the recycled pyrite from the leach process with silver ions overcomes these difficulties.

Effects of chloride concentration on the kinetics of chalcopyrite leaching was studied and it was found that chloride concentration up to 200 ppm has little or no detrimental effect. At higher concentrations, the rate of the leaching reaction is slightly slower. Under these conditions, silver-enhanced pyrite retained its catalytic properties upon recycle and the addition of 10% silver-enhanced pyrite was sufficient to ensure the optimum catalytic properties of pyrite.

Chapter 5 The Role of Galena Associated with Silver-enhanced Pyrite in the Kinetics of Chalcopyrite Leaching during the Galvanox™ Process

5.1 Objectives

As described in Chapter 4, in this work, catalytic properties of pyrite have been enhanced. In spite of differences in the catalytic properties of natural pyrite from different sources, silver-enhanced pyrite samples have identical effect on chalcopyrite leaching. It has been shown that the catalytic properties of pyrite can be improved by pretreating ground samples of natural pyrite with small amounts of silver ions.

In this chapter, the morphology and elemental compositions of pyrite samples were analyzed after pretreatment with silver ions. It has been noted that silver could only be detected in association with galena. In addition, it has been reported that the dissolution of chalcopyrite is favored in the presence of galena (Nova and Gonzalez, 2006). These authors compared the electrochemical behavior of pure chalcopyrite and chalcopyrite concentrate containing galena and they observed that the dissolution current was significantly higher in the concentrate containing galena. Therefore, it was a subject of interest to examine the effect of galena on accelerating the rate of chalcopyrite leaching in both the absence and presence of pyrite and silver in the leaching slurry. Based on the detection of silver in galena, it was also important to determine whether chalcopyrite oxidation could be accelerated by pretreating galena with silver ions.

In another study (Cruz *et al*., 2005), the galvanic effects of galena and pyrite have been investigated. Previously, electrochemical studies were carried out to analyze the reactivity of pyrite associated with galena. It has been indicated that galena has negative influences on the electrochemical reactivity of pyrite. This behavior has been attributed to the lower rest potential of galena relative to the

rest potential of pyrite (Cruz *et al.*, 2005). For semiconductive minerals, contact of different minerals with dissimilar rest potentials in an oxidizing condition initiates the galvanic effect where the mineral with the higher rest potential acts as cathode and the one with lower rest potential acts as anode, with oxidation of the latter favored due to the flow of electrons from areas with lower potential to those with higher potential.

5.2 Experimental

5.2.1 Pyrite and Galena Pretreatment with Silver Ions

Pyrite and galena were pretreated with silver ions according to the procedure described in section 4.2.1.

5.2.2 Leaching Experiments

Batch leaching experiments were conducted by following the procedure explained in section 4.2.2. In all of the experiments shown in this chapter, the mass of copper concentrate in solution was 70 g/L.

5.2.3 XRD Analysis

XRD analysis was carried out on a Rigaku Rotaflex 200 diffractometer using Cu Kα radiation at 40 kV and 20 mA, scanning from 10° to 90° (2θ) with the scanning rate of 0.02° (2θ).

5.2.4 Materials

In this study, a copper concentrate containing 27% copper, two pyrite samples containing 97.6% and 99.9% pyrite from two different sources, and pure galena (99.5%) were used.

To obtain the elemental compositions of the minerals, representative samples were sent to a local commercial laboratory (International Plasma Laboratory (IPL), Richmond, BC) for Induction Coupled Plasma (ICP) analysis. The mineralogical compositions of minerals were obtained by quantitative Rietveld XRD analysis. The sample was reduced into fine powder to the optimum grain-size range for X-ray analysis (<10μm) by grinding under ethanol in a vibratory McCrone Micronizing Mill for 7 minutes. Step-scan X-ray powder-diffraction data were collected over a range 3-80°2θ with Co (Kα) radiation on a Bruker D8 Focus Bragg-Brentano diffractometer equipped with an Fe monochromator foil, 0.6 mm (0.3°) divergence slit, incident- and diffracted-beam Soller slits and a LynxEye detector. The long fine-focus Co X-ray tube was operated at 35 kV and 40 mA, using a take-off angle of 6°.

Mineralogical and elemental compositions of the copper concentrate and pyrite samples are summarized in Table 5.1 and Table 5.2, respectively. The copper concentrate was leached in the as-received condition. A Malvern Mastersizer was used to obtain particle size distributions of the samples. The copper concentrate and galena were not ultrafine, with an 80%-mass-passing size (P_{80}) of 46 μm and 51 μm. The pyrite particles were considerably larger, with a P_{80} of 290 μm, giving the consistency of fine sand.

Table 5.1 Rietveld XRD analysis of copper concentrate and pyrite samples

Mineral	Ideal Formula	Copper Conc (%)	Pyrite #1 (%)	Pyrite #4 (%)	Galena (%)
Pyrite	FeS_2	15.9	97.6	99.9	—
Chalcopyrite	$CuFeS_2$	78	—	—	—
Galena	PbS	—	—	—	99.5
Quartz	SiO_2	1	0.6	—	—
Biotite	$K(Mg,Fe^{2+})_3AlSi_3O_{10}(OH)_2$	1.8	—	—	—
Dolomite	$CaMg(CO_3)_2$	1.1	—	—	—
Plagioclase	$NaAlSi_3O_8 – CaAl_2Si_2O_8$	2.2	—	—	—
Anhydrite	$CaSO_4$	—	1.8	—	—

Table 5.2 Elemental analysis of copper concentrate and pyrite samples

Element	Copper Conc	Pyrite #1	Pyrite #4	Galena
Cu	27.00 %	0.13 %	44 ppm	22 ppm
Fe	31.14 %	45.43 %	46.51 %	0.1 %
S	36.70 %	52.62 %	53.40 %	13.4 %
Mg	0.27 %	0.04 %	—	—
Co	0.16 %	—	20 ppm	—
Pb	—	0.14 %	< 2 ppm	86.2 %
As	130 ppm	—	6 ppm	—
Ag	15.5 ppm	21 ppm	1.4 ppm	7.7 ppm
Ca	0.47 %	0.56 %	0.03 %	0.03 %
Al	0.51 %	0.02 %	—	0.03 %
Zn	0.01 %	—	159 ppm	27 ppm
Si	1.14 %	0.28 %	—	—

5.3 Results and Discussion

A number of experiments were conducted in order to evaluate the effects of addition of silver-enhanced pyrite with and without galena on the kinetics of chalcopyrite leaching. Table 5.3 presents a matrix, containing the experimental conditions of all the tests.

Table 5.3 Experimental conditions

Test ID	Cu Concentrate Mass (g)	Pyrite Mass (g)	Galena Associated with Py (g)	Galena Mass (g)	Ag Concentration of Pyrite (ppm)	Ag (g)/ kg Cu	Comments
T1	105	0	0	0	0	0	
T2	105	175	0.283	0	0	0	
T3	105	17.5	0.0283	0	0	0	used residue* from T2
T4	105	175	0	0	0	0	
T5	105	17.5	0	0	0	0	used residue* from T4
T6	105	175	0.283	0	100	0.61	
T7	105	17.5	0.0283	0	-	0.061	used residue* from T6
T8	105	175	0	0	100	0.61	
T9	105	17.5	0	0	-	0.061	used residue* from T8
T10	105	0	0	0.283	0	0	
T11	105	0	0	81.88	0	0	
T12	105	0	0	0.283	0	0.61	
T13	105	0	0	0.0283	-	0.061	used residue from T12
T14	105	0	0	0	0	0.51	14.5 g silver were added
T15	105	0	0	0	0	0.051	used residue from T14
T16	105	175	0	2.26	-	0.61	
T17	105	17.5	0	0.226	-	0.061	used residue* from T14
T18	105	0	0	0	0	0	added 5 mg silver after 140 hours
T19	105	0	0	0	0	0.61	

*Residue contained both copper concentrate residue and pyrite

The first test was conducted in order to observe the rate of copper extraction in ferric/ferrous sulfate solution at 450 mV (all redox potentials are reported *vs* the KCl-saturated Ag/AgCl reference electrode) in the absence of added pyrite. The solution potential set point of 450 mV was selected based on the results obtained earlier in this work (Chapter 4) which showed that the maximum copper extraction was attained at this potential. Very slow kinetics and incomplete copper extraction under these conditions was observed as shown in Figure 5.1.

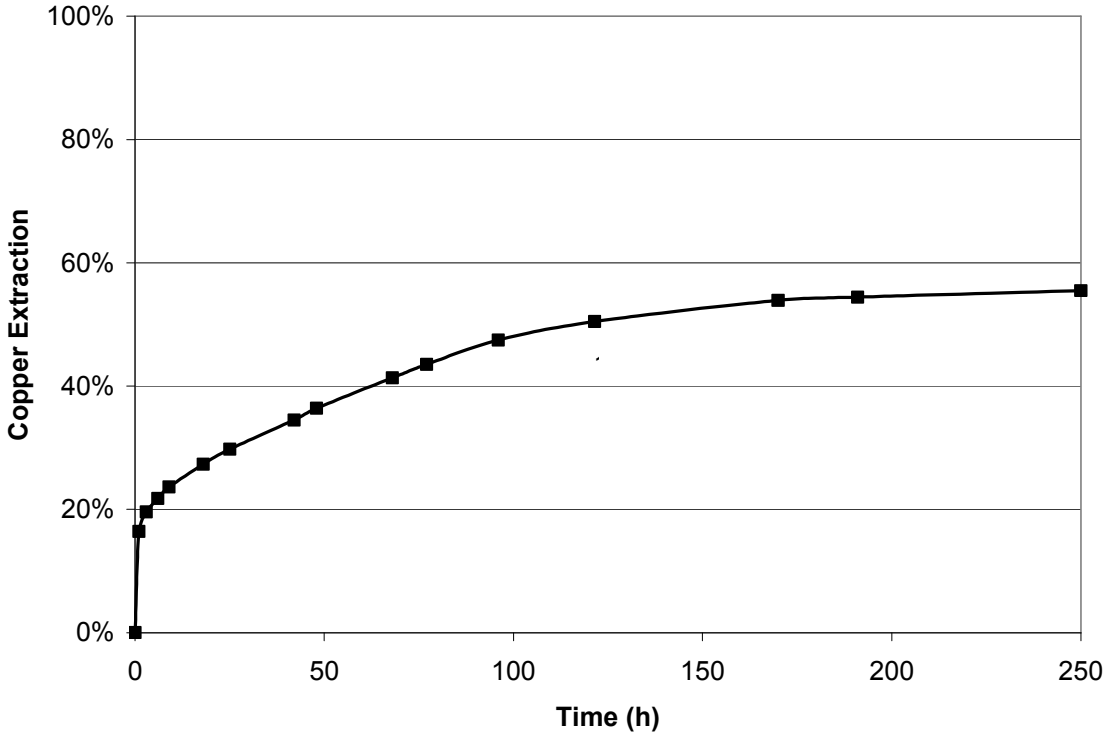

Figure 5.1 Chalcopyrite leaching in ferric sulfate media at a potential set point of 450 mV and 80°C (T1)

Two tests were conducted to examine the effect of adding two pyrite samples on the kinetics of chalcopyrite leaching. Upon completion of the first tests, recycle tests were conducted to examine the effectiveness of recycled pyrite. As shown in Figure 5.2, both added pyrite samples accelerated the rate and extent of copper extraction, but relatively long leach times were still required.

In order to enhance the catalytic properties of pyrite, samples were pretreated with silver ions. The finely divided pyrite reacted with all of the silver from solution in just a few minutes. Leaching experiments were conducted at a pyrite-to-chalcopyrite ratio of 2, a silver-to-pyrite ratio of 100 ppm, and a solution potential set point of 450 mV (T6 and T8). The effectiveness of recycling pyrite was also examined (T7 and T9). In the recycle tests, solid residues from the previous tests were recycled with fresh charges of copper concentrate and an additional 10% of the silver-enhanced pyrite (17.5 g) to make up for any silver and pyrite lost during the first experiments. All results are presented in Figure 5.2.

Obviously, a dramatic improvement in the leaching kinetics of chalcopyrite was observed as a result of pretreating pyrite with minor amounts of silver ions. The morphology and elemental composition of pyrite after pretreatment with silver ions were studied using a Hitachi S-3000N Scanning Electron Microscope (SEM). Energy Dispersive X-Ray spectroscopy (EDX) was used to determine the chemical composition of samples. The main purpose of this analysis was to detect silver on pyrite samples.

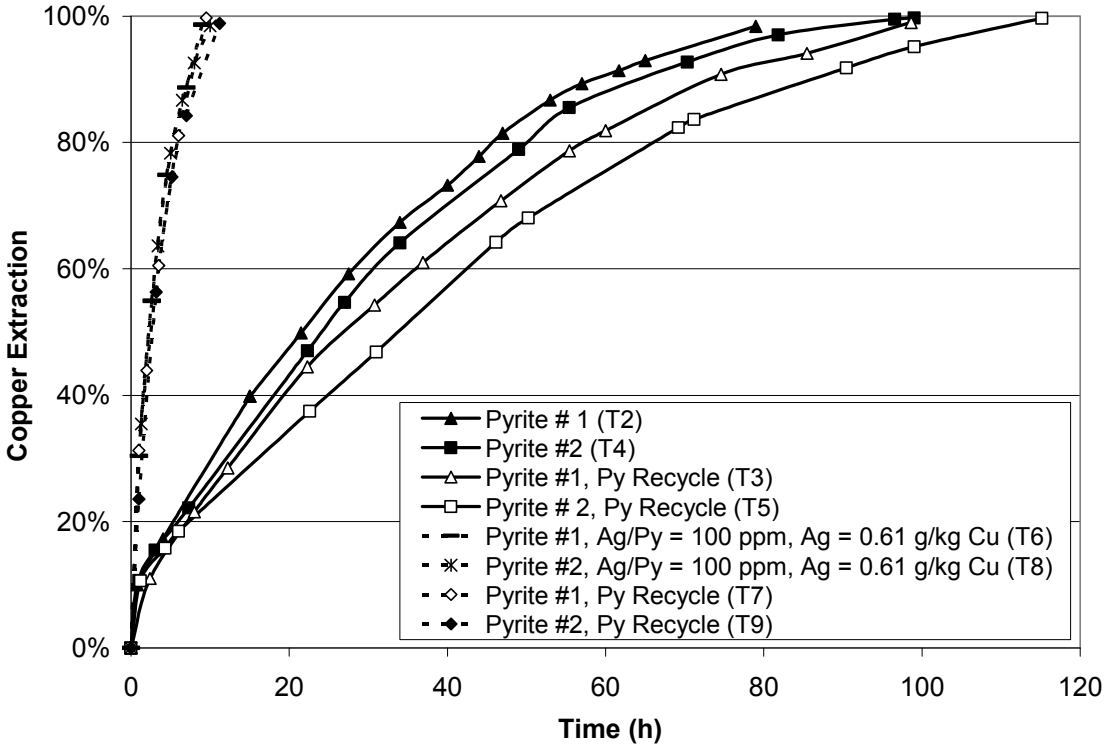

Figure 5.2 Effect of addition of pyrite (T2 and T4), silver-enhanced pyrite at a silver-to-pyrite ratio of 100 ppm (T6 and T8), and the recycled pyrite (T3, T5, T7, and T9) on copper extraction using two different pyrite samples at a potential set point of 450 mV and 80°C

(a)

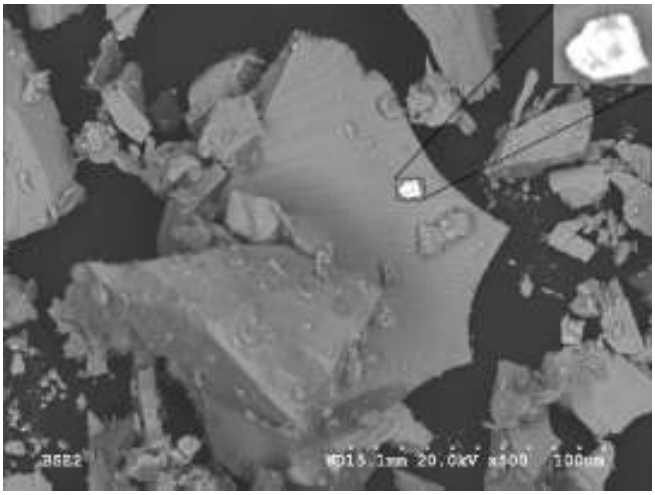

(b)

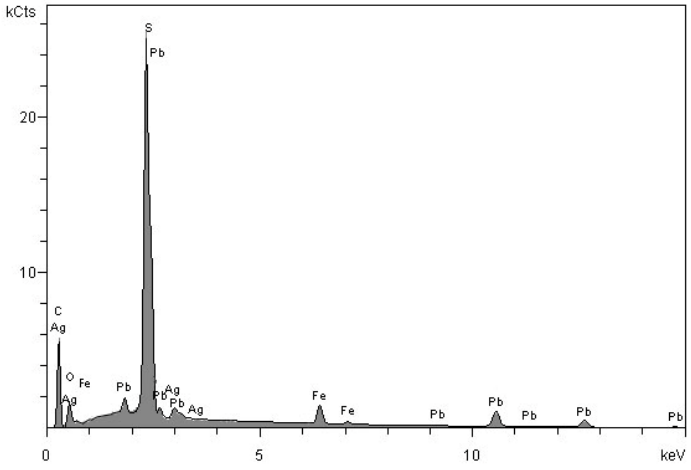

Elements	Concentration (wt%)
Carbon	49.56
Oxygen	11.81
Sulfur	8.60
Iron	3.87
Silver	2.17
Lead	23.99

(c)

Figure 5.3 (a) SEM micrographs, (b) EDX analysis, and (c) elemental analyses of the selected area of Pyrite #1 pretreated with silver at a silver-to-pyrite ratio of 100 ppm

SEM and EDX analyses of Pyrite #1 are shown in Figure 5.3. According to the EDX analysis, shown in Figure 5.3 (b) and Figure 5.3 (c), the detected silver was mostly associated with lead. Silver was not detected on Pyrite #2 which had a very low amount of lead (Figure 5.4). It is important to note that the concentration of silver on the pyrite sample was very low (100 ppm) and this value is lower than the detection limit of EDX. Hence, silver could only be detected on those areas where the silver concentration was higher than 1%.

It might be hypothesized that when a pyrite sample includes some amount of lead mineral, silver is mostly adsorbed to the lead mineral rather than pyrite. Hence, it was important to examine the effects of galena with and without added silver on the kinetics of chalcopyrite leaching.

Two experiments were conducted to study the effects of galena at two different concentrations. The amount of galena associated with Pyrite #1 was obtained and corresponded to 0.283 g ([239.26 (g/mol) / 207.2 (g/mol) × 0.0014 g / g × 175 g]) at a pyrite-to-chalcopyrite ratio of 2. Then, the same amount of galena was added but with no pyrite (T10). Another test was also conducted at a higher ratio of galena to chalcopyrite; specifically, a galena-to-chalcopyrite ratio of 1 (T11). The results, shown in Figure 5.5, clearly indicate that galena has no effect on the kinetics of chalcopyrite leaching.

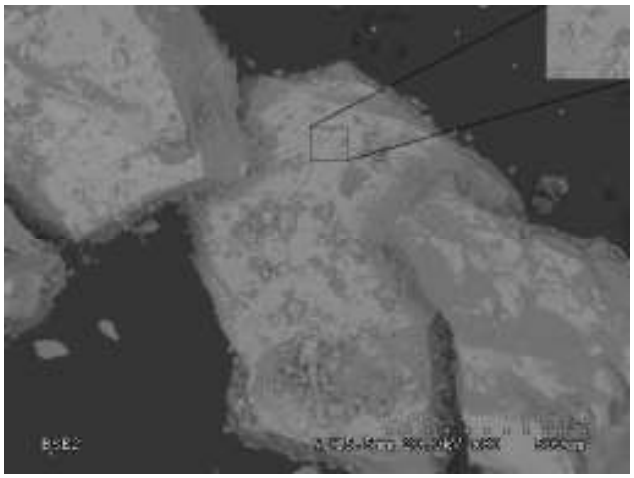

(a)

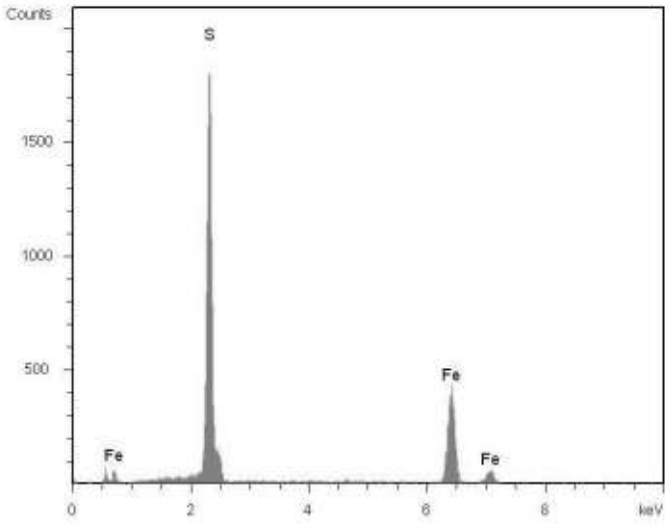

(b)

Elements	Concentration (wt%)
Sulfur	51.49
Iron	48.51

(c)

Figure 5.4 (a) SEM micrograph (b) EDX analysis (c) Elemental analysis of selected area of Pyrite #2 pretreated with silver at a silver-to-pyrite ratio of 100 ppm

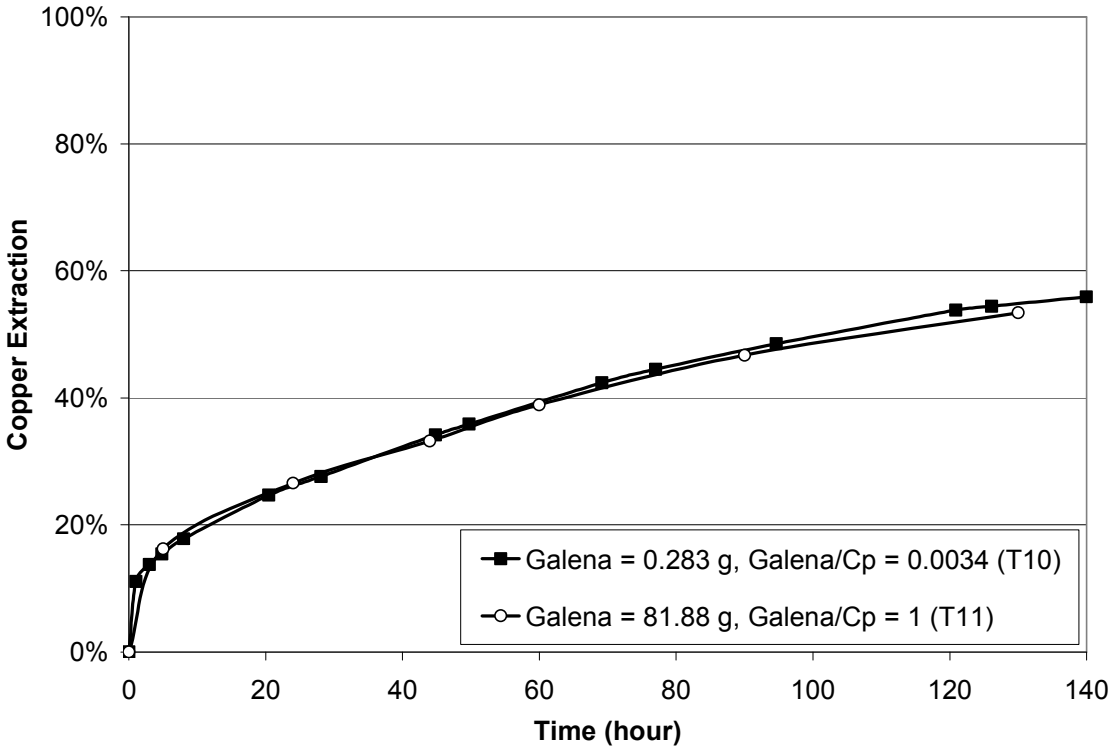

Figure 5.5 Effect of galena addition on copper extraction at two different galena to chalcopyrite ratios of 0.0034 (T10) and 1 (T11) at a potential set point of 450 mV and 80°C

In one experiment, the same amount of galena that was present in Pyrite #1 with the same amount of added silver was introduced into the reactor (without pyrite) (T12). After pretreating galena with silver for 30 minutes, a charge of copper concentrate was added. Upon completion of the first test, the residue was collected and recycled into the subsequent test to recover copper from a new charge of copper concentrate (T13). The results are shown in Figure 5.6 and indicate that the rate of copper extraction has been accelerated by the addition of silver. However, the copper extraction in the presence of the recycled residue was considerably slower than the first test, indicating that silver in the leaching residue does not maintain its catalytic properties. The results of recycling the residue in Figure 5.6 shows that after about 40 hours, the rate of reaction gradually increases. Silver mainly remains in the residue in the form of Ag_2S

particles embedded in elemental sulfur. This silver cannot be recycled directly; hence it does not maintain its catalytic properties. The EDX analysis of the residue shown in Figure 5.9 also indicated the presence of silver on the surface of lead mineral (mostly anglesite). The acceleration of the rate of chalcopyrite leaching after 40 hours is attributed to the gradual dissolution and release of silver ions from lead mineral to the solution. This would increase the availability of silver ions in the solution which would also enhance their catalytic properties. It is also important to note that unlike recycling the pyrite residue, recycling the lead residue is not a convenient process step. Due to the reaction of galena with sulfuric acid in the oxidizing condition of the experiment, fine particles of anglesite are formed. Separation of these fine particles from the chalcopyrite residue (mainly sulfur) and recycling them to the subsequent test cannot be achieved conveniently.

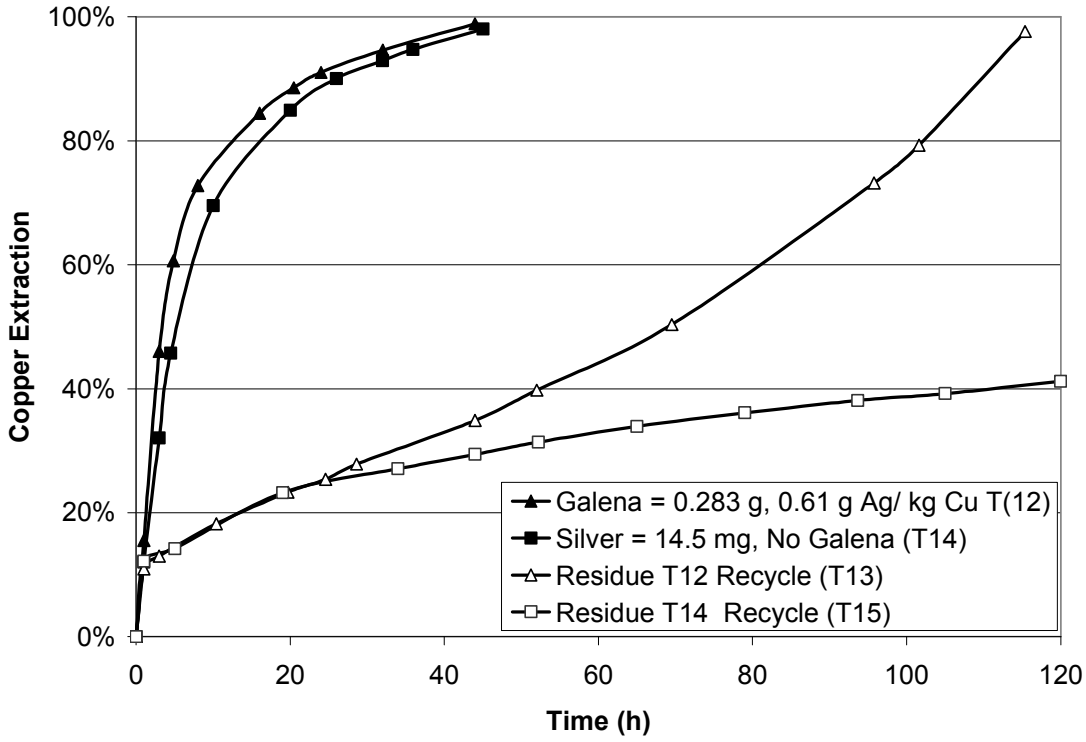

Figure 5.6 Effect of silver-pretreated galena (T12), silver (T14), recycled galena (T13), and recycled silver residue (T15) at a potential set point of 450 mV and 80°C

5.3.1 Interaction of Silver with Galena

In order to understand the effect of added silver and galena on the rate of leaching, the rate and extent of the interaction of silver with galena were examined. 2 g of galena were pretreated with silver in solutions containing silver in its soluble form at different silver concentrations. The required amounts of silver were added to the solutions to obtain a silver to galena ratio of 100 ppm, 1000 ppm, 5000 ppm, and 10,000 ppm if all the silver ions are reacted with galena. In this experiment, silver could either exist in the solution or on galena samples. Hence, the silver concentration on galena was determined by following and analyzing the silver concentration in the aqueous phase at various time intervals as described earlier. Galena was added one second after starting the experiment (i.e. at time t = 0, galena had not yet been introduced to the system). Given these conditions, $[Ag]_t/[Ag]_0 = 1$ at the beginning of the experiment where $[Ag]_0$ and $[Ag]_t$ represent the initial and instantaneous silver concentrations in solution, respectively. The results are shown in Figure 5.7.

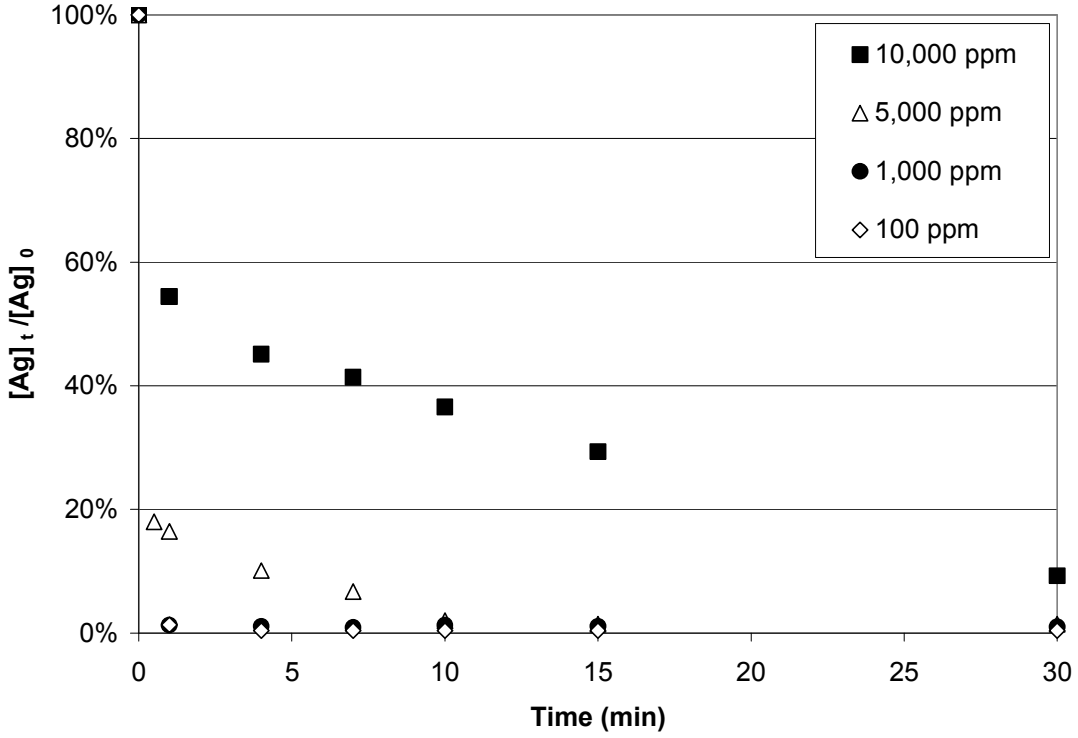

Figure 5.7 Rate of interaction of silver ions with galena at various silver concentrations

Figure 5.7 shows very rapid interaction of silver ions with galena and indicates a high affinity for silver adsorption. After one minute at maximum silver to galena ratios of 100 ppm and 1000 ppm, almost no silver was detected in the solution. At 5000 ppm, complete adsorption of silver onto galena occurred after about 30 min. At 10000 ppm, adsorption was incomplete even after 30 minutes.

$[Ag]_t/[Ag]_0$ attained values of 16.44% and 54.42% after one minute at maximum silver concentrations of 5000 ppm and 10000 ppm, respectively. Assuming homogeneous distribution of silver on galena, these values are equivalent to silver to galena ratio of 4178 ppm (5000 × [100% − 16.44%]) and 4558 ppm (10000 × [100% − 54.42%]), suggesting that this particular galena sample adsorbed silver to a concentration of roughly 4600 ppm very rapidly (in less than one minute).

In the experiment shown in Figure 5.6 (T12), 0.283 g of galena were pretreated with 17.5 mg silver and after 30 minutes copper concentrate was added. This pretreatment scenario was investigated separately, with solution samples taken at various time intervals. The results are shown in Figure 5.8. The results indicate that in the experiment with 0.283 g galena, $[Ag]_t/[Ag]_0$ is 92.64% after one minute. This is equivalent to a silver concentration of 4551 ppm ([17.5 mg / 0.283 g] × 1000 g/kg × [100% − 92.64%]) on galena. This concentration increased to 10593 ppm ([17.5 mg / 0.283 g] × 1000 g/kg × [100 − 82.87%]) and then became constant. This value probably represents the maximum amount of silver that can be adsorbed onto the galena. Therefore, 14.5 mg (82.87% × 17.5 mg) of the added silver were still dissolved in the solution at the beginning of the leach test (T12) shown in Figure 5.6.

Another experiment was conducted and 14.5 mg silver was added in the absence of galena (T14). After completion of the first test, the residue was recycled (T15). The results are shown in Figure 5.6. The results indicate that the rate of copper extraction in experiment T12 and T14 are almost identical.

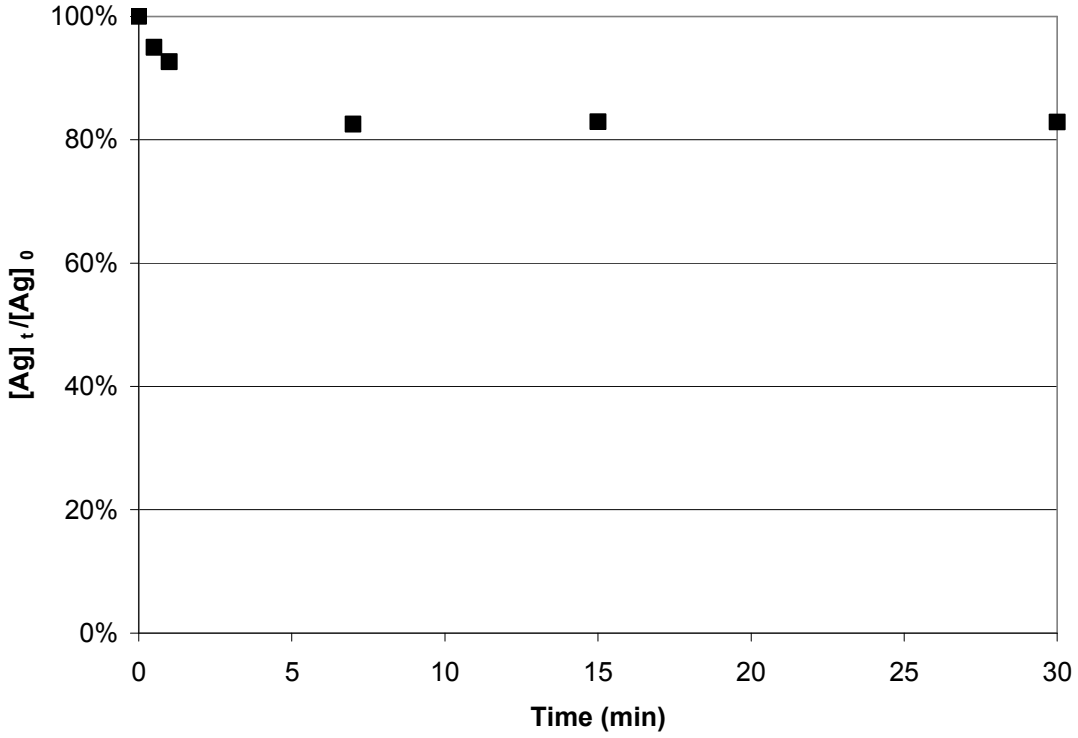

Figure 5.8 Rate of interaction of 17.5 mg silver ions with 0.283 g galena

Considering this analysis and the results of adding silver in the absence of galena in test T14, clearly, the increased rate of chalcopyrite leaching in the presence of galena and silver in test T12 is due to the direct catalytic effect of silver ions on the rate of chalcopyrite leaching. Therefore, unlike pyrite, galena samples pretreated with silver ions have no beneficial effect on the kinetics of chalcopyrite leaching.

The rapid interaction of silver with galena observed in this study is in agreement with previous studies by Scaini *et al*. (1995, 1997), who report the rapid interaction of silver ions with galena to form metallic Ag^0 and Ag_2S according to the following reactions:

$$PbS + 2\ Ag^+ = Ag_2S + Pb^{2+} \qquad (5.3.1)$$

$$2\ PbS + 10\ Ag^{+} + 4\ H_2O = 2\ Pb^{2+} + Ag_2S + 8\ Ag^{0} + SO_4^{2-} + 8\ H^{+} \quad (5.3.2)$$

The morphology and elemental compositions of the leach residues were analyzed. Samples mounted in epoxy were polished with 1200 grit SiC (silicon carbide) and rinsed with water to reveal cross sections. Figure 5.9 shows the morphology of chalcopyrite residue and galena after leaching (T12). The results shown in these micrographs indicate the preferential adsorption of silver onto the lead compound rather than the sulfur residue.

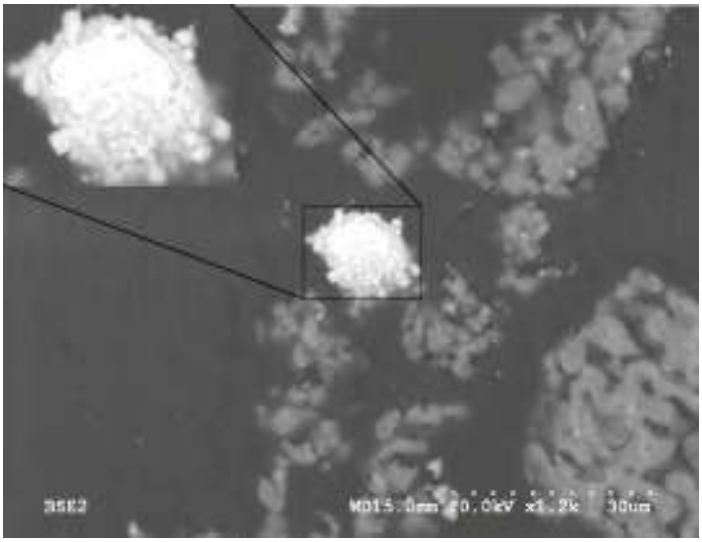

(a)

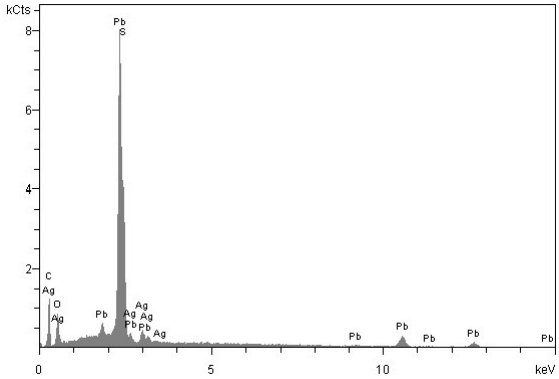

(b)

Elements	Concentration (wt%)
Carbon	37.45
Oxygen	21.55
Sulfur	8.23
Silver	1.67
Lead	31.11

(c)

Figure 5.9 (a) SEM micrograph (b) EDX analysis (c) Elemental analysis of selected area of completely leached chalcopyrite in the presence of galena and silver (T12)

In addition, X-Ray Diffraction (XRD) analysis was performed on the solid residue of reacted chalcopyrite in the presence of galena (T11). The diffraction pattern was compared with the XRD of the galena samples used in these experiments. The results are shown in Figure 5.10.

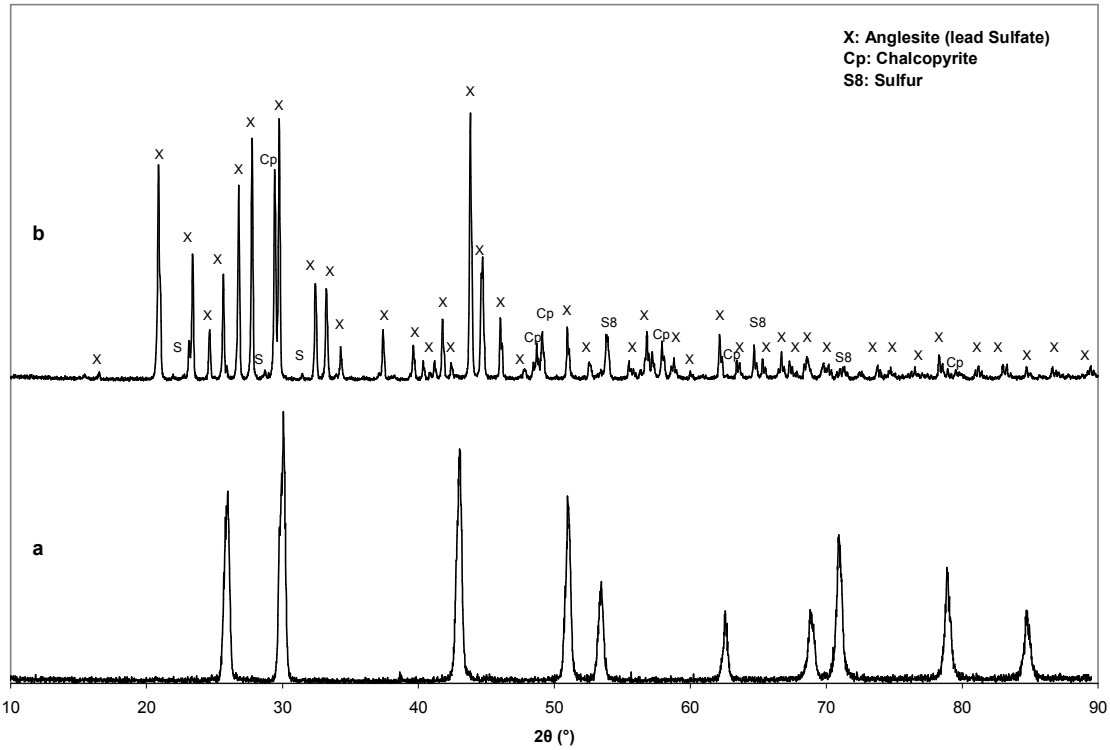

Figure 5.10 XRD patterns of (a) the galena sample and (b) reacted chalcopyrite concentrate (T11)

The XRD pattern shown in Figure 5.10(b) reveals several new peaks. These peaks (denoted “X”) match well with anglesite (lead sulfate). None of the galena peaks, presented in Figure 5.10(a), were observed on the XRD pattern of the residue after the leaching experiment. This analysis indicates that due to the oxidizing condition of the experiment, galena was transformed into anglesite according to the following reaction:

$$PbS + {}^{1}/_{2}\,O_2 + H_2SO_4 = PbSO_4 + S^0 + H_2O \qquad (5.3.3)$$

The XRD pattern also displays the characteristic reflections of chalcopyrite and sulfur (S_8).

In addition, the pH of the solution in experiment T11 was followed and a dramatic increase was noted. Since oxidation of chalcopyrite was slow, this increase in pH is attributed to the oxidation of galena to anglesite. This observation is in agreement with the XRD analysis.

5.3.2 The Catalytic Effects of Galena in the Presence of Pyrite and Silver

An experiment was conducted to examine the effect of galena in the presence of pyrite and silver. In this experiment, pyrite was added at a pyrite-to-chalcopyrite ratio of 2 and a silver-to-pyrite ratio of 100 ppm (similar to tests T6 and T7). To highlight the effect of galena on the kinetics, galena was added at a higher concentration (8 times higher) than was naturally present (0.14%) in Pyrite #1 (T16). The results, shown in Figure 5.11, indicate the slower rate of reaction in the presence of galena. As explained earlier, silver is preferentially adsorbed to galena rather than to pyrite. Galena has no catalytic effect on chalcopyrite oxidation, as already established. Hence, the reason for the slower kinetics in T16 and T17 than T6 and T7, respectively, may be attributed to the adsorption of some silver ions to galena rather than pyrite. Figure 5.11 shows that the total leach time in the recycle test was similar to the first test, indicating that the silver-enhanced pyrite maintained its catalytic properties.

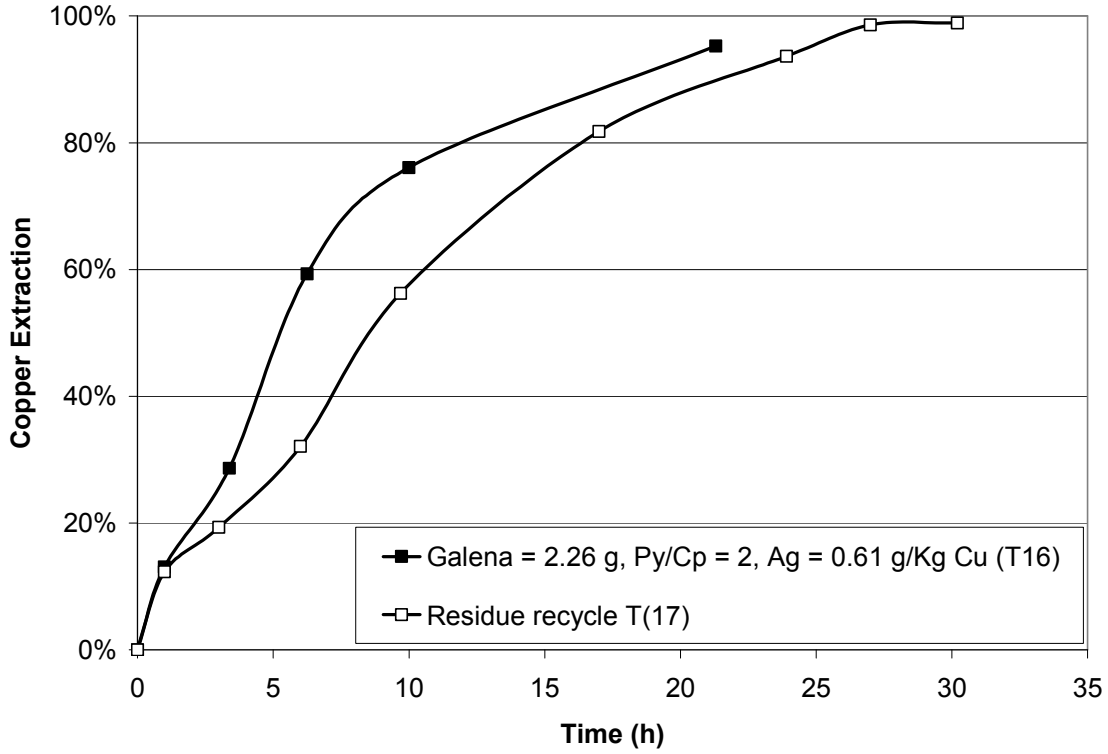

Figure 5.11 Effect of silver-pretreated pyrite and galena (T16) on copper extraction and recycled pyrite and galena (T17) at a potential set point of 450 mV and 80°C

5.3.3 Interaction of Galena and Pyrite with Silver Ions

In order to examine the hypothesis regarding adsorption of a lower amount of silver onto pyrite in the presence of galena, a new set of experiments was designed. In the previous experiment shown in Figure 5.11, after preparing the desired silver solution, galena and pyrite were added simultaneously. Pretreatment continued for 30 minutes and samples were taken at various time intervals. The silver concentrations of samples were determined by atomic absorption spectroscopy. Although galena and pyrite were pretreated with silver for 30 minutes before introducing the chalcopyrite concentrate, no silver was detected in the solution after one minute. In another experiment, 175 g of pyrite were added to the same silver solution and the silver concentration was followed.

The same experiment was repeated with 2.26 g galena (8 × 0.283 g galena). The results are shown in Figure 5.12.

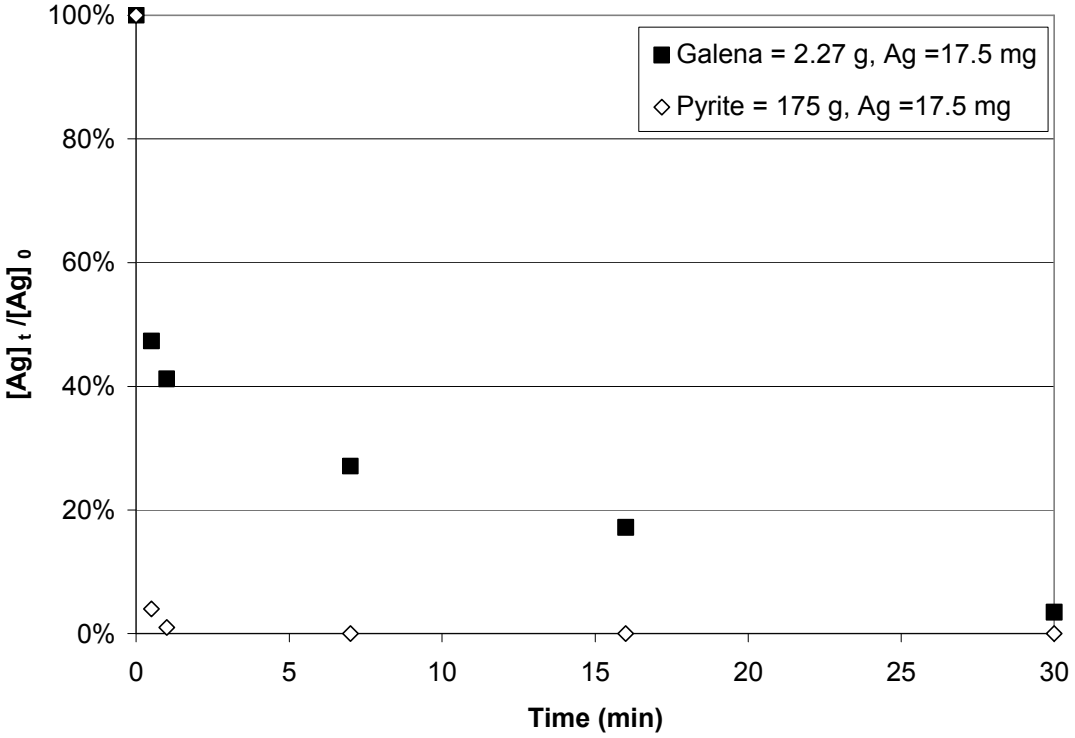

Figure 5.12 Rate of interaction of 17.5 mg silver ions with 2.27 g galena and 175 g pyrite

This analysis also confirms that in the presence of pyrite, the silver concentration of the solution reached zero after one minute. The silver concentration on galena after one minute was 4533 ppm. It was shown above that this particular galena sample attains a silver concentration of roughly 4600 ppm during the first minute of its interaction with silver. Since the rest potential of galena is lower than that of pyrite, silver reacts with galena preferentially. Therefore, the silver concentration of galena increases to about 4533 ppm (17.5mg / 2.27 g × 1000 g/kg × [100% − 41.19%]). The reaction of silver with pyrite is also rapid so that unreacted silver ions quickly react with pyrite. According to this analysis, the concentration of silver on pyrite was about 41 ppm ([41.19% × 17.5 mg] / 175 g). The silver concentration of pyrite was 100 ppm in the absence of galena. This analysis

further confirms the hypothesis that the rate of reaction in tests T16 and T17, shown in Figure 5.11, is slower in the presence of galena due to the reaction of some amount of silver with galena rather than pyrite.

5.3.4 Morphology

The morphology of chalcopyrite samples after leaching under different conditions was studied using SEM. In previous studies (Ballester *et* al., 2007; Price *et al.,* 1986; Miller and Portillo., 1979; Miller *et al*., 1981), it has been stated that in the absence of catalysts, an impermeable sulfur layer forms on the surface of chalcopyrite and inhibits the diffusion of reactants to the surface of chalcopyrite. These studies also indicate that the morphology of the sulfur layer is modified in the presence of catalysts such as silver ions (Ahonen and Touvinen, 1990; Cordoba *et al.,* 2008(II); Palencia *et al*., 1998; Romero *et al.,* 1998; Sukla *el al.,* 1990). The higher rate of copper extraction has therefore been attributed to the formation of a porous and non-protective sulfur layer which allows the diffusion of reactants to the chalcopyrite core.

In order to compare the morphology of partially leached chalcopyrite particles in the absence and presence of catalysts, 105 g of copper concentrate were leached in the absence of catalysts. It was observed that after 140 hours, chalcopyrite leaching proceeded very slowly, as expected. 5 mg of silver ions were added to the system after 140 hours (T18). The results are shown in Figure 5.13. A rapid increase in the rate of chalcopyrite leaching was observed after 140 hours, when the silver ions were introduced to the leaching reactor.

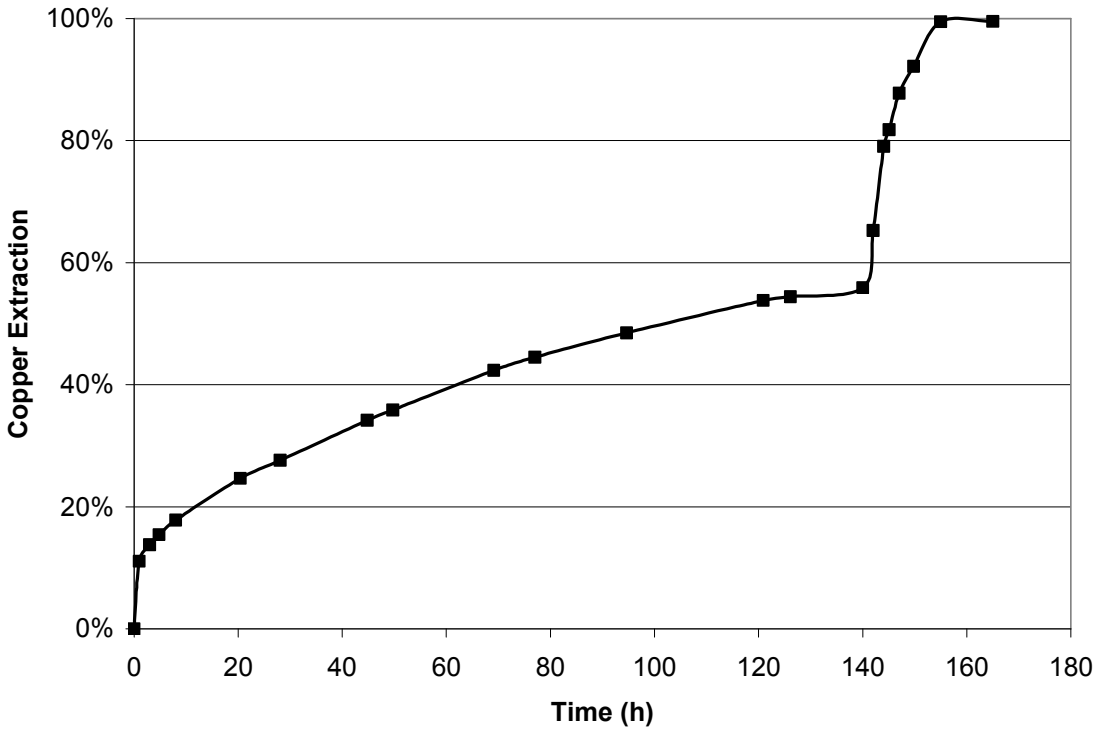

Figure 5.13 Effect of adding silver after chalcopyrite passivation at a potential set point of 450 mV and 80°C (T18)

Samples were taken after 140 hours (before adding the silver) and after 165 hours (after complete copper extraction). Samples were studied by SEM and the results are shown in Figure 5.14 and Figure 5.15. Figure 5.14 shows the morphology of partially leached chalcopyrite particles in test T18 after 140 hours before introducing silver ions to the leach solution. Figure 5.14(a) shows the formation of a thin non-porous sulfur layer around chalcopyrite particles. Figure 5.14(b) presents the thicker sulfur layer around chalcopyrite particles. Figure 5.14(b) clearly shows the porosity of the sulfur layer. However, it is interesting to note that in spite of the formation of a porous layer on the surface of chalcopyrite, the leaching reaction had ceased.

(a)

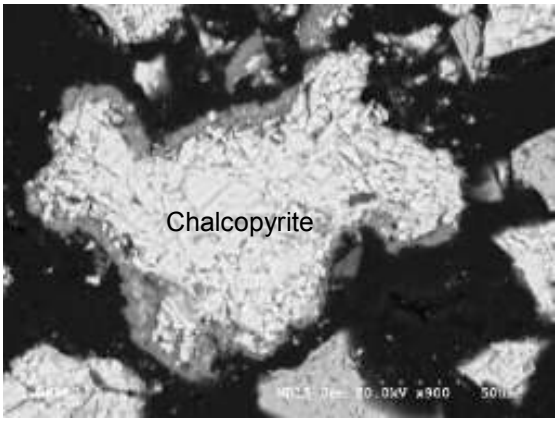

(b)

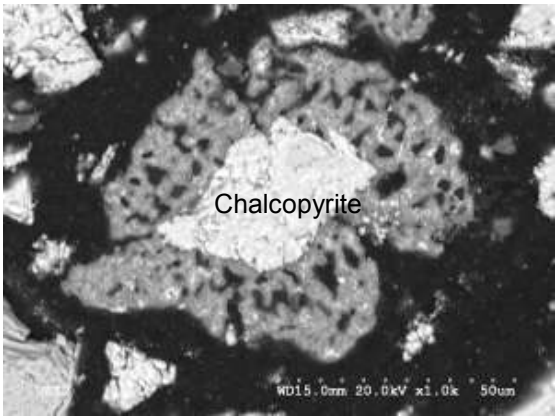

Figure 5.14 SEM micrographs of chalcopyrite particles partially leached in the absence of catalysts, test T18 after 140 hours, cross-sectioned and epoxy mounted, covered by (a) a thin non-porous and (b) a thick porous sulfur layer

Figure 5.15 shows the morphology of chalcopyrite in test T18 after 165 hours. Comparing Figure 5.14 and Figure 5.15, it can be concluded that the morphology of sulfur layers on the surface of chalcopyrite is similar in the absence and the presence of the catalyst. In Figure 5.15(a), one might report a non-porous protective sulfur layer; while in fact, this observation can be attributed to the formation of a thin layer. Due to the low copper and iron dissolution of this chalcopyrite particle, the sulfur layer is not thick enough to reveal the dendritic shape of the interstitial regions between the sulfur layers and if the leaching had proceeded further, it might have been seen as a porous layer. In addition, the sulfur layer was not observed on two sides of the particle shown in Figure

5.15(a). A review of the literature reveals that the formation of localized sulfur layer has been reported in previous studies (Biegler and Swift, 1979; Jones and Peters, 1976; Venkatachalam, 1991). However, samples were mounted and polished; hence there is a possibility of destruction of this layer during polishing.

(a)

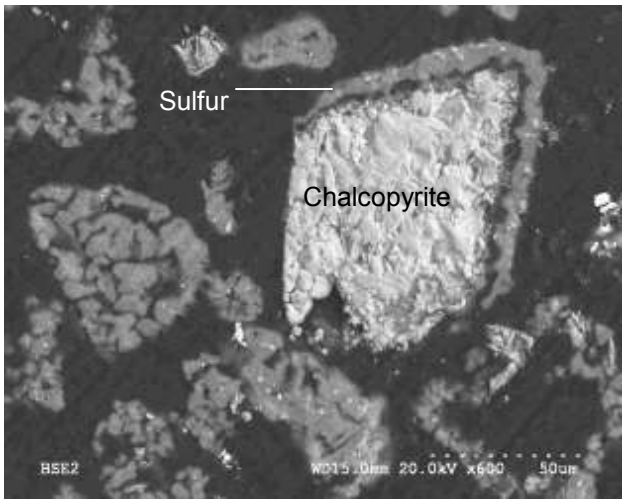

(b)

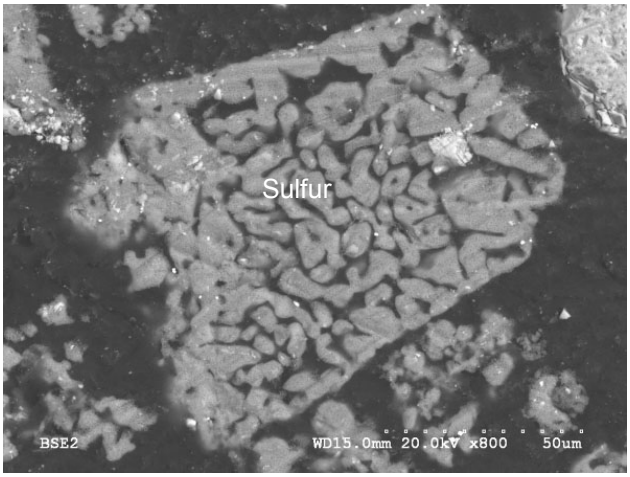

Figure 5.15 SEM micrographs of chalcopyrite particles leached in the presence of silver as a catalyst, test T18 after 165 hours, cross-sectioned and epoxy mounted, covered by (a) a thin non-porous, and (b) a thick porous sulfur layer

Figure 5.16 shows the rate of copper extraction in the silver catalyzed leaching process at 450 mV and 80°C. In this experiment, 0.61 g Ag/kg Cu was added

(T19). The results show that although silver accelerated the rate of copper recovery, with the same amount of silver, the rate was significantly slower in the absence of pyrite (T6 and T8). SEM micrographs of samples from this test are shown in Figure 5.17, which clearly show that the morphology of the sulfur layer is independent of the presence or absence of catalysts. In Figure 5.17(a) and Figure 5.17(b), relatively non-porous and relatively porous sulfur layers are shown, respectively, even though all particles were leached under the same conditions.

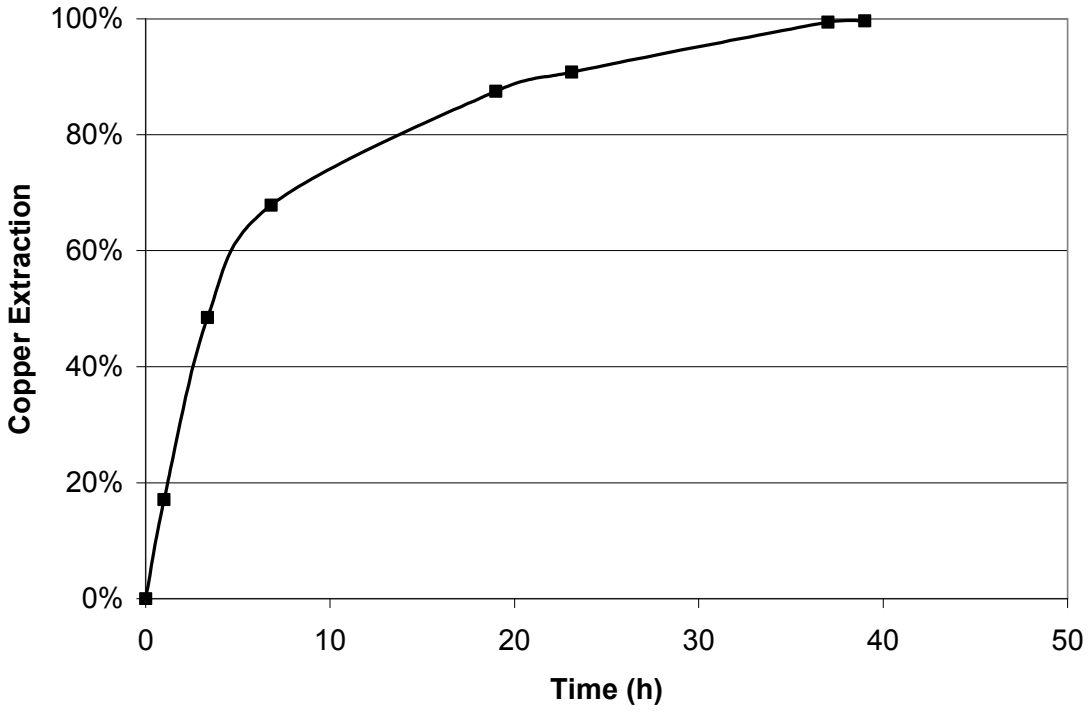

Figure 5.16 Effect of adding silver on chalcopyrite leaching at a potential set point of 450 mV and 80°C (T19)

(a)

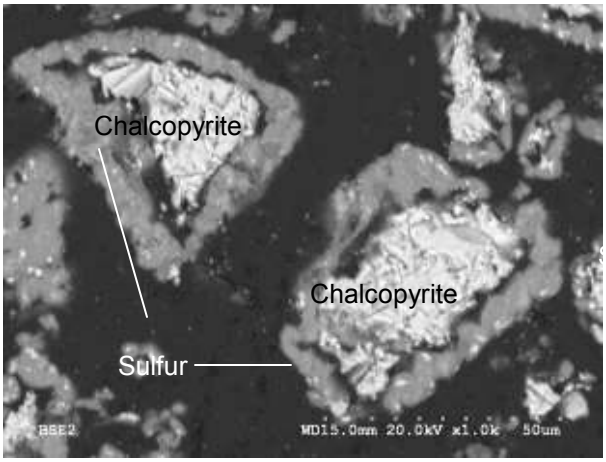

(b)

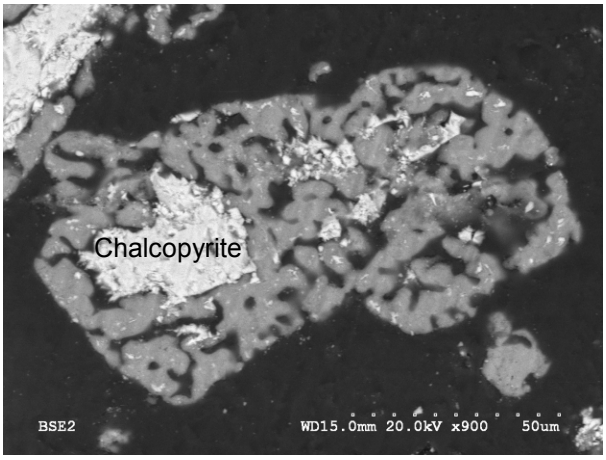

Figure 5.17 SEM micrographs of chalcopyrite particles leached in the presence of silver, test T19, cross-sectioned and epoxy mounted, covered by (a) a thin non-porous, and (b) a thick porous sulfur layer

SEM micrographs of chalcopyrite residues leached in the presence of galena are also presented in Figure 5.18. These images again show that relatively porous and non-porous sulfur layers can be formed around chalcopyrite particles regardless of the presence or absence of catalysts. Figure 5.18(b) clearly shows that the outer layer of the chalcopyrite particle is completely non- porous, but due to the progress of copper extraction through inner layers, the formation of a porous sulfur structure is observed.

(a)

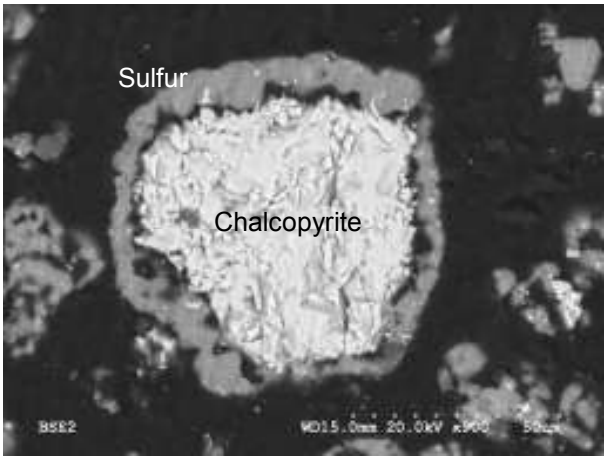

(b)

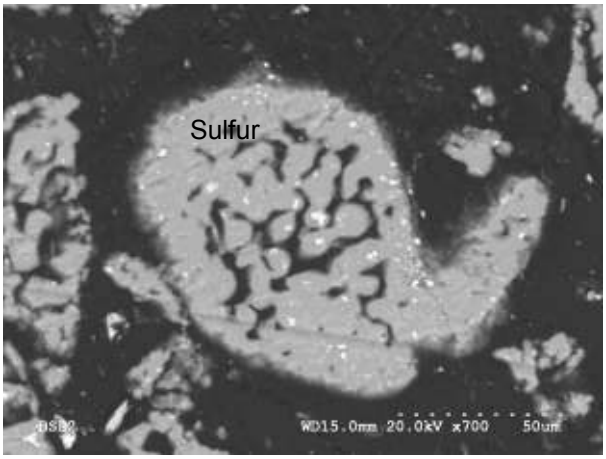

Figure 5.18 SEM micrographs of chalcopyrite particles leached in the presence of galena, test T10 after 140 hours, cross-sectioned and epoxy mounted, covered by (a) a thin non-porous, and (b) a thick porous inner and a non-porous outer sulfur layer

SEM micrographs of samples of partially leached chalcopyrite particles in the absence of catalysts and the presence of galena are shown in Figure 5.19(a) and Figure 5.19(b), respectively. To avoid destruction of the sulfur layer around the particles, SEM samples were prepared without mounting or polishing. This figure shows that leaching of chalcopyrite occurs along preferential directions. This observation is in agreement with previous studies (Biegler and Swift, 1979; Jones and Peters, 1976; Venkatachalam, 1991).

(a)

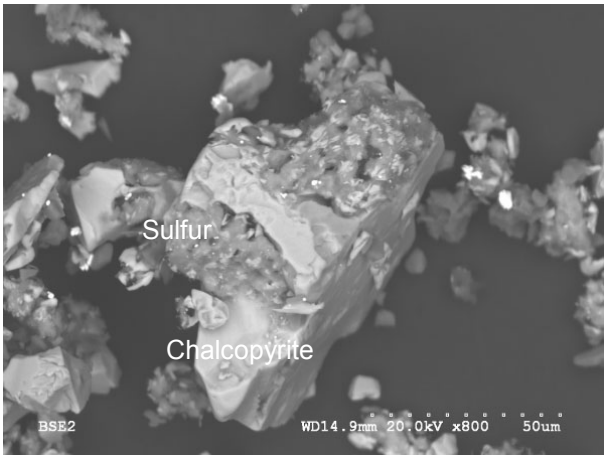

(b)

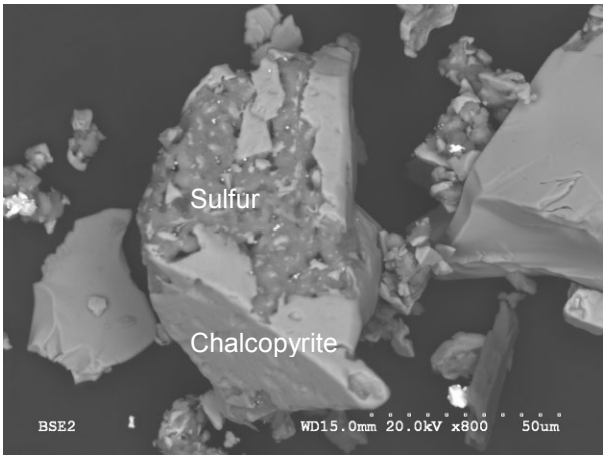

Figure 5.19 SEM micrographs of non-polished partially leached chalcopyrite particles from (a) test T18, and (b) test T10 after 140 hours

Figure 5.20 shows the SEM micrographs of non-polished leached chalcopyrite particles in the presence of silver, from test T19. Particles shown in Figure 5.20(a) have been completely leached from all sides while in Figure 5.20(b), almost pure elemental sulfur was observed at some surfaces and clean, unleached chalcopyrite was observed at other surfaces. Figure 5.20 also validates the previous observation that leaching of chalcopyrite occurs in preferential directions.

(a)

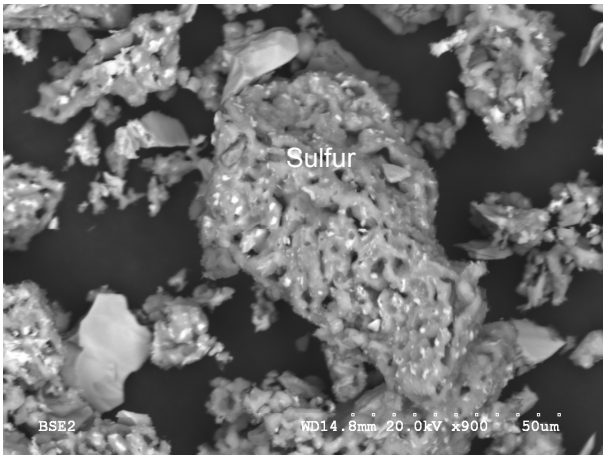

(b)

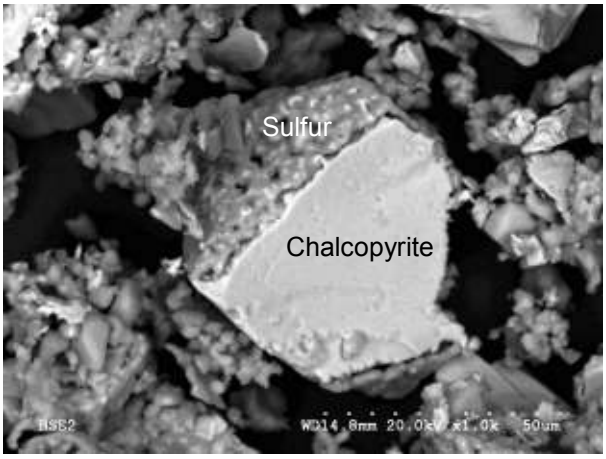

Figure 5.20 SEM micrographs of non-polished leached chalcopyrite particles in the presence of silver, from test T19, showing leaching in preferential directions

It has been observed that, under leaching conditions described earlier, both porous and non-porous sulfur layers form on the surfaces of chalcopyrite regardless of the absence or presence of silver catalyst. The observation of only a non-porous sulfur layer in the absence of catalysts, reported in previous studies, can be attributed to low copper extraction under this condition which leads to the formation of only a thin sulfur layer on the surface of chalcopyrite. However, continued leaching leads to the formation of a porous sulfur layer. Conversely, in the presence of catalysts, the extents of chalcopyrite dissolution are considerably higher which leads to the formation of a thicker sulfur layer.

Hence, the porous structure can be clearly observed. These results also indicate that the dissolved copper and iron ions can be easily transferred to the solution through the porous sulfur layer which is formed around chalcopyrite.

5.4 Conclusions

In this study, the influences of galena and pyrite on the rate of chalcopyrite leaching have been investigated. Pyrite and galena samples were pretreated with silver ions. It has been noted that in the presence of both pyrite and galena, silver reacts with galena preferentially. However, galena pretreated with silver does not enhance the kinetics of chalcopyrite leaching, whereas silver ions, pyrite, and pyrite pretreated with silver ions all accelerate the rate of chalcopyrite leaching significantly. The process of using silver to accelerate copper extraction is costly unless silver can be efficiently recovered from the residue and recycled. In this study, it has been shown that direct recycle of the silver catalyst is not feasible; however, silver-enhanced pyrite can be efficiently recycled to subsequent tests.

SEM and EDX techniques were applied to study the morphology and elemental composition of residues after completion of experiments. The results indicate that both porous and non-porous layers form on the surface of chalcopyrite regardless of the presence or absence of catalysts. Hence, acceleration of the rate of chalcopyrite leaching in the presence of catalysts is not due to the alteration of morphology of sulfur layers around chalcopyrite particles.

Chapter 6 Comparison between Conventional Silver-catalyzed Leaching and Leaching with Silver-enhanced Pyrite

6.1 Introduction

Chalcopyrite can be chemically activated with silver ions to improve its leachability under acid oxidizing conditions. Several authors have demonstrated the ability of silver to catalyze copper dissolution from chalcopyrite in both chemical and biological leaching systems (Banerjee *et al.*, 1990; Miller *et al.*, 1981; Price and Warren, 1986).

According to various authors, the dissolution of metals from mineral sulfides can be accelerated by the addition of soluble foreign ions. These ions alter the electrochemical behaviour of the sulfide after they become fixed onto its surface (Ballester *et al.*, 1990; Barriga *et al.*, 1987).

Initially it was shown by Snell and Fords (1976) that copper extraction from chalcopyrite increased in ferric sulfate solution by addition of silver as a soluble silver salt. In this work, it was claimed that the solid residue contained over 90% of the silver. To recover the silver, it was proposed to separate the elemental sulfur from the solid residue by aromatic liquid extraction to produce a tailings with less than 2% elemental sulfur and then to dissolve the silver using oxygen in a leaching solution containing 80% sulfuric acid. This reaction occurs at temperatures between 95 and 110°C (Snell and Fords, 1976).

Miller and Portillo (1979) proposed the first model to explain the catalytic effect of silver. Based on this model, the enhanced rate of leaching is due to the formation of an intermediate Ag_2S film which forms on the chalcopyrite surface by an exchange reaction. They have suggested that, under these conditions, the elemental sulfur forms a non-protective reaction product on the Ag_2S crystallites, in contrast to uncatalyzed ferric sulfate leaching, in which a dense elemental

sulfur layer forms on the mineral surface and acts as a diffusion barrier, thus delaying the oxidation of chalcopyrite by ferric ions. The following reaction has been proposed for the silver-catalyzed leaching of chalcopyrite:

$$CuFeS_2 + 4\ Ag^+ = 2\ Ag_2S_{(chalcopyrite\ surface)} + Cu^{2+} + Fe^{2+} \qquad (6.1.1)$$

In the presence of Fe^{3+}, the silver sulfide film is oxidized to Ag^+ and S^0:

$$Ag_2S + 2\ Fe^{3+} = 2\ Ag^+ + 2\ Fe^{2+} + S^0 \qquad (6.1.2)$$

The rate of the reaction is controlled by the intermediate electrochemical reaction of the silver sulfide film with ferric (reaction 6.1.2) since the first stage (reaction 6.1.1) occurs rapidly. Hence, increasing the ferric concentration improves the catalytic effect of silver.

Additionally, Ahonen and Tuovinen (1990) have shown that increase in the rate of copper dissolution is due to the galvanic interaction between chalcopyrite and silver sulfide where chalcopyrite behaves anodically in the $CuFeS_2$-Ag_2S galvanic couple.

The electrochemical response of silver sulfide in sulfuric acid solutions was also studied by Price *et al*. (1986) (Figure 6.1). Beginning the scan from the rest potential, the voltammogram shows an increase in anodic current at approximately 1.2 V (*vs* SHE). The anodic reaction in this potential region was described by reaction (6.1.3).

$$Ag_2S = 2\ Ag^+ + S^0 + 2\ e^- \qquad (6.1.3)$$

During the cathodic scan, metallic silver was formed at the electrode both from the reduction of silver sulfide and from the reduction of dissolved silver to elemental silver at 0.55 to 0.6 V (*vs* SHE) according to the following reaction:

$$Ag^{+} + e^{-} = Ag^{0} \qquad (6.1.4)$$

Subsequently, the oxidation of metallic silver produced a large and distinctive anodic peak at 0.70 V (*vs* SHE).

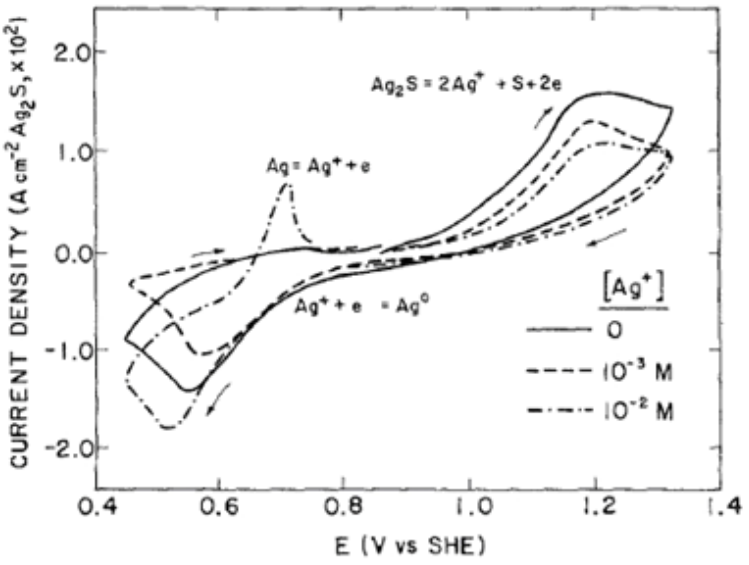

Figure 6.1 Cyclic Voltammograms for pressed pellets of Ag_2S in 1 M H_2SO_4 solutions with varying additions of silver ion (Price *et al*., 1986).

Figure 6.1 also confirms that oxidation of silver sulfide occurs at high potential which corresponds to a high ratio of ferric to ferrous ions. However, high ferric concentration also leads to ferric sulfate hydrolysis, and therefore to iron precipitation (jarosite formation) and sulfuric acid generation:

$$3\ Fe_2(SO_4)_3 + 14\ H_2O = 2\ (H_3O)Fe_3(SO_4)_2(OH)_6 + 5\ H_2SO_4 \qquad (6.1.5)$$

Silver is preferentially incorporated into the jarosite structure to form argentojarosite, $AgFe_3(SO_4)_2(OH)_6$. Hence, silver is trapped in the jarosite structure and loses its activity as a catalyst. This is one of the main drawbacks associated with silver-catalyzed leaching of chalcopyrite.

Along with reaction (6.1.1), in a study by Price and Warren (1986), the following reaction was proposed to describe the reaction of dissolved silver with chalcopyrite:

$$CuFeS_2 + 4\ Ag^+ \rightarrow 4\ Ag^0 + Cu^{2+} + Fe^{2+} + 2\ S^0 \qquad (6.1.6)$$

Price and Warren (1986) believed that a change in morphology or conductivity of the sulfur layer due to the presence of metallic silver enhances the kinetics of chalcopyrite leaching.

In summary, based on the model of Miller and Portillo (1979), in the absence of silver ions, the oxidation of chalcopyrite with ferric sulfate is retarded by the formation of a dense elemental sulfur layer on the mineral surface during leaching which acts as a diffusion barrier. However, in the presence of silver, a mixed product layer of elemental sulfur and silver sulfide forms on the surface which is porous and non-protective. The same model was proposed in other studies to explain the behaviour of chalcopyrite leaching in the presence of silver ions (Ballester, 1987; Gomez *et al.*, 1999; Muñoz *et al.*, 2007; Price and Warren, 1986).

Recently, Hiroyoshi *et al.*, (2002) proposed a new model to explain the role of silver ions in chalcopyrite leaching. In this model, chalcopyrite transforms into an intermediate phase consisting of Cu_2S and then this intermediate phase is oxidized by ferric and/or dissolved oxygen to release cupric ions. Chalcopyrite is reduced to Cu_2S thus:

$$2\ CuFeS_2 + 6\ H^+ + 2\ e^- = Cu_2S + 2\ Fe^{2+} + 3\ H_2S \qquad (6.1.7)$$

$$2\ Cu^{2+} + S + 4\ e^- = Cu_2S \qquad (6.1.8)$$

The standard reduction potentials for reactions (6.1.7) and (6.1.8) are −0.221 V and 0.561 V (*vs* SHE), respectively. The redox potential has to be higher than the half-cell potential of reaction (6.1.8) and lower than that of reaction (6.1.7) to obtain copper recovery according the model proposed by Hiroyoshi *et al*. (2002). This does not occur unless the hydrogen sulfide activity is lower than about 10^{-10}. Such a low hydrogen sulfide activity would not be achieved in a leaching system involving metal sulfides such as chalcopyrite, and, therefore, formation of the intermediate Cu_2S would not occur. However, according to Hiroyoshi *et al. (*2002), in the presence of silver ions, hydrogen sulfide activity would be extremely low because silver ions react with hydrogen sulfide to form silver sulfide and therefore the concentration of hydrogen sulfide decreases:

$$2\ Ag^{+} + H_2S = Ag_2S + 2\ H^{+} \qquad (6.1.9)$$

By combining reactions (6.1.7) and (6.1.9), the following reaction is obtained.

$$2\ CuFeS_2 + 6\ Ag^{+} + 2\ e^{-} = Cu_2S + 2\ Fe^{2+} + 3\ Ag_2S \qquad (6.1.10)$$

This reaction has a standard reduction potential (E°) of 2.365 V (*vs* SHE) (Hiroyoshi *et al.*, 2002), which is considerably higher than the standard reduction potential of Cu_2S (0.561 V). According to this model, under these conditions, chalcopyrite is reduced to the intermediate phase Cu_2S, which leaches more rapidly.

Carranza *et al.* (1997) have developed a new process for copper recovery from chalcopyrite known as BRISA. This process is comprised of two steps: chalcopyrite leaching in ferric sulfate solution, and biooxidation of ferrous to ferric using mesophilic bacteria. Silver may be recovered from the leach residue by acidic brine leaching (Romero *et al.*, 1998). Leaching was performed at 70°C and pH 1.25 with 2 g Ag per kg concentrate. The concentrate contained 8.9% copper (*i.e.*, 22.5 g Ag per kg Cu). A copper recovery of 95% was obtained after 8 hours.

Palencia *et al.* (1998) have shown that all silver added as a catalyst remains in the leached residue as Ag_2S and Ag^0. Furthermore, due to the acidity, temperature and ferric sulfate concentration in the BRISA process, silver is also precipitated as argentojarosite. Formation of this phase under similar conditions was also confirmed by Dutrizac and Jambor (1987), who state that silver is preferentially incorporated into jarosite precipitated from sulfate media.

At high temperature and high potential, silver sulfide is oxidized and silver ions are released into solution and subsequently taken up by jarosite. Formation of jarosite increases with increasing temperature, ferric concentration, and pH. Silver precipitation is rapid, and is complete before ferric precipitation (Bolorunduro *et al.*, 2003), which leads to the zoning of the silver-rich jarosite in the core of the jarosite. In order to extract silver from jarosite, the leaching solution has to diffuse through the core of jarosite.

In order to recover silver from the residue, the following method has been proposed by Palencia *et al.*, (1998). The first step is to separate the elemental sulfur from the residue. The residue is heated with steam at 140°C. The melting point of sulfur is about 125°C; hence, the sulfur melts to form sulfur droplets which agglomerate and form a continuous liquid sulfur phase. Then, this phase can be separated from the solid residue by vacuum filtration. The next step is to extract silver from the residue, for which various methods have been proposed. One method involves the dissolution of silver in hydrochloric or sulfuric acid containing 20% NaCl. Acid is required to dissolve argentojarosite whereas chloride ions are required to leach silver sulfide and elemental silver (Palencia *et al.*, 1998).

Silver is the most effective catalyst yet proposed for chalcopyrite leaching, but processes requiring silver are expensive and would typically be avoided in practice, unless the ores themselves contained sufficient silver (Hiroyoshi *et al.*, 2002). Hence, in spite of extensive research, no commercial process has been

developed successfully which uses silver as a catalyst for copper recovery from chalcopyrite concentrates (Ballester *et al.*, 2007).

There are two fundamental problems associated with silver-catalyzed leaching in both chemical and biological contexts:

1. Silver availability

Silver availability is affected by formation of precipitates during leaching (Muñoz *et al*., 2007). As shown in reaction (6.1.2), the catalytic effect of silver is increased by increasing the ferric concentration. However, as ferric concentration increases, hydrolysis of ferric sulfate leads to the formation of argentojarosite, which limits the availability of silver.

2. Silver toxicity (in biological leaching)

Solubility of silver in bioleaching experiments is low due to the bioaccumulation of silver. In addition, silver ions are toxic to most microorganisms. Silver toxicity has been attributed to a competing mechanism between silver and ferrous ions for active sites on bacterial cell walls (Muñoz *et al*., 2007). The accumulation of silver sulfide on ferrooxidant cells has been also observed (Pooley, 1982). It has been reported that biooxidant growth is inhibited in the presence of even miniscule amounts of silver (as low as 0.1 ppm) (Hoffman and Hendrix, 1976).

6.2 Objectives

In the process of silver-enhanced pyrite catalyzed chalcopyrite leaching, considering the known catalytic properties of silver to accelerate the leaching of copper from chalcopyrite and a stronger affinity of silver to interact with chalcopyrite than with pyrite, one might conclude that adding silver to pyrite initially and then introducing this pyrite into the reactor would give similar results

as adding silver to the chalcopyrite, directly. A series of experiments was conducted to evaluate this hypothesis.

6.3 Experimental

6.3.1 Pyrite Pretreatment with Silver Ions

Pyrite samples were pretreated with silver ions according to the procedure described in section 4.2.1.

6.3.2 Leaching Experiments

Batch leaching experiments were conducted by following the procedure explained in section 4.2.2.

6.3.3 Materials

In this study, a copper concentrate containing 27% copper and Pyrite #1 containing 97.6% pyrite were used. Mineralogical and elemental compositions of the concentrate and pyrite samples were summarized in Table 4.1 and Table 4.2, respectively.

6.4 Results and Discussion

Initially, two leaching experiments were conducted under identical conditions. In one test, silver-enhanced pyrite was added. In the other test, the same amount of silver was added directly to the chalcopyrite with no pyrite present. As shown in Figure 6.2, the presence of pyrite is a critical factor to achieve rapid and complete copper extraction. Although the initial rates of copper extraction in both tests were similar, the rate declined sharply after just a few hours in the test without pyrite, and complete copper extraction was not achieved even after 70

hours of leaching. However, in the presence of the silver-enhanced pyrite, leaching was very rapid for the duration of the test, and complete copper extraction was achieved within about 12 hours.

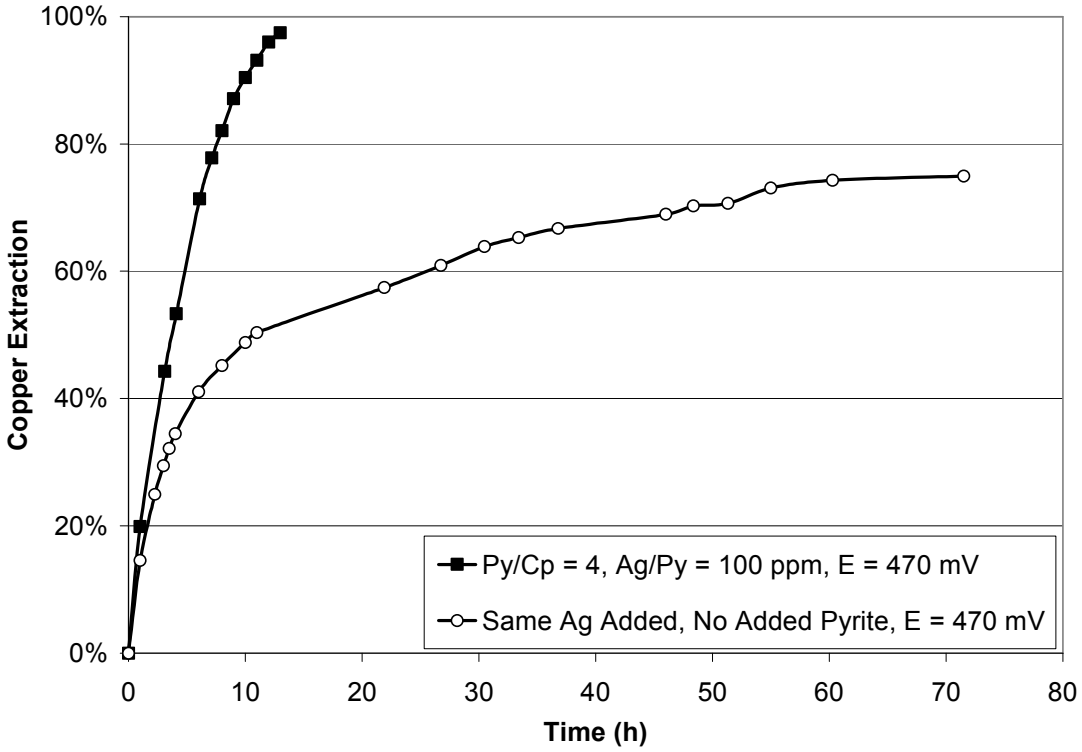

Figure 6.2 Comparison between conventional silver-catalyzed leaching and leaching with silver-enhanced pyrite at 1.23 g Ag per kg of contained Cu, a potential set point of 470 mV, and 80°C

As shown in Chapter 4, in the presence of silver-enhanced pyrite, faster leaching was observed at a redox potential of 450 mV than 470 mV. The tests shown in Figure 6.2 were repeated at 450 mV, and the results are shown in Figure 6.3. These results confirm the beneficial effect of lower solution potential, and also confirm the dramatic increase in both the rate and the extent of copper extraction in the presence of pyrite. It also bears noting that these tests were conducted with only half the amount of silver of the previous tests (shown in Figure 6.2), but the leaching rates were significantly faster in both the presence and the absence of pyrite. This further confirms the benefit of operating at a lower redox potential.

An important reason to explain the faster kinetics of silver catalyzed leaching at lower redox potential is decreasing or inhibiting the formation of jarosite. At lower redox potential, ferric concentration is lower which decreases the formation of jarosite and argentojarosite. As discussed earlier in this chapter, once argentojarosite is formed, silver loses its catalytic properties. In addition, dissolution of this species in ferric sulfate media at 80°C and atmospheric pressure is not feasible.

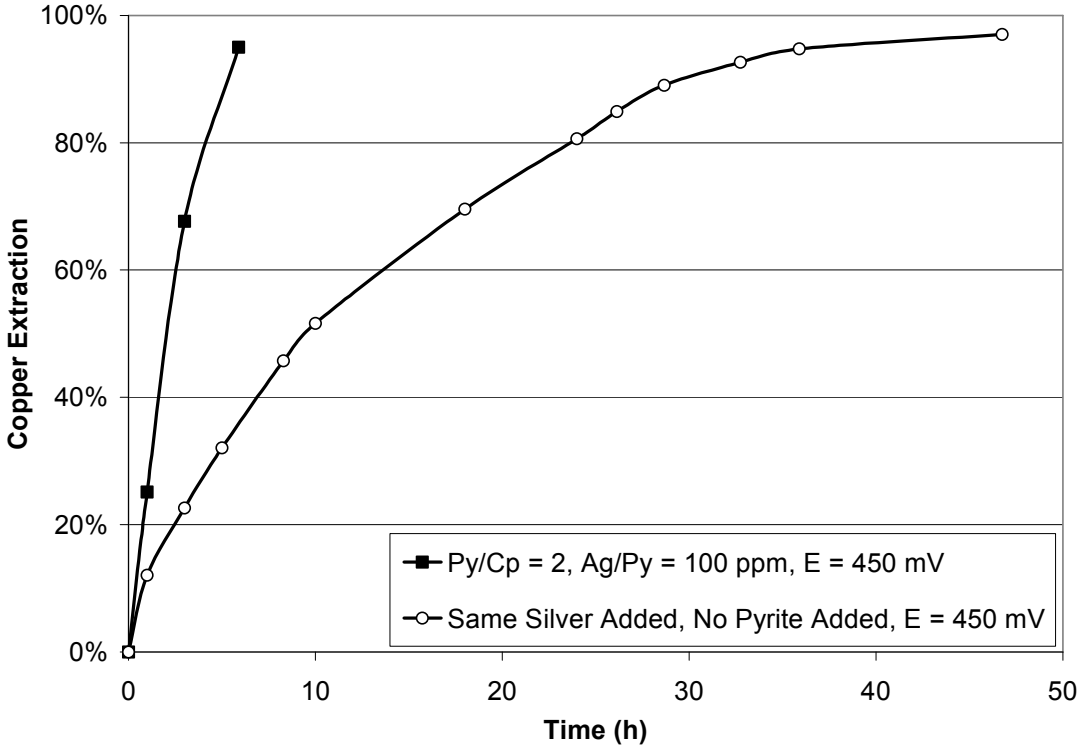

Figure 6.3 Comparison between conventional silver-catalyzed leaching and leaching with silver-enhanced pyrite with 0.65 g Ag per kg of contained Cu, and at a potential set point of 450 mV, and 80°C

The two tests shown in Figure 6.3 were repeated with recycled solid residues to confirm that silver-enhanced pyrite retains its effectiveness as a catalyst upon recycle, and to determine whether the solid residues from the test in the absence of pyrite retained any similar catalytic ability. As shown in Figure 6.4, copper extraction in the presence of the recycled pyrite was rapid and complete within

about 20 hours. However, the residue in the absence of added pyrite retained little or no catalytic ability. Any silver remaining in this residue was probably in the form of tiny Ag_2S particles embedded in elemental sulfur, as it is unlikely that argentojarosite would have formed to a significant extent at a redox potential of only 450 mV. Even so, the results shown in Figure 6.4 indicate that silver used in conventional silver catalyzed leaching cannot be recycled directly, but must first be recovered in soluble form. Dutrizac (1994) also showed that the dissolution of Ag_2S in ferric sulfate media at less than 110°C is negligible. As mentioned above, recovering silver in a soluble form is a complicated undertaking which can only be achieved at significant expense.

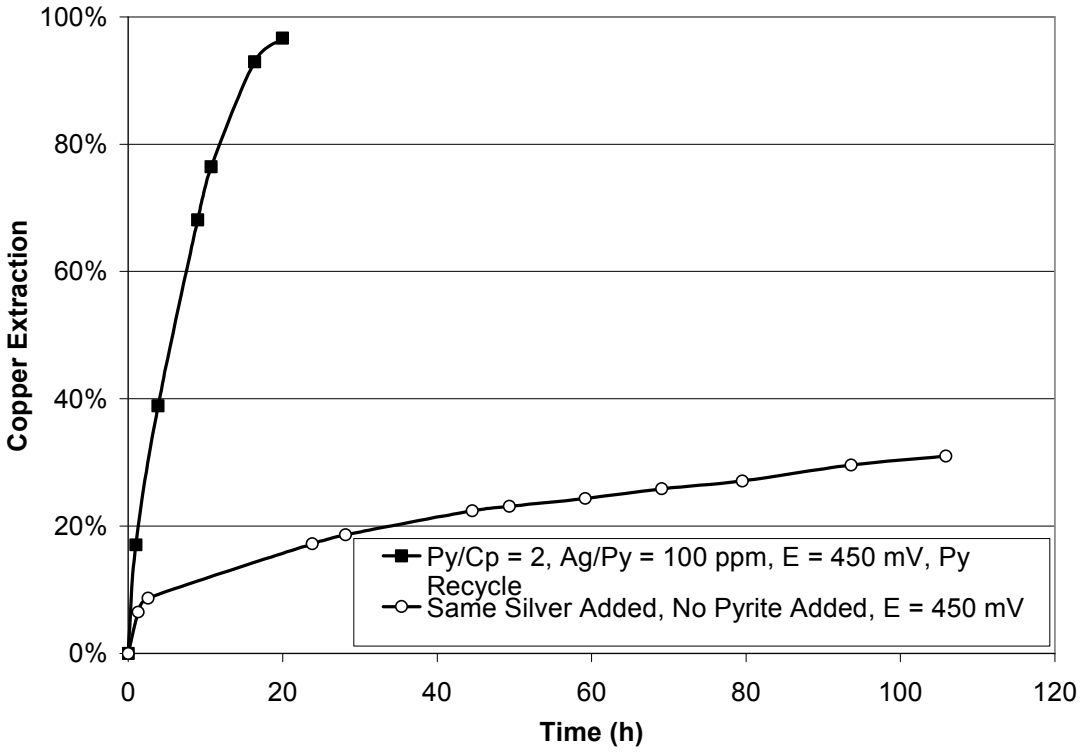

Figure 6.4 Comparison between leaching with recycled residue from a conventional silver-catalyzed leaching test and with recycled silver-enhanced pyrite, both with 0.65 g of Ag added initially per kg of contained Cu, and at a potential set point of 450 mV, and 80°C

In addition, experiments were conducted at optimum conditions discovered in Chapter 4 (i.e. at solution potential set point of 450 mV, 80°C, and 70 g/L Cu concentrate). Two experiments were conducted under identical conditions. In one experiment, silver-enhanced pyrite was added. In the other, an identical amount of silver was added directly to the chalcopyrite in the absence of pyrite. The results, shown in Figure 6.5, indicate the important role of pyrite in achieving fast and complete copper extraction. Considering the high cost of silver, after completion of the first test, the solid residues in both experiments were recycled to a subsequent leaching test in order to examine their effectiveness as catalysts upon recycling. In each test, 10% makeup of the catalyst was added. In one test, silver ions were added directly to the chalcopyrite slurry, and in the other, the same amount of silver was added in the form of silver-enhanced pyrite. As shown in Figure 6.5, the silver-enhanced pyrite retained its catalytic effectiveness. However, the residue without pyrite displayed little catalytic ability and could not be successfully recycled.

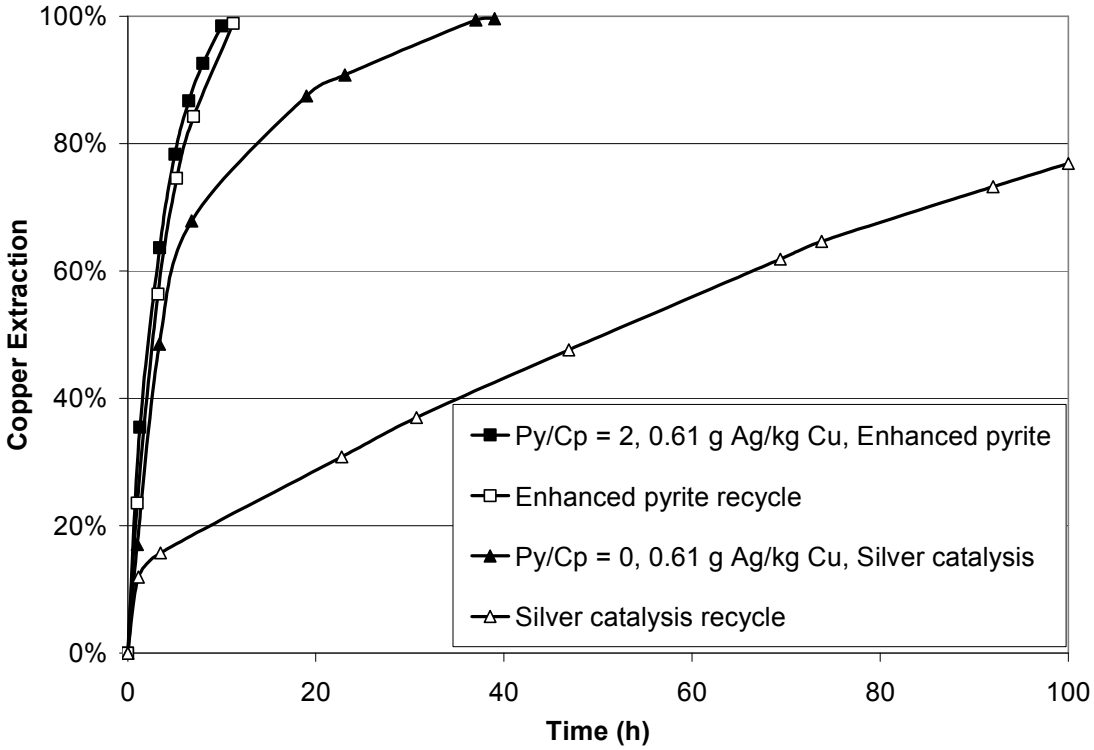

Figure 6.5 Comparison between silver catalyzed leaching and silver-enhanced pyrite catalyzed leaching of chalcopyrite in ferric sulfate media, at 0.61 g Ag/kg Cu and a potential set point of 450 mV and 80°C

According to the results shown in Figure 6.5, the addition of about 10% silver-enhanced pyrite was necessary to ensure optimum catalytic effectiveness. These results were in agreement with solid assay results which showed roughly 10% silver loss from the recycled pyrite. The silver concentrations on the recycled pyrite and the fresh enhanced pyrite were 85 – 89 ppm and 97 -102 ppm, respectively. The concentration of silver dissolved in solution was obtained by AAS. This concentration in all experiments was very low (0.2 to 0.5 ppm). Hence, any silver loss from pyrite is most likely to sulfur as silver sulfide.

In a study by Muñoz *et al*. (2008), chalcopyrite was shown to have a higher affinity for silver ions than pyrite. Hence, one might hypothesize that upon introducing silver-enhanced pyrite to chalcopyrite slurry, a portion of the added

silver leaves the pyrite and reacts with chalcopyrite. Furthermore, one might be tempted to assume that silver-enhanced pyrite does not possess any special catalytic ability *per se*, and that the only catalytic effect is that of the 10% silver makeup (which corresponds to 0.061 g Ag per kg Cu in these tests). To test this hypothesis, two experiments were conducted under identical conditions. In each of these tests, a full charge of copper concentrate (105 g) was introduced to the reactor, with 0.061 g Ag added per kg Cu (to correspond to the 10% makeup of the test shown in Figure 6.5). In one of these experiments, 17.5 g of natural (non-enhanced) pyrite were also introduced to the leaching slurry while the other experiment was conducted in the absence of pyrite. The results are shown in Figure 6.6. For comparison purposes, the results of leaching in the absence of catalysts are also shown.

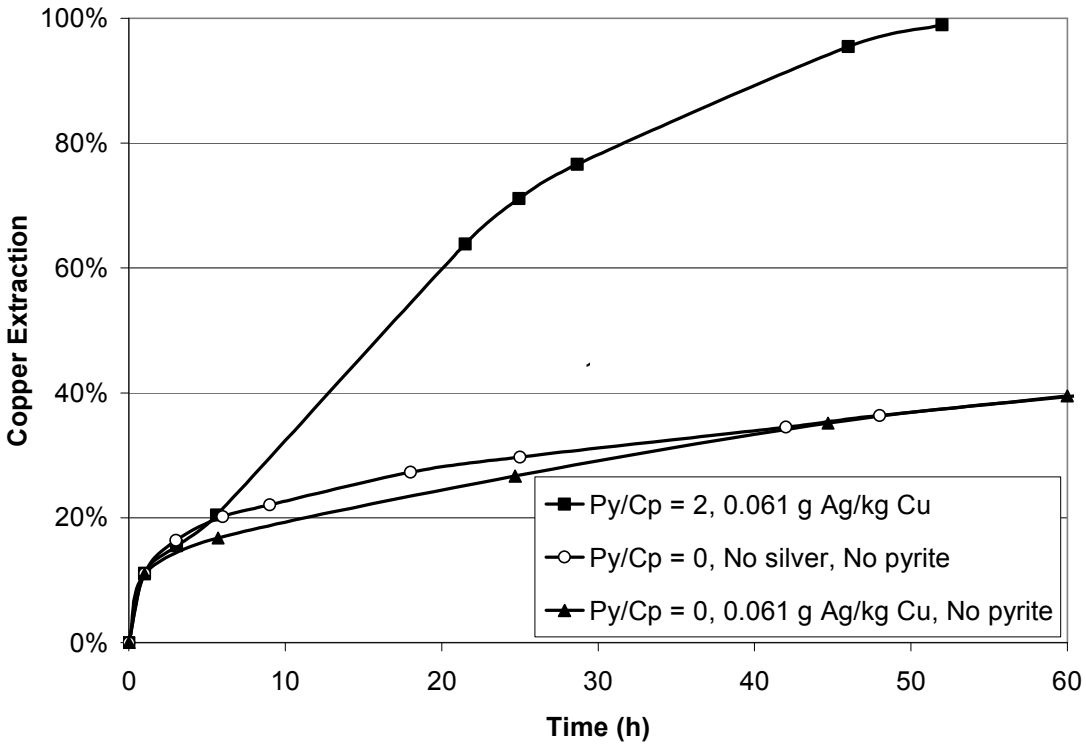

Figure 6.6 Effects of addition of 0.061 g Ag/kg Cu (equivalent to 10% silver make up shown in Figure 6.5) in the absence and the presence of pyrite at a potential set point of 450 mV and 80°C

Figure 6.6 shows that, with the addition of 0.061 g Ag per kg Cu and at a natural pyrite-to-chalcopyrite ratio of 2, leaching is complete after 55 hours. Recall that leaching was complete in just 10 hours in the presence of silver-enhanced pyrite at the same level of silver consumption (Figure 6.5). These results clearly indicate that the 10% silver makeup, by itself, was not sufficient to ensure rapid copper extraction. Moreover, the addition of 0.061 g Ag per kg Cu in the absence of pyrite had no effect on the kinetics of chalcopyrite leaching whatsoever.

Tests were also conducted to compare the addition of silver-enhanced pyrite with the BRISA process, which is based on conventional silver-catalyzed leaching and which has been the subject of several recent publications (Carranza *et al*., 1997; Romero *et al*., 1998; Romero *et al*., 2003). The first test was run under conditions identical to those recommended for the BRISA process, including the proposed amount of added silver. The results, shown in Figure 6.7, agree very closely with the work of Romero *et al*. (2003). Leaching kinetics is reasonably rapid, but complete copper extraction is not achieved. This confirms similar results reported in Romero *et al*. (2003), which also showed incomplete copper extraction from every test. It bears noting that the amount of silver used in the BRISA process is nearly 40 times higher than the initial amount of silver used to enhance pyrite in the Galvanox™ process.

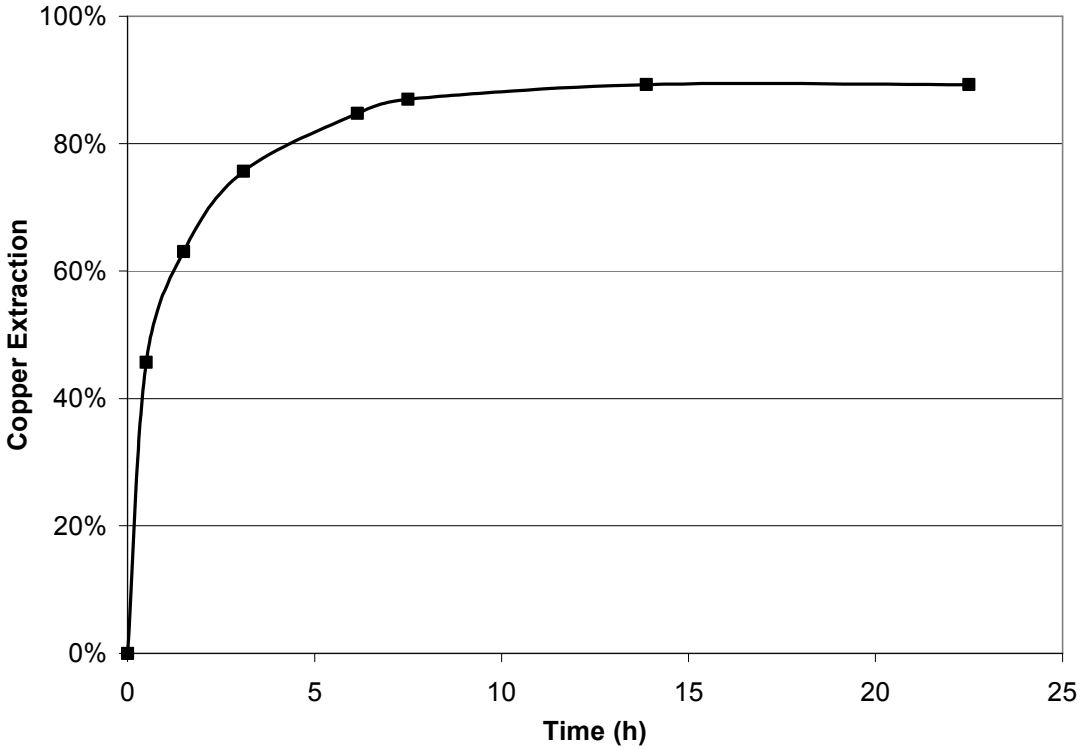

Figure 6.7 Typical results of the BRISA process with 22.2 g Ag per kg of contained Cu, initial Fe^{3+} concentration of 24 g/L, 20 g/L Cu concentrate, and 70°C.

This experiment was repeated with the same amount of silver required for silver-enhanced pyrite in the Galvanox™ process using silver-enhanced pyrite. Figure 6.8 compares results of high-potential silver-catalyzed leaching and low-potential silver-enhanced pyrite, both using the same amount of silver. The main difference between these low-silver tests and the conventional silver-catalyzed tests shown in Figure 6.3 and Figure 6.8 is that the latter were initiated at a much higher redox potential (roughly 600 mV). For comparison purposes, another test was also run under conditions identical to the BRISA process, but without added silver. Obviously, at the very low levels of silver addition used in the Galvanox™ process using silver-enhanced pyrite, high-potential silver-catalyzed leaching gives very similar results to leaching chalcopyrite with no catalyst present at all. The higher redox potential corresponds to the high ratios of ferric to ferrous

recommended in Romero *et al*. (2003). Obviously, this practice is antithetical to rapid oxidation of chalcopyrite, for the reasons alluded to above.

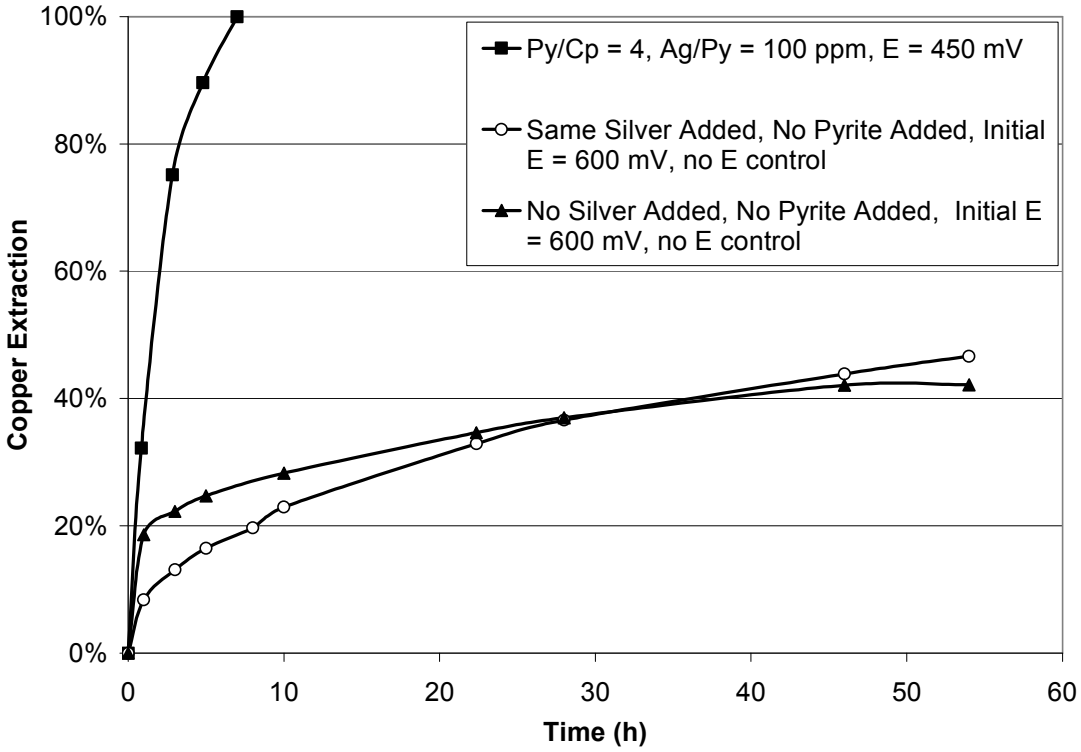

Figure 6.8 Comparison between high-potential silver-catalyzed leaching and silver-enhanced pyrite-catalyzed leaching, both with 1.23 g Ag per kg of contained Cu, at 80°C

The results of the experiments shown in this chapter clearly indicate that the presence of pyrite is a critical factor to ensure rapid and complete copper extraction. Although silver accelerate the rate of chalcopyrite leaching, adding the same amount of silver used in silver-enhanced catalyzed leaching, no/little improvement is observed on leaching kinetics.

6.5 Conclusions

In this chapter, a comparison between silver-catalyzed leaching and silver-enhanced catalyzed leaching was done. The catalytic ability of silver to

accelerate the kinetics of chalcopyrite leaching in ferric sulfate media is well-known. Hence, it was the subject of interest to evaluate the role of silver and silver-enhanced pyrite in this process. Under identical conditions, the same amount of silver was introduced to the leaching process in the absence and the presence of pyrite. It has been observed that the rate of copper extraction in the presence of pyrite is significantly higher. In addition, due to the high cost of silver, evaluation of recycling the silver into subsequent leaching tests is very important. Using silver-enhanced pyrite, the addition of only 0.061 g Ag/Kg Cu is sufficient to ensure rapid and complete chalcopyrite leaching. It has been found that at this level of silver, the process of silver catalyzed leaching is considerably slower and in fact there is not a significant difference in the absence or presence of silver at this level (0.061 g Ag/kg Cu). Consequently, the results of all experiments shown in this chapter indicate that the presence of pyrite is a critical factor in this process. In addition, unlike silver-catalyzed leaching, in the presence of silver-enhanced pyrite, silver can be efficiently recycled to subsequent leaching tests. In the presence of silver-enhanced pyrite, both silver and pyrite maintain their catalytic properties through recycle leach tests, while in silver-catalyzed leaching, silver is lost by formation of argentojarosite or silver sulfide and it is not recoverable unless an additional series of inconvenient process steps is followed.

Chapter 7 Interaction of Silver Ions with Pyrite Minerals

7.1 Introduction

As described in Chapter 4, the most recent studies of the Galvanox™ process have shown that pyrite samples from various sources influence the kinetics of chalcopyrite leaching differently. Some pyrite samples accelerate the rate of leaching significantly, while others only have minor effects on the kinetics. In this chapter, the variations of pyrite minerals in terms of impurities, minor and trace elements are discussed.

In addition, it was shown, in Chapter 4, that the catalytic properties of pyrite in the Galvanox™ process are improved by pretreating pyrite with silver ions. In this chapter the nature of the interaction of silver with pyrite is studied.

7.1.1 Variations in Pyrite Minerals

Pyrite is the most common sulfide mineral and is typically an abundant component of both simple and complex sulfide ores (Abraitis *et al*., 2004). The behaviour of pyrite in leaching processes is variable. This variation can be attributed to the differences in the structural, and crystallographic, chemical and/or electrical properties of pyrite (Abraitis *et al*., 2004).

Iron and sulfur are the essential elements in pyrite. The molar ratio of iron to sulfur is close to 1:2 in most natural specimens (Oberthur *et al*., 1997). All natural pyrites contain small quantities of minor and trace elements. A minor element is present in detectable quantities but is not an essential component of the mineral phase. A trace element is present in smaller quantities but still detectable (<1 wt%). Previous studies reported the presence of Ag, As, Au, Bi, Cd, Co, Cu, Hg, Mo, Ni, Pb, Ru, Sb, Se, Sn, Te, Tl, and Zn. These elements can be substituted in pyrite lattices (Fleischer, 1955; Vaughan and Craig, 1978). This substitution can

be stoichiometric such as substitution of Ni, Co, for Fe or Se and Te for S. Non-stoichiometric substitution may also occur, such as substitution of As for S, and may lead to significant variation in the electrical properties of pyrite (Abraitis *et al*., 2004). Along with those substitutions that occur during mineral formation, trace and minor elements may be present in pyrite mainly in the form of inclusions.

Non-stoichiometric substitution may cause significant changes in the electrical properties of pyrite. For example, the presence of arsenic in pyrite increases its electrical conductivity significantly. Non-stoichiometric substitution of As for S in the disulphide group leads to the formation of the AsS_3^- group within the lattice (Klein and Hurlbut, 1993). This group is likely to present *p*-type semiconductor properties, thereby trapping electrons and resulting in high electrical conductivity (Abraitis *et al*., 2004). Previous studies reported the presence of Au in most pyrite containing As (Arehart *et al*., 1993). This may be attributed to the formation of the AsS_3^- group, which can be charge compensated by Au^{3+} in the mineral lattice. Therefore, the incorporation of As into pyrite has important consequences in terms of both electrical conductivity and the ability of the mineral to hold minor and trace elements (Griffin *et al*., 1991).

The measured silver content of pyrite was reported to vary between 8 and 656 ppm (Chenery *et al*., 1995; Huston *et al*., 1995). This element is mainly present in the form of inclusions of other phases. It was observed that the Ag concentration in pyrite correlates with the concentration of Pb and Cu associated with argentiferrous galena, tetrahedrite or tennantite (Abraitis *et al*., 2004). Greenwood and Earnshaw (1984) reported the presence of Ag^{3+} in pyrite. This substitution may be analogous to Au^{3+} substitution through coupling with AsS_3^-.

The differences in pyrite behaviour during leaching can be attributed largely to its electrical properties. Semiconductivity reveals the presence of charge carriers, which may be related to deviation from stoichiometry and/or the presence of

impurities in solid solution and/or thermal excitation across the energy gap (Pridmore and Shuey, 1976).

Deviations from stoichiometry in pyrite are very small. Some researchers reported that pyrites with a deficit of sulfur tend to be *n*-type semiconductors (Favorov *et al*., 1974; Vaughan and Craig, 1978). This *n*-type behaviour is due to excess of iron atoms, which are expected to act as electron donors (Schieck *et al*., 1990). Conversely, pyrites with excess sulfur act as *p*-type semiconductors. This can be attributed to the fact that sulfur atoms are electron acceptors.

Minor and trace elements within the pyrite lattice can significantly change the semiconducting properties of pyrite. As discussed above, various elements may enter into the pyrite via stoichiometric and non-stoichiometric substitution or as inclusions. Different impurities confer either *p*-type or *n*-type properties on the pyrite. For instance, As is an important electron acceptor (*p*-type) impurity in pyrite (Pridmore and Shuey, 1976). Therefore, the amount of impurities in pyrite and their semiconducting behaviour may affect the semiconducting properties of pyrite.

The mean conductivity value of 46 pyrite samples was measured to be 47.64 $(\Omega\ cm)^{-1}$ and the median was 2.27 $(\Omega\ cm)^{-1}$ (Doyle and Mirza, 1996). Conductivity values ranged between 0.02 and 562 $(\Omega\ cm)^{-1}$. There was also a distinction between the conductivity of *n*-type and *p*-type pyrites. The mean conductivity of *n*-type pyrite was 56.08 $(\Omega\ cm)^{-1}$, but only 0.53 $(\Omega\ cm)^{-1}$ for *p*-type pyrite. The higher conductivities of *n*-type pyrite have been attributed to the higher mobility of charge carriers (Abraitis *et al*., 2004).

It has been shown that inclusion of metal of a higher valence state in an insulator may provide clouds of excess electrons surrounding the individual inclusions as space charge layers without charge compensation by other defects in the insulator (Wagner, 1972). Hence, it is expected that the electrical conductivity of

a material (even an insulator) is altered by addition of dispersed conductors (Wan *et al*., 1984).

Thermal excitation across the energy gap was another source of variation in the semiconducting properties of pyrite. However, this factor may only affect the conductivity at elevated temperatures. As temperature is raised, some electrons from the valence band are able to jump across to the conduction band. Heat-induced conductivity is called intrinsic, while conductivity attributable to extra electrons from impurity atoms is called extrinsic. It has been noted that pyrite samples exhibit intrinsic conductivity at temperatures above 500°C (Schieck *et al*., 1990).

Pyrite has the highest rest potential of all common sulfide minerals (Majima, 1969). Reported values are shown in Table 7.1. In a previous study, the rest potentials of 12 pyrites were measured (Doyle and Mirza, 1996) and a rest potential for pyrite in the range of 0.558 to 0.699 V (*vs* SHE) at 25°C and pH 1 was reported. These data suggest that the rest potentials of pyrite are not dependent on chemical composition or bulk conductivity.

Table 7.1 Standard state rest potential *vs* SHE at 25°C and pH = 4 (Majima, 1969)

Mineral	Rest Potential (V)	Mineral	Rest Potential (V)
Pyrite	0.66	Bornite	0.42
Marcasite	0.63	Galena	0.40
Chalcopyrite	0.56	Argentite	0.28
Sphalerite	0.46	Stibnite	0.12
Covellite	0.45	Molybdenite	0.11

As discussed above, deviation from stoichiometry in pyrite is generally small. The significant variation in electrochemical properties of pyrite cannot be related to

these minor deviations. Natural pyrites contain minor and trace elements that may affect their conductivity and, therefore, their electrochemical properties.

7.1.2 Reactions of Silver Ions with Pyrite

Interaction of silver ions with pyrite was investigated in various studies. Different mechanisms and reactions were suggested to explain the electrochemical behaviour of the product layer on the surface of the pyrite. Pyrite is one of the most common gold-bearing sulfide minerals. Leaching the precious metals from pyrite was suggested to lead to the formation of the tenacious layer of elemental sulfur which could inhibit the leaching rate (Mathews and Robins, 1974; Peters, 1984). Hence, the interaction of silver ions with pyrite was the subject of interest mainly to improve the oxidation of pyrite to recover precious metals.

Hiskey *et al*. (1987) investigated the reaction of silver ions with pyrite with the aim of enhancing the pyrite leaching rate in ferric sulfate media. It has been reported that the rate of silver transfer to the pyrite surface is considerably slower than the rate of transfer to chalcopyrite and exhibits higher activation energy. In this study, X-ray Photoelectron Spectroscopy (XPS) and X-ray Diffraction (XRD) analyses were performed on pyrite particles pretreated in a silver nitrate solution. Hiskey *et al*. (1987) reported that the results obtained using XPS was inconclusive, due to the minor difference between binding energy of silver and silver sulfide. It has been noted that the width of the peaks at half-height was roughly 2 eV and that was considerably wider than the difference between the peak positions for different silver compounds (silver, silver sulfide, silver oxide). However, their XRD results indicated that elemental sulfur and elemental silver were the main products of this interaction. In this study, the following reaction was proposed:

$$FeS_2 + 2\ Ag^+ = Fe^{2+} + 2\ S^0 + 2\ Ag^0 \qquad (7.1.1)$$

According to this study, the metallic silver forms on ground pyrite particles very rapidly when pyrite is in contact with the silver in solution. The reduction of Ag^+ on pyrite surface is similar to an electrochemical cementation reaction where a more noble metal is precipitated by a more electropositive metal.

Oxidation of elemental silver has been proposed in the presence of ferric ions. When 1 M ferric sulfate is contacted with pyrite which has been pretreated in a solution containing silver, most of the silver immediately redissolves and does not redeposit when ferric ions are present (Hiskey *et al*., 1987). This observation implies that the kinetics of the transfer reaction between Ag^+ and pyrite is slower than the reaction between Fe^{3+} and pyrite. This suggests that Ag^+ does not likely enhance the ferric sulfate leaching of pyrite.

Silver sulfide and polysulfide were also observed on the pyrite surface at different pH values and silver concentrations (Bancroft and Hyland, 1990; Buckley *et al*., 1989; Scaini *et al*., 1995). According to these studies, when pyrite is in contact with silver ions, the first step is the formation of silver sulfide followed by deposition of the metal at longer exposure times. They have also confirmed the presence of polysulfide on the surface of the mineral. Scaini *et al*. (1995) have proposed the following reaction to explain the interaction of silver ions with pyrite which indicates the presence of both elemental silver and silver sulfide:

$$FeS_2 + 8\ Ag^+ + 4\ H_2O = Fe^{2+} + Ag_2S + 6\ Ag^0 + SO_4^{2-} + 8\ H^+ \qquad (7.1.2)$$

Maddox *et al*. (1996) proposed the replacement of ferrous ions with silver ions at room temperature:

$$2y\ Ag^+ + Fe_{1-x}S_2 = Fe_{1-x-y}Ag_{2y}S_2 + y\ Fe^{2+} \qquad (7.1.3)$$

In reaction (7.1.3), initial loss of ferrous ions by dissolution of pyrite by the following reaction has been assumed:

$$FeS_2 = Fe_{1-x}S_2 + x\,Fe^{2+} + 2x\,e^- \quad (7.1.4)$$

In these studies, it was also speculated that some other oxidizing species in addition to silver must be present in solution to interact with pyrite causing oxidation of the mineral substrate, thus allowing the mineral to adsorb silver from solution.

Silver ions react very rapidly with an iron-deficient sulfide to form an iron-silver sulfide surface species, leading to a decrease in silver ion concentration at the surface. The interaction with ferrous ions is reported to be a simple ion exchange reaction (Maddox *et al*., 1996). Similar interaction between silver and galena has been observed in another study by Scaini *et al*. (1995).

Buckley *et al*. (1989) proposed the following reaction to explain the interaction of pyrite with silver ions:

$$4\,FeS_2 + 14\,Ag^+ + 4\,H_2O = 4\,Fe^{2+} + 7\,Ag_2S + SO_4^{2-} + 8\,H^+ \quad (7.1.5)$$

They also reported that pH affects the silver deposit thickness. They observed the same thickness of silver deposit in unacidified 10^{-3} M silver ions after 10 min on the pyrite surface versus 60 min for an acid-containing solution (0.25 M H_2SO_4) and 10^{-3} M silver ions. This result is in agreement with their proposed reaction for silver sulfide deposition since this reaction generates acid.

The influence of Ag^+ concentration on silver-pyrite interactions has been also examined (Hiskey and Pritzker, 1988; Hiskey *et al*, 1987). Based on these electrochemical studies, there is no evidence that any silver deposition occurs at Ag^+ concentration lower than 10^{-3} M.

Another important aspect to consider is the effect of the initial state of the pyrite surface on its interaction with silver ions. It has been observed that when the

initial anodic scan is extended high enough for pyrite to be oxidized, silver deposition on the pyrite surface is inhibited. This is due to the formation of surface products which passivate the pyrite surface. Various factors such as Ag^+ concentration and the degree of agitation in the electrolyte have an important effect on the degree by which pre-oxidation of the pyrite inhibits silver deposition. For instance, Hiskey and Pritzker (1988) observed that in a solution containing 10^{-2} M Ag^+, a considerable amount of deposition still occurs after the potential has been increased to 1.07 V (the potential at which pyrite oxidation increases significantly) and the mineral has been severely oxidized. Hence, silver deposition on pyrite is highly sensitive to Ag^+ concentration.

Pyrite samples reacted with dissolved silver were compared with pyrite samples containing silver naturally. In both samples, the silver surface concentration is much higher than in the bulk. It was also noted that the thickness of the Ag-rich layer was about 10 nm on pyrite reacted for 48 hours with silver solution, and about 100 nm on natural pyrite containing silver. These differences were attributed to deposition rate, solution composition, formation of the rock around the pyrite grain, and temperature (Scaini *et al*., 1997).

7.2 Objectives

In previous studies, the formation of either elemental silver or silver sulfide or both species was reported. In this chapter, the interaction of silver and pyrite was studied under the conditions of silver-enhanced pyrite preparation in the Galvanox™ process.

7.3 Experimental

7.3.1 Pyrite Pretreatment with Silver Ions

Pyrite samples were pretreated with silver ions at various silver concentrations in solution. 5 g of the pyrite sample were added to 400 mL solution containing the desired amount of silver ions according to Table 7.2. Silver ions were added as standard 1000 ppm silver nitrate solution. The interaction of silver with pyrite was studied by following the concentration of silver in solution using Atomic Absorption Spectroscopy (AAS).

Table 7.2 The amounts and concentrations of silver ions in solution containing 5 g of pyrite

Ag/Py ppm	Ag (mg)	Initial [Ag] in solution (ppm)
600	3	7.5
1000	5	12.5
4000	20	50
10000	50	125

After silver pretreatment, samples were filtered. The solutions were sent to Acme Labs (Vancouver, BC) for Induction Coupled Plasma (ICP) analysis. The solid residues were washed, dried, and analyzed by XRD. These analyses were performed under the conditions described in section 5.2.3.

7.3.2 XRD Analysis

XRD analysis was carried out on a Rigaku Rotaflex 200 diffractometer using Cu Kα radiation at 40 kV and 20 mA, scanning from 10° to 90° (2θ) with the scanning rate of 0.02° (2θ).

7.3.3 Materials

In this study, Pyrite #3 containing 98.7% pyrite was used. The mineralogy and elemental composition were shown above (Table 4.1 and Table 4.2).

7.3.4 Electrochemical Measurements

Electrochemical experiments were carried out using a three-electrode cell. Pyrite was used as the working electrode and graphite was used as a counter electrode. A saturated Hg/Hg_2SO_4 electrode was used as a reference electrode. However, in this study, the results were converted and reported with respect to saturated Ag/AgCl to be consistent with the redox potentials in batch leaching experiments. The electrolyte used in these experiments was identical to the solution in batch leaching experiments and contained 86 g/L sulfuric acid, 0.57 g/L ferric, and 13.4 g/L ferrous. The experiments were conducted at room temperature.

Massive electrodes were prepared by cutting the pyrite sample into small cubes. The samples were mounted in epoxy resin, leaving one surface exposed to the electrolyte. The sample was polished with 1200 grit SiC (silicon carbide) to obtain a surface area with less defects, cracks and pores.

7.4 Results and Discussion

The pyrite sample was ground and sieved through No. 500 (25 μm) and No. 400 (38 μm) mesh screens. Particles larger than 25 μm and smaller than 38 μm were selected for the experiments shown in this chapter. Pyrite particles in a narrow size range were used to reduce the variability between particles. The BET surface area of the pyrite sample was confirmed to be 0.69 m^2/g. Pyrite samples were pretreated with silver ions and 2 mL samples were taken at various time intervals. The solutions were analyzed by AAS. Figure 7.1 shows the rate of

interaction of silver ions with pyrite at various silver concentrations. In solution containing 3 mg silver ions, silver concentration was 0.63 ppm after one minute. This corresponds to a silver-to-pyrite ratio of 550 ppm. The silver concentration in solution gradually decreased. No silver was detected in solution after 5 minutes. At silver concentrations of 12.5 ppm and 50 ppm, all silver ions were reacted with pyrite after 2.5 and 7 hours. At the higher silver concentration of 125 ppm, even after 7 hours, the silver concentration in the solution was 48.23 ppm, and 62% of silver ions reacted with pyrite. This corresponds to a silver-to-pyrite ratio of 6200 ppm. This value represents the maximum concentration of silver on this pyrite sample.

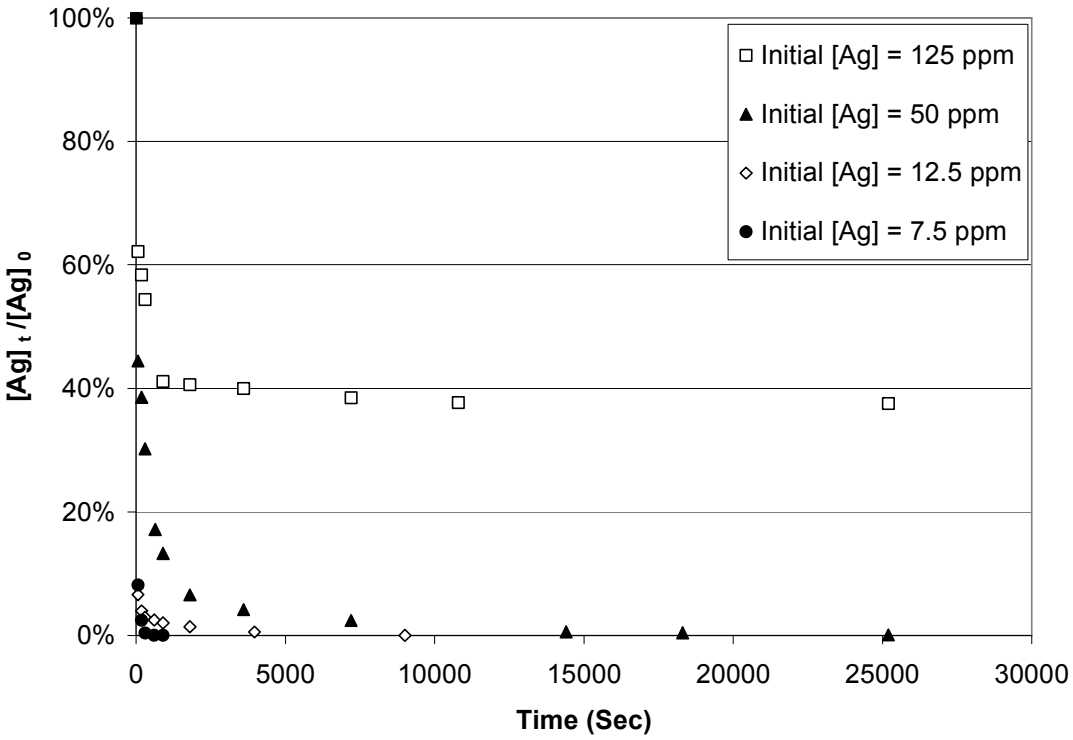

Figure 7.1 Rate of interaction of silver ions with pyrite at various silver concentrations

Table 7.3 shows the ICP analysis of final solutions after pretreatment of pyrite with silver ions at various silver concentrations.

Table 7.3 Elemental compositions of solutions after pyrite treatment with silver

Elements	$[Ag]_0$ = 7.5 ppm	$[Ag]_0$ = 12.5 ppm	$[Ag]_0$ = 50 ppm
Ag (ppb)	1.53	1.24	298.76
Cu (ppb)	45.9	49	87.4
Cr (ppb)	1.2	40	60.2
Fe (ppb)	880	1374	1594
Mn (ppb)	84.67	92.88	94.87
Ni (ppb)	96.2	114.7	127
Pb (ppb)	7.2	14.1	15.2
S (ppm)	<1	<1	2
Sb (ppb)	<0.05	0.09	0.26
Si (ppb)	1367	1433	1462
Th (ppb)	<0.05	0.21	0.54
Zn (ppb)	15.5	24.1	17.1
Zr (ppb)	<0.02	0.04	0.12

Table 7.3 shows that concentration of many of trace and minor elements increase by increasing the silver concentration. This finding implies that silver displaces these impurities from the pyrite surface layer. The major element in the solution is iron. The following reactions may occur under these conditions:

$$FeS_2 + 2\ Ag^+ = Fe^{2+} + 2S^0 + 2\ Ag^0$$
$$\Delta G^O = -86.929\ kJ/mol \qquad (7.3.1)$$

$$FeS_2 + 2\ Ag^+ = Ag_2S + Fe^{2+}$$
$$\Delta G^O = -127.312\ kJ/mol \qquad (7.3.2)$$

.

The Gibbs free energies of reactions per mole of pyrite were determined using the data shown in Table 7.4.

At higher silver concentration, sulfur in its soluble form was also detected in solution. In addition, there is no linear correlation between the silver and iron level at high silver concentration. Under these conditions, the following reactions may occur:

$$4\ FeS_2 + 14\ Ag^+ + 4\ H_2O = 4\ Fe^{2+} + 7\ Ag_2S + SO_4^{2-} + 8\ H^+$$
$$\Delta G^O = -222.220\ kJ/mol \qquad (7.3.3)$$

$$FeS_2 + 8\ Ag^+ + 4\ H_2O = Fe^{2+} + Ag_2S + 6\ Ag^0 + SO_4^{2-} + 8\ H^+$$
$$\Delta G^O = -385.794\ kJ/mol \qquad (7.3.4)$$

Table 7.4 Standard Gibbs free energy of formation of species involved in this process at 298 K, 1 atm

Species	ΔG^O (kJ/mol)
FeS_2	−158.824
Fe^{2+}	−91.525
Ag^+	77.114
Ag_2S	−40.383
H_2O	−237.141
SO_4^{2-}	−744.362

The solid residue at high silver concentrations of 4000 and 6200 ppm were studied using XRD to detect the crystal structure of silver species formed on the pyrite. The results are shown in Figure 7.2 and Figure 7.3. For comparison purposes, the XRD pattern of natural pyrite (before silver treatment) was also added. The XRD pattern of pyrite samples pretreated with silver reveals several peaks that are not observed in the XRD pattern of the natural pyrite sample. These peaks match with silver and/or silver sulfide. The XRD reference pattern of the assigned peaks was also added to Figure 7.2 and Figure 7.3 for clarity purposes.

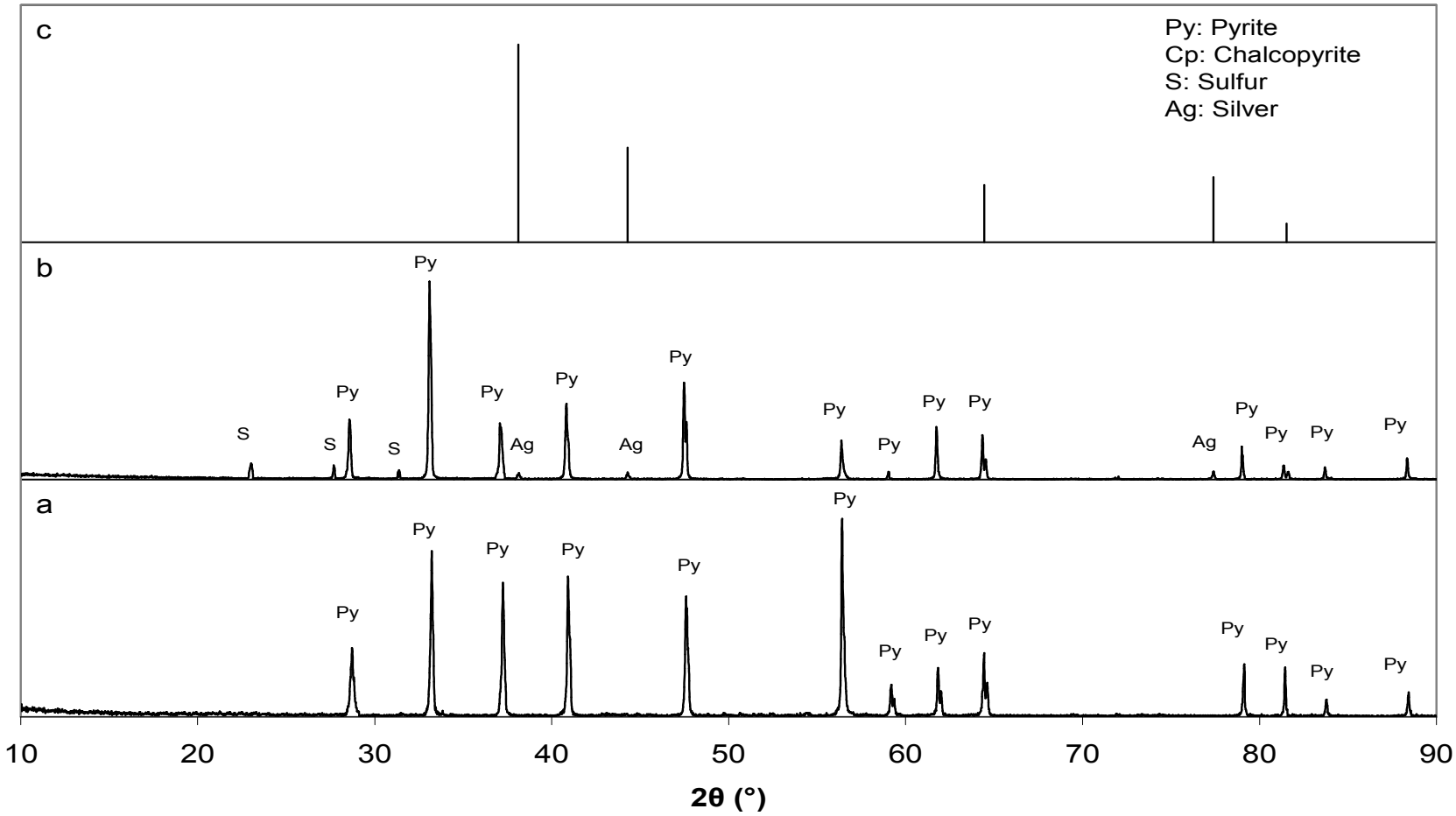

Figure 7.2 XRD patterns of (a) natural pyrite sample (b) pyrite sample pretreated with silver at a silver-to-pyrite ratio of 4000 ppm (c) silver

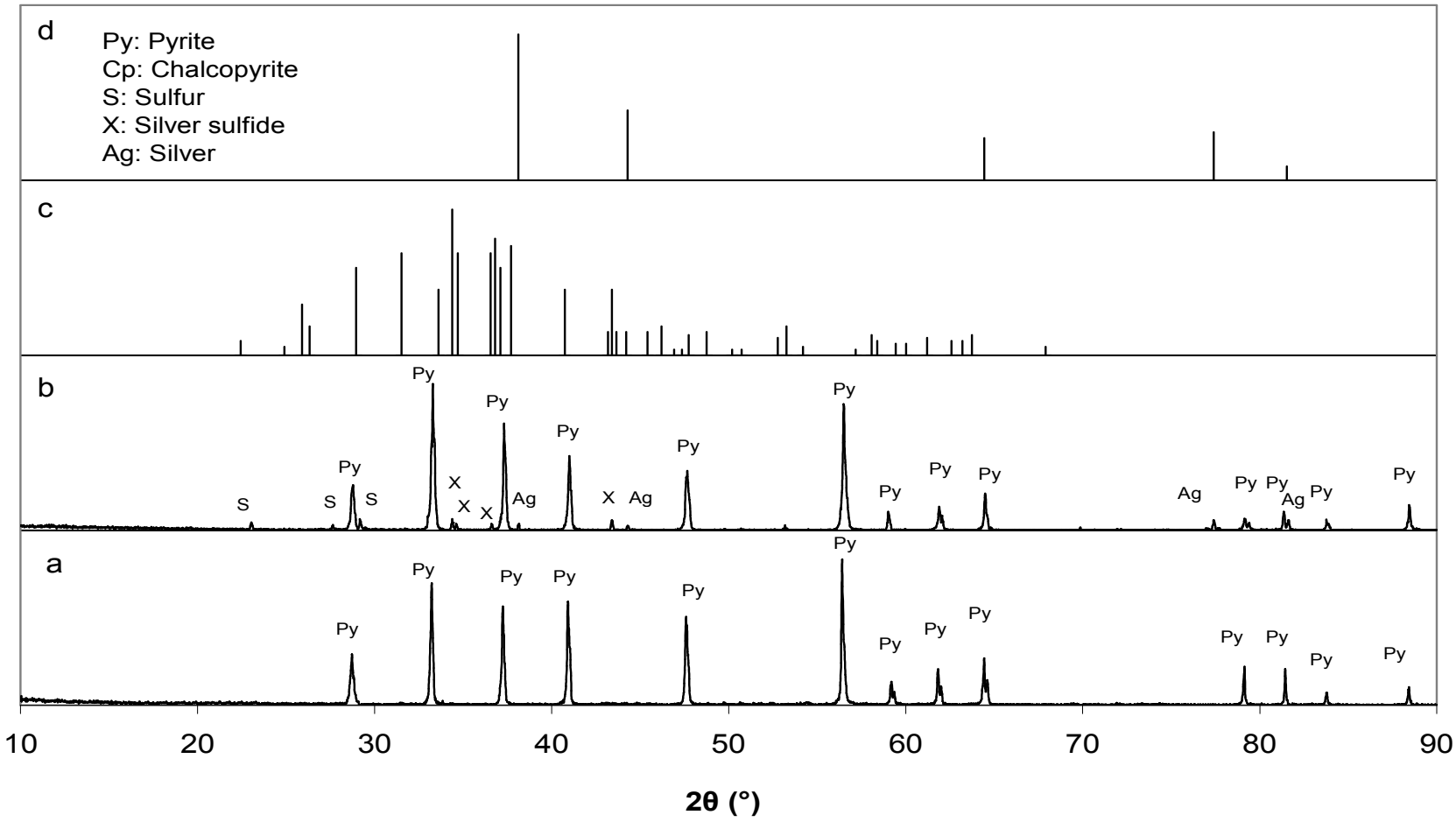

Figure 7.3 XRD patterns of (a) natural pyrite sample (b) pyrite sample pretreated with silver at a silver-to-pyrite ratio of 6200 ppm (c) silver sulfide (d) silver

According to the XRD analyses shown in Figure 7.2, the silver ions react with pyrite to form elemental silver. Hence, the proposed reaction under these conditions is reaction (7.3.1).

The results of ICP analysis also confirm this reaction as the number of moles of iron produced in the solution is approximately half of the number of moles of silver consumed and reacted with pyrite. This reaction can be also shown as two half-cell reactions as follows:

$$FeS_2 = Fe^{2+} + 2S^0 + 2\,e^- \qquad E^O = 0.340 + 0.0295 \log [Fe^{2+}] \qquad (7.3.5)$$

$$2\,Ag^+ + 2\,e^- = 2\,Ag^0 \qquad E^O = 0.799 + 0.059 \log [Ag^+] \qquad (7.3.6)$$

Therefore, silver ions are reduced on pyrite at its rest potential to form elemental silver.

XRD patterns of the pyrite sample at the higher silver-to-pyrite ratio (Figure 7.3), shows both silver and silver sulfide peaks. Sulfur peaks are also observed in this pattern. Thus, one might conclude that elemental silver forms at lower silver-to-pyrite ratios, followed by the formation of silver sulfide at higher silver-to-pyrite ratios.

The electrochemical behavior of pyrite in solutions containing sulfuric acid, ferric and ferrous solutions has been examined using cyclic voltammetry. Figure 7.4 shows the cyclic voltammograms obtained with a polished pyrite electrode in a solution prepared from sulfuric acid and ferric and ferrous sulfate. Each experiment was initiated at the rest potential followed by scanning to 400 mV above the open circuit potential, subsequently alternating to a cathodic sweep reaching 700 mV below the open circuit potential before returning to the rest potential; a constant sweep rate of 10 mV s^{-1} was used.

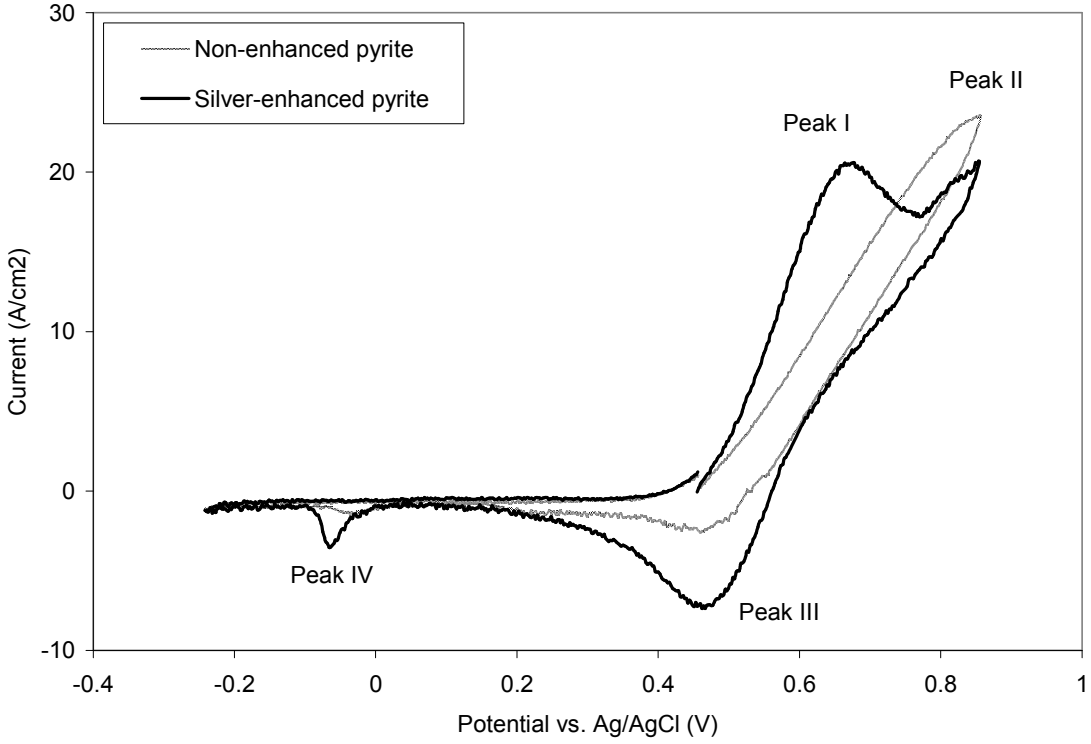

Figure 7.4 Cyclic voltammograms for non-enhanced and enhanced pyrite initiated at the open circuit potential in the anodic direction, at a sweep rate of 10 mV s^{-1}

Silver-enhanced pyrite was prepared by immersing the working electrode in a solution containing 10^{-3} M silver ions for 24 hours at the open circuit potential. The scan of non-enhanced pyrite shows typical pyrite behavior, as presented in previous studies (Biegler, 1976; Buckley *et* al., 1989; Hiskey and Pritzker, 1988). The scan of silver-enhanced pyrite clearly shows a new peak (Peak I), which is not observed in the scan of non-enhanced pyrite. A sharp peak in the first anodic cycle was assigned to the anodic dissolution of Ag^0 to Ag^+. The steep increase in current is typical of metal dissolution processes (Fletcher *et al*., 1983). Attributing the peak to silver dissolution also adds further evidence in favour of the previously proposed reaction (7.3.1) that metallic silver deposits on the surface of the pyrite at open circuit potential.

The peak of the scan in the cathodic region is about 450 to 455 mV (*vs* Ag/AgCl). This value is very close to the Ag^+ deposition potential according to the Nernst equation in a system containing 10^{-3} M Ag^+ (7.3.6). Interestingly, this value is also very close to the open circuit potential of pyrite, which further confirms the likely deposition of Ag^+ as Ag^0 on the surface of the pyrite at open circuit potential. The higher intensity of this peak in the scan of silver-enhanced pyrite has been attributed to the reduction of silver ions to elemental silver in addition to reduction of product of pyrite oxidation.

Continuing the scan to a more negative potential prior to reversal, Peak IV is observed, which has been assigned to reduction of elemental sulfur (Buckley *et al*., 1989; Price and Warren, 1986; Price *et al*., 1986):

$$S^0 + H^+ + 2\ e^- = H_2S$$
$$E = -\ 0.055 - 0.059\ pH - 0.295\ \log\ [H_2S]\ \textit{vs}\ Ag/AgCl \qquad (7.3.7)$$

Similarly, the higher intensity of peak IV in the scan of silver-enhanced pyrite than that of non-enhanced pyrite agrees with the proposed reaction (7.3.1) and thus it can be concluded that elemental silver and sulfur form on pyrite when pyrite is in contact with silver ions in solution.

It was also important to understand the behaviour of silver and pyrite after introducing silver-enhanced pyrite to the leach slurry. As described earlier, upon completion of the first test, the solid residues were sent to a local commercial laboratory for analysis by induction coupled plasma (ICP) spectroscopy. Solid assay results confirmed that the recycled pyrite contained less adsorbed silver than the freshly enhanced pyrite. The concentration of silver dissolved in the leach solution at the end of each test was always about the same (0.2 to 0.5 ppm), and probably represented a solubility limit for silver under the prevailing conditions. The chalcopyrite residue of an experiment conducted at a high silver-to-pyrite ratio of 4000 ppm was collected, separated from pyrite, and studied

using XRD to detect the crystal structure of silver species formed on the chalcopyrite residue. The results are shown in Figure 7.5(c) and Figure 7.6(b). For comparison purposes, the XRD pattern of the copper concentrate before leaching test was added to these figures and shown in Figure 7.5(a) and Figure 7.6(a). In addition, the XRD pattern of chalcopyrite residue after complete copper extraction at a silver-to-pyrite ratio of 100 ppm was obtained and shown in Figure 7.5(b). The XRD pattern of the chalcopyrite residue at higher silver-to-pyrite ratio reveals several peaks that are not observed in the XRD pattern of the copper concentrate before leaching and after leaching at low silver-to-pyrite ratio. These peaks match with silver sulfide. The XRD reference pattern of the silver sulfide is shown in Figure 7.6(c). These results clearly confirm the presence of silver sulfide formed in the sulfur residue during chalcopyrite leaching in the presence of silver-enhanced pyrite.

It is important to note that the concentration of silver in the residue shown in Figure 7.5(b) is approximately 80-90 ppm based on the solid assay results. This value is lower than the detection limit of XRD. Hence, the XRD pattern of this sample does not show the silver sulfide peaks.

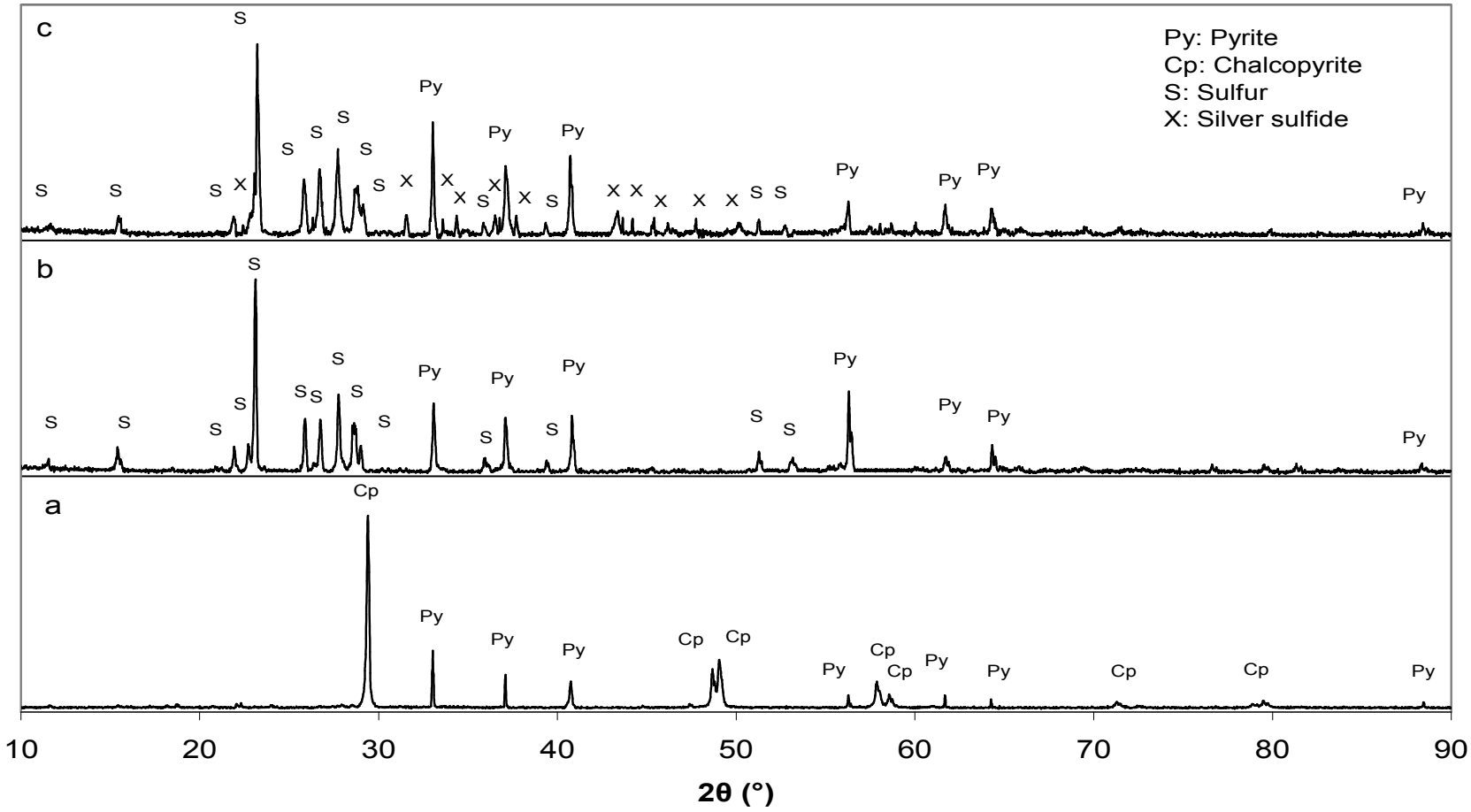

Figure 7.5 XRD patterns of (a) chalcopyrite concentrate (b) chalcopyrite residue of silver-enhanced pyrite catalyzed leaching at a silver-to-pyrite ratio of 100 ppm (c) chalcopyrite residue of silver-enhanced pyrite catalyzed leaching at a silver-to-pyrite ratio of 4000 ppm

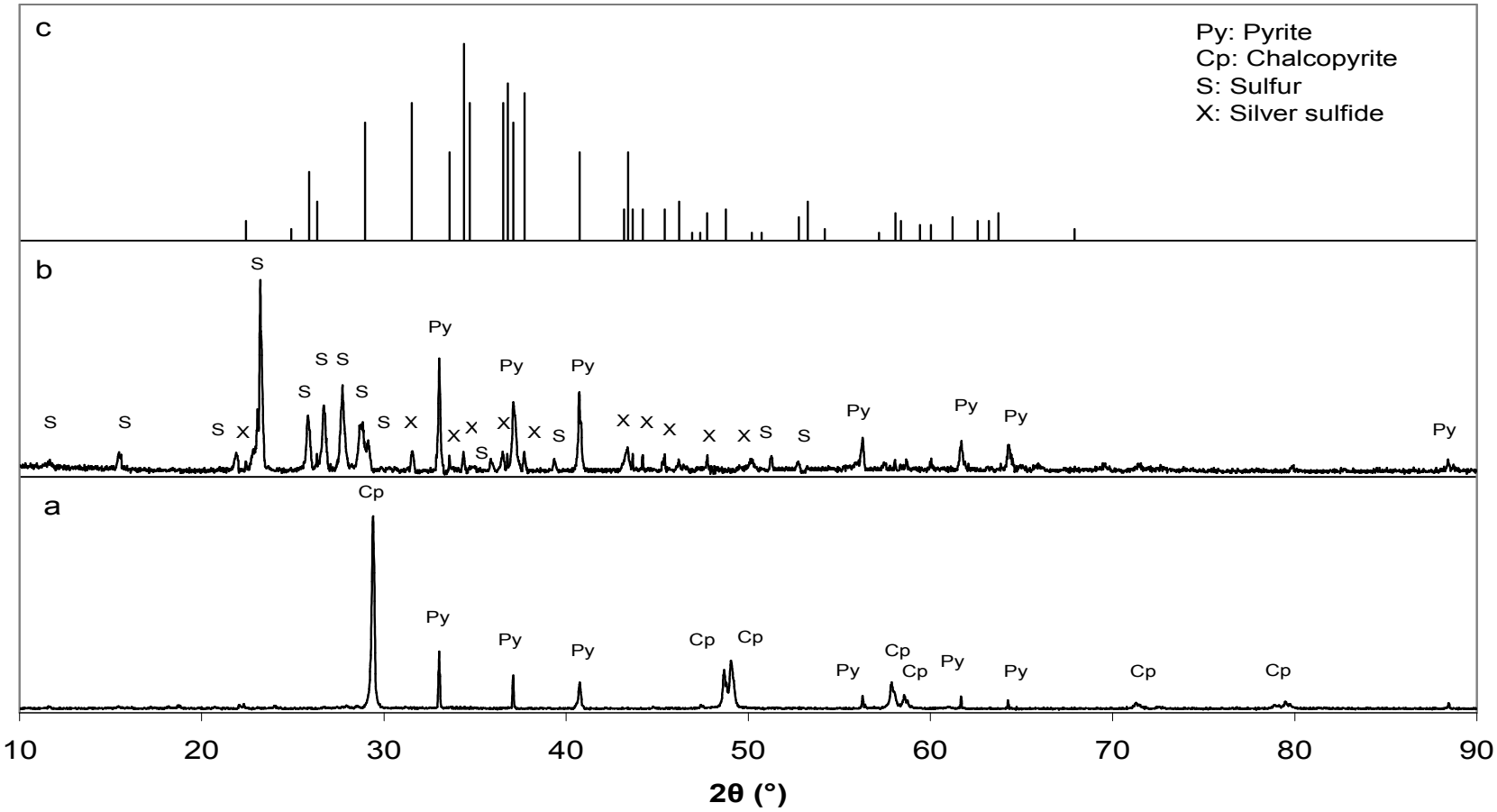

Figure 7.6 XRD patterns of (a) chalcopyrite concentrate (b) chalcopyrite residue of silver-enhanced pyrite catalyzed leaching at a silver-to-pyrite ratio of 4000 ppm (c) silver sulfide

The XRD pattern of the chalcopyrite residue shown in Figure 7.5(c) reveals silver sulfide peaks along with the sulfur residue. It is worth noting that the copper concentrate contained 15.9% pyrite; hence, the pyrite peaks observed in Figure 7.5 and Figure 7.6 belong to the pyrite associated with the copper concentrate.

Furthermore, the chalcopyrite residue of leaching experiments conducted at a silver-to-pyrite ratio of 4000 ppm was studied using SEM and EDX. The results are shown in Figure 7.7. These analyses also provide further evidence regarding the presence of silver in the sulfur layer.

(a)

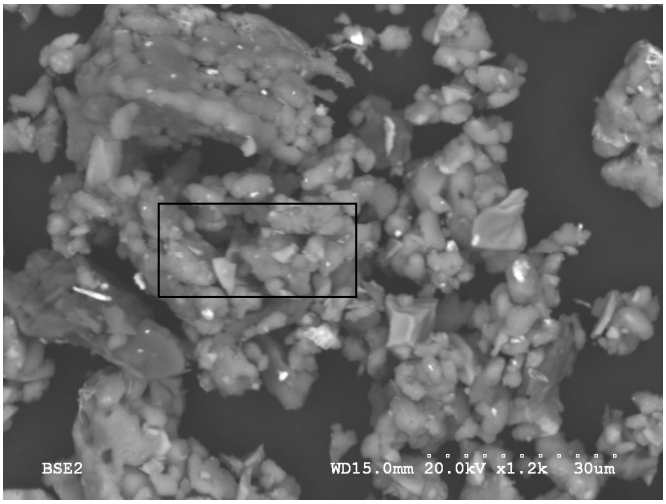

(b)

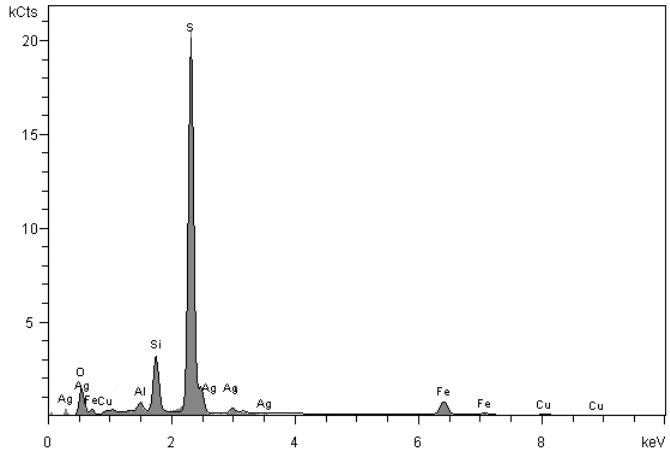

Elements	Concentration (wt%)	Elements	Concentration (wt%)
Oxygen	26.35 wt%	**Iron**	8.29 wt%
Aluminum	1.01 wt%	**Copper**	0.86 wt%
Silicon	6.47 wt%	**Silver**	0.98 wt%
Sulfur	56.04 wt%		

(c)

Figure 7.7 a) SEM micrographs, (b) EDX analysis, and (c) elemental analyses of selected area of chalcopyrite residue of silver-enhanced pyrite catalyzed leaching at a silver-to-pyrite ratio of 4000 ppm

7.5 Conclusions

In this chapter, the interaction of silver ions with pyrite was investigated. Pyrite samples were pretreated with silver ions according to the same procedure applied for silver-enhanced pyrite preparation during the Galvanox™ process. The results of ICP and XRD analyses confirmed the formation of elemental silver as a dominant species under these conditions. However, at higher silver-to-pyrite ratios, formation of silver sulfide was also observed. In addition, it was shown that silver reacted with pyrite up to a silver-to-pyrite ratio of 6200 ppm. The analyses also confirmed a very rapid (about one minute) reaction of silver ions with pyrite at a silver-to-pyrite ratio of 50 to 200 ppm used in the Galvanox™ process. Upon introducing silver-enhanced pyrite, a fraction of silver from silver-enhanced pyrite dissolved in the leaching solution and reacted with the sulfur around chalcopyrite to form silver sulfide. The presence of silver in the product sulfur layer was confirmed using EDX analysis. The solid residue was further studied to reveal the crystal structure of silver species. The XRD pattern of solid residue confirmed the presence of silver sulfide.

Chapter 8 The Mechanism of Chalcopyrite Leaching in the Presence of Silver-enhanced Pyrite

8.1 Introduction

As described in Chapter 4, a dramatic improvement in the leaching kinetics of chalcopyrite in ferric sulfate media was observed upon the addition of silver-enhanced pyrite. In this process, pyrite samples are pretreated with a miniscule amount of silver and used as a catalyst in atmospheric leaching of chalcopyrite. It has been shown that the addition of 10% makeup of silver-enhanced pyrite in each recycle test is required to ensure optimum catalytic effectiveness in subsequent leach tests. The results indicate that about 10% of the added silver leaves pyrite and reacts with sulfur formed around chalcopyrite.

In Chapter 5, it has been shown that acceleration of the rate of chalcopyrite leaching in the presence of catalysts is not due to alteration of the morphology of sulfur around chalcopyrite, since the formation of a porous sulfur layer around chalcopyrite was observed in both the presence and absence of catalysts. This observation also indicates that the rate of reaction is not mass transfer controlled. The transfer of copper and iron ions from the surface of unreacted chalcopyrite can occur easily through the pores of the sulfur layer.

In Chapter 6, the process of silver-enhanced pyrite catalyzed leaching was compared with the process of silver-catalyzed leaching. Considering the known catalytic properties of silver to accelerate the leaching of copper from chalcopyrite and a stronger affinity of silver to interact with chalcopyrite than with pyrite, it was important to evaluate the role of silver in both processes. The results showed that if the same amounts of silver used in the silver-enhanced catalyzed leaching process were added in the absence of pyrite, no improvement in the leaching kinetics would be observed. The results, shown in Chapter 6, indicate the critical role of pyrite in accelerating the rate of chalcopyrite leaching.

8.2 Objectives

Originally, the Galvanox™ process has been described as the galvanically assisted leaching of chalcopyrite, where pyrite provides an alternative surface for ferric reduction. As the leaching reaction proceeds, in the absence of silver-enhanced pyrite, a non-conductive sulfur layer forms on the surface of chalcopyrite. This layer may prevent electrical contact between pyrite and chalcopyrite particles in the slurry. The aim of this study was to understand the mechanism of this process and to reveal the role of silver and pyrite in enhancing the kinetics of chalcopyrite leaching in ferric sulfate media.

8.3 Experimental

8.3.1 Leaching Experiments

Leaching experiments were carried out according the procedure explained in section 4.2.1.

8.3.2 XRD Analysis

XRD analysis was carried out on a Rigaku Rotaflex 200 diffractometer using Cu Kα radiation at 40 kV and 20 mA, scanning from 10° to 90° (2θ) with the scanning rate of 0.02° (2θ).

8.3.3 Materials

In this study, a copper concentrate containing 27% copper, and Pyrite #4 containing 99.9% pyrite were used. Mineralogical and elemental compositions of the copper concentrate and the pyrite sample were summarized in Table 5.1 and Table 5.2, respectively. The copper concentrate was leached in the as-received condition. A Malvern Mastersizer was used to obtain particle size distributions of

the samples. The copper concentrate was not ultrafine, with an 80%-mass-passing size (P_{80}) of 46 µm. The pyrite particles were considerably larger, with a P_{80} of 290 µm, giving the consistency of fine sand.

8.3.4 Electrochemical Measurements

Electrochemical experiments were carried out using a three-electrode cell. Pyrite was used as the working electrode and graphite was used as a counter electrode. A saturated Hg/Hg_2SO_4 electrode was used as a reference electrode. However, in this study, the results were converted and reported with respect to saturated Ag/AgCl to be consistent with the redox potentials in batch leaching experiments. The electrolyte used in these experiments was identical to the solution in batch leaching experiments and contained 86 g/L sulfuric acid, 0.57 g/L ferric, and 13.4 g/L ferrous. The experiments were conducted at room temperature.

Massive electrodes were prepared by cutting the pyrite sample into small cubes. The samples were mounted in epoxy resin, leaving one surface exposed to the electrolyte. The sample was polished with 1200 grit SiC (silicon carbide) to obtain a surface area with less defects, cracks and pores.

8.3.5 Silver Sulfide Leaching

The silver sulfide formed during chalcopyrite leaching in the presence of silver-enhanced pyrite was dissolved according to the following procedure. Initially, cupric oxide was dissolved in hydrochloric acid to form cupric chloride.

$$CuO + 2\ HCl = CuCl_2 + H_2O \qquad (8.2.1)$$

After complete copper extraction from copper concentrate, the silver in the residue was leached in cupric chloride at pH 0 and 60°C, where pH was adjusted by addition of hydrochloric acid. The process was continued for 10 days.

$$Ag_2S + 2\ CuCl_2 = 2\ AgCl + Cu_2Cl_2 + S^0 \qquad (8.2.2)$$

Then, the sample was filtered and rinsed with distilled water and the solid residue was collected. The solid sample contained elemental sulfur and silver chloride. Thiosulfate is a divalent anion which tends to form stable complexes with low-spin d^8 metal ions (Pd(II), Pt(II), Au(III)) and (Cu(I), Ag(I), Au(I), Hg(II)) (Livingstone, 1965; Wilkinson, 1987). Hence, the solid residue was treated with sodium thiosulfate to dissolve silver from silver chloride via formation of silver complex ions. However, an important factor in thiosulfate stability is the pH of the solution, since thiosulfate rapidly decomposes in acidic media (Li *et al*., 1995). The solution pH was controlled with sodium hydroxide within the stability region of thiosulfate (pH ~10). This experiment was conducted at room temperature.

$$AgCl(s) + 2\ Na_2S_2O_3^{2-}(aq) + S^0(s) = Na_3Ag(S_2O_3)_2(aq) + NaCl(aq) + S^0(s) \qquad (8.2.3)$$

This reaction occurs rapidly as $[Ag(S_2O_3)_2]^{3-}$ is highly soluble.

$$Ag^+ + 2\ S_2O_3^{2-} = [Ag(S_2O_3)_2]^{3-} \qquad K_f = 2.9\times10^{19} \text{ (Kotz } et\ al\text{., 2009)} \qquad (8.2.4)$$

where K_f is the formation constant

The concentration of silver in solution was followed with Atomic Absorption Spectroscopy (AAS). The dissolution of silver chloride in thiosulfate solution was stopped when the silver concentration in the solution became constant. The dissolution reaction was complete in just a few minutes. Elemental sulfur is the sole solid product in this reaction. The solid residue was collected and rinsed with

distilled water. The sample was dried at room temperature. The dried sample was coned and quartered to obtain a representative sample for analysis. The sample was sent to Acme Labs (Vancouver, BC) for Induction Coupled Plasma (ICP) analysis to confirm the complete dissolution of silver from sulfur.

8.3.6 Synthesis of Silver Colloids

The most common method for synthesis of silver colloids is the chemical reduction of a silver salt with a reducing agent such as sodium borohydride, citrate, and ascorbate (Chou and Ren, 2000; Leoppold and Lendle, 2003; Nersisyan *et al*., 2003; Nickel *et al*., 2000; Sondi *et al*., 2003; Zhang *et al*., 1996). In this study a standard silver nitrate solution (1000 ppm) and sodium borohydride (99% $NaBH_4$) were used. The chemical reaction is as follows:

$$AgNO_3 + NaBH_4 = Ag + ½\ H_2 + ½\ B_2H_6 + NaNO_3 \qquad (8.2.5)$$

1mM silver nitrate and 2mM sodium borohydride solutions were prepared. Depending on the desired level of silver on sulfur samples, the required amounts of 1 mM silver nitrate and 2 mM sodium borohydride solutions were added at a ratio of 1 to 6. A large excess of sodium borohydride was added to ensure the complete reduction of silver (Solomon *et al*., 2007).

Initially, the required amount of sodium borohydride was added to a beaker. The beaker was placed into an ice bath, which was set on a stir plate. The sodium borohydride solution was cooled for 20 minutes. Then the required amount of silver nitrate solution was added dropwise, at a rate of 1 drop/second while solution was mixed with a magnetic stirrer. The solution turned yellow after the addition of a few drops of silver. Silver colloids show different colors due to light absorption and scattering in the visible region (Zielinska *et al*., 2009), which depends on their size and shape. The solution turns orange-yellow, violet, and eventually gray. The solution color varies with the speed of silver nitrate addition

and the ratio of reagents (silver nitrate and sodium borohydride solutions). To achieve consistency in all experiments, all experiments were conducted under identical conditions and stable yellow silver colloids were prepared. The stirring was stopped after addition of the last drop of silver nitrate solution. Then, the complete reduction of silver ions was confirmed by determining the silver concentration in the solution by AAS.

Once colloidal silver was prepared, 5 g of sulfur of 99.999% purity (-75 +45 μm) were added to the beaker. The solution was heated to 50°C to accelerate the reaction kinetics of the sulfur with the silver colloids. After 12 hours, the slurry was filtered and rinsed with distilled water. The solid residue was dried at room temperature. After coning and quartering, representative samples were collected and sent to Acme Labs for ICP analysis.

8.3.7 Sample Preparation for Conductivity Measurements

1 g of sulfur particles was mixed with three drops of distilled water and pressed at 7 kN into pellets of 1.45 cm in diameter (42.4 MPa). The pellets were held in an oven at 50°C for 72 hours. Given the density of sulfur (2.07 g/cm^2), the amount of material used, and the specimen volume, one can calculate the porosity. Due to the similarity of sulfur particle sizes and the applied pressure, the porosity of all specimens is in the same range and the results are comparable.

8.3.8 Conductivity Measurements

Copper wires were affixed to each side of a pellet with silver epoxy. Then, the resistance across the pellet was determined by passing AC potential at 1 kHz and measuring the current flowing across the pellet. The measurements were performed with a Lock-in Amplifier, Model SR810, Stanford Research Systems. Each measurement was performed on three pellets to evaluate the reproducibility

of the data. Using the geometric dimensions of each pellet, the resistivity was determined.

8.4 Results and Discussion

The first experiment was conducted to observe the rate of chalcopyrite leaching in ferric/ferrous sulfate solution at 450 mV (all redox potentials are reported *vs* the KCl-saturated Ag/AgCl reference electrode) in the absence of added pyrite. The second experiment was conducted to examine the effect of adding the natural pyrite sample at a pyrite-to-chalcopyrite ratio of 2. In order to enhance the catalytic properties of pyrite, the pyrite sample was pretreated with silver ions. Hence, the third experiment was carried out at a pyrite-to-chalcopyrite ratio of 2 and a silver-to-pyrite ratio of 100 ppm (i.e., 100 mg Ag per kg pyrite). As shown in Figure 8.1, copper extraction is incomplete and slow in the absence of a catalyst. In the presence of the natural (non-enhanced) pyrite sample with virtually no silver content, complete copper extraction was achieved after 100 hours. Hence, while complete copper extraction and faster kinetics are observed in the presence of the natural pyrite, a long residence time is required for complete copper extraction. Finally, in the presence of silver-enhanced pyrite complete copper extraction was achieved in just 10 hours.

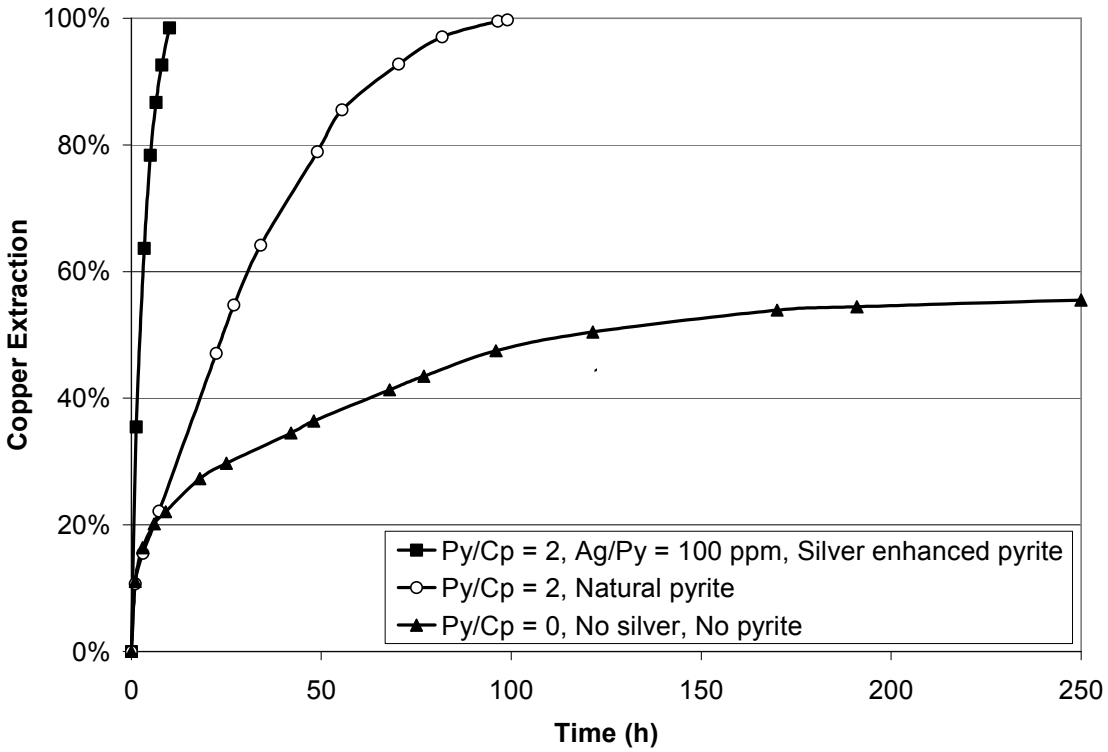

Figure 8.1 Chalcopyrite leaching in ferric sulfate media, in the absence of catalysts, in the presence of natural pyrite, and in the presence of enhanced pyrite at a potential set point of 450 mV and 80°C

The Galvanox™ process has been described as galvanically-assisted leaching (Dixon *et al.*, 2008). However, the formation of a non-conductive elemental sulfur layer around chalcopyrite particles would seem to limit the transfer of electrons from chalcopyrite to pyrite, thus preventing the electrical contact between pyrite and chalcopyrite particles which is generally required for galvanic coupling to occur (Mehta and Murr, 1983).

Due to the porous nature of the sulfur layer around chalcopyrite, one might assume that pyrite particles may approach to the surface of the unreacted chalcopyrite and, hence, electrons can be directly transferred from chalcopyrite to pyrite. However, it is important to note that pyrite particles are considerably larger than the pores of the sulfur layer. Therefore, the porous nature of the sulfur

layer allows the transfer of ions from/ to chalcopyrite to/ from the solution but does not provide a path for the direct contact between pyrite and chalcopyrite.

As mentioned earlier, in this process, during chalcopyrite leaching a small proportion of the added silver leaves pyrite and reacts with the elemental sulfur around chalcopyrite particles to form silver sulfide. In this study, it is hypothesized that even a very miniscule amount of silver sulfide decreases the resistivity of the sulfur layer significantly. Although the amount of silver sulfide is very low and the sulfur layer does not become very conductive, it does become conductive enough to allow the transport of electrons at a rate sufficient to support the leaching reactions. With a conductive path between pyrite and chalcopyrite, the galvanic interaction between these minerals can now occur. In this process, pyrite provides an alternative surface for ferric reduction. Therefore, the oxidation rate must increase to compensate for the increased electron consumption through ferric reduction and to thereby maintain charge neutrality in the solution. Since, pyrite is largely inert under these conditions due to its high rest potential (Majima, 1969 and Abraitis *et al.*, 2004), the only oxidation reaction is chalcopyrite leaching. Hence, the rate of copper recovery increases. Figure 8.2 shows the effect of increasing the ratio of cathodic to anodic area on the mixed potential and leaching rate. It is important to note that current and not current density is shown in abscissa.

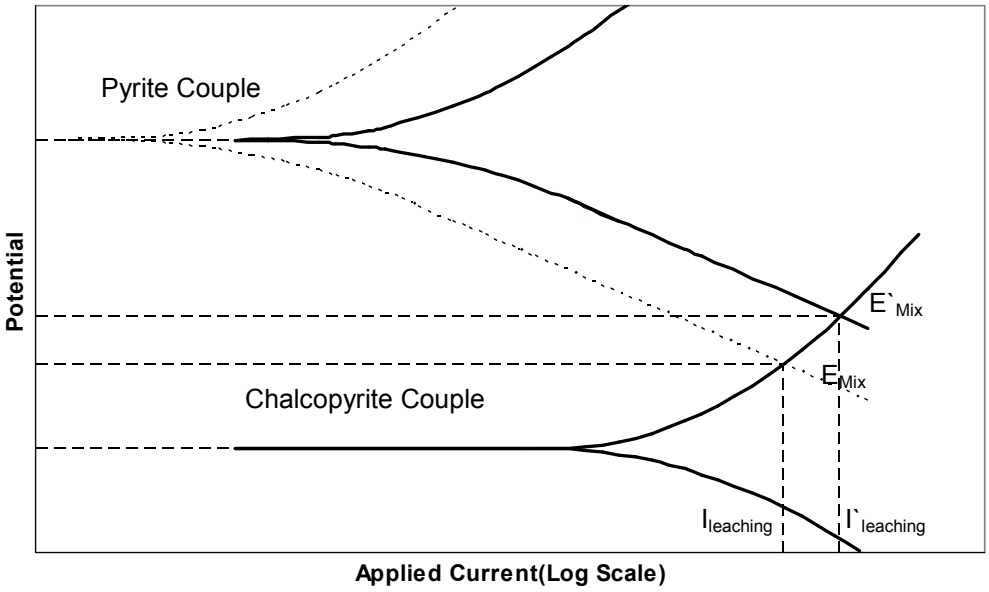

Figure 8.2 Shift in polarization curves for a case in which the cathodic area is larger than the anodic area (Nazari and Asselin, 2009)

Figure 8.2 shows that by increasing the cathodic surface area, both the anodic and the cathodic current increase. Since the anodic surface area remains constant, the rate of oxidation reaction increases.

In order to better understand the role of pyrite and chalcopyrite as a galvanic couple and the role of silver in decreasing the resistivity of the elemental sulfur layer, the following series of experiments was designed.

Copper concentrate was sieved through a No. 270 mesh (53 µm) screen, and only the portion that passed through the sieve was used in this study. Similarly, the pyrite sample was sieved through No. 45 (354 µm) and No. 60 (250 µm) mesh screens. Only the portion with particles larger than 250 µm and smaller than 354 µm was used.

The first test was run using natural pyrite at a pyrite-to-chalcopyrite ratio of 2. Copper extraction was complete after 200 hours. The second test was run under

identical conditions, but the pyrite was pretreated with silver to a ratio of 100 ppm. Under these conditions, copper extraction was complete after 27 hours. Tests were then performed where the leaching was stopped after 1 hour, 5 hours, and 10 hours. After stopping the experiment, pyrite and chalcopyrite in the leach residues were separated by screening. Since the pyrite particles were considerably larger than the chalcopyrite particles, they could be separated easily using a No. 270 (53 µm) mesh screen. Next, the copper concentrate was divided into two parts; one part was leached in the absence of pyrite and the other part was leached in the presence of natural (non-enhanced) pyrite. The results are shown in Figure 8.3.

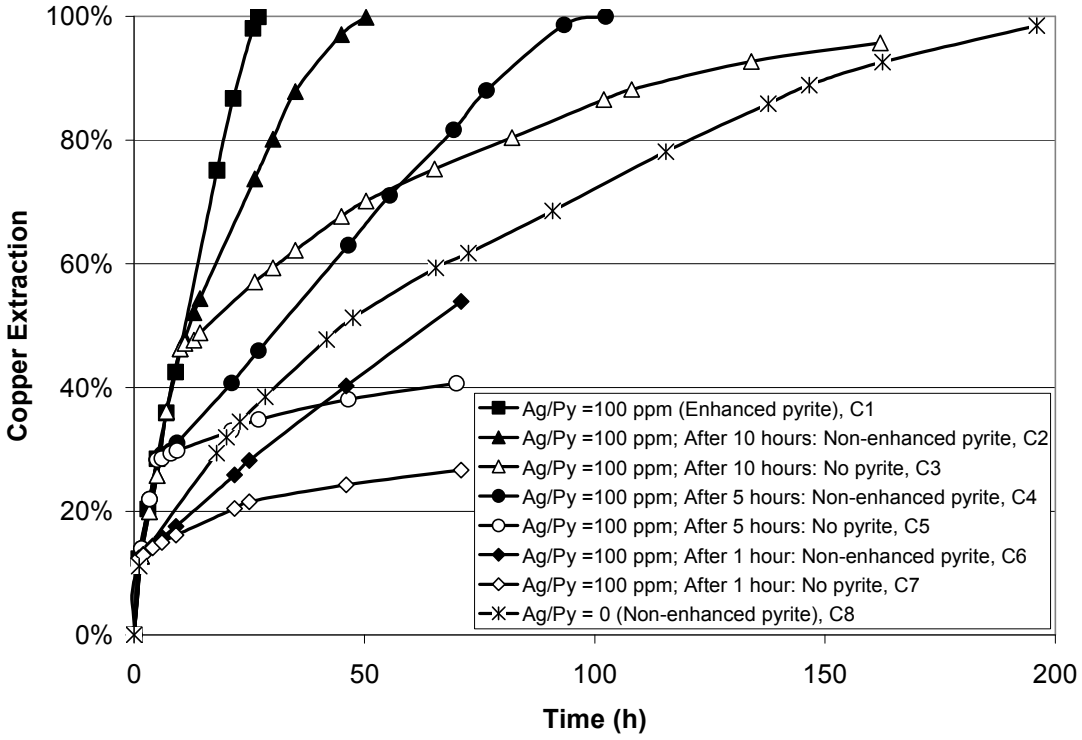

Figure 8.3 Chalcopyrite leaching in the presence of non-enhanced pyrite and the absence of pyrite upon pyrite removal after 1, 5, and 10 h at an initial pyrite-to-chalcopyrite ratio of 2 and a potential set point of 450 mV and 80°C

In the presence of natural pyrite (C8), complete copper extraction was achieved, although a long retention time was required. Upon addition of silver-enhanced pyrite (C1), the rate of chalcopyrite leaching increased and the required leach time decreased by a factor of 8, from 200 to 27 hours.

Upon removing the silver-enhanced pyrite after 1 hour (C7) and 5 hours (C5), the rate of copper extraction decreased significantly. These results indicate that the 10% loss of silver from silver-enhanced pyrite does not occur immediately upon introducing the pyrite to the leach slurry. If the pyrite were to lose that 10% silver at the beginning of the experiment, one would expect to observe similar kinetics in those tests that were continued with no pyrite after 1 hour (C7), 5 hours (C5), and 10 hours (C3), because the same amount of silver would have reacted with the chalcopyrite in each case, and therefore would have catalyzed its oxidation at the same rate. However, Figure 8.3 clearly shows that the reaction was much faster in the absence of pyrite when the pyrite was removed after 10 hours (C3). In this experiment, complete copper extraction was obtained after 170 hours, whereas, in those experiments where pyrite was removed after only 1 (C7) and 5 hours (C5), copper extraction proceeded extremely slowly.

When the silver-enhanced pyrite was removed after 10 hours, copper extraction continued rapidly in the presence of non-enhanced pyrite (C2). However, rapid copper extraction was not observed in the experiments where silver-enhanced pyrite was replaced with non-enhanced pyrite after 1 hour (C6) and 5 hours (C4). This observation is attributed to the formation of silver sulfide particles dispersed in the sulfur layer. As mentioned above, it is hypothesized tat the formation of silver sulfide decreases the resistivity of elemental sulfur, significantly. This layer may allow the transport of electrons from chalcopyrite either directly to ferric ions or to pyrite. Therefore, under these conditions, even in the presence of non-enhanced pyrite, the copper extraction proceeds rapidly. In the other two experiments, copper extractions of 12% and 28% were obtained after 1 hour (C6) and 5 hours (C4), respectively. Therefore, the thickness of the conductive sulfur

layer at that point was insufficient to ensure the transport of electrons to the end of the process. Consequently, in these experiments, fast kinetics was not observed.

It is also important to note that, upon removing the silver-enhanced pyrite from the system and substituting it with the natural pyrite (C2, C4, and C6), the leaching rates decreased immediately. This abrupt decrease in the rates cannot be due to a change in the conductivity of the sulfur layer, since copper extraction did not proceed very rapidly and the thickness of the sulfur layer did not vary significantly in the next few hours after silver-enhanced removal. This observation is attributed rather to the catalytic properties of pyrite. In order to evaluate the catalytic properties of pyrite, the rates of ferric reduction on silver-enhanced pyrite and natural pyrite were measured and compared. The reduction of ferric ions was studied at potentials lower than the rest potential of pyrite. The effect of the applied potential on the rate of ferric reduction on natural (non-enhanced) and silver-enhanced pyrite is shown in Figure 8.4.

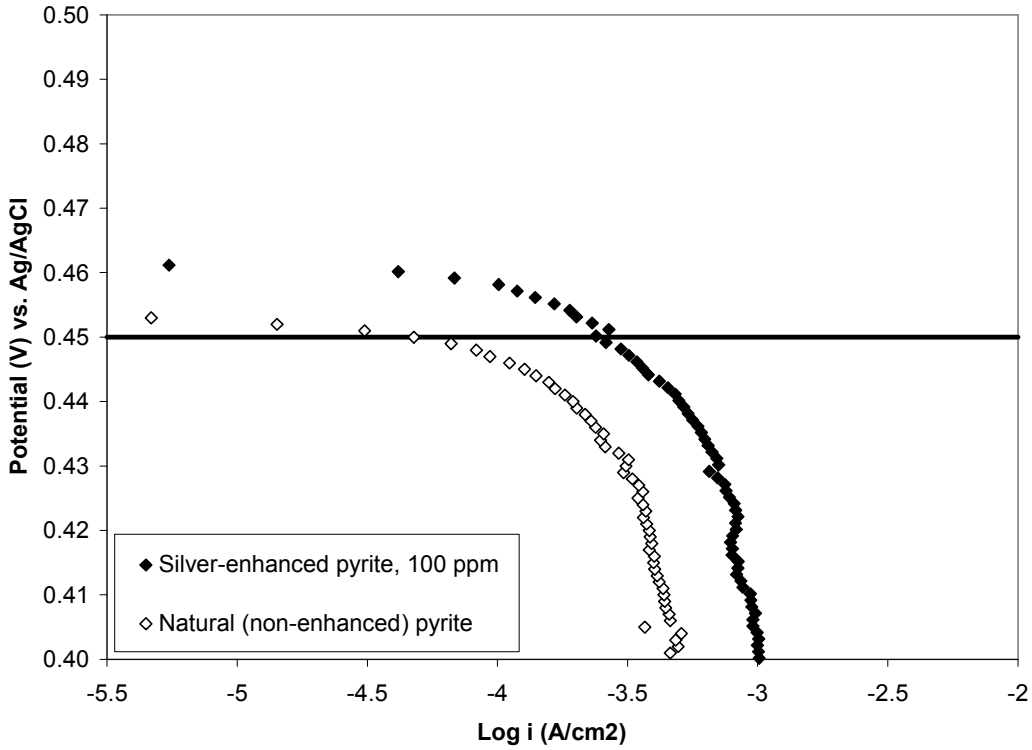

Figure 8.4 Reduction of ferric on silver-enhanced pyrite and natural pyrite

Figure 8.4 shows the potentiodynamic curves at the scan rate of 1 mV s^{-1} starting from the rest potential of pyrite to −300 mV *vs* OCP. This figure clearly shows that the rate of ferric reduction on silver-enhanced pyrite is faster than the rate on natural (non-enhanced) pyrite, by roughly a factor of 2.

The results shown above prove the hypothesis regarding the galvanic interaction between pyrite and chalcopyrite, and the important role of both pyrite and silver in that interaction. The main role of silver is to decrease the resistivity of the elemental sulfur layer and to enhance the catalytic properties of pyrite, while the role of pyrite is to provide additional surface for ferric reduction. These observations are in agreement with the results of silver catalyzed leaching shown in Chapter 6. It has been shown that, although low amounts of silver ions accelerate the rate of copper extraction, the leach time required for complete copper recovery is much longer than the time required in the Galvanox™ process

using silver-enhanced pyrite. There are two critical factors to ensure the galvanic interaction between two minerals. One is an electrical connection between the two minerals, and the other is additional cathodic surface area. Under identical conditions, the slower kinetics of silver-catalyzed leaching than Galvanox™ leaching with silver-enhanced pyrite can be attributed to the absence of a cathodic surface. As mentioned above and shown in previous studies, providing a larger surface area for the cathodic reaction on pyrite than for the anodic reaction on chalcopyrite also increases the anodic dissolution rate (Tshilombo, 2004). This effect can be explained in terms of area ratios and mixed potential theory. The ratio of cathodic to anodic area may be expressed as follows (Tshilombo, 2004):

$$\theta = \frac{A_c}{A_a} = \frac{\lambda A_{cp} + A_{py}}{(1-\lambda)A_{cp}} \tag{8.3.1}$$

where A_c and A_a are the cathodic and anodic surface areas, A_{cp} and A_{py} represent surface areas of chalcopyrite and pyrite, and λ represents the fraction of the cathodic to anodic area on chalcopyrite. At the mixed potential, the cathodic current is equal to the anodic current. Hence, the anodic current on chalcopyrite is given as follows:

$$I_{a,cp} = I_{c,cp} + I_{c,py} \tag{8.3.2}$$

$I_{a,cp}$ is the anodic current on chalcopyrite and $I_{c,cp}$ and $I_{c,py}$ are the cathodic currents on chalcopyrite and pyrite, respectively. Therefore, by addition of pyrite, the cathodic surface area increases and the anodic rate of copper dissolution has to increase to compensate for the extra electron consumption (Tshilombo, 2004). Leaching of chalcopyrite occurs slowly due to the formation of the passivating layer at a potential higher than the passive potential. Therefore, it is important to control the potential of the system such that it remains in the active region of chalcopyrite oxidation. Reaction 4.2.1 shows that when chalcopyrite is oxidized,

ferrous ions are produced. The oxidation of ferrous to ferric is known to occur rapidly and readily at elevated temperature in the presence of oxygen such that the oxidation-reduction potential (ORP) of the leach solution also increases readily. Therefore, the potential of the system shifts to the passive region of the mineral (Elsherif, 2002). The role of ferric in passivating the chalcopyrite surface has been also confirmed by Cordoba *et al*. (2008(I)). They have reported that although suitable ferric concentration favors the oxidation of chalcopyrite, high ferric concentration causes its passivation and inhibits copper and iron dissolution (Cordoba *et al*., 2008(I)). However, when pyrite is present in the leach slurry, ferric reduction increases and this allows the system to maintain the solution potential within the active region of the mineral.

In a study by Parker *et al*. (1981), it has been shown that electron transfers from corroding chalcopyrite to ferric or cupric in solutions are very slow step. They suggested that the transfer of electrons from chalcopyrite to ferric is the rate limiting step in ferric sulfate processes. According to this study, the electron transfer from corroding chalcopyrite occurs in following series:

Br_2, I^{2-}, $CuCl_2$ > $FeCl_3$> $Fe_2(SO_4)_3$

Hence, the slow electron transfer in ferric sulfate media might be one of the reasons that leaching is slower than cupric or ferric chloride media. In this study, it is also shown that the presence of pyrite or silver sulfide mineral associated with chalcopyrite increases the rate of chalcopyrite leaching. Pyrite and silver sulfide are semiconductors and more noble than chalcopyrite. Hence, the surface of these minerals remains uncoated during the leaching process. The presence of the uncoated surfaces facilitates the electron transfer to ferric. Hence, the rate limiting step is no longer the electron transfer from chalcopyrite to ferric ions. Under these conditions, the rate limiting step might be slow diffusion of ions to the anodic sites (Parker *et al*., 1981).

Four experiments were conducted to evaluate the effect of pyrite particle size on the kinetics of chalcopyrite leaching. In this series of experiments, chalcopyrite particles were smaller than 53 µm. Pyrite particles in the range of 25 to 75 µm, 75 to 125 µm, 125 to 150 µm, 250 to 354 µm were used. Tests were carried out at a pyrite-to-chalcopyrite ratio of 2 and a silver-to-pyrite ratio of 100 ppm. The results shown in Figure 8.5 indicate the important role of pyrite particle size on the rate of chalcopyrite leaching. The rate of reaction increases as pyrite particles size decreases.

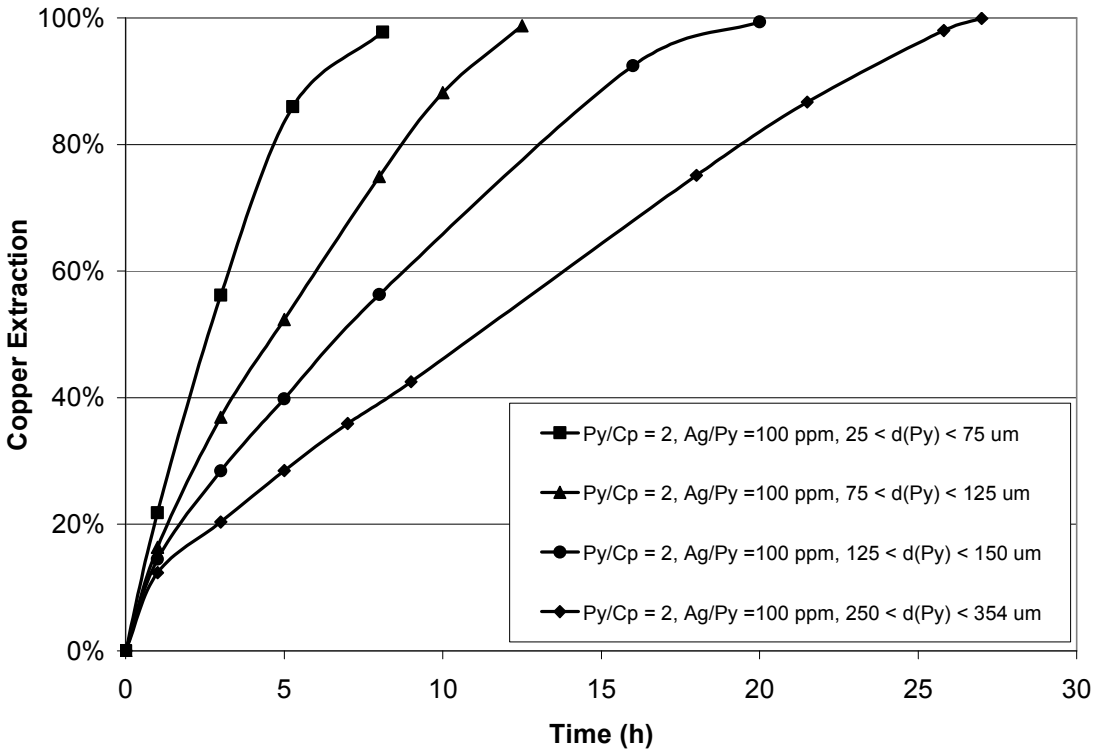

Figure 8.5 Effects of pyrite particle size at a pyrite-to-chalcopyrite ratio of 2, a silver to pyrite ratio of 100 ppm, a potential set point of 450 mV, and 80°C

By reducing the pyrite particle size, the total surface area increases. Hence, the cathodic surface area increases. Quantachrome Autosorb-1 was used to determine the BET surface area of pyrite in each experiment. The results are shown in Table 8.1.

Table 8.1 BET surface area of pyrite samples

Pyrite Particle Size (μm)	25 to 75	75 to 125	125 to 150	250 to 354
BET Specific Surface Area (m^2/g)	0.3052	0.1335	0.0487	0.0190
Normalized to the largest size	16.06	7.03	2.56	1

Faster kinetics in the presence of smaller pyrite particle sizes, shown in Figure 8.5, can be attributed to the presence of larger surface area for cathodic reaction, as explained earlier.

As mentioned above, an important factor in any galvanic process is an electrical contact between the couple to ensure the transport of electrons from one mineral (anode) to the other (cathode). In the presence of silver-enhanced pyrite, a small proportion of the added silver leaves pyrite and reacts with sulfur around chalcopyrite to form silver sulfide. Although the resulting silver level in the sulfur layer is very low, it has been hypothesized that the presence of conductive silver sulfide particles dispersed in a non-conductive sulfur layer decreases the resistivity of the product layer significantly. Hence, in the Galvanox™ process, the electrical contact between pyrite and chalcopyrite can be maintained via the formation of this product layer.

In a study by Wan *et al*. (1984), chalcopyrite leaching experiments were interrupted after 40% copper extraction. Then, sulfur was removed by distillation under a N_2 atmosphere. When the leaching reactions were resumed, after removal of the sulfur layer, the initial reaction rates were obtained. This observation also confirms that the sulfur product layer limits the transport of electrons and by elimination of this layer, a rapid copper extraction can be reached.

Wan *et al*. (1984) also investigated the kinetics of chalcopyrite leaching in a ferric sulfate medium. They reported that the rate of copper extraction can be enhanced in the presence of conductive carbon particles. According to this study,

carbon particles dispersed in the sulfur product layer increase its conductivity. In their study, the rate of leaching was increased by 4 to 6 times depending on the conductivity and size of the carbon particles.

In addition, the influence of dispersed phases on the conductivity of sulfides has been demonstrated by several investigators (Beckman *et al.*, 1982; Wan *et al.*, 1984). Changes in conductivity of an insulator at very low volume fractions of dispersed phase have been reported in previous studies. At very low concentrations of conductive elements in an insulator matrix, although volume fractions are not high enough to establish a connected conductive path, a number of phenomena have been invoked to explain the increase of conductivity of an insulator. Tunneling of electrons from surface states of the insulator to the dispersed phase, tunneling of electrons between the dispersed phase particles and thermal injection of electrons from the dispersed phase particle to the insulator's conduction band are some of these phenomena (Liang, 1973; Morris, 1998; Morris and Coutts, 1977). In a study by Wagner (1972), it was reported that conductive particles embedded in a matrix phase may act as a source or a sink for electrons which leads to the formation of a cloud of excess electrons or holes in the space charge adjacent to the particle. According to this study, if the concentration of electrons or holes in the matrix phase is low comparing to those of the dispersed phase, then the electrical conductivity of a two-phase mixture is determined by the concentration of carriers emitted by the particles and the excess electrons establishes the electrical conductivity of the mixture. In a study by Wan *et al*. (1984), it was reported that the electrical conductivity of an insulator is altered by addition of dispersed conductors. Another study by Beckman *et al*. (1982) showed that the electrical conductivity of elemental sulfur is increased by 8 to 12 orders of magnitude by the addition of small amounts of carbon.

It was critical to evaluate the conductivity of the sulfur product layer in the absence and presence of silver-enhanced pyrite to fully prove the model

proposed in this study. In this section, the current and current density during a typical Galvanox™ process were determined. Applying Ohm's law, the maximum resistivity of the sulfur layer that still allows the transport of electrons during the leach time was obtained. This analysis was of interest to ensure that the increase in conductivity of sulfur at low concentrations of silver was sufficient to maintain electrical contact between pyrite and chalcopyrite in the presence of a sulfur product layer.

In order to determine the role of silver sulfide dispersed in sulfur product layer in the presence of silver-enhanced pyrite, a leaching test was carried out using 30 g of copper concentrate in 1.5 L of leaching solution, at a pyrite-to-chalcopyrite ratio of 2, a silver-to-pyrite ratio of 100 ppm, a potential set point of 450 mV *vs* Ag/AgCl, and a temperature of 80°C. Pyrite particles in the range of 125 to 150 µm and copper concentrate particles in the range of 30 to 53 µm were used. The results are shown in Figure 8.6.

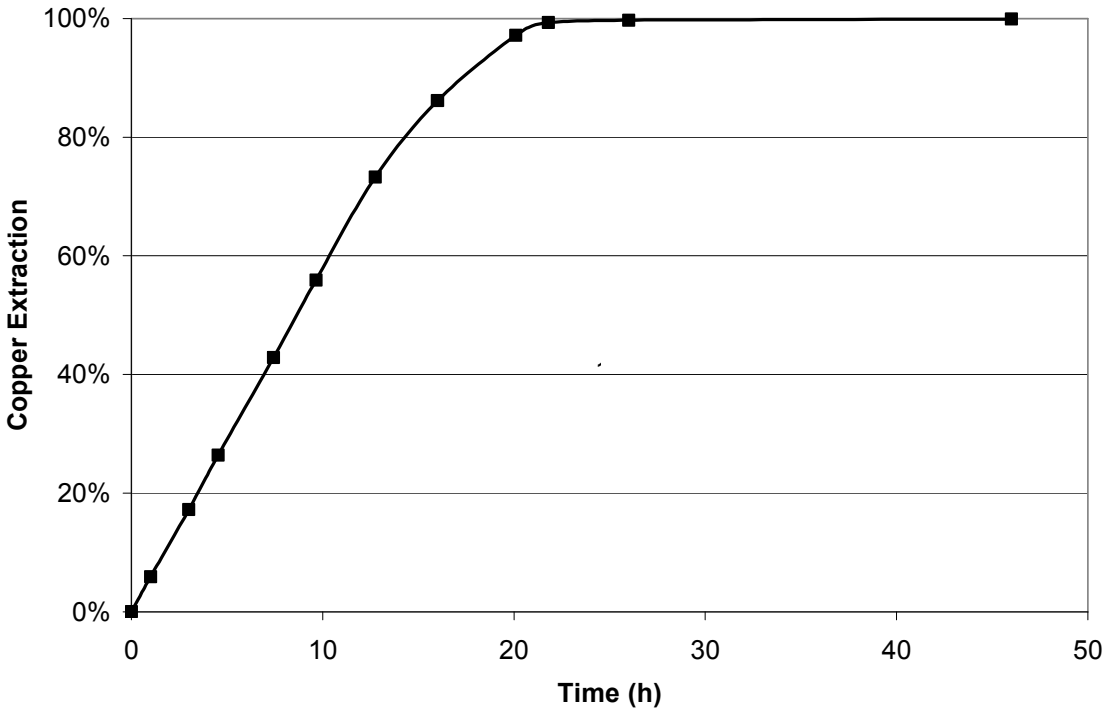

Figure 8.6 Chalcopyrite leaching in the presence of silver-enhanced pyrite at a pyrite-to-chalcopyrite ratio of 2, silver-to-pyrite ratio of 100 ppm, 450 mV *vs* Ag/AgCl, and 80°C

After complete copper extraction, pyrite and chalcopyrite residue (sulfur) were separated using a 53 µm sieve. A very small proportion of pyrite was also passed the 53 µm sieve due to the pyrite attrition during the leaching process. Ultimately, the sulfur residue and pyrite were separated using an elutriation column. The sulfur residue was divided into two parts. The silver sulfide formed during leaching in sulfur residue from one part was leached according to the procedure explained earlier. The solid assay results of sulfur residue before and after silver sulfide leaching are shown in Table 8.2.

Table 8.2 Elemental analysis of sulfur residue

Elements	Sulfur residue containing silver sulfide	Sulfur residue after silver sulfide leaching
Ag	75.8 ppm	1.8 ppm
Cu	27 ppm	19 ppm
Zn	6 ppm	11 ppm
Pb	11 ppm	9 ppm
Mo	2 ppm	2 ppm
Fe	<0.01 %	<0.01 %
Co	16 ppm	28 ppm

1 g of each sample was pressed and two pellets were prepared as described earlier for the resistivity measurement. The resistivity of both samples was measured. Similarly, each measurement was performed on three pellets to evaluate the reproducibility of the data. The results are shown in Table 8.3.

Table 8.3 The resistivity values of sulfur residues in the presence and absence of silver sulfide

Sample ID	Resistivity (Ω cm)
Sulfur residue containing silver sulfide	$1.06 \pm 0.10 \times 10^{7}$
Sulfur residue after silver sulfide leaching	$8.05 \pm 0.15 \times 10^{10}$

Table 8.3 shows that the resistivity of the product sulfur without silver is about 3 orders of magnitude higher than that of the sulfur with silver. This limits the electrical contact between pyrite and unleached chalcopyrite. The galvanic interaction between the couple can be maintained by decreasing the resistivity of the product layer. The results shown in Table 8.3 indicate that the resistivity of sulfur layer in the presence of minuscule amounts of silver is considerably lower.

However, the resistivity of the product layer in the presence of silver at this level is still very high. Hence, it is important to determine if the observed improvement

in the conductivity was sufficient to ensure electron transfer from chalcopyrite to pyrite at a rate commensurate with the leaching rate shown in Figure 8.6.

Faraday's law was applied and the rate of copper dissolution (current) in ferric sulfate media in the Galvanox™ process using silver-enhanced pyrite was estimated.

$$m = \frac{ItM}{Fz} \tag{8.3.3}$$

where m is the total mass of the dissolved copper, I is the current, t is the total time, M is the molar mass of copper (63.546 g/mol), F is Faraday's constant (96485 C/mol), and z is the number of electrons produced per mole of copper (+4) according to reaction (8.3.4).

$$CuFeS_2 = Cu^{2+} + Fe^{2+} + 2\ S^0 + 4\ e^- \tag{8.3.4}$$

Figure 8.6 shows that the rate of copper extraction during the first 12.75 hours of the experiment was constant and followed a straight line. After 12.75 hours, the rate changes as it deviates from the straight line. Hence, during the first 12.75 hours, the current is constant and Faraday's law can be applied to calculate the current.

According to the results shown in Figure 8.6, 73.28% copper extraction was obtained in 12.75 hours. Considering the mineralogical and elemental compositions of copper concentrate, shown in Table 5.1 and Table 5.2, one may obtain the amount of copper dissolved in this leach time. The copper concentrate contained 27% copper. Hence, 5.94 g copper were dissolved from chalcopyrite, and Faraday's law gives the following current:

$$5.94 = \frac{I \times 12.75 \times 3600 \times 63.546}{96485 \times 4} \Rightarrow I = 0.785\text{A} \tag{8.3.5}$$

The BET surface area of the copper concentrate was confirmed to be 0.741 m^2/g, thus giving a total surface area of 22.2 m^2 = 222000 cm^2. Hence, the initial current density may be calculated as follows:

$$i_1 = \frac{I}{A} = \frac{0.785}{222000} = 3.54 \times 10^{-6}\,\text{A/cm}^2 \tag{8.3.6}$$

The surface area of unleached chalcopyrite varies during the leaching process which leads to the variation of the current density. Hence, only the initial current density was determined. However, the current is constant during the first 12.75 hours of leaching. The current during that time is 0.785 A and the initial current density and rate are 3.54 $\mu A/cm^2$ and 9.17×10^{-12} $mol/cm^2/s$, respectively. These results are in agreement with values reported in the literature. In a previous study, the galvanic interactions between pyrite and chalcopyrite were studied and the corrosion current was measured when pyrite and chalcopyrite were in contact in ferric sulfate media (Mehta and Murr, 1983). Under these conditions, the corrosion current of 5 $\mu A/cm^2$ was obtained. In another study, it has been shown that the current density on the surface of chalcopyrite at 450 mV *vs* Ag/AgCl is about 1 $\mu A/cm^2$ (Ghahremaninezhad *et al*., 2010). It is important to note that the initial current density in the presence and absence of catalysts is very similar. However, the initial reaction rates decline rapidly with time in the absence of catalysts, while in the presence of an effective catalyst the initial reaction rates are maintained.

Using Ohm's law, the resistivity of the product layer may be determined, thus:

$$R = \frac{\Delta E}{I_1} = \rho \frac{L}{A} \tag{8.3.7}$$

Electrical resistance depends on the length and the cross-sectional area, and the area varies during copper dissolution. The resistance should be calculated at very small sulfur layer thicknesses ($\Delta r \rightarrow 0$) where the inner and outer areas are almost equal. Hence, the sample resistance was obtained by integration from the inner radius r_1 to the outer radius r_2, thus:

$$R = \rho \frac{L}{A} = \rho \int_{r_1}^{r_2} \frac{dr}{4\pi r^2} = \frac{\rho}{4\pi}\left(\frac{1}{r_1} - \frac{1}{r_2}\right) \tag{8.3.8}$$

The differential and cumulative particle size distributions of the chalcopyrite sample are shown in Figure 8.7. The average particle size is 39.8 μm. The leaching experiment was conducted using a sample with a narrow particle size range so that the average particle size to be used in the calculation would be representative of the sample. This would limit the variability between particles throughout the sample based on particle size.

Having the total current, total surface area, and initial average particle size, one may then calculate the average current passed through a single particle, thus:

$$I_1 = I \frac{A_1}{A} \tag{8.3.9}$$

Assuming the particles are spherical, the current passed through one particle of diameter 39.81 μm (outer radius 19.9 μm) would be 1.76×10^{-10} A.

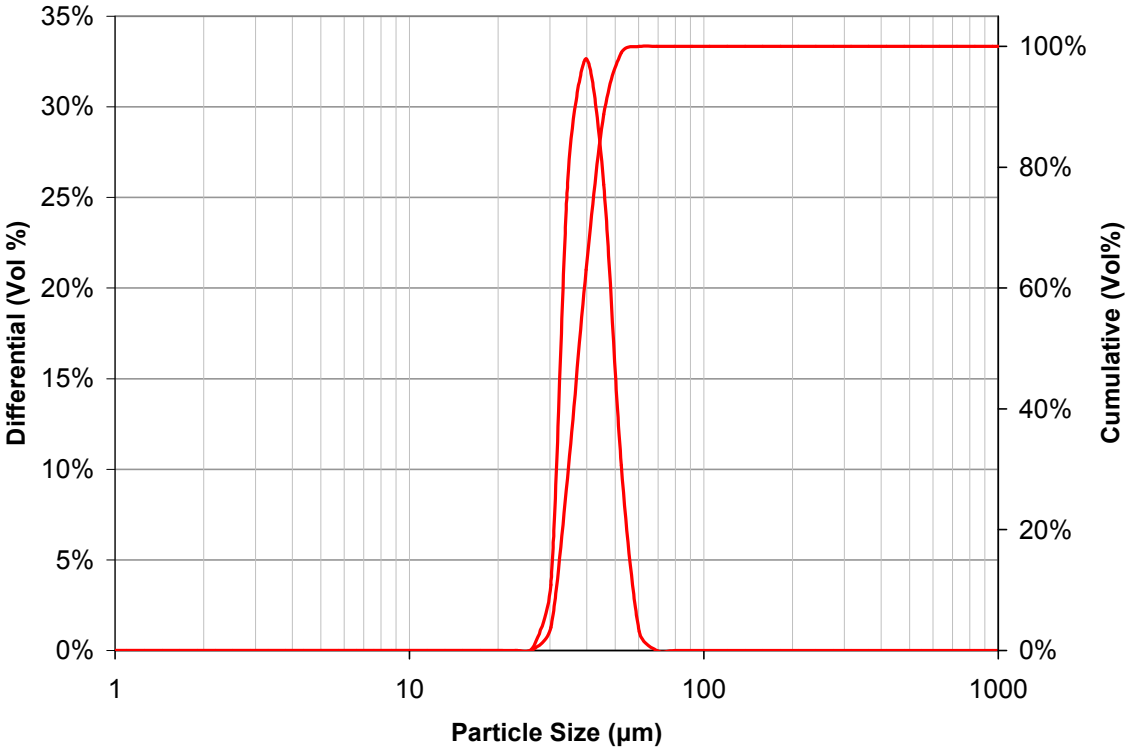

Figure 8.7 Differential and cumulative particles size distribution of copper concentrate

After 73.28% copper extraction, the average unleached core diameter would be 10.64 µm (inner radius 5.32 µm). The driving force for the leaching reaction is the potential difference between the solution and the rest potential of chalcopyrite. The average rest potential of chalcopyrite under the prevailing conditions is 205 mV *vs* Ag/AgCl (Cordoba *et al*., 2008(II); Gomez *et al*., 1996; Lazaro and Nicol, 2006; Nova and Gonzalez, 2006; Price and Warren, 1986) and the solution potential is 450 mV *vs* Ag/AgCl; thus giving a potential difference of 245 mV. The potential difference between solution and chalcopyrite was the driving force for transfer of electrons through the sulfur layer, and the anodic overpotential required for chalcopyrite oxidation. The anodic overpotential required to obtain the current density of 3.54 µA/cm^2 was determined by applying the Tafel equation.

$$\eta_a = \frac{RT}{\alpha ZF}\left[Ln\left(\frac{i_1}{i_2}\right)\right] \tag{8.3.10}$$

where η_a is the anodic overpotential, α is the charge transfer coefficient, i_1 and i_2 are current densities in the Tafel region and z is the number of electrons produced per mole of copper (+4) according to reaction (8.3.4).

The dissolution current density, i_d, of approximately 5×10^{-7} A/cm^2 under the prevailing condition has been reported in previous studies (Rivera Vasquez, 2010; Viramontes-Gamboa *et al*., 2007). Equation 8.3.10 can be applied if the anodic overpotential is not very large. It has been shown that the dissolution rate of the mineral follows Tafel behavior in the potential range of OCP to 485 mV (*vs* Ag/AgCl) (Rivera Vasquez *et al*., 2012). Assuming α = 0.5 and i_1 = initial current density = 3.54×10^{-6} A/cm^2 and $i_2 = i_d = 5\times10^{-7}$ A/cm^2, and T = 80°C, the anodic overpotential would be 30 mV.

Hence, the anodic overpotential accounts for only a small proportion of the total driving force and the rest (215 mV) is required for transfer of electrons through the sulfur layer. Applying these results to the integral and rearranging gives an estimate of the maximum sulfur layer resistivity which allows leaching to occur at the observed rate:

$$\Delta E = I_1 R = I_1 \frac{\rho}{4\pi}\left(\frac{1}{r_1} - \frac{1}{r_2}\right) \Rightarrow 0.215 = 1.76\times10^{-10}\times\frac{\rho}{4\pi}\left(\frac{1}{5.3\times10^{-4}} - \frac{1}{19.9\times10^{-4}}\right) \tag{8.3.11}$$

$$\rho = 1.11\times10^{7}\,\Omega\text{cm} \tag{8.3.12}$$

This implies that the resistivity of the elemental sulfur product layer must be lower than 1.11×10^7 Ω cm to allow the transfer of electrons at the rate shown in Figure

8.6. This value is in agreement with the resistivity of sulfur layer with silver shown in Table 8.3 (1.06×10^{7} Ω cm).

The same methodology was applied to obtain the resistivity of an anodic oxide passive layer, a common and well-characterized system. This process was used to confirm the validity of the calculation shown above.

The field strain and current density of the passive oxide film have been reported in previous studies. Typically, the field strain through oxide film is 1.0×10^{6} to 1.1×10^{6} V/cm and the current density in a 0.5 M H_2SO_4 is 2 to 5 μA/cm^2 (Chao *et al*., 1982; Hermas and Morad, 2008; Raja and Jones, 2006; Sato *et al*., 1971). Since the area of the passive film is constant, the resistance does not vary through the passive layer.

$$\Delta E = \frac{I\rho L}{A} = i\rho L \tag{8.3.13}$$

Substituting the average values in the above equation, the following results were obtained.

$$\frac{\Delta E}{L} = i\rho \Rightarrow 1.05\times10^{6}\left[\frac{\text{V}}{\text{cm}}\right] = 3.5\times10^{-6}\left[\frac{\text{A}}{\text{cm}^2}\right].\rho\left[\Omega\text{cm}\right] \Rightarrow \rho = 3\times10^{11}\Omega\text{cm} \tag{8.3.14}$$

In the literature, the resistivity of the passive oxide layer has been reported to be about 10^{11} Ω cm (Chao *et al*., 1982; Yin *et al*., 2001). This value is in agreement with the resistivity value obtained above, which validates the methodology that was applied in this study.

Hence, according to the model described in this study, in order to observe the copper extraction with the rate shown in Figure 8.6, the resistivity of the product layer can be as high as 1.11×10^{7} Ω cm. The model would have been disproved

had the actual resistivity of the product layer been significantly higher than this value, and the reaction was still proceeding with the rate shown in Figure 8.6.

In order to obtain a broader understanding of the effects of silver ratio of sulfur on the electrical resistivity, sulfur samples at various silver levels were prepared according to the procedure outlined above. As described earlier, colloidal silver was prepared and then sulfur samples were added to the solution containing colloidal silver to form silver sulfide. Although the reaction of silver ions and sulfur are thermodynamically favorable, as shown in reaction (8.3.15), the kinetics of this reaction is extremely slow at low temperature. The slow kinetics of sulfur oxidation at low temperature and low pressure was discussed in Chapter 3. Hence, sulfur particles were added to react with elemental silver rather than silver ions (reaction 8.3.16).

$$6\ Ag^{+} + 4\ S^{0} + 4H_2O = 3\ Ag_2S + 7\ H^{+} + HSO_4^{-}$$
$$\Delta G^{O} = -390.934\ kJ/mol \qquad (8.3.15)$$

$$Ag^{0} + S^{0} = Ag_2S$$
$$\Delta G^{O} = -40.383\ kJ/mol \qquad (8.3.16)$$

In the first experiment, after colloidal silver preparation, the solution was allowed to evaporate and the solid sample was collected and studied using XRD to confirm the formation of elemental silver. The results are shown in Figure 8.8(a). For comparison purposes, the XRD reference pattern of silver was also added and shown in Figure 8.8(b). The XRD pattern reveals only peaks of elemental silver as expected.

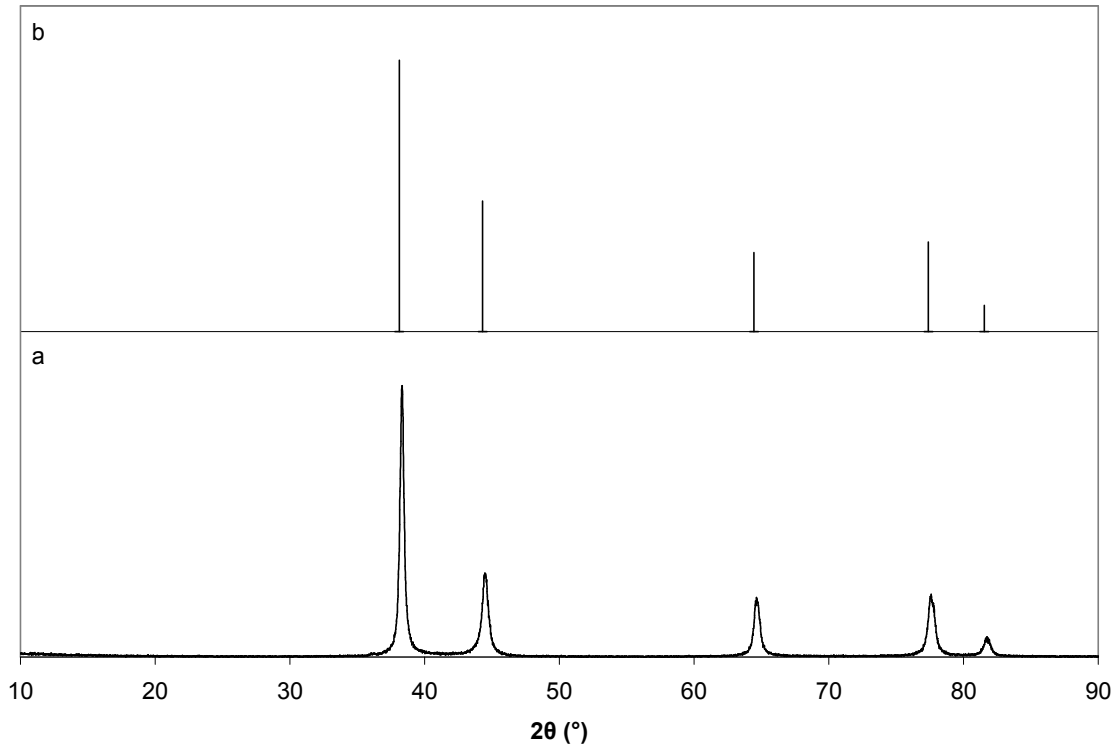

Figure 8.8 XRD pattern of (a) prepared silver particles (b) reference silver

Table 8.4 shows the amount of sodium borohydride and silver nitrate added to each sample and the porosity of pressed sulfur pellets prepared for the purpose of resistivity measurements. The concentrations of silver on sulfur samples were verified using ICP analysis. The sulfur pellets are highly porous which is analogous to the structure of the sulfur layer formed around chalcopyrite during the Galvanox™ leaching process.

Table 8.4 The amounts of reagents for 5 g sulfur at various silver concentrations

Ag/S ppm	$NaBH_4$ [0.002M] (mL)	$Ag(NO_3)$ [0.001M] (mL)	Porosity (%)
0	0	0	22.2
20	3	1	22.2
40	6	2	22.3
60	9	3	22.1
80	12	4	22.4
100	15	5	22.1
200	30	10	22.1
500	75	25	22.2
1000	150	50	22.2

A sample was prepared at a silver-to-sulfur ratio of 15000 ppm or silver concentration of 1.5%. The purpose of preparing this sample was to study the crystal structure of silver species formed via reaction of colloidal silver and sulfur. The results are shown in Figure 8.9(b). The XRD pattern of pure sulfur was also obtained and shown in Figure 8.9(a) along with the XRD reference peaks of silver sulfide (Figure 8.9(c) and silver (Figure 8.9(d)). The XRD pattern of sulfur sample containing silver reveals several new peaks. These peaks match with silver sulfide. None of the silver peaks were matched to this pattern. Due to low intensity of these new peaks and the large number of sulfur peaks, the x-axis was expanded between $2\theta = 30°$ to 50°. The results are shown in Figure 8.10. This figure clearly shows the presence of several new peaks which match well with silver sulfide. The peaks observed at the following 2θ were assigned to silver sulfide: 33.56, **34.38**, 34.76, **36.56**, **36.80**, 37.10, 40.74, 43.40, 43.64, 44.20, 45.42, 48.76, 53.28, and 58.06.

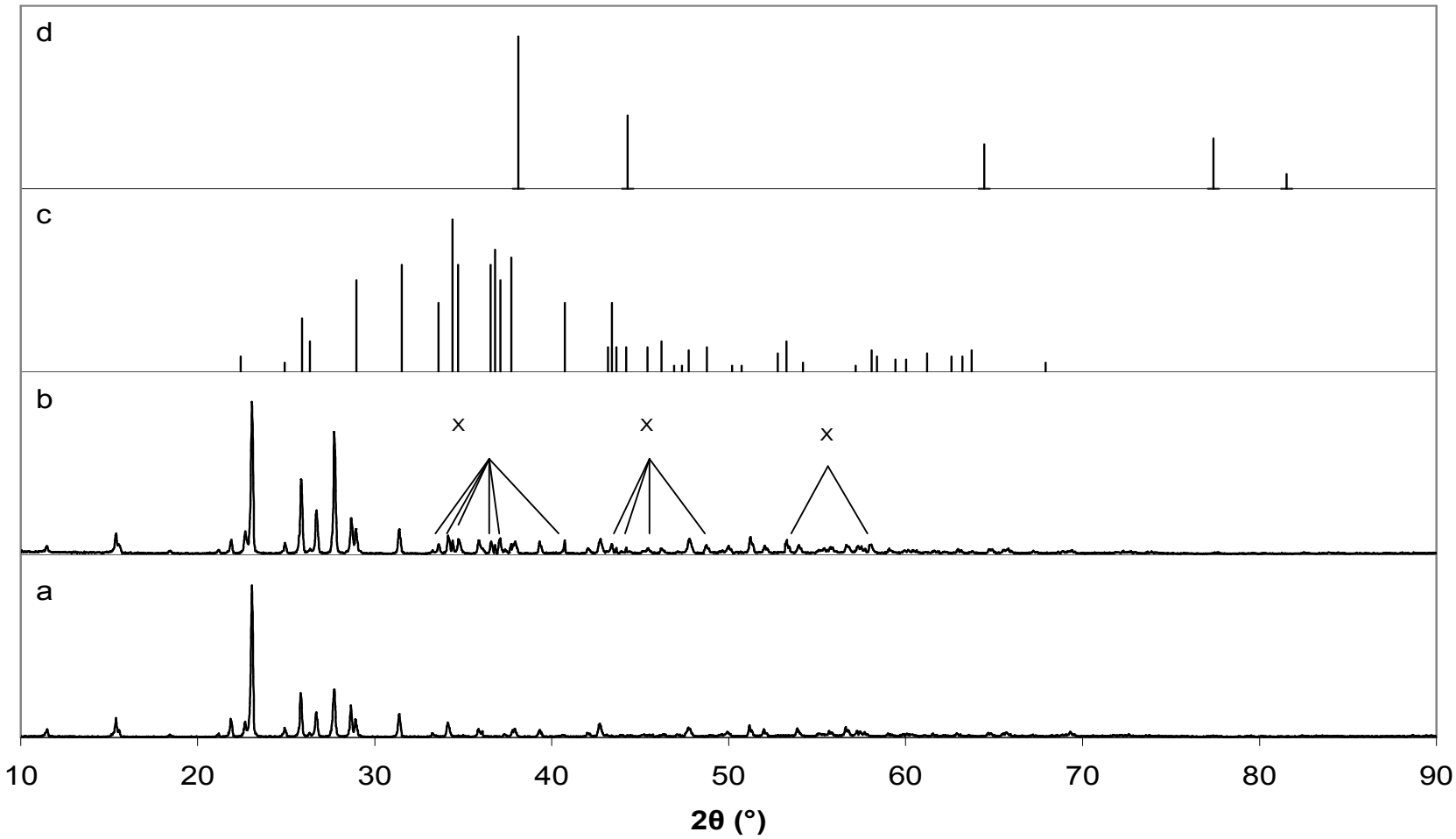

Figure 8.9 XRD patterns of (a) 99.999% sulfur, (b) silver treated sulfur at a silver to sulfur concentration of 1.5%, (c) silver sulfide, and (d) silver, “x” denotes silver sulfide

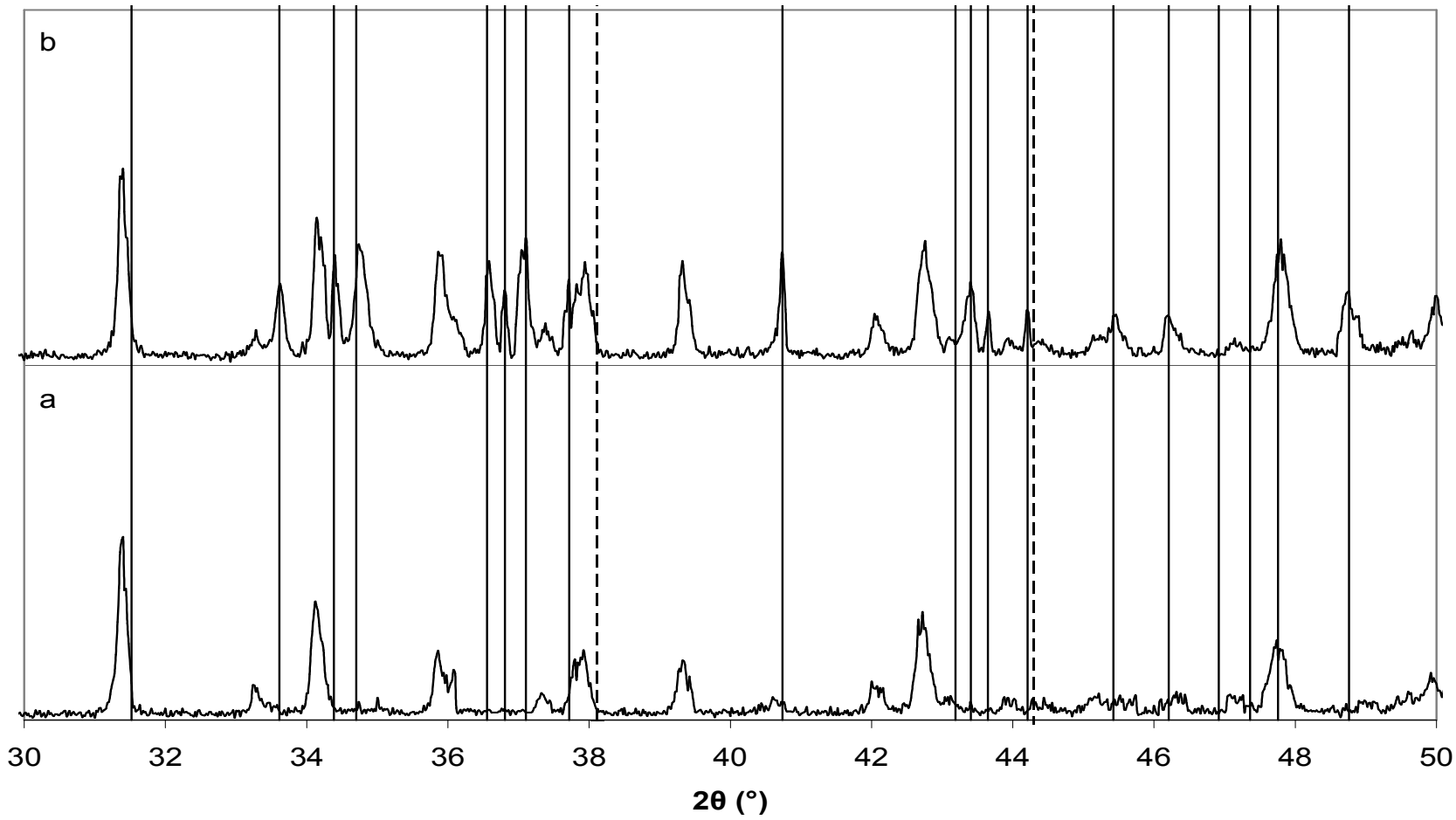

Figure 8.10 XRD patterns of (a) 99.999% sulfur, (b) silver treated sulfur at a silver to sulfur concentration of 1.5%, dashed and solid vertical lines denote silver and silver sulfide reference diffraction patterns, respectively

The resistivity values of sulfur samples at different silver levels are shown in Figure 8.11. The results indicate that the presence of a miniscule amount of silver as silver sulfide in the product layer enhances electrical conductivity significantly. At silver concentrations higher than 80 ppm, the resistivity is low enough to allow the transport of electrons from the surface of an unleached chalcopyrite particle to the surface of the sulfur layer at the rate shown in Figure 8.6, and as a result maintain the electrical contact between pyrite and chalcopyrite. At a silver level lower than 80 ppm, this electron transfer can occur at a slower rate. The average resistivity of the sulfur pellets without silver was 6.94×10^{12} Ω cm. This resistivity is roughly five orders of magnitude higher than the required maximum resistivity of 1.11×10^{7} Ω cm obtained in this study.

The structure of the elemental sulfur product layer during chalcopyrite leaching in the Galvanox™ process is porous as shown in Chapter 5. Similarly, the pressed silver pretreated sulfur pellets are also porous, as shown in Table 8.4.

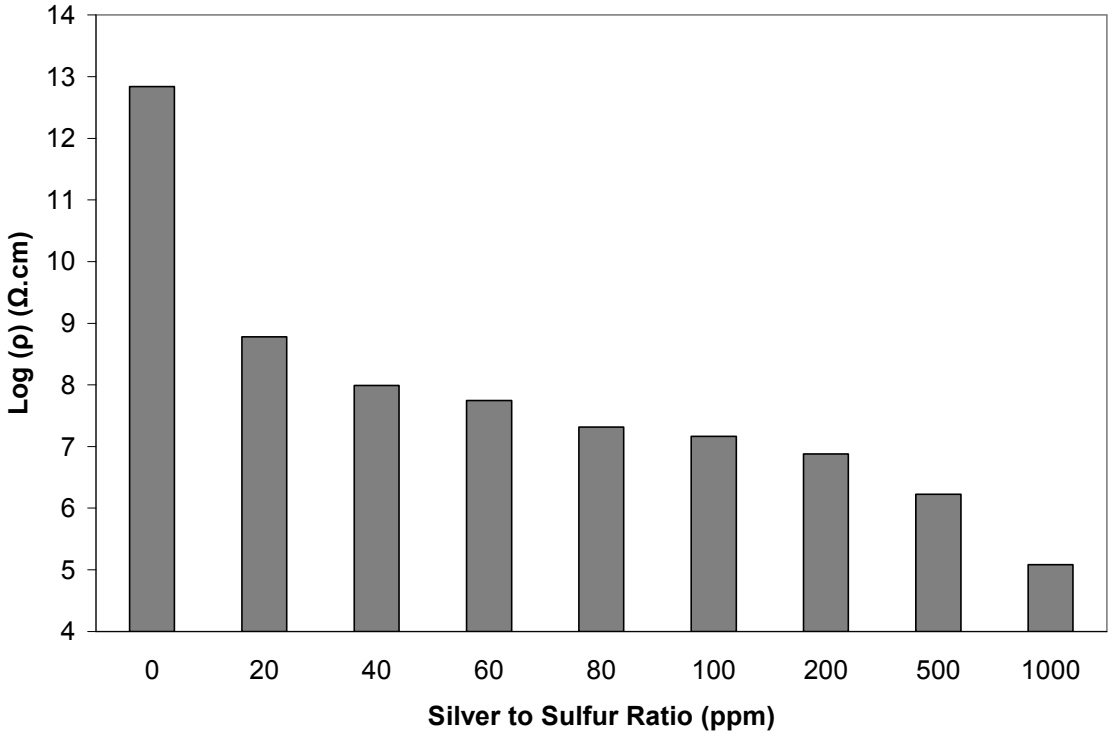

Figure 8.11 Resistivity of sulfur at various silver concentrations

Copper and iron ions are both conductive and are present in chalcopyrite leaching media. Thus, one might hypothesize that the presence of these elements would decrease the resistivity of sulfur layer sufficiently. However, the reactions of copper and/or iron ions with sulfur/sulfide under the oxidizing conditions of leaching are not thermodynamically possible and these phases are not stable. The standard Gibbs free energies of possible reactions were calculated using the standard free energies of formation for species shown in Table 8.5.

Table 8.5 Standard Gibbs free energy of formation of species involved in this process at 298 K, 1 atm*

Species	ΔG^O (kJ/mol)
Cu^{2+}	65.522
Fe^{2+}	−91.525
Fe^{3+}	−17.183
Ag^{+}	77.114
$CuFeS_2$	−190.493
CuS	−56.611
Ag_2S	−40.383
H_2O	−237.141
Hg^{2+}	164.697
HgS	−52.212

It is well known (Miller *et al*., 1981; Price and Warren, 1986) that silver ions react with chalcopyrite according to reaction (8.3.17).

$$CuFeS_2 + 4\ Ag^{+} = Cu^{2+} + Fe^{2+} + 2\ Ag_2S \qquad \Delta G^O = -224.702\ kJ/mol \qquad (8.3.17)$$

In this reaction, copper and iron are replaced with silver. The standard free energy is negative indicating that this reaction is thermodynamically favorable. Oxidation of silver sulfide in ferric media may occur according to reaction (8.3.18).

$$Ag_2S + 2\ Fe^{3+} = Ag^{+} + 2\ Fe^{2+} + S^0 \qquad \Delta G^O = +45.927\ kJ/mol \qquad (8.3.18)$$

The free energy of this reaction is positive which indicates that this reaction is not favorable at 25°C. The oxidation of silver sulfide in ferric sulfate solution has been studied previously (Dutrizac, 1994), and it was shown that the oxidation of silver sulfide in ferric sulfate solution was not possible even at elevated temperatures, high potential and high acidity due to the refractory behavior of

* Obtained from the HSC Chemistry database (version 5.11, Outokumpu Research Oy, Finland

silver sulfide in ferric sulfate solutions. According to this study, silver sulfide does not dissolve in concentrated acidic ferric sulfate solution at temperatures lower than 100°C.

One might assume that the same reaction may occur between cupric ions and chalcopyrite to generate CuS.

$$CuFeS_2 + Cu^{2+} = Fe^{2+} + 2\ CuS \qquad \Delta G^O = -79.806\ kJ/mol \qquad (8.3.19)$$

$$CuS + 2\ Fe^{3+} = Cu^{2+} + 2\ Fe^{2+} + S^0 \qquad \Delta G^O = -29.521\ kJ/mol \qquad (8.3.20)$$

Although reaction (8.3.19) is thermodynamically favorable, CuS is not stable in the presence of ferric ions. Reaction (8.3.20) shows that oxidation of CuS can occur readily. In addition, it has been reported that CuS (covellite) and Cu_2S (chalcocite) are more amenable to oxidation than chalcopyrite (Hiroyoshi *et al*., 1997, 1998, 2000). Hence, the sulfides of copper (I) and copper (II) are not stable in acidic ferric sulfate solutions and therefore cannot decrease the resistivity of the sulfur layer. Conversely, as mentioned above, silver sulfide is very stable under atmospheric leaching in acidic ferric sulfate solution at 450 mV *vs* Ag/AgCl. Thus, once it is formed, it does not dissolve under these conditions.

To further validate the model and describe the mechanism of silver-enhanced pyrite catalyzed leaching of chalcopyrite in ferric sulfate solution, silver was substituted with mercury. Mercury was selected given its similarity to silver in respect to its high electrical conductivity and similar redox potential. Mercuric sulfide is highly conductive, although its conductivity is lower than that of silver sulfide. In addition, similar to silver, the redox potential of mercury is higher than the rest potential of pyrite. Hence, mercury ions reduce on pyrite.

$$Ag^+ + e = Ag^0 \qquad E^O = 0.80\ V\ vs\ SHE\ at\ 25°C\ and\ 1\ atm \qquad (8.3.21)$$

$Hg^{2+} + 2e = Hg^{0}$ $E^{O} = 0.85$ V *vs* SHE at 25°C and 1 atm (8.3.22)

In addition, once formed, mercuric sulfide is not oxidized in ferric sulfate solution. The free energy of mercuric sulfide dissolution is calculated using the data shown in Table 8.5.

$HgS + 2\ Fe^{3+} = Hg^{2+} + 2\ Fe^{2+} + S^{0}$ $\Delta G^{O} = +68.225$ kJ/mol (8.3.23)

Three experiments were conducted to evaluate the effects of addition of mercury to pyrite samples on the kinetics of chalcopyrite leaching. In one experiment, pyrite was pretreated with mercury instead of silver. Pyrite samples were pretreated with mercury (II) in its soluble form (mercury nitrate) at a mercury-to-pyrite ratio of 600 ppm, according to the procedure described in the previous study for pretreatment of pyrite with silver. Another experiment was carried out using silver-enhanced pyrite at a silver-to-pyrite ratio of 100 ppm. In the third experiment, natural pyrite was used with no pretreatment. The results of chalcopyrite oxidation in the presence of natural pyrite, silver-pretreated pyrite, and mercury-pretreated pyrite are compared in Figure 8.12. In these experiments, pyrite particles are between 25 and 75 μm and copper concentrate particles are smaller than 53 μm.

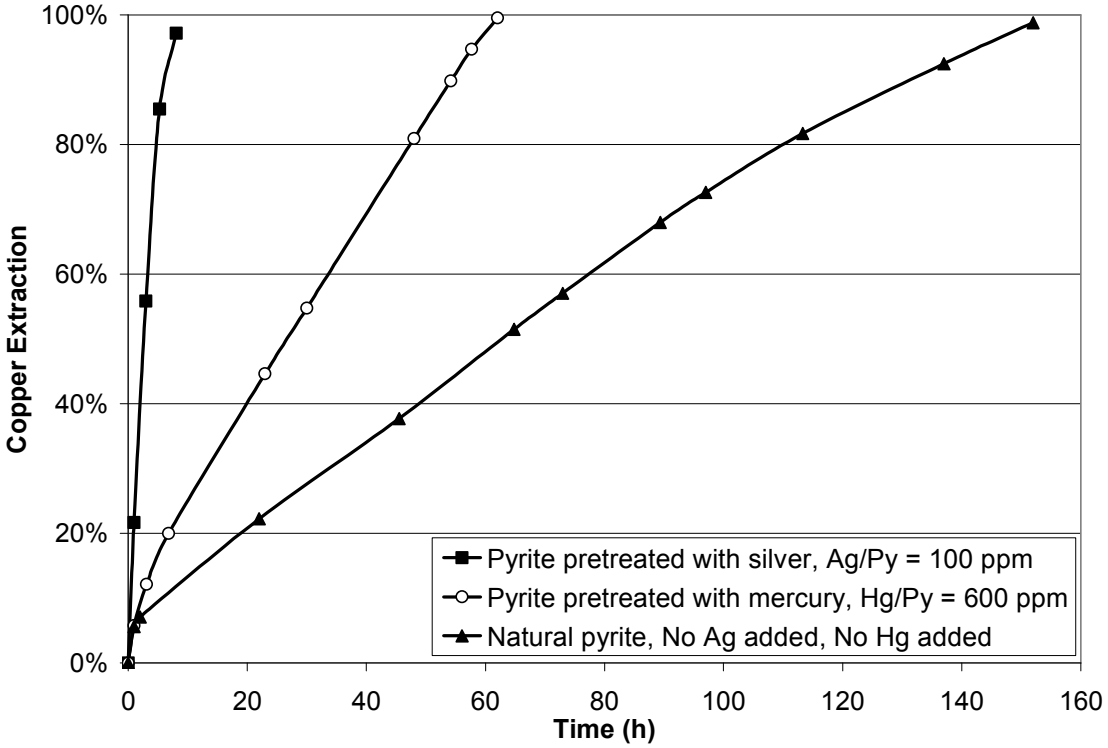

Figure 8.12 Chalcopyrite leaching in the presence of natural pyrite, pyrite pretreated with mercury, and pyrite pretreated with silver, at a pyrite-to-chalcopyrite ratio of 2, 450 mV *vs* Ag/AgCl, and 80°C

The conductivity of silver sulfide and mercuric sulfide in average are 1.8×10^{-2} and $3\times10^{-4}/\Omega$/cm, respectively (Hebb, 1952; Martienssen and Warlimont, 2005). Hence, the conductivity of silver sulfide is approximately 60 times higher than that of mercury sulfide. Therefore, it is expected that the sulfur product containing mercury sulfide has a lower conductivity than the one containing silver sulfide. This may explain the slower rate of copper extraction in the presence of mercury.

Figure 8.12 clearly shows the fastest kinetics in the presence of silver and the slowest kinetics in the presence of natural pyrite. These results further confirm the role of a conductive element on decreasing the resistivity of the sulfur layer and maintaining the electrical contact between two minerals and sustaining the galvanic interaction in order to enhance the kinetics of chalcopyrite oxidation.

8.5 Conclusions

In this study, a model was proposed to explain the mechanism of silver-enhanced pyrite catalyzed leaching of chalcopyrite in ferric sulfate media. The rapid rate of chalcopyrite leaching in the Galvanox™ process has been attributed to the galvanic interaction between pyrite and chalcopyrite. Pyrite under the conditions of the Galvanox™ process is inert and acts as a cathode. Pyrite thus facilitates the cathodic reduction of ferric to ferrous. Acceleration of the reduction rate also increases the rate of oxidation as charge neutrality must be obtained. In this study, it has been shown that in the process of silver-enhanced pyrite catalyzed leaching, the catalytic properties of pyrite is enhanced in the presence of silver. It has been shown that the rate of ferric reduction on silver-enhanced pyrite is considerably faster than the rate on natural pyrite.

As chalcopyrite oxidation proceeds, sulfur layers of extremely high electrical resistivity form around chalcopyrite particles. The formation of this layer limits the transport of electrons from chalcopyrite to pyrite and inhibits the galvanic interaction between these two minerals. However, it has been shown that in the presence of silver-enhanced pyrite, small amounts of silver leave the pyrite surface and react with the sulfur product layer. Although the resulting silver level in the sulfur layer is very low, the resistivity of this layer decreases dramatically. The electrical resistivity of the sulfur layer is low enough to allow the transfer of electrons from chalcopyrite to pyrite at a rate sufficient to sustain the leaching process. The electrical resistivity of sulfur at various silver concentrations was determined. It has been shown that the electrical resistivity of sulfur layer decreases about five orders of magnitude in the presence of low amounts of silver (60 to 100 ppm) dispersed in sulfur particles. In the absence of silver, the resistivity of sulfur is extremely high which hinders the electrical contact between the couple.

Chapter 9 Conclusions and Recommendations

9.1 Enhancing the Kinetics of Chalcopyrite Leaching in the Galvanox™ Process

In this project, a new process has been developed whereby pyrite, pretreated with miniscule amounts of soluble silver, is used as a catalyst for atmospheric leaching of chalcopyrite in iron sulfate media. It has been shown that by pretreating natural pyrite samples with miniscule amounts of silver ions, the rate of chalcopyrite leaching increases dramatically. As little as 50 ppm silver on pyrite, or about 50 g silver (about 1.5 troy ounces) per tonne of pyrite, is sufficient to ensure rapid chalcopyrite leaching kinetics in the Galvanox™ process. In this process, the catalytic properties of pyrite are improved such that all pyrite samples regardless of their sources accelerate the rate of copper extraction from chalcopyrite significantly.

The effects of several variables such as the mass ratio of pyrite to chalcopyrite, the ratio of silver to pyrite, solution potential, and pulp density were evaluated in order to discover the optimized conditions for this process and to render it industrially feasible. The rate of leaching reaction increases by increasing the ratio of pyrite to chalcopyrite and ratio of silver to pyrite. The maximum recovery and the most efficient pyrite recycle were obtained at a solution potential of 450 mV *vs* Ag/AgCl. In this process, the redox potential has to be high enough to provide enough driving force for anodic oxidation and low enough to prevent oxidation of pyrite and loss of silver from pyrite. Under optimized conditions, the addition of 10% freshly silver-enhanced pyrite in each recycle test is sufficient to ensure the complete copper extraction within 10 to 15 hours of leaching which corresponds to the addition of as little as 61 mg of silver per kg of copper. Hence, recycled pyrite is equally as effective as freshly enhanced pyrite as a catalyst, which adds significantly to the commercial attractiveness of the process.

Effects of impurities associated with pyrite samples in the process of silver-enhanced pyrite catalyzed leaching were also investigated. It has been demonstrated that even a pyrite sample with a high level of impurities could be enhanced with silver ions. However, due to the presence of impurities and possible reactions of silver ions with this species, some pretreatment steps were required to obtain the optimum catalytic properties. It was shown that the detrimental effects of impurities were eliminated when pyrite was pretreated in leach solutions containing sulfuric acid, ferric and ferrous sulfate. Hence, pretreating the recycled pyrite from the leach process with silver ions overcomes these difficulties.

Due to possibility of presence of dissolved chloride in hydrometallurgical process water, the effects of chloride concentration on silver-enhanced catalyzed leaching were examined. It has been found that chloride concentrations up to 200 ppm have little or no detrimental effect on the kinetics of leaching. At higher chloride concentrations the rate of reaction is slightly slower but concentrations up to 1000 ppm can be still tolerated. Under these conditions, the recycled pyrite retains its catalytic properties and is as effective as freshly enhanced pyrite.

9.2 Understanding the Mechanism of Silver-enhanced Pyrite Catalyzed Leaching

An important aim of this research project was to understand the mechanisms involved in the process of leaching chalcopyrite in the presence of silver-enhanced pyrite and reveal the role of silver, silver-enhanced pyrite, and pyrite. In this process, the acceleration of chalcopyrite leaching was attributed to the galvanic interaction between pyrite and chalcopyrite. Pyrite provides an additional surface for only the cathodic reaction as it is inert under conditions of this process. Thus, the rate of ferric reduction increases which leads to the faster consumption of electrons. As charge neutrality in solution must be obtained, the rate of chalcopyrite oxidation must increase. In this study, it has been shown that

the rate of ferric reduction is faster on silver-enhanced pyrite than on natural pyrite; hence, the catalytic properties of pyrite are improved in the presence of silver.

Upon leaching of chalcopyrite, a non-conductive sulfur layer forms around the chalcopyrite which hinders the electrical contact between the couple. However, in the presence of silver-enhanced pyrite, a small fraction of the silver leaves the pyrite and reacts with the sulfur layer around chalcopyrite to form silver sulfide. It has been shown that this minuscule amount of silver decreases the resistivity of the sulfur layer sufficiently, rendering the sulfur layer conductive enough to allow the transport of electrons from the surface of unleached chalcopyrite to pyrite and thus facilitate electrical contact between the two minerals.

The electrical resistivities of the sulfur layer in the presence and absence of silver-enhanced pyrite were determined. In addition, the current and current density during typical Galvanox™ leaching were determined. Applying Ohm's law, the maximum resistivity of the sulfur layer that still allows the transport of electrons during the leaching time was obtained. This analysis was of interest to ensure that the decrease in resistivity of sulfur at low concentrations of silver was sufficient to facilitate electrical contact between pyrite and chalcopyrite. The results have shown that although the amount of silver sulfide is very low and the sulfur layer does not become very conductive, it does become conductive enough to allow the transport of electrons at a rate sufficient to support the leaching reactions at the rates observed in this process. With a conductive path between pyrite and chalcopyrite, the galvanic interaction between these minerals can now occur. Conversely, in the absence of silver, the resistivity of the sulfur layer is very high which limits the electrical contact between the two minerals.

The process of silver-enhanced pyrite-catalyzed leaching was compared with silver catalyzed leaching. It has been found that, at the level of silver added in the Galvanox™ process (60 mg Ag/kg Cu), the silver-catalyzed leaching process is

considerably slower and in fact there is no significant difference in leaching kinetics in the absence or presence of silver at this level. The results indicate that the presence of pyrite is a critical factor in this process. In addition, unlike silver-enhanced pyrite-catalyzed leaching, in the absence of pyrite, silver cannot be efficiently recycled to subsequent leaching tests unless several additional and inconvenient process steps are taken. In the silver-catalyzed leaching process, silver forms argentojarosite or silver sulfide and its catalytic properties are lost. Furthermore, it has been proven that silver-catalyzed leaching plays no role in the process of silver-enhanced pyrite-catalyzed leaching.

It was important to understand the nature of interaction of silver with pyrite prior to the leaching process and also to identify where the silver goes as the reaction proceeds.

The results have indicated that, by pretreating pyrite with silver ions at the low ratios used in the process, silver is reduced on the pyrite surface to form elemental silver. The possibility of reducing silver ions on pyrite at the rest potential of pyrite was confirmed.

9.3 Recommendations for Engineering Design

The proposed flowsheet of silver-enhanced catalyzed leaching in the Galvanox™ process is shown in Figure 9.1. This flowsheet comprises the following steps: pyrite pretreatment with silver, atmospheric copper leach, autoclave copper leach and oxyhydrolysis, pyrite elutriation, thickening, filtration, solvent extraction, electrowinning, and neutralization.

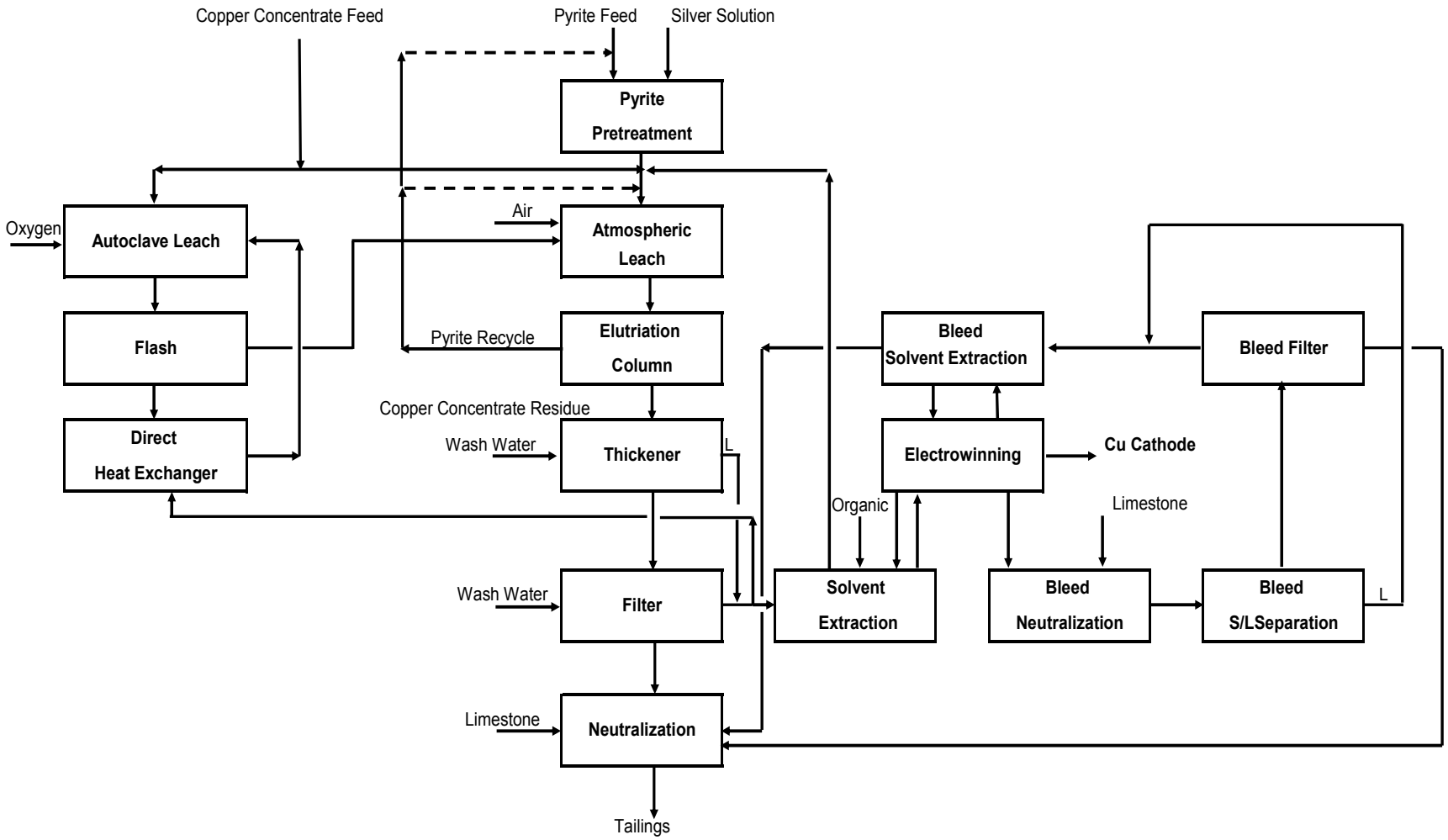

Figure 9.1 Process flowsheet

Pyrite particles are pretreated with silver ions before they are added to the atmospheric leaching reactor. The major portion of the concentrate is leached via atmospheric leaching and the rest enters a high pressure/high temperature autoclave. The purpose of the autoclave is to generate heat, sulfuric acid, and ferric sulfate required in atmospheric leaching. The autoclave discharge slurry from flash letdown is advanced to the atmospheric leach.

After atmospheric leaching, the slurry enters an elutriation column to separate pyrite from the slurry. The pyrite underflow is recycled to the atmospheric leaching tank and the overflow advances to the thickener. Then, the thickener underflow stream is filtered and the solid residue proceeds to the neutralization stage and on to tailings impoundment, while the thickener overflow and the leach solution from the filter advances to SX-EW to produce pure copper cathode. A portion of this stream (PLS) is returned to the autoclave. PLS has a high concentration of ferric sulfate which is precipitated as hematite in the autoclave and generates sulfuric acid.

After solvent extraction, the raffinate is recycled to the atmospheric leach since it is the main source of sulfuric acid for the leaching reaction. A raffinate bleed stream is neutralized and after solid/liquid separation proceeds to a bleed solvent extraction circuit.

It is important to note that the pretreatment of pyrite with silver ions is only feasible if the sources of pyrite and copper concentrate are separate. Such would be the case when the copper concentrate contains only a very small amount of pyrite and pyrite is provided from an external source.

If the copper concentrate contains sufficient pyrite, then separate pyrite enhancement with silver is not feasible. Under these conditions, silver may be added directly to the copper concentrate. However, it should be noted that pyrite is not recycled and all the added silver leaves the system along with the residue.

Under these circumstances, it might be advantageous to separate pyrite from the copper concentrate prior to atmospheric leaching (i.e., during cleaner flotation).

9.4 Recommendations for Future Work

Based on the results of this research study, several suggestions can be offered for future work:

- In this project, the mechanism of the Galvanox™ process using silver-enhanced pyrite was studied and the role of pyrite, silver-enhanced pyrite, and silver were revealed. Knowing the mechanism of the process and having the experimental data, one can now develop a mathematical model for the kinetics of chalcopyrite leaching using this process.

- An increase in electrical conductivity of an insulator at very low volume fractions of conductive dispersed phase have been reported in previous studies. It has been shown that, at very low concentrations of conductive elements in an insulator matrix, although volume fractions are not high enough to establish a connected conductive path, electron conductivity can be increased. In addition, in this study, it has been shown that the electrical conductivity of the sulfur layer increases by about five orders of magnitude in the presence of minuscule amounts of silver (60 to 100 ppm) dispersed in sulfur particles. The mechanism of electron transfer through sulfur should be explored further.

- In this study, the Galvanox™ process using silver-enhanced pyrite was examined at laboratory batch scale. The next step is to evaluate the process in continuous mode.

References

Abraitis, P.K., Pattrick, R.A.D., Vaughan, D.J. 2003. Variation in compositional, textural and electrical properties of natural pyrite: a review. *International Journal of Mineral Processing* 74, 41–59.

Agrawal, A., Sahu, K.K. Problems, prospects and current trends of copper recycling in India: An overview. *Resources, Conversation and Recycling* 54, 401–416.

Ahonen, L., Touvinen, O.H. 1990. Catalytic effects of silver in the microbiological leaching of finely ground chalcopyrite-containing ore materials in shake flasks. *Hydrometallurgy* 24, 219–236.

Ahonen, L., Tuovinen, O.H. 1993. Redox potential-controlled bacterial leaching of chalcopyrite ores. *Proceedings of International Biohydrometallurgy Symposium* 1, 571–578.

Almeida, C.M.V.B., Giannetti, B.F. 2003. The electrochemical behavior of pyrite-pyrrhotite mixtures. *Journal of Electroanalytical Chemistry* 553, 27–34.

Andersen, T., Boe, Y.H., Danielssen, T., Finne, P.M. 1980. Production of Base Metals from Complex Concentrates by Ferric Chloride Route in a Small, Continuous Pilot Plant, Complex Sulfide Ores. *Rap. Conf.*, Rome–London, 186–192.

Anderson, C.G., Harrison, K.J., Krys, L.E. 1996. Theoretical considerations of sodium nitrite oxidation and fine grinding in refractory precious metals concentrate pressure leaching. *Transactions of the Society for Mining, Metallurgy and Exploration* 299, 4–11.

Anderson, C.G. 1999. The treatment of chalcopyrite concentrate with nitrogen species catalyzed oxidative pressure leaching. *Proceeding of Copper 99-Cobre 99 International conference*, Volume IV, 139–149.

Anderson, C.G. 2003. Treatment of copper ores and concentrates with industrial nitrogen species catalyzed pressure leaching and non-cyanide precious metals recovery. *JOM* 55, 32–36.

Arbiter, N., Fletcher, A. W. 1994. Copper hydrometallurgy- Evolutions and milestones. *Mining Engineering*, 118-123.

Arbiter, N., McNulty, T. 1999. Ammonia leaching of copper sulfide concentrates. *Proceeding of Copper 99-Cobre 99 International conference*, Volume IV, 197–212.

Arehart, G.B., Eldridge, C.S., Chryssoulis, S.L., Kesler, S.E. 1993. Ion microprobe determination of sulfur isotope variations in iron sulfides from the Post/Betze sediment hosted disseminated gold deposit, Nevada, USA. *Geochimica et Cosmochimica Acta* 57, 1505–1519.

Asano, S., Imamura, M., Takeda, K, Ando, K., Nagase, N. 2007. Hydrometallurgical process for treating copper concentrates at Sumitomo metal mining. *The John Dutrizac International Symposium on Copper Hydrometallurgy,* Book 1, Volume IV, 177–187.

Ballester, A, 1987. Separation Process in Hydrometallurgy. Ellis Horwood Publishers, London, 99–110.

Ballester, A., Gonzalez, F., Blazquez, M.L., Mier, J.L. 1990. The influence of various ions in the bioleaching of metal sulfides. *Hydrometallurgy* 23, 221–235.

Ballester, A., Blazquez, M.L., Gonzalez, F., Muñoz, J.A. 2007. Catalytic role of silver and other ions on the mechanism of chemical and bioleaching leaching. Editors: Donati, E.R., Sand, W. Microbial Processing of Metal Sulfides, 77–101.

Bancroft, G.M., Hyland, M.M. 1990. Spectroscopic studies of adsorption/reduction reactions of aqueous metal complexes of sulfide surfaces. *Mineralogical Society of America* 23, 511–558.

Banerjee, P.C., Chakrabarti, B.K., Bhattacharyya, S., Das, A. 1990. Silver-catalyzed hydrometallurgical extraction of copper from sulfide ores from Indian Mines. *Hydrometallurgy* 25, 349–355.

Barr, G., Grieve, W., Jones, D., Mayhew, K. 2007. The new CESL gold process. *ALTA Copper Conference*, Perth, Australia.

Barriga F., Palencia I., Carranza F. 1987. The passivation of chalcopyrite subjected to ferric sulfate leaching and its reactivation with metal sulfides. *Hydrometallurgy* 19, 159–167.

Baur, J.P., Gibbs, H.L., Wadsworth, M.F. 1974. Initial stage sulfuric acid leaching kinetics of chalcopyrite using radiochemical techniques, *U.S Bureau of Mines Report of Investigations* 7823, 37.

Baxter, K., Scriba, H. Vega, I. 2010. Treatment of high arsenic copper gold concentrates– An option. *Proceeding of copper 2010*, 1783–1802.

Beckman, J. M., Birchenall, A.K., Simkovich, G. 1982. Electrical conductivity of dispersed phase systems. *Material Science Monographs* 15, 8–28.

Berry, V.K., Murr, L.E., Hiskey, J.B. 1978. Galvanic interaction between chalcopyrite and pyrite during bacterial leaching of low grade waste. *Hydrometallurgy* 3, 309–326.

Biegler, T. 1976. Oxygen reduction on sulfide minerals. Part II. Relation between activity and semiconducting properties of pyrite electrodes. *Journal of Electroanalytical Chemistry and Interfacial Electrochemistry* 159, 267–285.

Biegler, T., Swift, D.A. 1979. Anodic electrochemistry of chalcopyrite. *Journal of Applied Electrochemistry* 9, 545-554.

Bolorunduro, S.A., Dreisinger, D.B., Van Weert, G. 2003. Fundamental study of silver deportment during the pressure oxidation of sulfide ores and concentrates. *Minerals Engineering* 16, 695–708.

Braithwaite, J.W., Wadsworth, M.E. 1976. Oxidation of chalcopyrite under simulated conditions of deep solution mining. Editors: Yannopoulos, J.C., Agarwal, J.C. *Extractive Metallurgy of Copper 2, AIME*, New York, 752–775.

Bruynesteyn, A., Hackl, R.P., Lawrence, R.W., Vizsolyi, A.I. 1986. Biological acid leach process. United States Patent No. 4, 571,387.

Buckley, A.N., Wouterlood, H.J., Woods, R. 1989. The interaction of pyrite with solutions containing silver ions. *Journal of Applied Electrochemistry* 19, 744–751.

Buttinelli, D., Lavecchia, R., Pochetti, F., Geveci, A., Guresin, N., Topkaya, Y. 1992. Leaching by ferric sulfate of raw and concentrated copper-zinc complex sulfide ores, *International Journal of Mineral Processing* 36, 245–257.

Carranza, F., Palencia, I., Romero, R. 1997. Silver catalyzed IBES process: application to a Spanish copper–zinc sulfide concentrate. *Hydrometallurgy* 44, 29–42.

Chao, C.Y., Lin, L.F., Macdonald, D.D. 1982. A point defect model for anodic passive films. III. Impedance response. *Journal of the Electrochemical Society* 129. 1874–1879.

Chenery, S., Cook, J.M., Stylus, M., Cameron, E.M., 1995. Determination of the 3-dimensional distributions of precious metals in sulfide minerals by laser-ablation microprobe inductively coupled plasma-mass spectrometry (LAMP-ICP-MS). *Chemical Geology* 124, 55–65.

Chou, K., Ren, C. 2000. Synthesis of nanosized silver particles by chemical reduction method. *Materials Chemistry and Physics* 64, 241–246.

Chmielewski, T., Wodka, J., Iwachow, L. 2009. Ammonia pressure leaching for lubin shale middlings. *Physicochemical problems of Mineral Processing* 43, 5–20.

Collins, M.J., Kofluk, D.K. 1998. Hydrometallurgical process for the extraction of copper from sulphide concentrates. United States Patent. 5,730,776.

Cordoba, E.M., Muñoz, J.A., Blazquez, M.L., Gonzalez, F., Ballester, A. 2008(I). Leaching of chalcopyrite with ferric ion. Part I: General aspects. *Hydrometallurgy* 93, 81–87.

Cordoba, E.M., Muñoz, J. A., Blazquez, M.L., Gonzalez, F., Ballester, A. 2008(II). Leaching of chalcopyrite with ferric ion. Part III: Effect of redox potential on the silver-catalyzed process. *Hydrometallurgy* 93, 97–105.

Corrans, I.J., Angove, J.E. 1993. Activation of a Mineral Species, United States Patent 5,232,491.

Corriou, J.P., Kikindai, T. 1981. The aqueous oxidation of elemental sulfur and different chemical properties of the allotropic forms S_λ and S_μ. *Journal of Inorganic and Nuclear Chemistry* 43, 9–15.

Cruz, R., Luna-Sanchez, R. M., Lapidus, G.T., Gonzalez, I., Monroy, M. 2005. An experimental strategy to determine galvanic interactions affecting the reactivity of sulfide mineral concentrates. *Hydrometallurgy* 78, 198–208.

Dalton, R.F., Diaz, G., Price R., Zunkel, A.D. 1991. The Cuprex metal extraction process recovering copper from sulfide ores. *Journal of Metals* 43, 51–56.

Defreyne, J., Cabral, T. 2009. Early copper production results from Vale's hydrometallurgical CESL refinery. *ALTA Copper Conference*, Perth, Australia.

Dixon, D.G., Tshilombo, A.F. 2005. Leaching process for copper concentrates. United States Patent Application 2005/0269208 A1.

Dixon, D.G., Baxter, K.G., Sylwestrzak, L.A. 2007. Galvanox™ treatment of copper concentrates. *Proceedings of the ALTA 2007 Copper Conference, ALTA Metallurgical Services*, www.altamet.com.au.

Dixon, D.G., Mayne, D.D., Baxter, K.G. 2008. Galvanox™- A novel process for recovery of copper from primary copper concentrates. *Canadian Metallurgical Quarterly* 47, 327–336.

Doyle, F.M., Mirza, A.H. 1996. Electrochemical oxidation of pyrite samples with known composition and electrical properties. *Electrochemical Proceedings* 96, 203– 214.

Dreisinger, D.B., Steyl, J.D.T., Sole, K.C., Gnoinski, J., Dempsey, P. 2003. The Anglo American Corporation/University of British Columbia (AAC/UBC) chalcopyrite process: An integrated pilot–plant evaluation. *Hydrometallurgy of copper proceedings of the Copper 2003–Cobre 2003 conference*, Book 1, Volume VI, 223–237.

Dreisinger, D. B. 2006. Copper leaching from primary sulfides: Options for biological and chemical extraction of copper. *Hydrometallurgy* 83, 10–20.

Dutrizac, J.E., MacDonald, R.J.C., Ingraham, T.R. 1969. The kinetics of dissolution of synthetic chalcopyrite in aqueous acidic ferric sulfate solutions. *Trans. Metall. Soc. AIME* 245, 955–959.

Dutrizac, J.E., MacDonald, R.J.C. 1974. Ferric ion as a leaching medium. *Minerals Science and Engineering* 6, 59–100.

Dutrizac, J.E., 1978. The kinetics of dissolution of chalcopyrite in ferric ion media. *Metallurgical Transactions* 9B, 431–439.

Dutrizac, J.E. 1982. Ferric ions leaching of chalcopyrite from different localities. *Metallurgical Transaction* 13B, 303–309.

Dutrizac, J.E., Jambor, J.L. 1987. Behaviour of silver during jarosite precipitation. *Trans. IMM* 96, C206–C217.

Dutrizac, J.E., 1989. Elemental sulfur formation during the ferric sulfate leaching of chalcopyrite. *Canadian Metallurgical Quarterly* 28, 337–344.

Dutrizac, J.E. 1994. The leaching of silver sulphide in ferric ion media. *Hydrometallurgy* 35, 275–292.

Duyvesteyn, W.P.C., Sabacky,B.J. 1993. The Escondida process for copper concentrates. *Extractive Metallurgy, Copper, Nickel, Cobalt, Proceedings Paul E. Queneau International Symposium* 881–910.

Elsherif, A.E., 2002. The influence of cathodic reduction, Fe^{2+} and Cu^{2+} ions on the electrochemical dissolution of chalcopyrite in acidic solution. *Minerals Engineering* 15, 215–223.

Favorov, V.A., Krasnikov, V.J., Sychugov, V.S. 1974. Variations in semiconductor properties of pyrite and arsenopyrite and their determinants. *International Geology Review* 16, 385– 394.

Ferron, C.J., Fleming, C.A., O'Kan, P.T., Dreisinger, D.B. 2001. Application of the PLATSOL process for simultaneous dissolution of copper, nickel, gold, and PGMs from sulfide concentrates and autocatalysts. *Precious Metals*, 129–157.

Ferron, C.J., Fleming, C.A., O'Kan, P.T., Dreisinger, D.B. 2002. Pilot plant demonstration of the PLATSOL process for the treatment of the NorthMet copper–nickel–PGM deposit. *Mining Engineering* 54, 33–39.

Fleischer, M., 1955. Minor elements in some sulphide minerals. *Economic Geology*, 970–1024.

Fletcher, S., Holliday, C.S., Gates, D., Westcott, M., Lwin, T., Nelson, G. 1983. The response of some nucleation/growth processes to triangular scans of potential. *Journal of Electroanalytical Chemistry* 159, 267–285.

Fletcher, A.W. 1986. Future potential for chloride metallurgy. *SME Annual Meeting, New Orleans, LA,* March 3–5.

Garrels, R.M., Christ, C.L., 1965. Solution, Minerals, and Equilibria. Harper & Row, New York, 213–233.

Gericke, M., Pinches, A. 1999. Bioleaching of copper sulfide concentrate using extreme thermophilic bacteria. *Minerals Engineering* 12, 893–904.

Ghahremaninezhad, A., Asselin, E., Dixon, D.G. 2010. Electrochemical evaluation of the surface of chalcopyrite during dissolution in sulfuric acid solution. *Electrochemical Acta* 55, 5041–5056.

Glen, J.R., Richmond, G.D., Arnold, S.N., Mitchell, D.J. 2003. The Mount Gordon ferric leach process–plant upgrade to treat lower grade feed stocks. *Hydrometallurgy of copper, Proceedings of the Copper 2003–Cobre 2003*, Volume VI, 239–251.

Gomez, C., Figueroa, M., Muñoz, J., Blazquez, M.L. 1996. Electrochemistry of chalcopyrite. *Hydrometallurgy* 43, 331–344.

Gomez, E., Ballester, A., Blazquez, M.L., Gonzalez, F. 1999. Silver-catalyzed bioleaching of chalcopyrite concentrate with mixed cultures of moderately thermophilic microorganisms. *Hydrometallurgy* 51, 37– 46.

Greenwood, N.N., Earnshaw, A. 1984. The Chemistry of the Elements. Pergamon, Oxford.

Griffin, W.L., Ashley, P.M., Ryan, C.G., Soey, H.S., Suter, G.F. 1991. Pyrite geochemistry in the North Arm epithermal Ag–Au deposit, Queensland, Australia: a proton-microprobe study. *Canadian Mineralogist* 29, 185–198.

Habashi, F., Bauer, E.L. 1966. Aqueous oxidation of elemental sulfur. *Industrial and Engineering Chemistry Fundamentals* 5, 469–471.

Hackl, R.P., 1995. The leaching and passivation of chalcopyrite in acid sulfate media, PhD Thesis, The University of British Columbia, Vancouver, BC, Canada.

Hackl, R.P., Dreisinger, D.B., Peters, E. King J.A., 1995. Passivation of chalcopyrite during oxidative leaching in sulfate media. *Hydrometallurgy* 39, 25–48.

Hamalainen, M., Hyvarinen, O., Jyrala, M. 2003. Solution purification in the Outokumpu Hydrocopper process. *Hydrometallurgy 2003–Fifth International Conference in Honor of Ian Ritchie*, Volume I, 545–553.

Havlik, T., Kammel, R. 1995. Leaching of chalcopyrite with acidified ferric chloride and carbon tetrachloride addition. *Mineral Engineering* 8, 1125–1134.

Hebb, M.H. 1952. Electrical conductivity of silver sulfide. *The Journal of Chemical Physics* 20, 185–190.

Hermas, A.A., Morad, M.S. 2008. A comparative study on the corrosion behaviour of 304 austinitic stainless steel in sulfamic and sulfuric acid solution. *Corrosion Science* 50, 2710–2717.

Hirato, T., Majima, H., Awakura, Y. 1987. The leaching of Chalcopyrite with Ferric Sulfate. *Metallurgical Transactions* 18B, 489–496.

Hiroyoshi, N., Hirato, M., Hirajima, T., Tsunekawa, M. 1997. A case of ferrous sulfate addition enhancing chalcopyrite leaching. *Hydrometallurgy* 47, 37–45.

Hiroyoshi, N., Maeda, H., Miki, H., Hirajima, T., Tsunekawa, M. 1998. Ferrous promoted chalcopyrite leaching – ferric formation and its effect on the leaching. *Journal of MMIJ* 114, 795–800.

Hiroyoshi, N., Miki, H., Hirajima, T., Tsunekawa, M. 2000. A model for ferrous-promoted chalcopyrite leaching. *Hydrometallurgy* 57, 31–38.

Hiroyoshi, N., Miki, H., Hirajima, T., Tsunekawa, M. 2001. Enhancement of chalcopyrite leaching by ferrous ions in acidic ferric sulfate solutions. *Hydrometallurgy* 60, 185–197.

Hiroyoshi, N., Arai, M., Miki, H., Tsunekawa, M., Hirajima, T. 2002. A new reaction model for the catalytic effect of silver ions on chalcopyrite leaching in sulfuric acid solutions. *Hydrometallurgy* 63, 257–267.

Hiroyoshi, N., Kuroiwa, S., Miki, H., Tsunekawa, M., Hirajima, T. 2004. Synergic effect of cupric and ferrous ions on active-passive behaviour in anodic dissolution of chalcopyrite in sulfuric acid solutions. *Hydrometallurgy* 74, 103–116.

Hiroyoshi, N., Kuroiwa, S., Miki, H., Tsunekawa, M., Hirajima, T. 2007. Effects of coexisting metal ions on the redox potential dependence of chalcopyrite leaching in sulfuric acid solutions. *Hydrometallurgy* 87, 1–10.

Hiroyoshi, N., Kitagawa, H., Tsunekawa, M. 2008. Effect of solution composition on the optimum redox potential for chalcopyrite leaching in sulfuric acid solutions. *Hydrometallurgy* 91, 144–149.

Hiskey, J.B., Phule, P.P., Pritzker, M.D. 1987. Studies on the effect of addition of silver ions on the direct oxidation of pyrite. *Metallurgical Transactions* 18B, 641–647.

Hiskey, J.B., Pritzker, M.D. 1988. Electrochemical behavior of pyrite in sulfuric acid solutions containing silver ions. *Journal of Applied Electrochemistry* 18. 484–490.

Hoffman, J.E. 1991. Winning copper via chloride chemistry– An elusive technology, *JOM* 43, 48–49.

Hoffman, L.E., Hendrix, J.L., 1976. Inhibition of Thiobacillus ferrooxidans by soluble silver. *Biotechnology and Bioengineering* 18, 1161–1165.

Holliday, R.J., Richmond, W.R. 1990. An electrochemical study of the oxidation of chalcopyrite in acidic solution. *Journal of Electroanalytical Chemistry* 288, 83–98.

Hourn, M., Halbe, D. 1999. The NENATECH process: Results on Frieda River copper gold concentrates. *In: Proceedings of the International Conference of Randol Copper Hydromet Roundtable '99, Golden, Colorado, Randol International*, 97–102.

Huston, D.L., Sie, S.H., Suter, G.F., Cooke, D.R., Both, R.A. 1995. Trace elements in sulfide minerals from Eastern Australian volcanic- hosted massive sulfide deposits: Part 1. Proton microprobe analyses of pyrite, chalcopyrite and sphalerite, and Part II. Selenium levels in pyrite: comparison with Δ34S values and implications for the source of sulfur in volcanogenic hydrothermal systems. *Economic Geology* 90, 1167–1196.

Jibiki, K. 1971. An electrochemical study of pyrrhotite. MASc Thesis, The University of British Columbia, Vancouver, BC, Canada.

Johansson, C., Shrader, V., Auissa, J., Adutwum, K., Kohr, W. 1999. Use of the Geocoat process for the recovery of copper from chalcopyrite, *Proceeding of the international Biohydrometallurgy Symposium IBC 99*, Part A, 569–576.

Jones, D.L. 1974. The leaching of chalcopyrite. PhD Thesis, The University of British Columbia, Vancouver, BC, Canada.

Jones, D. L., Peters, E. 1976. The leaching of chalcopyrite with ferric sulfate and ferric chloride. Extractive Metallurgy of Copper, Editors: Yannopoulos, I.C., Agrawal, J.C. AIME, New York, NY. 663.

Jones, D.L., Hestrin, J. 1998. CESL process for copper sulfide: Operation of the demonstration plant. *Alta 1998 Copper Sulfide Symposium*. Australia.

Jones, D. L. 2002. Process for the recovery of Nickel and/or Cobalt from a concentrate. United States Patent No. 6,383,460.

Jones, D. 2011. Process for gold and silver recovery from a sulphide concentrate. United States Patent. US 8,025,859 B2.

Kametani, K., Aoki, A. 1985. Effect of suspension potential on the oxidation rate of copper concentrate in a sulfuric acid. *Metallurgical Transactions* 18B, 489–496.

King, J.A., Dreisinger, D.B., Knight, D.A. 1993. The total pressure oxidation of copper concentrates. Editors: Reddy, R.G., Weizenbach, R.N. Extractive Metallurgy of Copper, Nickel, and Cobalt: Fundamental Aspects. *The Minerals, Metals, and Materials Society of AIME*, Warrendale, PA, USA, 735–756.

King, J.A., Dreisinger, D.B. 1995. Autoclaving of copper concentrates. *Proceedings of Copper 95–Cobre 95 International Conference*, 511–534.

Klauber, C., Parker, A., van Bronswijk, W., Watling, H., 2001. Sulphur speciation of leached chalcopyrite surfaces as determined by X-ray photoelectron spectroscopy. *International Journal of Mineral Processing* 62, 65–94.

Klein, C., Hurlbut Jr., C.S., 1993. Manual of Mineralogy, 21st edition. Cambridge University Press, Cambridge.

Kotz, J.C., Treichel, P., Townsend, J.R. 2009. Chemistry and Chemical Reactivity, Volume 2.

Lawrence, R.W., Vizsolyi, A., Vos, R.J. 1985. The silver catalyzed bioleach process for copper concentrate. Editors: Clum, J.A., Haas, L.A. Microbiological effects on metallurgical processes, New York, TMS, Warren dale, 65–82.

Lazaro, I., Nicol, M.J. 2006. A rotating ring-disk study of the initial stages of the anodic dissolution of chalcopyrite in acidic solutions. *Journal of Applied Electrochemistry* 36, 425–431.

Le Houillier, R., Ghali, E. 1982. Contribution to the study of the leaching of chalcopyrite. *Hydrometallurgy* 9, 169–194.

Leimala, R., Hyvarinen, O., Hamalanien, M., Jyrala, M. 2003. The Outokumpu HydroCopper Process–Design, implementation, and operation of a demonstration plant. *Hydrometallurgy of copper, Proceedings of the Copper 2003–Cobre 2003*, Volume VI, 281–288.

Leoppold, N., Lendle, B. 2003. A New Method for Fast Preparation of Highly Surface-Enhanced Raman Scattering (SERS) Active Silver Colloids at Room Temperature by Reduction of Silver Nitrate with Hydroxylamine Hydrochloride. *Journal of Physical Chemistry* 107B, 5723–5727.

Li, J., Miller, J.D., Wan, R.Y., Le Vier, M. 1995. The ammoniacal thiosulfate system for precious metal recovery. Proceedings of the XIX International Mineral Processing Congress (IMPC), San Fransisco, CA, USA. SME, Littleton, CO, USA.

Liang, C.C. 1973. Conduction characteristics of the lithium iodide-aluminum oxide solid electrolyte. *Journal of the Electrochemical Society* 120, 1289–1292.

Liddicoat, J., Dreisinger, D. 2007. Chloride leaching of chalcopyrite. *Hydrometallurgy* 89, 323–331.

Linge, H.G., 1976. A study of chalcopyrite dissolution in acidic ferric nitrate by potentiometric titration. *Hydrometallurgy* 2, 51–64.

Livingston, S.E. 1965. Metal complexes of ligands containing sulfur, selenium or tellurium as donor atoms. *Quarterly Reviews of Chemical Society* 19, 386–425.

Lundstrom, M., Aromaa, J., Forsen, O., Hyvarinen, O., Barker, M. 2005. Leaching of chalcopyrite in cupric chloride solution, *Hydrometallurgy* 77, 89–95.

Maddox, L.M., Bancroft, G.M., Lorimer, J.W. 1996. Interaction of aqueous silver ions with the surface of pyrite. *Journal of Applied Electrochemistry* 26. 1185–1193.

Majima, H., 1969. How oxidation affects selective floatation of complex sulfide ores. *Canadian Metallurgical Quarterly* 8, 269–282.

Marsden, J.O., Brewer, R.E., Hazen, N. 2003. Copper Concentrate Leaching Developments by Phelps Dodge Corporation. Editor: Courtney Young. *Hydrometallurgy 2003, Proceedings of the International Symposium honoring Professor Ian M. Ritchie*, 1429–1446.

Martienssen, W., Warlimont, H. 2005. Springer Handbook of Condensed Matter and Material Data.

Mathews, C.T., Robins, R.G. 1974. Aqueous oxidation of iron disulfide by molecular oxygen. *Australian Chemical Engineering* 15*,* 19–24.

McLean, D.C. 1982. Chloride leaching of copper concentrates, practical operational aspects. *AIME Annual Meeting*, Dallas, TX, Feb14–18.

McMillan, R.S., MacKinnon, D.J., Dutrizac, J.E. 1982. Anodic dissolution of n-type and p-type chalcopyrite. *Journal of Applied Electrochemistry* 12, 743–757.

Mehta, A.P., Murr, L.E. 1983. Fundamental studies of the contribution of galvanic interaction to acid-bacterial leaching of mixed metal sulfides. *Hydrometallurgy* 9, 235–256.

Milbourne, J., Tomlinson, M., Gormely, L. 2003. Use of hydrometallurgy in direct processing of base metal/PGM concentrates. *Hydrometallurgy 2003–Fifth International Conference in Honor of Professor Ian Ritchie*, Volume: Leaching and Solution Purification, 617–630.

Miller, J.D., Portillo, H.Q. 1979. Silver catalysis in ferric sulfate leaching of chalcopyrite. Mineral Processing. Editor: J. Laskowski. XIII International Min Proc Conf. Elsevier, Amsterdam, 851–901.

Miller, J.D., McDonough, P.J., Portillo, H.Q. 1981. Electrochemistry in silver catalyzed ferric sulfate leaching of chalcopyrite. In: Process and Fundamental Considerations of Selected Hydrometallurgical Systems (Editor: Kuhn, M.C.), SME-AIME, New York, 327–338.

Morris, J. E., Coutts, T.J. 1977. Electrical conduction in discontinuous metal films: A discussion. *Thin Solid Films* 47, 3–65.

Morris, J. E. 1998. Recent developments in discontinuous metal thin film devices. *Vacuum* 50, 107–113.

Moyes, J., Sammut, D., Houllis, F. The Intec copper process: activity in British Columbia.

Moyes, J., Houllis, F. 2002. Intec base–metal processes realizing the potential of chloride hydrometallurgy. Chloride Metallurgy 2002. *Canadian institute of mining, metallurgy and petroleum*, Volume 2, 577–592.

Muir, D. 2008. The Parker copper process– A new approach ahead of its time. Hydrometallurgy 2008, *Proceedings of the Sixth International Symposium*, 685–694.

Muñoz, P.B., Miller, J.D., Wadsworth, M.E. 1979. Reaction mechanism for the acid ferric sulfate leaching of chalcopyrite. *Metallurgical Transactions* 10B, 149–158.

Muñoz, J.A., Dreisinger, D.B., Cooper, W.C., Young, S.K., 2007. Silver catalyzed bio-leaching of low-grade copper ores. Part II: Stirred tank tests. *Hydrometallurgy* 88, 19–34.

Muñoz, J.A., Dreisinger, D.B., Cooper, W.C., Young, S.K. 2008. Interaction of silver ions with sulphide minerals with special emphasis on the chalcopyrite/pyrite galvanic couple. *Canadian Metallurgical Quarterly* 47, 259–268.

Nazari, G., Asselin, E. 2009. Morphology of chalcopyrite leaching in acidic ferric sulfate media. *Hydrometallurgy* 96, 183–188.

Nersisyan, N.H., Lee, J.H., Son, H.T., Won, C.W., Maeng, D.Y. 2003. A new and effective chemical reduction method for preparation of nanosized silver powder and colloid dispersion. *Materials Research Bulletin* 38, 949–956.

Nickel, U., Castell, A., Poppl, K., Shneider, S. 2000. A silver colloid produced by reduction with hydrazine as support for highly sensitive surface enhanced Raman spectroscopy. *Langmuir* 16, 9087–9091.

Nova, D., Gonzalez, I. 2006. The influence of galena galvanic interaction on the reactivity of chalcopyrite floatation concentrate. *ECS Transactions* 2, 255 –264.

Nowak, P., Krauss, E., Pomianowski, A. 1984. The electrochemical characteristics of the galvanic corrosion of sulphide minerals in short-circuited model galvanic cells. *Hydrometallurgy* 12, 95 –110.

Oberthur, T., Cabri, L.J., Weiser, T.W., McMahon, G., Muller, P. 1997. Pt, Pd and other trace elements in sulfides of the main sulfide zone, Great Dyke, Zimbabwe: *a reconnaissance study. Canadian Mineralogist* 35, 597–609.

Okamoto, H., Nakayama, R., Tsunekawa, M., Hiroyoshi, N. 2003. Improvement of chalcopyrite leaching in acidic sulfate solutions by redox potential control. Editors: Riveros, P.A., Dixon, D.G., Dreisinger, D.B., Menacho, J. Hydrometallurgy of copper leaching and process development, 67–81.

Okamoto, H., Nakayama, R., Hiroyoshi, N. Tsunekawa, M. 2004. Redox potential dependence and optimum potential of chalcopyrite leaching in sulfuric acid solutions. *Journal of MMIJ* 120, 592–599.

Okamoto, H., Nakayama, R., Kuroiwa, S., Hiroyoshi, N., Tsunekawa. M. 2005. Normalized redox potential used to assess chalcopyrite column leaching. *Journal of MMIJ* 121, 246–254.

Palencia, I., Romero, R., Carranza, F. 1998. Silver Catalyzed IBES process: Application to a Spanish copper–zinc sulfide concentrate. Part 2. Biooxidation of the ferrous iron and catalyst recovery. *Hydrometallurgy* 48, 101–112.

Parker, A.J. Paul, R.L., Power, G.P. 1981. Electrochemistry of the oxidative leaching of copper from chalcopyrite. *Journal of Electroanalytical Chemistry* 118, 305–316.

Parker, A., Klauber, C., Kougianos, A., Watling, H.R., Bronswijk, W. 2003. An X-ray photoelectron spectroscopy study of the mechanism of oxidative dissolution of chalcopyrite. *Hydrometallurgy* 71, 265–276.

Peacey, J., Guo, X.J., Robles, E. 2003. Copper hydrometallurgy–current status, preliminary economics, future direction and positioning versus smelting. *Hydrometallurgy of copper proceedings of the Copper 2003–Cobre 2003 conference*, Volume VI (Book 1), 205–221.

Peters, E. 1984. Electrochemical mechanisms for decomposing sulphide minerals. *Proceedings of the Electrochemical Society* 84, 343–361.

Peters, E. 1986. Leaching of sulfides. Advances in Mineral Processing, Editor: P. Somasasundaran. The Society for Mining, Metallurgy, and Exploration, Inc., of AIME, Littleton, CO, USA. 445–462.

Peters, E. 1992. Hydrometallurgical process innovation. *Hydrometallurgy* 29, 431–459.

Petersen, J., Dixon, D.G. 2006. Competitive bioleaching of pyrite and chalcopyrite. *Hydrometallurgy* 83, 40–49.

Pinches, A., Al-Jaid, F.O., Williams, D.J.A., 1976. Leaching of chalcopyrite concentrates with thiobacillus ferrooxidans in batch culture. *Hydrometallurgy* 2, 87–103.

Pinches, J. 1997. A process for the leaching of chalcopyrite. Republic of South Africa Patent Application. No.97/1307.PCT/GB97/00585.

Pooley, F.D., 1982. Bacteria accumulate silver during leaching of sulfide ore minerals. *Nature* 296, 642–643.

Price, D.W, Warren, G.W. 1986. The influence of silver ion on the electrochemical response of chalcopyrite and other mineral sulfide electrodes in sulfuric acid. *Hydrometallurgy* 15, 303–324.

Price, D.W., Warren, G.W., Drouven, B. 1986. The electrochemical behaviour of silver sulphide in sulfuric acid solutions. *Journal of Applied Electrochemistry* 16, 719–731.

Pridmore, D.F., Shuey, R.T. 1976. The electrical resistivity of galena, pyrite, and chalcopyrite. *American Mineralogist* 61, 248– 259.

Raja, K.S., Jones, D.A. 2006. Effects of dissolved oxygen on passive behaviour of stainless alloys. *Corrosion Science* 48, 1623–1638.

Ramachandran, V., Lakshmanan. V.I., Kondos, P.D. 2007. Hydrometallurgy of copper sulfide concentrate: An update. . *The John Dutrizac International Symposium on Copper Hydrometallurgy,* Book 1, Volume IV, 101–128.

Rivera Vasquez, B.F. 2010. Electrochemical and leaching studies of enargite and chalcopyrite. PhD Thesis, The University of British Columbia, Vancouver, BC, Canada.

Rivera Vasquez, B., Viramontes Gamboa, G., Dixon, D.G. 2012. Transpassive Electrochemistry of chalcopyrite particles. *Journal of Electrochemical Society* 159, C8–C14.

Romero, R., Palencia, I., Carranza, F. 1998. Silver catalyzed IBES process: application to a Spanish copper–zinc sulfide concentrate. Part 3. Selection of the operational parameters for a continuous pilot plant. *Hydrometallurgy* 49, 75–86.

Romero, R., Mazuelos, A., Palencia, I., Carranza, F. 2003. Copper recovery from chalcopyrite concentrates by the BRISA process. *Hydrometallurgy* 70, 205–215.

Sandstrom, A.m., Shchukarev, A., Paul, J. 2005. XPS characterization of chalcopyrite chemically and bio-leached at high and low redox potential. *Minerals Engineering* 18, 505–515.

Sato, N., Kudo, K., Noda. 1971. The anodic oxide film of iron in neutral solution. *Electrochemical Acta* 16, 1909–1921.

Scaini, M.J., Bancroft, G.M., Lorimer, J.W., Maddox, L.M. 1995. The interaction of aqueous silver species with sulphur- containing minerals as studied by XPS, AES, SEM, and electrochemistry. *Geochimica et Cosmochimica Acta* 59, 2733–2747.

Scaini, M.J., Bancroft, G.M., Knipe, S.W. 1997. An XPS, AES, and SEM study of the interactions of gold and silver chloride species with PbS and FeS2:

Comparison to natural samples. *Geochimica et Cosmochimica Acta* 61, 1223–1231.

Schieck, R., Hartmann, A., Fiechter, S., Konenkamp, R., Wetzel, H. 1990. Electrical properties of natural and synthetic pyrite (FeS2) crystals. *Journal Materials Research* 5, 1567– 1572.

Schweiter, F.W., Livingstone, R. 1982. Duval's CLEAR hydrometallurgical process. Editor: P.D. Parker. *AIME*. 221–227.

Snell, G., Fords, N.J., 1976. Leaching of copper ore to recover sulfur and silver catalyst. United States Patent 3,974,253.

Solomon, S., Bahadory, M., Jeyarajasingam, A.V, Rutkowsky, S.A. 2007. Synthesis and study of silver nanoparticles. *Journal of Chemical Education* 84, 322–325.

Sondi, I., Gola, D.V., Matijevic, E. 2003. Preparation of highly concentrated stable dispersions of uniform silver nanoparticles. *Journal of Colloid and Interface Science* 260, 75–81.

Stanczyk, M.H. 1963. Oxidation leaching of copper sulfides in acidic pulps at elevated temperatures and pressures. U.S Bureau of Mines report of Investigations RI6193, 19.

Stanely, R. W., Subramanian, K.N. 1977. Recovering copper from concentrates with insolubale sulfate forming leach. United States Patent 4,039,406.

Stott, M.B., Watling, H.R., Franzmann, P.D., Sutton, D.C. 2001. The effect of solution chemistry on jarosite deposition during the leaching of chalcopyrite by the thermophilic archaeon. Sulfolobus metallicus. *Process Metallurgy* 11, 207–215.

Sukla, L.B., Chaudhury, G.R., Das, R.P., 1990. Effect of silver ion on kinetics of biochemical leaching of chalcopyrite concentrate. *Transactions of the Institution of Mining and Metallurgy* 99, C43–C46.

Sullivan, J.D. 1933. Chemical and physical features of copper leaching. *Transactions of the American Institute of Mining and Metallurgical Engineers* 106, 515–546.

Szymanowski, J. 1993. Hydroxyoxime and Copper Hydrometallurgy; CRC *Press: Boca Raton, FL*.

Third, K.A., Cord-Ruwisch, R., Watling, H.R. 2000. The role of iron-oxidizing bacteria in stimulation or inhibition of chalcopyrite bioleaching. *Hydrometallurgy* 57, 225–233.

Third, K.A., Cord-Ruwisch, R., Watling, H.R. 2002. Control of the redox potential by oxygen limitation improves bacterial leaching of chalcopyrite. *Biotechnology and Bioengineering* 78. 433–441.

Tshilombo, A F. 2004. Mechanism and kinetics of chalcopyrite passivation and depassivation during ferric and microbial leaching solutions. PhD Thesis, The University of British Columbia, Vancouver, BC, Canada.

Tunley, T.H, Copper recovery. 1999. United States Patent 5,919,674.

Van der Merwe, C., Pinches, A., Myburgh, P.J. 1998. A process for the leaching of chalcopyrite. World Patent No. WO 9,839,491.

Van Staden, P.J. 1998. The Mintek/Bactech copper bioleach process. *Alta 1998 Copper Sulfides Symposium*. October 1998. Australia.

Vaughan, D.J., Craig, J.R. 1978. Mineral Chemistry of Metal Sulfides. Cambridge University. Press, Cambridge.

Venkatachalam, S. 1991. Treatment of chalcopyrite concentrates by hydrometallurgical techniques. *Minerals Engineering* 4, 1115–1126.

Viramontes-Gamboa, G., Rivera Vasquez, B.F., Dixon, D.G. 2007. The active-passive behaviour of chalcopyrite: Comparative study between electrochemical and leaching responses. *Journal of Electrochemical Society* 154, C299–C311.

Vizsolyi, A., Veltman, H., Warren, I.H., Mackiw, V.N. 1967. Copper and elemental sulfur from chalcopyrite by pressure leaching. *Journal of Metals* 19, 52–59.

Wagner, C. 1972. The electrical conductivity of semiconductors involving inclusions of another phase. *Journal of Physics and Chemistry of Solids* 33, 1051–1059.

Wang, S. 2005. Copper leaching from chalcopyrite concentrates. *JOM* 57, 48–51.

Wan, R. Y., Miller, J. D., Foley, J., Pons, S. 1984. Electrochemical Features of the Ferric Sulfate Leaching of CuFeS2/C Aggregates. Proceedings of the International Symposium on Electrochemistry in Mineral and Metal Processing, the Electrochemical Society, Editors: P. E. Richardson, S. Srinivasan and R. Woods. 391–416.

Wilkinson, G. 1987. Comprehensive Coordination Chemistry. Pergamon, Oxford.

Yin, Q., Kelsall, G.H.., Vaughan, D.J., Brandon, N.P. 2001. Mathematical Models for time-dependant impedance of passive electrodes. *Journal of the Electrochemical Society* 148, A200–A208.

Zhang, Z., Zhao, B., Hu, L. 1996. PVP Protective Mechanism of Ultrafine Silver Powder Synthesized by Chemical Reduction Processes. *Journal of Solid State Chemistry* 121, 105–110.

Zielinska, A., Skwarek, E., Zaleska, A., Gazda, M., Hupka, J. 2009. Preparation of silver nanoparticles with controlled particle size. *Procedia Chemistry* 1, 1560–1566.